UNIVERSITÀ DELLA CALABRIA

UNIVERSITA' DELLA CALABRIA

Dipartimento di Chimica e Tecnologie Chimiche

Dottorato di Ricerca in

Medicina Traslazionale

CICLO

XXXII

ANTICANCER DRUGS: A DETAILED COMPUTATIONAL ANALYSIS OF "NON CLASSICAL" COMPOUNDS MECHANISM OF ACTION

Settore Scientifico Disciplinare CHIM/03

Coordinatore: Ch.mo Prof. Sebastiano Andò

Firma

Supervisore: Prof.ssa Emilia Sicilia

Firma

Dottorando: Dott.ssa Fortuna Ponte

Firma

Table of Contents

Table of Contents

Table of Contents

Abstract

Metal containing drugs have attracted an enormous deal of interest for their use in cancer therapy. Transition metal compounds' richness offers extraordinary opportunities for the design of anticancer compounds, possessing pharmacokinetic properties inaccessible to purely organic compounds. The most successful and evident proof of their pivotal role is represented by cisplatin that, together with its carboplatin and oxaliplatin derivatives, continues to be routinely used worldwide in clinical practice. However, it is well known that the use of such drugs for fighting cancer is accompanied by severe side effects and intrinsic or acquired resistance that drastically limit their successful action. Therefore, decades of research efforts have been devoted to the search and the synthesis of safer and more effective and selective agents, either containing platinum or alternative metals, acting with similar or different mechanisms. In order to accomplish this aim is of decisive importance the elucidation of the mechanism of action of the drugs.

Molecular simulations, or *in silico* experiments, are able to provide detailed information at atomistic resolution, rarely accessible to experiments, that can complement laboratory experiments. The increasing accuracy of computational approaches and the growing performance of computer performance, allow to properly describe reaction paths and involved molecular orbitals, calculate electronic properties, simulate spectra without any limitation except those connected with the adopted level of theory and compuatational protocol.

The main aim of the present work was the detailed investigation, in the framework of the Density Functional Theory, of the mechanism of action of “non classical” platinum and transition metal non-platinum compounds, for some of them in collaboration with experimentalists, and the rationalization of their behaviors. In the next paragraphs all the studied systems will be shortly described together with the motivations that have prompted us to study such systems.

Both “non classical” platinum(IV) prodrugs, non-platinum drugs and photoactivatable Pt(II) and Pt(IV) complexes have been examined. In the development of new platinum-based anticancer drugs, is of great interest the emerging class of "dual action" Pt(IV) prodrugs that, undergoing a reductive elimination process, which is the key step for their activation, are able to release the active Pt(II) complexes and bioactive axial ligands that together lead to cell death. Indeed, the two axial ligands, in turn, can be chosen to possess physico-chemical and biopharmaceutical properties or even facilitate the incorporation into a drug delivery system.

According to the research lines mentioned above, the use of drug delivery systems has also grown, and many different strategies have been examined to encapsulate platinum drugs within macromolecules, including macrocyclic species, which are responsible for creating supramolecular host-guest structures. The encapsulation slows down and prevents the drug degradation by proteins and peptides. One of the most widely studied class of synthetic supramolecular macrocycles are Calix[n]arenes (CX), whose property, as molecular hosts and delivery systems, are of increasing interest.

Photodynamic Therapy (PDT) is a non-toxic therapeutic technique, clinically approved and minimally invasive, used for the treatment of several types of cancers based on the generation of reactive oxygen species (ROS), that acts as cytotoxic agents. In PDT applications three components are required: a photosensitizer (PS), a light of a specific wavelength and tissue oxygen.

A promising approach to increase the effectiveness of anticancer therapy is the combination of multimodal treatment methods into a single system. Recently, a strategy has been proposed providing the possibility to combine the classical Pt-based chemotherapy with photodynamic therapy (PDT) treatment. This approach involves the functionalization of a photosensitizer (PS) with a therapeutic drug such as cisplatin-like compounds.

Abstract

I farmaci contenenti metalli hanno riscosso un enorme interesse per il loro impiego nelle terapie antitumorali. La ricchezza chimica dei complessi dei metalli di transizione offre straordinarie opportunità per la progettazione di composti antitumorali, che presentano proprietà farmacocinetiche inaccessibili ai composti puramente organici.

La prova più riuscita ed evidente del loro ruolo cardine è rappresentata dal cisplatino che, insieme ai suoi derivati, carboplatino e ossaliplatino, continua ad essere utilizzato abitualmente a livello mondiale nella pratica clinica.

Tuttavia, è ben noto che l'uso di tali farmaci è accompagnato da gravi effetti collaterali e resistenza intrinseca o acquisita che limita drasticamente la loro efficacia. Pertanto, decenni di sforzi di ricerca sono stati dedicati all'individuazione e alla sintesi di agenti più sicuri, più efficaci e più selettivi, contenenti platino o metalli alternativi, che agiscono con meccanismi simili o diversi. Per raggiungere questo obiettivo, è necessario chiarire il meccanismo d'azione dei farmaci.

Le simulazioni molecolari (esperimenti in *silico)* sono in grado di fornire informazioni dettagliate con risoluzione atomistica, raramente accessibili agli esperimenti, che possono integrare gli esperimenti di laboratorio. La sempre maggiore accuratezza degli approcci computazionali e le crescenti prestazioni dei calcolatori, consentono di:

- descrivere correttamente i percorsi di reazione e gli orbitali molecolari coinvolti;
- calcolare le proprietà elettroniche;

- simulare gli spettri

senza alcuna limitazione, fatta eccezione per quelle connesse al livello di teoria adottato e al protocollo computazionale.

L'obiettivo del presente lavoro è stato quello di indagare dettagliatamente, nell'ambito della Teoria Funzionale della Densità, il meccanismo d'azione di complessi "non classici" del platino e di composti contenenti metalli di transizione diversi dal platino. Per alcuni di essi, l'indagine e la razionalizzazione dei loro comportamenti sono state condotte in collaborazione con gruppi sperimentali. Di seguito sono brevemente descritti tutti i sistemi studiati e le motivazioni che hanno condotto alla scelta di tali sistemi.

Sono stati esaminati i profarmaci di platino (IV), i farmaci a base di altri metalli e i complessi fotoattivabili di Pt(II) e Pt(IV).

Nello sviluppo di nuovi farmaci antitumorali a base di platino, è di grande interesse la classe emergente di profarmaci di Pt (IV) a "doppia azione" che, sottoposti ad un processo di eliminazione riduttiva, che rappresenta il passaggio chiave per la loro attivazione, sono in grado di rilasciare il complesso attivo di Pt(II) e i leganti assiali bioattivi che insieme portano alla morte cellulare. Infatti, i due leganti assiali, che a loro volta possono essere scelti in base alle loro proprietà chimico-fisiche e biofarmaceutiche, o sono anche in grado di facilitare l'incorporazione in un sistema di trasporto e rilascio di farmaci.

In accordo con quanto descritto in precedenza, anche l'uso di sistemi di trasporto di farmaci è cresciuto e sono state esaminate molte strategie diverse per incapsulare i farmaci del platino all'interno di

macromolecole, comprese specie macrocicliche, che sono responsabili della creazione di strutture host-guest supramolecolari. L'incapsulamento rallenta e previene il degrado del farmaco da parte di proteine e peptidi. Una delle classi di macrocicli supramolecolari maggiormente studiate è quella dei Calix[n]areni (CX), le cui proprietà, di *host* molecolari e di sistemi di rilascio, sono diventate oggetto di grande interesse della comunità scientifica.

La terapia fotodinamica (PDT) è una tecnica terapeutica non tossica, clinicamente approvata e poco invasiva, basata sulla generazione di specie reattive dell'ossigeno (ROS), che agisce come agente citotossico è utilizzata per il trattamento di diversi tipi di tumori. Nelle applicazioni della PDT sono richiesti tre componenti: un fotosensibilizzatore (PS), una luce di una lunghezza d'onda specifica e la presenza di ossigeno nei tessuti.

Un approccio promettente per aumentare l'efficacia della terapia antitumorale è la combinazione di metodi di trattamento multimodale in un unico sistema. Recentemente, è stata proposta una strategia che offre la possibilità di combinare la chemioterapia classica a base di Pt con il trattamento di terapia fotodinamica (PDT). Questo metodo prevede la funzionalizzazione di un fotosensibilizzatore (PS) con un farmaco terapeutico come i composti simili al cisplatino.

List of papers included in this thesis

1. **Glutathione activation of an organometallic half-sandwich anticancer drug candidate by ligand attack.**

X. Zhang, F. Ponte, E. Borfecchia, A. Martini, C.S Cano, E. Sicilia, P.J. Sadler, Chemical Communications, **2019**, 55, 14602—14605.

2. **Ligand-centred redox activation of inert organo-iridium(III) anticancer complexes.**

Wen-Ying Zhang, Samya Banerjee, George M. Hughes, Hannah Bridgewater, Ji-Inn Song, Ben Breeze, Guy J. Clarkson, James P. C. Coverdale, Fortuna Ponte, Emilia Sicilia, Peter J. Sadler

(Submitted to Chemical Science)

3. **A metadynamics perspective on the reduction mechanism of the Pt(IV) asplatin prodrug.**

F. Ponte, GM. Piccini, E. Sicilia, M. Parrinello, Journal of Computational Chemistry, Journal of Computational Chemistry, **2020**, 41, 290–294.

4. **Photophysical Exploration of Dual-Approach PtII−BODIPY Conjugates: Theoretical Insights.**

Fortuna Ponte, Marta E. Alberto, Bruna C. De Simone, Nino Russo, Emilia Sicilia, Inorganic chemistry, **2019**, *58*, 9882−9889.

5. **Elusive Intermediates in the Breakdown Reactivity Patterns of Prodrug Platinum(IV) complexes.**

D. Corinti, M. E. Crestoni, S. Fornarini, F. Ponte, N. Russo, E. Sicilia, E. Gabano, D. Osella, Journal of The American Society for Mass Spectrometry, **2019** , 30(10), 1881-1894.

6. **Antitumor Platinium(IV) Prodrugs: A Systematic Computational Exploration of Their Reduction Mechanism by L-Ascorbic Acid.**

E.Dabbish, F. Ponte, N. Russo, E. Sicilia, Inorganic chemistry **2019**, *58*, 3851−3860.

7. **Insights from computations on the mechanism of reduction by ascorbic acid of Pt(IV) prodrugs with Asplatin and its chlorido and bromido analogues as model systems.**

F. Ponte, N. Russo, E. Sicilia, Chemistry - A European Journal, **2018**, *24*, 9572 – 9580.

8. **BODIPY for photodynamic therapy applications: computational study of the effect of bromine substitution on 1O2 photosensitization.**

F. Ponte, G. Mazzone, N. Russo, E. Sicilia, Journal of Molecular Modeling, **2018**, *24*, 183.

9. **Investigation of the guest-host complexation between 4-sulfocalix[4]arene and nedaplatin for potential use as a drug delivery system**.

S. A. Fahmy, F. Ponte, M. K. Abd El-Rahman, N. Russo, E. Sicilia, T.Shoeib, Spectrochimica Acta Part A: Molecular and Biomolecular Spectroscopy, **2018**, *193*, 528–536.

10. **Theoretical determination of the aquation reaction mechanism of cyclometalated benzimidazole Ru(II) and Ir(III) anticancer complexes.**

F. Ponte, I. Ritacco, N. Russo, E. Sicilia, Inorganica Chimica Acta, **2017**, *470*, 325–330.

INTRODUCTION

Cisplatin and its congeners, carboplatin and oxaliplatin, are the most used platinum based anticancer drugs in the world. It is clinically proven that they combat diverse types of cancers but, despite their worldwide clinical application, their use is limited by considerable problems of inherent and acquired resistance, systemic toxicity and low water solubility.

The mechanism of action (MoA) of cisplatin has been clarified in its essential aspects both experimentally and theoretically. Activated by hydrolysis, the platinum compound causes cell death by the formation of DNA cross-links.

Recently, other strategies summarized below, have been proposed to combat the Pt compounds resistance, to increase the spectrum of activity and decrease side effects:

1. New platinum compounds, different in structure, whose mechanism of action is in part or totally different from that identified in the case of cisplatin.
2. Platinum (IV) prodrugs, an important class of compounds that are activated by reduction directly in the cell releasing the corresponding cytotoxic square-planar Pt(II) active complexes together with the axial ligands.

The chemical inertness obtained through the hexa-coordination of the platinum(IV) complexes makes the compounds stable in biological fluids. Moreover, the axial ligands, which might

possess antineoplastic or pharmacological properties, provide a means to control reduction potentials, lipophilicity, charge, selectivity, targeting and.

3. Complexes based on other metals with different chemical properties (charge, coordination, redox activity, etc.), which can act with the same or distinct mechanisms of action than platinum complexes.
4. Drug delivery systems for platinum complexes that are obtained by the encapsulation of anticancer drugs within macrocycles to slow down and prevent degradation before reaching the target. Interactions of hydrophobic type are established between the macrocycle (host) and the drug (guest) to generate a host-guest complexes. Three groups of macrocycles are relevant as delivery systems: calix[n]arenes, cucurbit[n]urils and n-cyclodextrins.
5. A less invasive therapeutic technique named Photodynamic Therapy (PDT) used to treat different types of tumors through the production of cytotoxic agents, the reactive oxygen species (ROSs). PDT uses a drug, named photosensitizer agent (PS), which upon irradiation with light of a specific wavelength, produces the highly cytotoxic singlet oxygen ($^1O_2$) (type I photoreaction) or other highly reactive radicals (type II photoreaction).

It is worth underlining that the knowledge of the mechanisms of action, the metabolic pathways and the chemical properties of

cisplatin derivatives, non-platinum metal based complexes and photosensitizing molecules is of paramount importance for the selection of new approaches to cure cancer. Laboratory experiments should be complemented by “in silico” experiments able to afford information not accessible differently and, in principle, without any limitation except those related to the adopted level of theory and computational protocol.

The aim of this research project was to study, through the strategies of the theoretical and computational chemistry, such as density functional theory (DFT), time dependent DFT (TD-DFT) and metadynamics:

- The reduction mechanisms of new Pt(IV) anticancer prodrugs aiming at proposing, in some cases, new compounds with higher anticancer activity. (Chapter 3)

- The mechanisms of action of new metal-based anticancer complexes. Classical hydrolysis mechanism of Ru(II) and Ir(III) anticancer complexes has been investigated. In addition, the reactivity of organometallic Ir(III) and Os(II) complexes able to kill cancer cells by novel mechanisms of action has been explored. (Chapter 4)

- The host/guest interaction between 4-sulfocalix[4]arene and a Pt(II) complex. (Chapter 5)

- The chemical properties of new photosensitizers operating as photodynamic agents in Photodynamic Therapy (PDT). A multitarget antineoplastic drug, a particular molecule that combines a light absorbing chromophore with a cisplatin unit, was studied. (Chapter 6)

1

ANTICANCER DRUGS: A BRIEF HISTORY AND NEW DEVELOPMENTS

1. Cisplatin and beyond

1.1. Cisplatin, Carboplatin and Oxaliplatin, classical Pt(II) drugs

Cisplatin, cis-[$Pt(NH_3)_2Cl_2$], whose cytotoxic activity has been serendipitously discovered in the 1960s by Rosenberg,[1] is the most well-known Pt based complex used as anticancer drug (Figure 1) and very efficacious in the treatment of a wide variety of cancers such as testicular, ovarian, head, neck and small cell lung.[2–7]

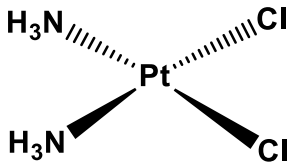

Figure 1. Chemical structure of the anticancer drug cisplatin

It is well known that the cisplatin complex activation starts inside the cell by hydrolysis of Pt-Cl bonds,[5,6] to generate Pt-H_2O complexes. The lower chlorido concentration (4–20 mM) inside the cells with respect to the bloodstream promotes the drug activation. Specifically, the first chlorido ligand is replaced by a water molecule leading to the formation of the mono-aqua complex cis-[$Pt(NH_3)_2(OH_2)Cl]^+$. The remaining chlorido ligand can be substituted by a further water molecule to form cis-[$Pt(NH_3)_2(OH_2)_2]^{2+}$, the di-aqua platinum complex (Scheme 1).

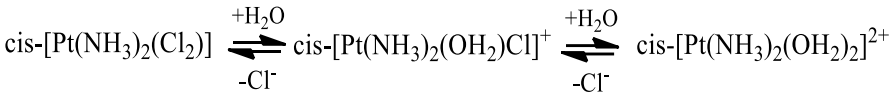

Scheme 1. Cisplatin, hydrolysis reaction

In the aquated compounds, the water molecules coordinated to the metal centre lower their pKa causing the formation of hydroxido complexes. At physiological pH, the equilibria associated with the formation of Pt-OH species, hence cis-[$Pt(NH_3)_2(OH_2)(OH)]^+$ and cis-[$Pt(NH_3)_2Cl(OH)$], become important.

The Pt aquo/hydroxido complexes are the active forms that, can interfere with the cell division processes by the formation of covalent adducts with DNA (Pt-DNA adducts), forming preferentially 1,2-intrastrand cross-links (65%) with the N7 position of guanines bases.[7–11] The 1,3-adduct intrastrand and the interstrand modes are significantly less important.[11]

The DNA lesions induce the cancer cell necrosis and/or apoptosis.[11,12]

Despite its success, severe side effects of cisplatin therapies: vomiting, kidney damage, hearing loss etc. and intrinsic and acquired drug resistance, limit its clinical use.

The cisplatin shortcomings have motivated, in the first moment, the exploration of a large number of cisplatin analogues, having reduced side effects, lower resistance and efficacy toward a wider range of cancers, acting following the same steps of cisplatin mechanism of action and, finally, binding to DNA.[13,14] Since the

discovery of cisplatin, over 3000 platinum compounds have been synthesized and screened for antitumor activity and among these, only two complexes have been approved for clinical use: *Carboplatin* a second generation of platinum (II) complex and *Oxaliplatin*, a third generation drug.[15] (Figure 2)

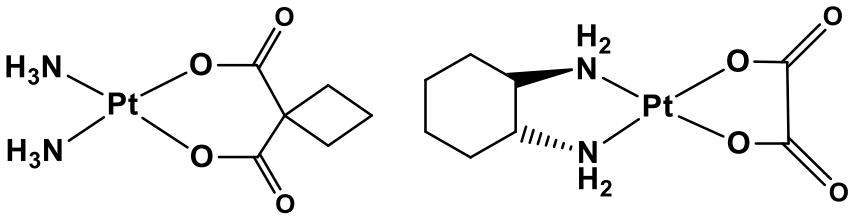

Figure 2. Chemical structure of the clinical carboplatin and oxaliplatin agents.

In addition, three other complexes have been approved for use in specific countries, named *Nedaplatin* (in Japan),[16] *Lobaplatin* (China), and *Heptaplatin* (Korea). [17,18]

Carboplatin (*cis*-diammine (1,1-cyclobutanedicarboxylato) platinum II) contains the chelating leaving group, the cyclobutane-1,1-dicarboxylate (CBDCA), instead of the two chlorido ligands of cisplatin. This chelating ligand is replaced by water molecules more slowly than cisplatin and causes the complex to be more stable and soluble compared to cisplatin. Furthermore, carboplatin exhibits improved nephrotoxicity, neurotoxicity, ototoxicity,[19] but it is less efficacious than the first generation of platinum drugs. The mechanism of action of

carboplatin involves the formation of covalent drug-DNA adducts where carboplatin mainly reacts whit guanine and to a lesser extent with adenine.[20]

The DNA-carboplatin monoadducts and diadducts involve the replacement of one or both "arms" of the bidentate dicarboxylate ligand.

Oxaliplatin (*trans*-R,R-diaminocyclohexane(oxalate) platinum II) is a third generation platinum derivative, which contains two bidentate ligands, a chelating oxalate as leaving group and a chelating R,R-diaminocyclohexane (DACH) as non leaving group. These chelating ligands confer greater stability to the complexes than cisplatin. Oxaliplatin is useful in the treatment of metastatic colorectal cancer, is active in cisplatin and carboplatin resistant tumours[21,22] and, moreover, reveals reduced haematological toxicity than carboplatin.[23,24] Oxaliplatin interacts with DNA forming adducts, whose detailed characteristics are not known yet.

1.2. Drug candidates with non-classical mechanisms of action: trans Pt(II) complexes and intercalating agents

Over the years, in an attempt to find drugs with improved features, a great deal of attention has been focused on new Pt(II) derivatives, able to interact with DNA in unconventional ways.

The first examples of such complexes consisted of platinum compounds with *trans* geometry.

Although transplatin (*trans*-diammine-dichlorido-platinum (II) is inactive, several platinum compounds with *trans* geometry exhibit promising anticancer activity.

One strategy to obtain active trans-Pt(II) complexes a is the replacement of the ammine ligand(s) with planar N-donor ligands such as pyridine, quinoline, isoquinoline, thiazole, or benzothiazole. An increased activity in cisplatin and oxaliplatin resistant is obtained.[25] Moreover, these trans complexes display different lesions of DNA compared to cisplatin, Pt(II) derivates, favouring monofunctional adducts and interstrand cross-links. Further trans-Pt(II) analogues complexes, with promising biological activity, have the amino group(s) substituted by iminoether ligands.[22, 23] These complexes are able to establish more stable monofunctional adducts with DNA.

Another strategy is to consider trans-Pt$(NH_3)_2$Cl unit to create **polynuclear platinum(II) compounds** with the aim to improve DNA binding ability and facilitate long distance interactions, for obtaining flexible intra- and inter-strand cross-links. This new proposal increases the affinity to DNA. The complex that has shown improved features is the trinuclear platinum(II) compound, BR3564,bis[trans-diammine-chlorido-platinum(II)][μ-trans-diammine-bis(hexanediamine)-platinum(II)] nitrate,[28] which generates adducts with DNA that

are not recognized during the repair phase. Nevertheless, during the phase II trials, the compound has shown a large toxicity and other side effects.

The systems proposed so far, despite having different properties, require further studies to mitigate problems of toxicity and drug resistance.

Another class of complexes studied and tested is represented by Pt(II) complexes that can bind to DNA in a non-covalent way, through an *intercalation process*. Intercalation is a reversible intermolecular process in which the drugs, containing □-conjugated heterocyclic ligands, can establish electrostatic interactions, H-bonding, van der Waals and hydrophobic interactions with DNA leading to its distortion. In particular, insertion and formation of π-π stacking interactions between a complex containing a planar aromatic ring ligand and the two adjacent basis of the double-stranded DNA occur, generating a structural change. The most common binders for these systems are bipyridine, terpyridine, and phenanthroline. This category includes the **monofunctional platinum(II)** complexes having an organic intercalator group and a classical leaving group such as a chlorido ligand. These complexes are able to play a double function, exhibiting DNA intercalation followed by platination to form monofunctional DNA adducts. These monofunctional DNA-damaging agents such as pyriplatin (*cis*-diamminepyridinechloroplatinum(II)) and phenanthriplatin (*cis*-

diamminephenanthridinechloroplatinum(II)) are able to inhibit DNA polymerases.[29,30]

1.3. Pt(IV) prodrugs as multi-action anticancer agents. Reduction and anticancer activity

The second and third-generation of Pt(II) drugs encounter the same drawbacks of cisplatin complex. In order to overcome these limits, new strategies have been adopted over the years including the use of Pt(IV) complexes capable to act as prodrugs.

The prodrugs are derivatives of drugs that undergoing *in vivo* transformation, can release the active drug able to perform the desired action. The Pt(IV) prodrugs, after administration, being relatively inert to substitution, can be directly activated inside the cells and consequently reduce undesired side effects making even oral administration feasible.[31] One of the best known orally active Pt(IV) complex, whose clinical trials have been stopped within Phase II, is Satraplatin (bis-acetato-ammine-dichlorido-cyclohexylamine-platinum (IV)) JM216, a cisplatin-based complex.[32] (Figure 3)

However, the clinical tests have been stopped within phase II[32] due to an irrelevant increase of survivors. Its advantage resides in a small number of collateral effects, especially after administration. No neurotoxicity, nephrotoxicity, and ototoxicity have been observed.

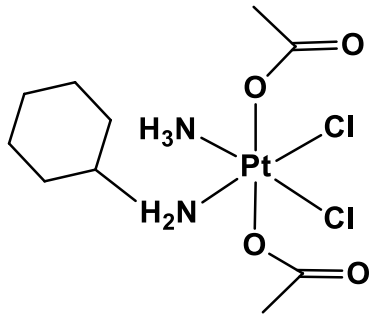

Figure 3. Chemical structure of the Pt(IV) prodrug Satraplatin

Pt(IV) complexes have low-spin d^6 electron configuration and adopt octahedral geometries with two additional axial ligands in the axial position with respect to Pt(II) complexes.[33] Pt(IV) complexes, thanks to their configuration, are more kinetically inert. The inertness makes Pt(IV) prodrugs more resistant toward ligand substitution reactions minimizing collateral reactions with biomolecules before reaching the target, and increases their lifetime in the blood. Moreover, the two axial ligands can modulate the biological features of the complex such as lipophilicity, redox stability, solubility in biological media etc., can inhibit reactions related to resistance to the drug and/or afford pharmacological properties to the complex.

The Pt(IV) complexes can be activated directly inside cancer cells by a two-electron reduction reaction that involves the loss of both axial ligands and the simultaneous release of cisplatin or its derivatives. The resulting square-planar Pt(II) complex binds the DNA and induces cellular death. (Scheme 2).

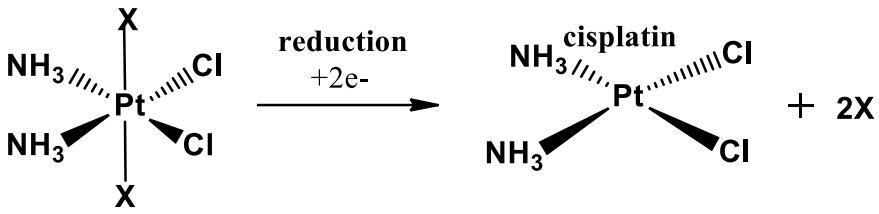

Scheme 2. Reduction reaction of Pt(IV) complexes

Therefore, the reduction reactions are the main chemical processes in which Pt(IV) complexes are involved and the complexes reduction potential is influenced by the nature of the ligands in both axial (much stronger influence) and equatorial positions[31] and by the biological reducing agent involved in the redox process.

For *in vitro* reduction tests, the reducing agents used to activate the Pt(IV) complexes are ascorbic acid (AA), or more properly its active monoanionic ($AscH^-$) form, and glutathione (γ-glutamylcysteinylglycine, GSH), which are believed to be the main bio-reducing agents in the cell.[34,35] Several experiments have been carried out using also cysteine, methionine [36] and in particular cases also the cytochrome c. [37]

It is worth mentioning that there are also cases of "spontaneous reduction" reactions of Pt(IV) through daylight or elevated temperatures, not only reduction accomplished by biomolecules.

Experimental information concerning the reduction is usually obtained by cyclic voltammetry, which allows measuring the reduction potential but not the standard redox potential because

the Pt(IV) complex is involved in an irreversible process that leads to the electron transfer and release of both the axial ligands. Several mechanistic hypotheses have been proposed for the reductive elimination of Pt(IV) complexes by ascorbate that are, generally, classified as:

- *inner sphere mechanism*, in which the two electron transfer occurs in one step thanks to a bridge formation between one of the ligands in axial position and the reducing agent, facilitating the electron flow. The corresponding reduced Pt(II) complex and the oxidized form of the reducing agent are the final products.
- *Pt(II) complex catalyzed inner sphere mechanism* that involves bridged Pt(II)-Pt(IV) dimers formation in the redox reaction.[38]
- *outer sphere mechanism*, a process in which the electrons are transferred without any contact between the complex and reducing agent, at least without the formation of new covalent bonds. [39]

Several studies on the activation step of Pt(IV) complexes indicate that the structural features of the prodrugs influence the activity and the type of mechanism of action followed by the complex. For example the inner sphere mechanism is active for complexes containing in axial positions halide ions, hydroxido ligands [24,38,40] or good leaving groups; in other cases the active mechanism is thought to be the outer sphere, [41] even if details are still poorly understood. Moreover, also the reduction rate can change based on the ligand identity.

Pt(IV) complexes with electron withdrawing groups in axial positions, able to destabilized the system, are more potent and are involved in a faster reduction.[42] For example, the Pt(IV) complexes with axial trifluoroacetate ligands are more potent compared to their analogues with acetate.

It is important to underline, as mentioned before, that the Pt(IV) behavior is based on the nature of the ligands and the enormous plethora of combinations of ligands can generate a large variety of Pt(IV) candidates with different physical and chemical properties, bioactivity etc.

An attractive strategy is to design Pt(IV) prodrugs with bioactive axial ligands (enzyme, drugs etc.) being the advantage that a single prodrug can play a multiple action and can act on different cellular targets. Several example can be found in recent literature and the number is growing over the years. [43–46]

For example, when the prodrug contains anti-inflammatory drugs in axial position, the complex can act combining both anti-inflammatory and chemotherapy actions. The Asplatin is a good example of dual action Pt(IV) prodrug with the ability to release, under reduction conditions, the corresponding Pt(II) complex, cisplatin, and aspirin, able to play its biological activity. [44,47] A computational study of the reduction mechanism of the Asplatin prodrug (Figure 4) in presence of the monodeprotonated form of L-ascorbic acid as reducing agent has been carried out. [48] Recent studies show also that the aspirin can be used to reduce the

incidence of colorectal cancer (CRC) and protect against other non-CRC associated adenocarcinomas. [49]

Further studies and novel development are going on Asplatin analogues and Pt(IV) complexes containing anti-inflammatory drugs able to act as multi-action anticancer drugs.

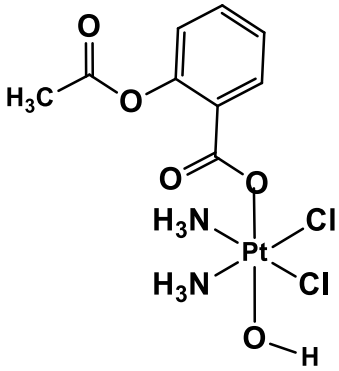

Figure 4. Asplatin, Pt(IV) prodrug

1.4. Metal-based non-platinum anticancer drugs

1.4.1 Anticancer activity of organometallic Os(II), Ir(III) and Ru(II) complexes

With the aim to overcome the well-known limitations of platinum-based complexes and increasing the range of treatable cancers, a new generation of complexes with alternative metals (in particular transition metals) provides a wide platform for the drug design with higher cancer cell selectivity, lower resistance, and reduced collateral effects.[49–52]

With respect to platinum drugs, non-platinum metal complexes offer several advantages that give the possibility of increasing selectivity and modulate their anticancer activity. For example,

their different accessible redox states and the wide range of geometries and coordination numbers allow the proper tuning of their chemical reactivity from both thermodynamic (strengths of metal−ligand bonds, redox potentials, etc.) and kinetic (rate of ligand substitution) points of view. In addition, also the ligands directly bound to the metal can play important roles in the biological activity.

Such new non-platinum metal-based therapeutic agents might have the same cisplatin's mode of action (classical chemotherapeutics) or can act with different mechanisms and on different target sites such as mitochondrial membranes, thiol-containing proteins, enzymes, metal transport protein and RNA (non-classical chemotherapeutics). The mechanism of action for non-classical metal complexes can include the perturbation of the redox state of cells (the redox balance, in several diseases, including cancer, is disturbed) which can occur through the direct participation of the redox metal centre and the ligands or through the coordination of biomolecules involved in redox processes.

A large number of non-platinum anticancer drugs (gold, gallium, arsenic, ruthenium, osmium, and iridium complexes) are involved in redox pathways. According to recent studies, a new way effective to kill cancer cells is the generation of reactive oxygen species, ROS.[53] This new strategy entails the use of intracellular antioxidant molecules such as glutathione (GSH) and organometallic complexes.

Several organometallic complexes have been widely explored and mainly Ru, Ir, and Os complexes have been studied in view of their use as antineoplastic agents. Especially, pseudo-octahedral half-sandwich complexes of Ru(II), Os(II), Rh(III) and Ir(III) [53–57] with cyclopentadienyl or arene ligands, chelating ligand such as N,N- or C,N- and a monodentate leaving group such as halide (e.g. Cl or I) or pyridine ligands, show promising antiproliferative activity towards human cancer cells and are active *in vivo*.

As demonstrated from Sadler and co-workers, organometallic complexes can exhibit their anticancer activity through multiple mechanisms. For instance, when N,N is a chelating diamine ligand (e.g., ethylenediamine, en), Osmium(II) arene complexes, Ruthenium(II) arene complexes and iridium(III) cyclopentadienyl (CpX) complexes $[M(arene/CpX)(N,N)(X)]^{n+}$ can bind the DNA and act with classical mechanisms of action.[58,59] If an azopyridine, instead, is the N,N bidentate ligand (Figure 5), the complexes are relatively inert toward the classical activation by hydrolysis and can cause, by redox reactions, an increasing of reactive oxygen species inside cancer cells.

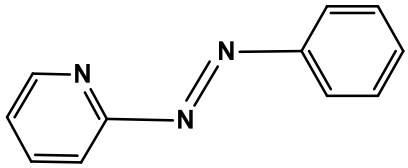

Figure 5. Azopyridine ligand

As experimental studies show, these azopyridine complexes provide novel and complex mechanism of actions because they are activated inside the cells by reduction reactions, in the presence of glutathione. In particular the proposed mechanism provides the attack of the reducing agent, GSH on the azo bond of the azopyridine ligand.

The glutathione, through the mediation of the azo group (inert toward the reduction reactions when it is not coordinated to the metal centre) can catalyze the metal complexes hydrolysis, can generate reactive adducts for which their interaction with DNA is facilitated and/or may include the metal complex in a redox cycle that appears to lead to the fast generation of ROS in cells.

It is possible to conclude that the use of non-platinum anticancer complexes is an effective strategy to increase the anticancer potency thanks to combination of more than one cytotoxic action.

1.5. Drug delivery systems

1.5.1. Calixarenes and related macrocycles as drug vehicles

In the pharmaceutical sector, one of the ongoing challenges, it is to increase the selectivity for cancerous cells over normal tissues and solving the intracellular degradation (by glutathione, proteins, peptides or other species) and further effects that disable the drug.

These problems can be overcome using drug delivery vehicles, macrocycles able to encapsulate and protect the drug within their cavity, allowing the formation of host-guest inclusion complexes. The formulation of the supramolecular complex, in addition, may improve the drug solubility and stability, slow down the drug release, reduce the systematic toxicity and overcome acquired drug resistance. [60]

The study of macrocycles used as drug delivery agents is a promising area of research, as highlighted by a large number of recent reviews.

A promising class of macrocyclic hosts, with little to null toxicity, relatively simple to synthesize and functionalized is that of **calix[n]arenes** (where n indicates the number of macrocycles subunits).

These macrocycles can be used, also, in molecular recognition and have shown potential as host molecules in selective extraction processes.

The calixarenes are more versatile hosts of bowl or cone shaped with hydrophobic π-electron rich mid-region cavity (accessible only through one portal), a larger flexibility of the macrocyclic backbone and a variable number of conformations, which increases with the size of the macrocycle.

They are synthesized through the condensation of p-substituted phenol derivatives with an aldehyde.[61]

The functionalization of these macrocycles at their wide and narrow rims allows to identify a wider range of applications with different mechanisms of action (they can act as anti-cancer, anti-obesity, anti-bacterial and anti-diabetic molecules), and allows them to possess improved drug carrier properties leading the development of new drug-delivery system.[62,63]

Here, the main aspect which we are interested in engages the calixarenes as drug delivery systems able to encapsulate the drug of interest with the aim to improve the pharmacokinetic and pharmacodynamics effects and to better target cancerous tissues. The nature of the drug-macrocycle complexes depends of the type of used anticancer drug.

Generally, the supramolecular complex is stabilised through hydrophobic effects within the macrocycle cavity and ion–dipole or hydrogen bonding to the macrocycles' portals.

For platinum-based drugs, the most studied macrocycles are para-sulfonatocalix[4]arenes (SC_4) [64] (Figure 6), bowl-shaped water soluble drug vehicles with a hydrophobic cavity and four negatively charged sulphate groups.

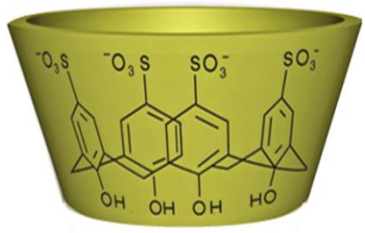

Figure 6. Chemical Structure of para-sulfonatocalix[4]arene.

Compared to native calixarenes, the sulfonatocalixarens showed improved drug solubility, chemical stability, bioavailability, biodistribution and transport, and/or elimination of drug polymorphism in the solid state.[65,66]

This type of macrocycles is also capable of forming inclusion complexes with different types of platinum anticancer complexes, including dinuclear complexes.

In conclusion, the supramolecular strategy opens to a wide range of opportunities to build versatile delivery systems able to transport anticancer drugs, improving their properties and performance.

1.6. Photodynamic Therapy (PDT), general principles

Photodynamic Therapy (PDT) is a clinically approved, minimally invasive and non-toxic therapeutic technique for the treatment of different cancer cell types and other non-malignant diseases, based on the generation of cytotoxic active species.

This therapy has also proved to be highly efficacious to kill bacteria, fungi and viruses and can be used for the sterilization of blood plasma and water.[67]

PDT application is based on the combination of three components, namely an oxygen molecule, a photosensitizer (PS) and a light of a specific wavelength.

The therapy is based on the ability of the PS, a molecule with specific chemical and photophysical properties, to trigger, upon

activation, a series of photochemical and photobiological reactions that induce apoptosis and/or necrosis in the tumor cells through the production of intracellular reactive oxygen species (ROS), singlet oxygen $^1O_2$ and free radicals.

Specifically, the photosensitizer is injected into the bloodstream or can be administered intraperitoneally or topically and when is localized in cancer cells, is excited by irradiation from the ground state S0 to the singlet exited state S1 (PS: S0→ S1) with a laser light of a wavelength that falls in the range between 600–800 nm, the so-called therapeutic window. In order to maximize the tissue penetration is better to use a photosensitizer that absorbs a radiation around 800 nm (the penetration depth of approximately 1 cm) than visible radiation. So, the PDT application is limited to the treatment of superficial lesions.

The activation process of PS by light (in the form of photons), generates the exited state, usually S1 state, and is followed by competing of radiative or non-radiative processes.

The S1 state can relax back to the ground state via a radiative process by emitting fluorescent light (the singlet−singlet emission is called fluorescence) or by internal conversion (IC) into heat. The photochemical process, instead, that leads the tumor cells necrosis or apoptosis, consists in the S1 energy transfer, via nonradiative intersystem crossing (ISC), to a low-lying triplet state, forbidden by the selection rules in principle, but allowed by spin orbit couplings.

If the PS energy triplet state is sufficiently high and the lifetime is in the micro-millisecond range, it can generate cytotoxic species through two types of photodynamic reactions, known as:

1. Photochemical reactions of type I
2. Photochemical reactions of type II.

However, the deactivation of the excited T1 state can occur either by internal or external conversion or by triplet-singlet emission process (phosphorescence).

The type I photochemical reactions involves the formation of free radicals (anions and cations species) through the reaction (electron transfer or hydrogen transfer) between the triplet excited state of PS and substrates (e.g. lipids and other biological molecules) present in the environment, which, in turn, may produce, through reactions with oxygen, reactive oxygen species (i.e., O_2^{-}, H_2O_2, OH^{-}). In the photochemical reactions of type II, instead, the triplet exited state returns to the ground state S0 via energy transfer to molecular oxygen, which is excited from the triplet state to singlet-excited state (cytotoxic agent in PDT).

The active singlet oxygen $^1O_2$ can react with many biological species, such as lipids, proteins, and nucleic acids leading to cancer cell death.

The amount of energy required to promote the O_2 $^3\Sigma_g^-$ → $^1\Delta_g$ transition, and obtain the highly reactive and cytotoxic singlet oxygen is 0.98 eV and a PS in PDT must have an energy gap S0-T1 larger than this value. The typical process of PDT can be briefly summarized in an energy diagram. (Figure 7)

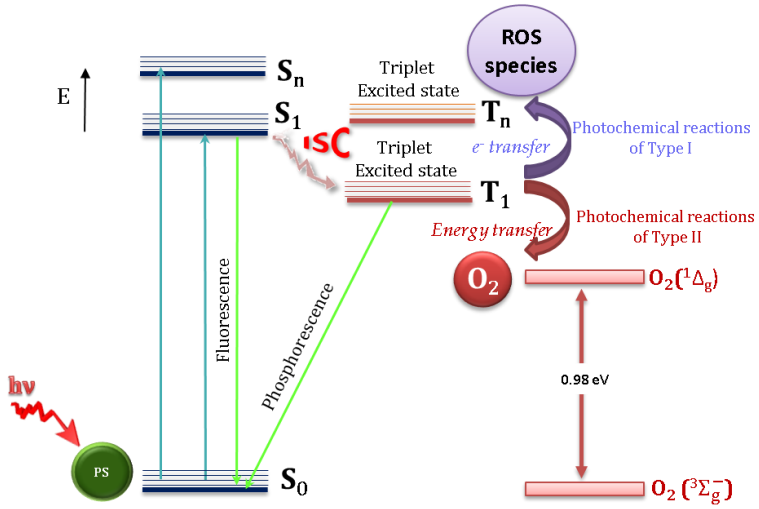

Fig.7 Jablonski diagrams and $^1O_2$ production

Obviously, the singlet oxygen production (cytotoxic agent) is possible only if an efficient intersystem crossing mechanism occurs and a quantitative analysis (it is possible to calculate the rate of the ISC mechanism, K_{isc}) is made on the basis of some rules such as Fermi golden rule and energy-gap rule. The K_{isc} depends partly on the relative magnitude of the spin–orbit matrix elements (SOC) between the wavefunctions of singlet (Sn) and triplet (Tn) that are engaged in the transition. According to the first rule, the K_{isc} is proportional to the square module of the SOC elements and roughly, proportional to the energy difference

between the electronic states that are involved (the energy-gap rule).

Furthermore, according to El-Sayed rules, the K_{isc} increases if during the transition there is an orbital change. So, to promote the type II photochemical reaction, a photosensitizer must possess a high value of spin-orbit coupling that ensures an efficient ISC mechanism, strong absorption in the therapeutic window and a singlet-triplet energy gap (ΔE_{S-T}) higher than 0.98 eV (the energy required to generate the singlet oxygen.

In the PDT field, an ideal photosensitizer, in addition, must have several properties such as chemical stability, water solubility, high and selective accumulation in tumour tissue, no cytotoxicity in the dark, high molar extinction coefficients.

Different classes of PSs have been proposed over the years. The first photosensitizer, approved in 1995, belongs to the family of porphyrins and it is the Photofrin (Fig.10),[68] a molecule formed by dimers and oligomers of hematoporphyrin, which, after several clinical tests, showed numerous limitations mainly due to low light absorption. In a series of states, other drugs are presently approved, such as: Foscan, [69] (Figure 11) with generic name "Temoporfin", the 5,10,15,20-tetrakis(m-hydroxyphenyl) chlorin, a benzoporphyrin derivative named Verteporfin[70] and a lutetium Texaphyrin.[71]

Porphyrins derivatives including chlorins, bacteriochlorins, phthalocianines, and related structures are the most commonly

used photosensitizers thanks to their well known photophysical properties. Other classes of PSs known for the production of ROS include tetrapyrrolic systems, fullerenes derivatives and aromatic ketones.

New photosensitizers, whose properties can be appropriately modulated by introducing into the macrocycles (typical photodynamic agents) various transition metals and heavy substituents, have been synthesized in recent years.

In this specific field, several attempts have been made to find a new type of functionalizable chromophores other than porphyrins.

Recently, the well known BODIPY, (the IUPAC name is 4,4-difluoro-4-bora-3a,4a-diaza-s-indacene), and its aza derivatives (aza BODIPY)[72] have been proposed as promising photosensitizers in PDT. The "*BODIPY* core" and its *IUPAC* numbering system representation are reported in Figure 8.

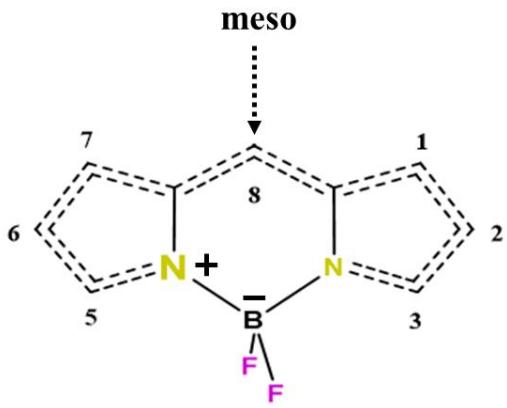

Figure 8. IUPAC labelling system for BODIPY dyes

These molecules have attracted considerable attention for their very favourable chemico-physical properties such as good thermodynamic stability, large absorption extinction coefficients in the visible region, non-dark toxicity, no dependence on environmental conditions (solvent polarity or pH), etc. [73]

Beside, thanks to these properties, the BODIPY family is widely used in several field as biological labelling, electroluminescent devices, tunable laser dyes, solid-state solar concentrators, fluorescent switches, and fluorophores in sensors.

Although the BODIPY exhibit a negligible efficiency of T1 formation due to the high fluorescence quantum yields, there are diverse strategies to enhance the mechanism of intersystem crossing and encouraging the spin–orbit coupling such as the direct incorporation of heavy atoms (i.e. Br, I) into the BODIPY core. Moreover, the substitution on the meso position, or atom number 8, with electron donors or acceptors, has been extensively studied for the reason that for the meso-modified BODIPY dyes the fluorescence can be quenched.[74]

Research currently conducted in this area is focused on the design of new PSs functionalized with classical Pt-based chemotherapeutics. These compounds are capable of carrying out a double action, because they can play both a photo-based treatment (through the dye) and a cytostatic activity (through the Pt-based chemotherapeutics, which can covalently bind DNA). The conjugation allows a different drug activity, which could

eliminate the drawbacks of classical anticancer drugs, and a better distribution of the drug in the cancer cells.

Recent literature reports the design and the synthesis of Pt-BODIPY conjugates, compounds in which the boron dipyrromethene (BODIPY) dye is functionalized with cis-$PtCl_2$ moiety.[75,76] This two-component systems show, upon radiation and at low concentration, an excellent phototoxicity and comparable toxicity with cisplatin. [75]

It is possible to conclude that to improve the effectiveness of photodynamic therapy treatments it is important to evaluate different factors such as the type of used light, the photosensitizers and their concentration, the site to be treated and its depth and finally the tumor oxygenation status. Moreover, the combination between PDT and chemotherapy should be an excellent method to develop new anticancer drugs.

References Chapter 1

(1) Rosenberg, B.; Camp, L. V.; Krigas, T. Inhibition of Cell Division in Escherichia Coli by Electrolysis Products from a Platinum Electrode. *Nature* **1965**, *205* (4972), 698–699. https://doi.org/10.1038/205698a0.

(2) Rosenberg, B. Platinum Complexes for the Treatment of Cancer: Why the Search Goes On. In *Cisplatin*; John Wiley & Sons, Ltd, 2006; pp 1–27. https://doi.org/10.1002/9783906390420.ch1.

(3) Lu, Q.-B. Molecular Reaction Mechanisms of Combination Treatments of Low-Dose Cisplatin with Radiotherapy and Photodynamic Therapy. *J. Med. Chem.* **2007**, *50* (11), 2601–2604. https://doi.org/10.1021/jm061416b.

(4) Ishida, S.; Lee, J.; Thiele, D. J.; Herskowitz, I. Uptake of the Anticancer Drug Cisplatin Mediated by the Copper Transporter Ctr1 in Yeast and Mammals. *Proceedings of the National Academy of Sciences* **2002**, *99* (22), 14298–14302. https://doi.org/10.1073/pnas.162491399.

(5) Hall, M. D.; Okabe, M.; Shen, D.-W.; Liang, X.-J.; Gottesman, M. M. The Role of Cellular Accumulation in Determining Sensitivity to Platinum-Based Chemotherapy. *Annu. Rev. Pharmacol. Toxicol.* **2008**, *48*, 495–535. https://doi.org/10.1146/annurev.pharmtox.48.080907.180426.

(6) Cisplatin : chemistry and biochemistry of a leading anticancer drug in SearchWorks catalog https://searchworks.stanford.edu/view/4264436 (accessed Sep 14, 2019).

(7) Wang, D.; Lippard, S. J. Cellular Processing of Platinum Anticancer Drugs. *Nat Rev Drug Discov* **2005**, *4* (4), 307–320. https://doi.org/10.1038/nrd1691.

(8) Guo, Z.; Sadler, P. J. Metals in Medicine. *Angew. Chem. Int. Ed. Engl.* **1999**, *38* (11), 1512–1531. https://doi.org/10.1002/(SICI)1521-3773(19990601)38:11<1512::AID-ANIE1512>3.0.CO;2-Y.

(9) Robertazzi, A.; Platts, J. A. A QM/MM Study of Cisplatin–DNA Oligonucleotides: From Simple Models to Realistic Systems. *Chemistry – A European Journal* **2006**, *12* (22), 5747–5756. https://doi.org/10.1002/chem.200501566.

(10) Jung, Y.; Lippard, S. J. Direct Cellular Responses to Platinum-Induced DNA Damage. *Chem. Rev.* **2007**, *107* (5), 1387–1407. https://doi.org/10.1021/cr068207j.

(11) Jamieson, E. R.; Lippard, S. J. Structure, Recognition, and Processing of Cisplatin-DNA Adducts. *Chem. Rev.* **1999**, *99* (9), 2467–2498.

(12) Brabec, V. DNA Modifications by Antitumor Platinum and Ruthenium Compounds: Their Recognition and Repair. *Prog. Nucleic Acid Res. Mol. Biol.* **2002**, *71*, 1–68.

(13) Siddik, Z. H. Cisplatin: Mode of Cytotoxic Action and Molecular Basis of Resistance. *Oncogene* **2003**, *22* (47), 7265–7279. https://doi.org/10.1038/sj.onc.1206933.

(14) Weiss, R. B.; Christian, M. C. New Cisplatin Analogues in Development. A Review. *Drugs* **1993**, *46* (3), 360–377. https://doi.org/10.2165/00003495-199346030-00003.
(15) Lebwohl, D.; Canetta, R. Clinical Development of Platinum Complexes in Cancer Therapy: An Historical Perspective and an Update. *European Journal of Cancer* **1998**, *34* (10), 1522–1534. https://doi.org/10.1016/S0959-8049(98)00224-X.
(16) Ota, K. [Nedaplatin]. *Gan To Kagaku Ryoho* **1996**, *23* (3), 379–387.
(17) Lobaplatin: D 19466. *Drugs R D* **2003**, *4* (6), 369–372. https://doi.org/10.2165/00126839-200304060-00008.
(18) Kim, D. K.; Kim, H. T.; Tai, J. H.; Cho, Y. B.; Kim, T. S.; Kim, K. H.; Park, J. G.; Hong, W. S. Pharmacokinetics and Antitumor Activity of a New Platinum Compound, Cis-Malonato[(4R,5R)-4,5-Bis(Aminomethyl)-2-Isopropyl-1, 3- Dioxolane]Platinum(II), as Determined by Ex Vivo Pharmacodynamics. *Cancer Chemother. Pharmacol.* **1995**, *37* (1–2), 1–6.
(19) Cleare, M. J.; Hoeschele, J. D. Studies on the Antitumor Activity of Group VIII Transition Metal Complexes. Part I. Platinum (II) Complexes. *Bioinorganic Chemistry* **1973**, *2* (3), 187–210. https://doi.org/10.1016/S0006-3061(00)80249-5.
(20) Stornetta, A.; Zimmermann, M.; Cimino, G. D.; Henderson, P. T.; Sturla, S. J. DNA Adducts from Anticancer Drugs as Candidate Predictive Markers for Precision Medicine. *Chem. Res. Toxicol.* **2017**, *30* (1), 388–409. https://doi.org/10.1021/acs.chemrestox.6b00380.
(21) Zhang, S.; Lovejoy, K. S.; Shima, J. E.; Lagpacan, L. L.; Shu, Y.; Lapuk, A.; Chen, Y.; Komori, T.; Gray, J. W.; Chen, X.; et al. Organic Cation Transporters Are Determinants of Oxaliplatin Cytotoxicity. *Cancer Res.* **2006**, *66* (17), 8847–8857. https://doi.org/10.1158/0008-5472.CAN-06-0769.
(22) Dilruba, S.; Kalayda, G. V. Platinum-Based Drugs: Past, Present and Future. *Cancer Chemother. Pharmacol.* **2016**, *77* (6), 1103–1124. https://doi.org/10.1007/s00280-016-2976-z.
(23) Pasini, A.; Zunino, F. New Cisplatin Analogues—On the Way to Better Antitumor Agents. *Angewandte Chemie International Edition in English* **1987**, *26* (7), 615–624. https://doi.org/10.1002/anie.198706151.
(24) Parish, J. H. Principles of Nucleic Acid Structure: By W Saenger. Pp 556. Springer-Verlag, New York. 1984. DM 79. ISBN 3-540-90761-0. *Biochemical Education* **1985**, *13* (2), 92–92. https://doi.org/10.1016/0307-4412(85)90046-9.
(25) Kelland, L. R.; Barnard, C. F.; Mellish, K. J.; Jones, M.; Goddard, P. M.; Valenti, M.; Bryant, A.; Murrer, B. A.; Harrap, K. R. A Novel Trans-Platinum Coordination Complex Possessing in Vitro and in Vivo Antitumor Activity. *Cancer Res.* **1994**, *54* (21), 5618–5622.
(26) Coluccia, M.; Nassi, A.; Loseto, F.; Boccarelli, A.; Mariggio, M. A.; Giordano, D.; Intini, F. P.; Caputo, P.; Natile, G. A Trans-Platinum

Complex Showing Higher Antitumor Activity than the Cis Congeners. *J. Med. Chem.* **1993**, *36* (4), 510–512. https://doi.org/10.1021/jm00056a012.

(27) Intini, F. P.; Boccarelli, A.; Francia, V. C.; Pacifico, C.; Sivo, M. F.; Natile, G.; Giordano, D.; De Rinaldis, P.; Coluccia, M. Platinum Complexes with Imino Ethers or Cyclic Ligands Mimicking Imino Ethers: Synthesis, in Vitro Antitumour Activity, and DNA Interaction Properties. *J. Biol. Inorg. Chem.* **2004**, *9* (6), 768–780. https://doi.org/10.1007/s00775-004-0572-x.

(28) Perego, P.; Caserini, C.; Gatti, L.; Carenini, N.; Romanelli, S.; Supino, R.; Colangelo, D.; Viano, I.; Leone, R.; Spinelli, S.; et al. A Novel Trinuclear Platinum Complex Overcomes Cisplatin Resistance in an Osteosarcoma Cell System. *Mol. Pharmacol.* **1999**, *55* (3), 528–534.

(29) Johnstone, T. C.; Wilson, J. J.; Lippard, S. J. Monofunctional and Higher-Valent Platinum Anticancer Agents. *Inorg. Chem.* **2013**, *52* (21), 12234–12249. https://doi.org/10.1021/ic400538c.

(30) X-ray structure and mechanism of RNA polymerase II stalled at an antineoplastic monofunctional platinum-DNA adduct | PNAS https://www.pnas.org/content/107/21/9584 (accessed Jan 30, 2020).

(31) Hall, M. D.; Hambley, T. W. Platinum(IV) Antitumour Compounds: Their Bioinorganic Chemistry. *Coordination Chemistry Reviews* **2002**, *232* (1), 49–67. https://doi.org/10.1016/S0010-8545(02)00026-7.

(32) Bhargava, A.; Vaishampayan, U. N. Satraplatin: Leading the New Generation of Oral Platinum Agents. *Expert Opinion on Investigational Drugs* **2009**, *18* (11), 1787–1797. https://doi.org/10.1517/13543780903362437.

(33) Creutz, C.; Ford, P. C.; Meyer, T. J. Henry Taube: Inorganic Chemist Extraordinaire. *Inorg. Chem.* **2006**, *45* (18), 7059–7068. https://doi.org/10.1021/ic060669s.

(34) Washko, P.; Rotrosen, D.; Levine, M. Ascorbic Acid in Human Neutrophils. *Am J Clin Nutr* **1991**, *54* (6), 1221S-1227S. https://doi.org/10.1093/ajcn/54.6.1221s.

(35) Michelet, F.; Gueguen, R.; Leroy, P.; Wellman, M.; Nicolas, A.; Siest, G. Blood and Plasma Glutathione Measured in Healthy Subjects by HPLC: Relation to Sex, Aging, Biological Variables, and Life Habits. *Clinical Chemistry* **1995**, *41* (10), 1509–1517.

(36) Jovanović, S.; Petrović, B.; Bugarčić, Ž. D.; van Eldik, R. Reduction of Some Pt(IV) Complexes with Biologically Important Sulfur-Donor Ligands. *Dalton Trans* **2013**, *42* (24), 8890–8896. https://doi.org/10.1039/c3dt50751c.

(37) Wexselblatt, E.; Gibson, D. What Do We Know about the Reduction of Pt(IV) pro-Drugs? *J. Inorg. Biochem.* **2012**, *117*, 220–229. https://doi.org/10.1016/j.jinorgbio.2012.06.013.

(38) Afrasiabi, Z.; Sinn, E.; Padhye, S.; Dutta, S.; Padhye, S.; Newton, C.; Anson, C. E.; Powell, A. K. Transition Metal Complexes of

Phenanthrenequinone Thiosemicarbazone as Potential Anticancer Agents: Synthesis, Structure, Spectroscopy, Electrochemistry and in Vitro Anticancer Activity against Human Breast Cancer Cell-Line, T47D. *J Inorg Biochem* **2003**, *95* (4), 306–314. https://doi.org/10.1016/S0162-0134(03)00131-4.

(39) Feng, J.; Garza, V. J.; Krische, M. J. Redox-Triggered C–C Coupling of Alcohols and Vinyl Epoxides: Diastereo- and Enantioselective Formation of All-Carbon Quaternary Centers via Tert-(Hydroxy)-Prenylation. *J. Am. Chem. Soc.* **2014**, *136* (25), 8911–8914. https://doi.org/10.1021/ja504625m.

(40) Dong, J.; Ren, Y.; Huo, S.; Shen, S.; Xu, J.; Tian, H.; Shi, T. Reduction of Ormaplatin and Cis-Diamminetetrachloroplatinum(IV) by Ascorbic Acid and Dominant Thiols in Human Plasma: Kinetic and Mechanistic Analyses. *Dalton Trans.* **2016**, *45* (28), 11326–11337. https://doi.org/10.1039/C6DT01804A.

(41) Sinisi, M.; Intini, F. P.; Natile, G. Dependence of the Reduction Products of Platinum(IV) Prodrugs upon the Configuration of the Substrate, Bulk of the Carrier Ligands, and Nature of the Reducing Agent. *Inorg Chem* **2012**, *51* (18), 9694–9704. https://doi.org/10.1021/ic300957v.

(42) Choi, S.; Filotto, C.; Bisanzo, M.; Delaney, S.; Lagasee, D.; Whitworth, J. L.; Jusko, A.; Li, C.; Wood, N. A.; Willingham, J.; et al. Reduction and Anticancer Activity of Platinum(IV) Complexes. *Inorg. Chem.* **1998**, *37* (10), 2500–2504. https://doi.org/10.1021/ic971047x.

(43) Gibson, D. Platinum(Iv) Anticancer Prodrugs – Hypotheses and Facts. *Dalton Transactions* **2016**, *45* (33), 12983–12991. https://doi.org/10.1039/C6DT01414C.

(44) Pathak, R. K.; Marrache, S.; Choi, J. H.; Berding, T. B.; Dhar, S. The Prodrug Platin-A: Simultaneous Release of Cisplatin and Aspirin. *Angewandte Chemie International Edition* **2014**, *53* (7), 1963–1967. https://doi.org/10.1002/anie.201308899.

(45) Dabbish, E.; Ponte, F.; Russo, N.; Sicilia, E. Antitumor Platinium(IV) Prodrugs: A Systematic Computational Exploration of Their Reduction Mechanism by l-Ascorbic Acid. *Inorg Chem* **2019**, *58* (6), 3851–3860. https://doi.org/10.1021/acs.inorgchem.8b03486.

(46) Petruzzella, E.; Sirota, R.; Solazzo, I.; Gandin, V.; Gibson, D. Triple Action Pt(IV) Derivatives of Cisplatin: A New Class of Potent Anticancer Agents That Overcome Resistance. *Chem. Sci.* **2018**, *9* (18), 4299–4307. https://doi.org/10.1039/C8SC00428E.

(47) Cheng, Q.; Shi, H.; Wang, H.; Min, Y.; Wang, J.; Liu, Y. The Ligation of Aspirin to Cisplatin Demonstrates Significant Synergistic Effects on Tumor Cells. *Chem. Commun.* **2014**, *50* (56), 7427–7430. https://doi.org/10.1039/C4CC00419A.

(48) Ponte, F.; Russo, N.; Sicilia, E. Insights from Computations on the Mechanism of Reduction by Ascorbic Acid of PtIV Prodrugs with

Asplatin and Its Chlorido and Bromido Analogues as Model Systems. *Chemistry – A European Journal* **2018**, *24* (38), 9572–9580. https://doi.org/10.1002/chem.201800488.

(49) Fu, Y.; Habtemariam, A.; Pizarro, A. M.; van Rijt, S. H.; Healey, D. J.; Cooper, P. A.; Shnyder, S. D.; Clarkson, G. J.; Sadler, P. J. Organometallic Osmium Arene Complexes with Potent Cancer Cell Cytotoxicity. *J. Med. Chem.* **2010**, *53* (22), 8192–8196. https://doi.org/10.1021/jm100560f.

(50) Fu, Y.; Habtemariam, A.; Basri, A. M. B. H.; Braddick, D.; Clarkson, G. J.; Sadler, P. J. Structure–Activity Relationships for Organometallic Osmium Arene Phenylazopyridine Complexes with Potent Anticancer Activity. *Dalton Trans.* **2011**, *40* (40), 10553–10562. https://doi.org/10.1039/C1DT10937E.

(51) Hearn, J. M.; Romero-Canelón, I.; Qamar, B.; Liu, Z.; Hands-Portman, I.; Sadler, P. J. Organometallic Iridium(III) Anticancer Complexes with New Mechanisms of Action: NCI-60 Screening, Mitochondrial Targeting, and Apoptosis. *ACS Chem. Biol.* **2013**, *8* (6), 1335–1343. https://doi.org/10.1021/cb400070a.

(52) Ude, Z.; Romero-Canelón, I.; Twamley, B.; Fitzgerald Hughes, D.; Sadler, P. J.; Marmion, C. J. A Novel Dual-Functioning Ruthenium(II)–Arene Complex of an Anti-Microbial Ciprofloxacin Derivative — Anti-Proliferative and Anti-Microbial Activity. *Journal of Inorganic Biochemistry* **2016**, *160*, 210–217. https://doi.org/10.1016/j.jinorgbio.2016.02.018.

(53) Trachootham, D.; Alexandre, J.; Huang, P. Targeting Cancer Cells by ROS-Mediated Mechanisms: A Radical Therapeutic Approach? *Nat Rev Drug Discov* **2009**, *8* (7), 579–591. https://doi.org/10.1038/nrd2803.

(54) Needham, R. J.; Sanchez-Cano, C.; Zhang, X.; Romero-Canelón, I.; Habtemariam, A.; Cooper, M. S.; Meszaros, L.; Clarkson, G. J.; Blower, P. J.; Sadler, P. J. In-Cell Activation of Organo-Osmium(II) Anticancer Complexes. *Angew Chem Int Ed Engl* **2017**, *56* (4), 1017–1020. https://doi.org/10.1002/anie.201610290.

(55) Lucas, S. J.; Lord, R. M.; Basri, A. M.; Allison, S. J.; Phillips, R. M.; Blacker, A. J.; McGowan, P. C. Increasing Anti-Cancer Activity with Longer Tether Lengths of Group 9 Cp* Complexes. *Dalton Trans.* **2016**, *45* (16), 6812–6815. https://doi.org/10.1039/C6DT00186F.

(56) Kandioller, W.; Balsano, E.; M. Meier, S.; Jungwirth, U.; Göschl, S.; Roller, A.; A. Jakupec, M.; Berger, W.; K. Keppler, B.; G. Hartinger, C. Organometallic Anticancer Complexes of Lapachol : Metal Centre-Dependent Formation of Reactive Oxygen Species and Correlation with Cytotoxicity. *Chemical Communications* **2013**, *49* (32), 3348–3350. https://doi.org/10.1039/C3CC40432C.

(57) Liu, Z.; Sadler, P. J. Organoiridium Complexes: Anticancer Agents and Catalysts. *Acc Chem Res* **2014**, *47* (4), 1174–1185. https://doi.org/10.1021/ar400266c.

(58) Kostrhunova, H.; Florian, J.; Novakova, O.; Peacock, A. F. A.; Sadler, P. J.; Brabec, V. DNA Interactions of Monofunctional Organometallic Osmium(II) Antitumor Complexes in Cell-Free Media. *J. Med. Chem.* **2008**, *51* (12), 3635–3643. https://doi.org/10.1021/jm701538w.

(59) Novohradsky, V.; Liu, Z.; Vojtiskova, M.; Sadler, P. J.; Brabec, V.; Kasparkova, J. Mechanism of Cellular Accumulation of an Iridium(III) Pentamethylcyclopentadienyl Anticancer Complex Containing a C,N-Chelating Ligand. *Metallomics* **2014**, *6* (3), 682–690. https://doi.org/10.1039/C3MT00341H.

(60) de Paula, E.; Cereda, C. M. S.; Fraceto, L. F.; de Araújo, D. R.; Franz-Montan, M.; Tofoli, G. R.; Ranali, J.; Volpato, M. C.; Groppo, F. C. Micro and Nanosystems for Delivering Local Anesthetics. *Expert Opin Drug Deliv* **2012**, *9* (12), 1505–1524. https://doi.org/10.1517/17425247.2012.738664.

(61) Redshaw, C. Coordination Chemistry of the Larger Calixarenes. *Coordination Chemistry Reviews* **2003**, *244* (1), 45–70. https://doi.org/10.1016/S0010-8545(03)00099-7.

(62) Yousaf, A.; Hamid, S. A.; Bunnori, N. M.; Ishola, A. Applications of Calixarenes in Cancer Chemotherapy: Facts and Perspectives. *Drug Des Devel Ther* **2015**, *9*, 2831–2838. https://doi.org/10.2147/DDDT.S83213.

(63) Trush, V. V.; Cherenok, S. O.; Tanchuk, V. Y.; Kukhar, V. P.; Kalchenko, V. I.; Vovk, A. I. Calix[4]Arene Methylenebisphosphonic Acids as Inhibitors of Protein Tyrosine Phosphatase 1B. *Bioorg. Med. Chem. Lett.* **2013**, *23* (20), 5619–5623. https://doi.org/10.1016/j.bmcl.2013.08.040.

(64) Guo, D.-S.; Liu, Y. Supramolecular Chemistry of P-Sulfonatocalix[n]Arenes and Its Biological Applications. *Acc. Chem. Res.* **2014**, *47* (7), 1925–1934. https://doi.org/10.1021/ar500009g.

(65) Danylyuk, O.; Suwinska, K. Solid-State Interactions of Calixarenes with Biorelevant Molecules. *Chem. Commun.* **2009**, No. 39, 5799–5813. https://doi.org/10.1039/B910331G.

(66) Perret, F.; Coleman, A. W. Biochemistry of Anionic Calix[n]Arenes. *Chem. Commun.* **2011**, *47* (26), 7303–7319. https://doi.org/10.1039/C1CC11541C.

(67) Garland, M. J.; Cassidy, C. M.; Woolfson, D.; Donnelly, R. F. Designing Photosensitizers for Photodynamic Therapy: Strategies, Challenges and Promising Developments. *Future Med Chem* **2009**, *1* (4), 667–691. https://doi.org/10.4155/fmc.09.55.

(68) Bonnett, R.; White, R. D.; Winfield, U. J.; Berenbaum, M. C. Hydroporphyrins of the Meso-Tetra(Hydroxyphenyl)Porphyrin Series as Tumour Photosensitizers. *Biochem. J.* **1989**, *261* (1), 277–280. https://doi.org/10.1042/bj2610277.

(69) Grahn, M. F.; McGuinness, A.; Benzie, R.; Boyle, R.; Jode, M. de; Dilkes, M. G.; Abbas, B. A.; Williams, N. S. Intracellular Uptake, Absorption Spectrum and Stability of the Bacteriochlorin Photosensitizer 5,10,15,20-Tetrakis(m-Hydroxyphenyl) Bacteriochlorin (MTHPBC). Comparison with 5,10,15,20-Tetrakis(m-Hydroxyphenyl) Chlorin (MTHPC); 1997. https://doi.org/10.1016/s1011-1344(96)07421-0.

(70) Houle, J.-M.; Strong, A. Clinical Pharmacokinetics of Verteporfin. *J Clin Pharmacol* **2002**, *42* (5), 547–557. https://doi.org/10.1177/00912700222011607.

(71) Sessler, J. L.; Hemmi, G.; Mody, T. D.; Murai, T.; Burrell, A.; Young, S. W. Texaphyrins: Synthesis and Applications. *Acc. Chem. Res.* **1994**, *27* (2), 43–50. https://doi.org/10.1021/ar00038a002.

(72) Byrne, A. T.; O'Connor, A. E.; Hall, M.; Murtagh, J.; O'Neill, K.; Curran, K. M.; Mongrain, K.; Rousseau, J. A.; Lecomte, R.; McGee, S.; et al. Vascular-Targeted Photodynamic Therapy with BF2-Chelated Tetraaryl-Azadipyrromethene Agents: A Multi-Modality Molecular Imaging Approach to Therapeutic Assessment. *Br J Cancer* **2009**, *101* (9), 1565–1573. https://doi.org/10.1038/sj.bjc.6605247.

(73) Yogo, T.; Urano, Y.; Ishitsuka, Y.; Maniwa, F.; Nagano, T. Highly Efficient and Photostable Photosensitizer Based on BODIPY Chromophore. *J. Am. Chem. Soc.* **2005**, *127* (35), 12162–12163. https://doi.org/10.1021/ja0528533.

(74) Gabe, Y.; Urano, Y.; Kikuchi, K.; Kojima, H.; Nagano, T. Highly Sensitive Fluorescence Probes for Nitric Oxide Based on Boron Dipyrromethene Chromophore-Rational Design of Potentially Useful Bioimaging Fluorescence Probe. *J. Am. Chem. Soc.* **2004**, *126* (10), 3357–3367. https://doi.org/10.1021/ja037944j.

(75) Liu, Y.; Li, Z.; Chen, L.; Xie, Z. Near Infrared BODIPY-Platinum Conjugates for Imaging, Photodynamic Therapy and Chemotherapy. *Dyes and Pigments* **2017**, *141*, 5–12. https://doi.org/10.1016/j.dyepig.2017.01.075.

(76) Xue, X.; Zhu, C.; Chen, H.; Bai, Y.; Shi, X.; Jiao, Y.; Chen, Z.; Miao, Y.; He, W.; Guo, Z. A New Approach to Sensitize Antitumor Monofunctional Platinum(II) Complexes via Short Time Photo-Irradiation. *Inorg Chem* **2017**, *56* (7), 3754–3762. https://doi.org/10.1021/acs.inorgchem.6b02148.

- Anticancer drugs: a brief history and new developments

2
COMPUTATIONAL METHODS

Preliminary Introduction

The quantum-mechanical study of the stationary properties of microscopic systems and their evolution over time is based on the equation of the Austrian physicist Erwin Schrödinger and from him it takes its name. The Schrödinger equation can only be solved for simple systems, while for multielectronic systems it is practically impossible to trace the energy of the system itself by solving this equation, due to its explicit dependence on the number of particles present in the system.

Based on the Heisenberg uncertainty principle, it is not possible to know exactly how a microscopic particle evolves over time because its position and moment cannot be known at the same time. For this reason, we resort to the use of a wavefunction, a function that depends on the spatial coordinates and time Ψ (r, t) [1] that contains all the information regarding the behavior of microscopic particles such as the electrons.

Given the impossibility of solving the Schrödinger equation and therefore representing the behavior of electrons with the wavefunction Ψ (r, t) in the case of polyelectronic systems, their quantum-mechanical study requires an approach that uses a function that is not directly related to the number of particles and able to describe the system itself. Starting from such premise the

theoretical method that goes under the name of *Density functional theory* (*DFT*) has been developed. DFT uses a functional detail strictly dependent on only three spatial coordinates, but independent of the whole number of particles in the system. Its rigorous physical treatment has been achieved through gradual theoretical developments starting from the first attempt carried out with the introduction of the Thomas-Fermi model, by which the energy of a multi-electronic system is evaluated without the explicit use of the wavefunction. The use of this statistical model gives the possibility to derive, for a homogeneous electron gas, a medium potential (VTF) expressible simply through the density ρ(r). However, the results obtained were based on a too coarse theoretical approximation.

The quantum mechanical DFT approach requires, for each energy contribution, a direct dependence on the density, but above all for a solid theoretical foundation, it was necessary to univocally express all the properties of a system through ρì (r) and formulate a variational principle allowing energy minimization.

The DFT method is now considered the theoretical method that most effectively approximates real multielectronic systems. In fact, the computational results, compared with those of traditional *ab initio* methods, also correlated, confirm the reliability of the method.

The Born-Oppenheimer Approximation

A quantum system can be described by *non-relativistic time-independent Schrödinger equation*. [2]

$$\hat{H}\psi = E\psi \qquad \textbf{(2.1)}$$

where $\hat{H}$ is the Hamiltonian operator for a system of nuclei and electrons described by position vectors R_A and r_i, respectively.

In atomic units, for a general N electrons and M nuclei the Hamiltonian and potential energy is:

$$\hat{H} = -\sum_{i=1}^{N}\frac{1}{2}\nabla_i^2 - \sum_{A=1}^{M}\frac{1}{2M_A}\nabla_A^2 - \sum_{i=1}^{N}\sum_{A=1}^{M}\frac{Z_A}{r_{iA}} + \sum_{i=1}^{N}\sum_{J>1}^{N}\frac{1}{r_{ij}} + \sum_{A=1}^{M}\sum_{B>A}^{M}\frac{Z_A Z_B}{R_{AB}} \qquad \textbf{(2.2)}$$

The first term in Eq. (2.2) is the operator for the kinetic energy of the electron while the second term is the operator for the kinetic energy of nuclei; the third term is the coulomb attraction between electrons and nuclei; the fourth and fifth terms are the repulsion between electrons and nuclei, respectively.

Due to the *Born-Oppenheimer* approximation, [3] in equation (2.2), the second term can be neglected, and the last term can be considered constant. The remaining terms in (2.2) compose the electronic Hamiltonian, that is the Hamiltonian describing the motion of N electrons in the field of M point charges.

$$\hat{H}_{elec} = -\sum_{i=1}^{N}\frac{1}{2}\nabla_i^2 - \sum_{i=1}^{N}\sum_{A=1}^{M}\frac{Z_A}{r_{iA}} + \sum_{i=1}^{N}\sum_{J>1}^{N}\frac{1}{r_{ij}} \qquad \textbf{(2.3)}$$

Quantum chemistry tries to find approximate solutions to the electronic Schrödinger equation, because it can be solved exactly only for one- electron systems, such as hydrogen atom or H_2^+ molecule.

The Hartree-Fock approximation

To find and to describe approximate solutions to the electronic Schrödinger equation results to be very difficult. To try to solve this problem another approximation is used, that is the Hartree-Fock (HF) approximation.[5-8] The simplest antisymmetric wave function, which can be used to describe the ground state of an N-electron system, is a single Slater determinant.

The variation principle states that the best wave function, of this functional form, is the one which gives the lowest possible energy and, in the Slater Determinant wave function, the variational flexibility is in the choice of spin orbitals.

Minimizing the energy with respect to the choice of spin orbitals lead to the HF equation, that is an eigenvalue equation of the form:

$$f(i)\psi(r_i s_i) = \varepsilon\psi(r_i s_i) \qquad \textbf{(2.4)}$$

where *f(i)* is the Fock operator that includes a one-electron contribute for the kinetic energy of ith electron and for the

coulomb attraction between the ith electron and nucleus, and two-electron contribute that measure the “field” seen by the ith electron due to the presence of the other electrons on the other spin orbitals.

Thus the Hartree-Fock equations depend on their eigenfunctions, so they are non-linear equations that must be solved iteratively, using the self-consistent-field (SCF) method. However, with the HF approach the motion of the electrons with opposite spins remains not correlated.

Electron correlation can be included explicitly with well-known extensions collectively called post-Hartree-Fock methods, [9] like *Moller-Plesset perturbation theory (MP*), the *generalized valence bond method (GVB), configuration interaction (CI), multiconfigurational self–consistent field (MCSCF) and coupled cluster theory (CC).*

These approaches improve the level of accuracy but become computationally much more demanding and thus are only suitable for relatively small systems. To handle larger systems an alternative approach has been developed.

2.1 Density Functional Theory (DFT)

Density Functional Theory (DFT) allows to deal with large molecular systems, including the electron correlation, with a

computational demanding much lower than post-HF methods. These DFT vantages are due to the use of the *electron density* $\rho(r)$ as basic variable.

$$\rho(r) = N \int \dots \int |\psi(x_1, x_2, \dots x_N)|^2 dx_1\, dx_2 \dots dx_N \qquad \textbf{(2.5)}$$

In contrast to the wave function, ψ_N, that depends on 3N variable excluding the spin variable, the electron density $\rho(r)$ depends on 3 variables only, also for many-electron systems.

In 1964, Hohenberg-Kohn introduced the existence of an unique relationship between $\rho(r)$ and all fundamental properties of a given system. [10]

The Hohenberg-Kohn theorems

The *first theorem* of *Hohenberg-Kohn*[10] affirms that every observable of a quantum mechanical system can be calculated exactly from the ground-state electron density $\rho(r)$, so every observable can be written as a functional of the ground-state electron density $\rho(r)$.

For a system defined by an external potential $v(r)$, acting on the electrons due to the nuclear charges, the energy E_v can be written as functional of the electron density.

Within the approximation of Born Oppenheimer, E_v can be splitted into three terms, which are kinetic energy T, electron-electron repulsion E_{ee} and the nuclei-electron attraction V:

$$E_v[\rho] = T[\rho] + E_{ee}[\rho] + V[\rho] = T[\rho] + E_{ee}[\rho] + \int \rho(r)v(r)dr \qquad \textbf{(2.6)}$$

Since the terms T and E_{ee} depend exclusively on the coordinates of the electrons and their forms are the same for all systems, depending only on the number of electrons, they are grouped together into the universal Hohenberg and Kohn functional $F^{HK}[\rho]$.

$$F^{HK}[\rho] = T[\rho] + E_{ee}[\rho] \qquad \textbf{(2.7)}$$

F^{HK} contains the functional for the kinetic energy $T[\rho]$ and that for the electron-electron interaction $E_{ee}[\rho]$. The explicit form of both these functionals are unknown.

However from term $E_{ee}[\rho]$ can be extracted at least, analytically, the classical part $J[\rho]$ that measures the coulomb electron-electron interaction, whereas $Vq[\rho]$ is a measure of the non-classical electronic interaction:

$$E_{ee}[\rho] = J[\rho] + Vq[\rho] = \frac{1}{2}\iint \frac{\rho[r]\rho[r']}{|r-r'|} dr\, dr' + Vq[\rho] \qquad \textbf{(2.8)}$$

The complete form of the ground state energy associated with the density $\rho(r)$, is the functional

$$E_v[\rho] = F^{HK}[\rho] + \int \rho(r)v(r)dr = T[\rho] + \frac{1}{2}\iint \frac{\rho[r]\rho[r']}{|r-r'|} dr\, dr' + Vq[\rho] + \\ + \int \rho(r)v(r)dr \quad \textbf{(2.9)}$$

The *second Hohenberg-Kohn theorem*, [10] affirms that for a trial electron density $\tilde{\rho}$(r), the energy is higher or equal to the real energy of system:

$$E_0 \leq E_v\,[\tilde{\rho}] \quad \textbf{(2.10)}$$

where E_0 is the correct energy and $E_v[\tilde{\rho}]$ is the energy, written as functional of trial electron density $\tilde{\rho}(r)$, of a system with an external potential v(r).

So, this theorem states the variational principle for the DFT theory. The applicability of the variational principle is limited to the ground state. Hence the strategy cannot be easily transferred to the problem of excited states. According to the two theorems, the energy can be known exactly when the electron density of the system is exact.

The Kohn-Sham equations

The explicit form of the functional $F^{HK}[\rho]$ is the major challenge of DFT. Since only the *J[ρ]* term is known, the main problem is to find the expression for *T[ρ]* and *Vq[ρ]*.

In 1927 Thomas and Fermi provided the first example of density functional theory. However the performance of their model had a deficiency due to the poor approximation of the kinetic energy.

To solve this problem Kohn and Sham proposed, in 1965, a new approach.[11]

They considered a reference system whit non-interacting electrons, having the same density of the real, interacting one.

For the reference system, both the kinetic energy and ground-state electron density can be written using one-electron orbital:

$$T_s[\rho] = \sum_{i=1}^{N} < \psi_i \left| -\frac{1}{2}\nabla_i^2 \right| \psi_i > \qquad \textbf{(2.11)}$$

$$\rho[r] = \sum_{i=1}^{N} \sum_s |\psi_i(r,s)|^2 \qquad \textbf{(2.12)}$$

The kinetic energy of the real system can be expressed as sum of two contributes: the kinetic energy of the reference system $T_s[\rho]$ and the kinetic energy that measures the electron correlation $T_c[\rho]$

$$T[\rho] = T_s[\rho] + T_c[\rho] \qquad \textbf{(2.13)}$$

Consequently, a new redefinition of the universal functional can be introduced:

$$F[\rho] = T_s[\rho] + J[\rho] + E_{xc}[\rho] \quad \textbf{(2.14)}$$

Where $E_{xc}[\rho]$ is the exchange and correlation functional that represents the sum of the terms having an unknown analytically form: i) the difference between the exact kinetic energy and the kinetic energy of the reference system; ii) the non-classical electron-electron interaction; iii) the self-interaction correction.

So the exchange and correlation functional can be defined as

$$E_{xc}[\rho] = (T[\rho] - T_s[\rho]) + (E_{ee}[\rho] - J[\rho]) \quad \textbf{(2.15)}$$

Including all these considerations the expression of energy for the real, interacting system is

$$E_v[\rho] = T_s[\rho] + J[\rho] + E_{xc}[\rho] + \int \rho(r)v(r)dr \quad \textbf{(2.16)}$$

The only term for which no explicit form can be given is $E_{xc.}$

Applying the variational method, imposing the wave function orthogonality condition and using the Lagrange multipliers method, the Kohn-Sham equations have been obtained:

$$-\frac{1}{2}\nabla_i^2 + v_s(r)\psi_i{}^{KS} = \varepsilon_i\psi_i{}^{KS} \quad \textbf{(2.17)}$$

Where vs is the local potential for the single particle that includes the exchange and correlation potential, v_{xc}, defined as the functional derivative of E_{xc} with respect to $\rho(r)$. So v_s depends on the density and therefore the Kohn-Sham equations have to be solved iteratively.

$$v_{xc} = \frac{\delta E_{xc}[\rho]}{\delta \rho(r)} \qquad \textbf{(2.18)}$$

Kohn-Sham equations led to a formalism that is exact and computationally accessible. The only one lack is the fact that the explicit form of the functional *Exc* is unknown. The major challenge in DFT is to find e improve approximate model for this unknown functional. Although there is no exact solution of this functional, an approximate functional have been proposed. One approach to calculate the functional *Exc* is the *Local (Spin) Density Approximation* (L(S)DA). This approach is based on assuming that the density ρ varies very slowly and locally with position and can thus be treated as a homogeneous electron gas[7]. In fact, the exchange energy of an electron gas with uniform density can be calculated exactly. Unfortunately, the L(S)DA approximation cannot be used for systems with no uniform electronic distribution. In this case, to yield accurate chemical description, *Gradient Corrected or Generalized Gradient*

Approximation (GGA) was introduced. This approximation depend not only on the density ρ, but also on the gradient Δ_{ρ}.

The development of GGA methods is based on two main lines.

The first one, also credited *Semiempirical approach* was proposed by Becke.[12-17]The basic idea is to choose a flexible mathematical functional form depending on one or more parameters extracted from molecular thermochemical data. Exchange functionals of this category are for example Becke88 (B), Perdew-Wang (PW) and modified-Perdew-Wang (MPW); [18-22]

The second set of GGA method, *Nonempirical approach, was proposed* by Perdew. This approach provides that the development of exchange- correlation functionals should depend on principles derived by quantum mechanics. Exchange functionals of this category are for example Perdew 86 (P), Perdew- Burke-Ernzerhof (PBE) and modified-Perdew-Burke-Ernzerhof (mPBE).[23-25]

GGA functionals have been shown to give more accurate predictions for thermochemistry than LSDA ones, but they still underestimate barrier heights. LSDAs and GGAs are “local” functionals because the electronic energy density at a single

spatial point depends only on the behaviour of the electronic density and kinetic energy at and near that point.[26]

Local functional can be mixed with non-local HF exchange (calculated via Kohn-Sham orbitals) leading to the hybrid functionals, that are often more accurate than local functional especially for main group thermochemistry.

One popular group of hybrid methods is Becke 3 parameter functional (*B3*), with the three empirical fitted parameters A,B and C:

$$E_{XC}^{B3} = (1 - A)E_x^{Dirac-Slater} + AE_x^{HF} + BE_x^{B88} + E_c^{VWN} + C\Delta E_C^{GGA} \quad \textbf{(2.19)}$$

LSDA exchange, $E_x^{Dirac-Slater}$, is given by the Dirac-Slater formula for a uniform electron gas, and LSA correlation energy E_c^{VWN} is the functional by Vosko, Wilk an Nusair (VWN).[27]

When ΔE_C^{GGA} gradient correction to correlation in eq. (2.19) is Lee, Yang and Parr functional (LYP),[28] the approximate functional is known as B3LYP. So A determines the extent of replacement of the Slater local exchange $E_x^{Dirac-Slater}$ by the exact HF exchange E_x^{HF}; B controls the addition of Becke's gradient-correction to the exchange functional E_x^{B88}; C defines the weight of the LYP correlation E_C^{LYP} and the VWN correlation E_c^{VWN} functionals.

In recent years, new density functionals have been developed, belonging to the M05-class and M06-class functionals (including M05, M052X, M06L, M06, M062X, M06HF).[29]

In this thesis, the B3LYP and M06L functionals are used to investigate the various reaction mechanisms.

2.2 Time-Dependent Density-Functional Theory (TD-DFT)

The fundamental ideas of DFT in the ground state are extended by means of time-dependent scheme to deal with the excitations or time-dependent phenomena in more general, so called TD-DFT. In the TD-DFT, the standard way to obtain the electron density, $\rho(r,t)$ is helped by a fictitious system with non-interacting electrons, i.e. the Kohn-Sham system. The equations for the systems are numerically simple to be solved. The scheme is general and there are two regimes as explained next. When the time dependent potential is weak, it is sufficient to resort to linear response theory and optical adsorption spectra can be calculated for instance. The spectra calculated within this framework agree with experimental results well, although the potential is approximated simply. If the TD potential is strong, full description of the Kohn Sham equations is required. The treatment of atoms or molecules in strong laser field is a

canonical example for this regime. In such case, TD-DFT can describe non-linear phenomena (e.g. high harmonic generation or multi-photon ionization).[30,31]The TD-DFT formulation is analogous derivation of the Kohn-Sham equation from the Schrödinger equation with time-independent regime, except for consideration of time-dependency.

Time Dependent Kohn-Sham Equations

The equations for a set of non-interacting electrons are described by single particle wavefunctions, $\{\phi_i(t)\}$ known as orbitals. The total electronic wavefunction in this context is taken to be a Slater determinant of the single particle orbitals as follow:

$$\psi(t) = \frac{1}{\sqrt{N!}}\begin{bmatrix} \phi_1(r_1,t) & \cdots & \phi_{1N}(r_1,t) \\ \vdots & \ddots & \vdots \\ \phi_1(r_N,t) & \cdots & \phi_N(r_N,t) \end{bmatrix}. \qquad \textbf{(2.20)}$$

Herein, the time-dependent density of the interacting system can be computed from the following equation:

$$\rho(r,t) = \sum_{i=1}^{N} \phi_i^*(r,t)\phi_i(r,t). \qquad \textbf{(2.21)}$$

The time-dependent Kohn Sham orbitals are obtained by solving the time-dependent Schrödinger equation of the non-interacting particle system shown below:

$$\left[-\frac{1}{2}\nabla^2 + v_s[\rho](r,t)\right]\phi_j(r,t) = i\frac{\partial\phi_j(r,t)}{\partial t}. \qquad \textbf{(2.22)}$$

The single particle Kohn Sham potential is given by the following formula:

$$v_s[\rho](r,t) = \int dr' \frac{\rho(r',t)}{|r-r'|} + v_{ext}(r,t) + V_{XC}. \quad \textbf{(2.23)}$$

The first and second terms represent the Coulomb and the external potentials, respectively, while the third term means the exchange-correlation potential which is approximated by the same exchange-correlation potential as in time-independent DFT. However, the time-dependent density at a particular time t is used in TD-DFT, rather than the time-independent density.

2.3 Metadynamics

To overcome the timescale problem, characteristic of many chemical reactions, a large number of enhanced sampling methods have been developed over the years. Metadynamics is one of such techniques, which allows to accelerate processes characterized by timescale problems and to reconstruct the free energy profile by adding a history-dependent potential, function of selected Collective Variables (CV).

In metadynamics, the external history-dependent bias potential can be written as a sum of Gaussians deposited in the CVs space

and it encourages the system under investigation to explore several configurations and different reaction pathways.

The metadynamics bias potential, at time t, can be written as:

$$V_G(S,t) = \int_0^t dt' \omega \, exp\left(- \sum_{i=1}^{d} \frac{\left(S_i(R) - S_i\left(R(t')\right)\right)^2}{2\sigma_i^2} \right) \quad \textbf{(2.24)}$$

Where S is a set of d functions of the miscoscopic coordinates R of the system, ω is an energy rate and σi is the Gaussian width. The energy rate is constant and depends on a Gaussian height W and a deposition stride τG according to the equation 2.25

$$\omega = \frac{W}{\tau \mathrm{G}} \quad \textbf{(2.25)}$$

The effect of V_G on the evolution of the system can be understood by considerying the simple case of the one-dimensional potential of Figure 1, in which three local minima A, B and C are present.

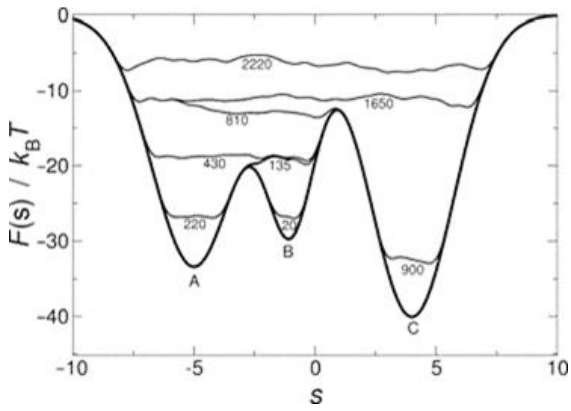

Figure 1. Example of metadynamics simulation in a one dimensional potential.

During the metadynamics simulation, the relative filling of the basins occurs until the thermodynamic bias is overcome in the whole (or a large region of) phase space. When this is accomplished, the system will visit all regions of phase space with equal probability and the biasing potential will approximately flatten the original profile $F(s)$, such that

$$V_G(S, t \rightarrow \infty) = -F(S) \qquad \textbf{(2.26)}$$

Nevertheless, Metadynamics presents two main problems:

VG, in a single run, does not converge modulo a constant to the free energy, but oscillates around it, causing the overfilling the underlying FES, pushing the system toward high energy regions of the CVs space. Moreover, it is not trivial to decide when to

stop a simulation and to choose proper collective variables for describing the processes.

The first problem can be solved by Well-tempered metadynamics

Well-tempered metadynamics

In well-tempered metadynamics, the external bias potential becomes smaller as the metadynamics simulation progresses. In this case the bias potential can be expressed as:

$$V_G(S,t) = K_B\,\Delta T\; ln\left(1 + \frac{\omega N(S,t)}{kb\;\Delta T}\right) \qquad \textbf{(2.27)}$$

In this case $\dot{V}(S, t)$ is the time derivative of the bias potential, N(S, t) is the histogram of the S variables collected during the simulation, and ΔT an input parameter with the dimension of a temperature. Respect to the standard metadynamics, the bias potential .

The bias potential, for a long time of analysis, converges to a value proportional to the F(s), free-energy surface, according to the formula:

$$V(s) = -\left(1 - \frac{1}{\gamma}\right) F(s) \qquad \textbf{(2.28)}$$

Where γ is the bias factor and (***s***) is the free energy associated to the CV**s.**

If the simulation has been properly carried out it is,thus, possible to obtain the FES of the studied reaction according to the chosen collective variable

Harmonic linear discriminant analysis

In order to select a proper set of CVs, some requirements must be fulfilled. The different metastable states have to be distinguished by the order parameters, the most relevant system slow modes have to be included and the CV number has to be limited. Thus, to reduce the complexity of the problem some outlines have been proposed in a new approach based on Fisher's Linear Discriminant Analysis (LDA), named Harmonic Linear Discriminant Analysis (HLDA).[32]

Here has been reported its simplest form.

It is assumed that there are two separated states identified by *Nd* descriptors (***R***), function of the microscopic atomic coordinates *R* and arranged to form a vector (***R***). It is assumed that the average values in the two basins (μA and μB) are different and there is no overlap between the two states in the *Nd* space. The (***R***)'s

fluctuation in the two states are given by the covariance matrices, indicated as Σ*A* and Σ*B*.

The idea of HLDA is to find the direction along which the projected data of the two metastables states is best separated. This is obtained by maximizing the ratio of the between-class variation $\boldsymbol{SB=(\mu A-\mu B)(\mu A-\mu B)^{T}}$ and the within-class variance calculated by a harmonic average $\boldsymbol{SW=\Sigma A\Sigma B/(\Sigma A+\Sigma B)}$, which leads to the function:

$$J(W) = \frac{W^{T}SBW}{W^{T}SWW} \qquad \textbf{(2.29)}$$

maximized by $$W = (\mu_A - \mu_B)\left(\frac{1}{\sum A} + \frac{1}{\sum B}\right) \qquad \textbf{(2.30)}$$

So, the CV based on HLDA is

$$s^{H}(R) = W^{T}d(R) = (\mu_A - \mu_B)^{T}\left(\frac{1}{\sum A} + \frac{1}{\sum B}\right) d(\mathbf{R}) \qquad \textbf{(2.31)}$$

For process that involve several metastable states, an extension of HLDA has named multi-class HLDA (MC-HLDA been proposed). [33]

It is assumed that there are c classes, the between-class variance matrix in this case isexpressed as:

$$S_B = \sum_{i=1}^{c}(\mu i - \mu)(\mu i - \mu)T, \qquad \textbf{(2.32)}$$

where $\mu = \frac{1}{c}\sum_{i=1}^{c}\mu i$ and the within-class variance matrix is expressed as

$$SW = \frac{1}{\left(\frac{1}{\Sigma 1}\right)+\left(\frac{1}{\Sigma 2}\right)+\cdots+\left(\frac{1}{\Sigma c}\right)} \quad (2.33)$$

The projection matrix $\mathbf{K} = [\boldsymbol{W1}|\boldsymbol{W2}|\ldots|\boldsymbol{Wc}]$ that maximizes the ratio $J(W) = \frac{K^T S_B K}{K^T S_W K}$ is the one whose columns are the eigenvectors corresponding to the generalized eigenvalue problem:

$$(\boldsymbol{S_B} - \lambda_i \boldsymbol{S_W})\boldsymbol{W_i} = 0. \quad (2.34)$$

Now, the optimized CVs are given by

$$s(\boldsymbol{R}) = \boldsymbol{W_i}^T \boldsymbol{d}(\boldsymbol{R}) \quad (2.35)$$

Notice that, because $\boldsymbol{S_B}$ is of rank (c-1) or less, there will be at most c-1 eigenvectors with non-zero eigenvalues λi.

References Chapter 2

(1) Green, N. J. B., *Quantum Mechanics 1: Foundations*,Oxford University,**1997**, page 6.
(2) Schrödinger, E., *Ann. Physik.*, **1926**, 79, 361.
(3) Born, M., Oppenheimer, J. *Ann. Physik.*, **1927**, 84, 457.
(4) Pauli, W. *Z., Physik.* **1925**, 31, 765.
(5) Szabo, A., Ostlund, N. S., *Modern Quantum Chemistry*, Dover Publication: New York, **1989**.
(6) Hartree, D., *Proc. Cambridge Phil. Soc*., **1928**, 24, 89.
(7) Hartree, D., *Proc. Cambridge Phil. Soc.*,**1928**, 24, 111.
(8) Hartree, D., *Proc. Cambridge Phil. Soc*., **1928**, 24, 426.
(9) Fock, V. Z., *Physik.*, **1930**, 61, 126.
(10) Bartlett, R. J., Stanton, J., *In Reviews in Computational Chemistry*; Lipkowitz, K. B., Boyd, D.B.: Eds., VCH Publishers: New York, **1994**, Vol.V.
(11) Hohenberg, P., Kohn, W., *Phys. Rev. B*, **1964**, 136, 864.
(12) Kohn, W., Sham, L., *J. Phys. Rev. A* **1965**, 136, 1133.
(13) Becke, A. D., *J. Chem. Phys.* **1986**, 84, 4524.
(14) Becke, A. D., *J. Chem. Phys.* **1992**, 96, 2155.
(15) Becke, A. D., *J. Chem. Phys.* **1992**, 97, 9173.
(16) Becke, A. D., *J. Chem. Phys.* **1993**, 98, 5648.
(17) Becke, A. D., *J. Chem. Phys.* **1996**, 104, 1040.
(18) Becke, A. D., *J. Chem. Phys.* **1997**, 107, 8544.
(19) Becke, A. D., *Phys. ReV. A*, **1988**, 38, 3098.
(20) Perdew, J. P., Wang, Y., *Phys. ReV. B*, **1986**, 33, 8800.
(21) Adamo, C., Barone, V., *J. Chem. Phys.*, **1998**, 108, 664.
(22) Handy, N. C., Cohen, A., *J. Mol. Phys.*, **2001**, 99, 403.
(23) Xu, X., Goddard, W. A., III. *Proc. Natl. Acad. Sci.* U.S.A.,**2004**, 101, 2673.
(24) Perdew, J. P., *Phys. ReV. B*, **1986**, 33, 8822.
(25) Perdew, J. P., Burke, K., Ernzerhof, M., *Phys. ReV. Lett.*, **1996**, 77, 3865.
(26) Adamo, C., Barone, V., *J. Chem. Phys.*, **2002**, 116, 5933.
(27) a) van Leeuwen, R., Baerends, E.J., *Phys. Rev. A*, **1994**, 49, 2421;
b) Becke, A. D., *J. Chem. Phys.*, **1998**, 109, 2092;
c) Mori-Sanchez, P., Cohen, A. J., Yang, W., *J. Chem. Phys*., **2006**, 124, 91102/1.
(28) Vosko, S. H.,Wilk, L., Nusair, M., *Can. J. Phys*. **1980**, 58, 1200.
(29) Lee, C., Yang, W., Parr, R.G., *Phys. Rev. B* **1988**, 37, 785.
(30) Koch, W.; Holthausen, M. C. A Chemist's Guide to Density Functional Theory, 2nd Edition, WILEY-VCH Verlag GmbH: Weinheim, **2001**.

(31) Hohenberg, P.; Kohn, W, *Phys. Rev.* **1964**, *136*, B864-B871.
(32) Mendels, D., Piccini, G., Parrinello, M *J. Phys, Chem. Lett.*, **2018**, *9*, 2776−2781.
(33) Piccini, G.; Mendels, D.; Parrinello, M., *J. Chem. Theory Comput.*, **2018**, *14 (10)*, 5040–5044.

3

PLATINUM (IV) PRODRUGS: NEW STRATEGIES FOR ENHANCING THE EFFICACY

Platinum (IV) Prodrugs: new strategies for enhancing the efficacy

Introduction

Pt(IV) complexes are an emerging novel class of anticancer drugs.

They can act as pro-drugs, which are activated inside the cells by reducing agents such as L-glutathione or L-ascorbic acid and can release, by various mechanisms, the active square-planar Pt(II) species and the ligands in axial position. In addition to their increased kinetic stability, the further advantage of the use of Pt(IV) prodrugs is the possibility to choose the axial ligands properly tuning their pharmacokinetic properties.

The reduction mechanism of these complexes, that involves a two electrons transfer, is still under investigation and it is matter of debate whether activation by reduction occurs following an inner-sphere mechanism (the formation of a chemical bridge between the ligand and the reducing agent is required) or outer-sphere mechanism (this mechanism does not require the formation of covalent bond and the electron transfer occurs from the reaction environment to the oxidizing species).

The information concerning the activation by reduction is usually obtained by cyclic voltammetry that allows to measure the reduction potential, but not the standard redox one because the platinum(IV)-to-platinum(II) reduction is irreversible. Baik and co-workers, thanks to a series of electrochemical experiments, have proposed a decomposition scheme able to give reliable

results for solution-phase redox processes, which allows separating the chemical events from the electrochemical events.

To understand which is the reduction mechanism followed by the platinum (IV) complexes, it is important to take into consideration the ligand bridging ability as, generally, the inner-sphere mechanism is more favored as the ligand bridging ability increases. Such ability leads to a lowering of the activation energy barriers and therefore an increase in the reduction rate. Viceversa, if bridging ability is low, the electron transfer by outer-sphere mechanism should prevail. Therefore, for the development of new platinum-based anticancer drugs, the knowledge of the Pt(IV) activation mechanism is crucial.

In the design of new Pt(IV) prodrugs, the species mainly used as axial ligands are chlorido, bromido, hydroxido and acetato groups, in connection with the role they should play as bridges, *trans* leaving species and proton acceptors.[1] In addition, a promising strategy, involves the incorporation of the axial ligands which can be biologically active and able to enhance the potential of the Pt(IV) drug through synergistic effects with classical platinum therapy.

Recently, a new cisplatin-based complex named Asplatin, a Pt(IV) prodrug with aspirin and hydroxido ligands in axial position, has been synthesized. [2,3] Asplatin, upon reduction by ascorbic acid, releases both cisplatin, which binds to DNA and

triggers cell apoptosis, and aspirin, a widely used anti-inflammatory drug that enhances the drug efficacy of the platinum complex and could modulate the apoptosis of cancer cells thanks to its newly discovered antineoplastic action.

Aim of the work

With the aim to identify the correct activation mechanism, a detailed computational investigation of the mechanism of reduction of some Pt(IV) prodrugs has been carried out. In particular, the study of the reduction mechanism of Asplatin and other Asplatin derivatives in presence of L-ascorbic acid as reducing agent has been carried out by means of Density Functional Theory (DFT). Moreover, the reduction potentials for all the examined complexes have been quantum-mechanically calculated (**Paper 1**)

After a detailed quantum-mechanical DFT study on Asplatin complex, the metadynamics sampling technique, which allows exploring the different paths of reduction and tracing the relative free energy surface, and a new method named Multi Class Harmonic Linear Discriminant Analysis (MC-HLDA) have been applied to investigate the reduction process of this complex. (**Paper 2**)

Furthermore, the reduction processes, in presence of ascorbate as a model reducing agent, and the reduction potentials of a set of platinum(IV) anticancer drugs have been computationally

explored by using DFT. The reduction process details have been examined as a function of the identity of both axial and equatorial ligands. (**Paper 3**)

Finally, for two sampled Pt(IV) complexes, DFT calculations have been performed to outline the free energy profiles for the gas-phase fragmentation pattern. (**Paper 4**)

3.1 Insights from Computations on the Mechanism of Reduction by Ascorbic Acid of Pt(IV) Prodrugs with Asplatin and Its Chlorido and Bromido Analogues as Model Systems

Here the outcomes of a DFT computational exploration of the possible pathways leading to the reduction by L-ascorbic acid of the "dual action" Asplatin Pt(IV) complex, *c,c,t*-[$PtCl_2(NH_3)_2(OH)$(aspirin)], have been reported.

In addition, the same reduction mechanisms have been explored for Asplatin analogues obtained by replacing the OH^- axial ligand with Cl^- and Br^- to assess the assumption that better bridging ligands (OH <Cl <Br) [2–4] should favour bridge formation and, therefore, the reduction of the complex (Scheme 1).

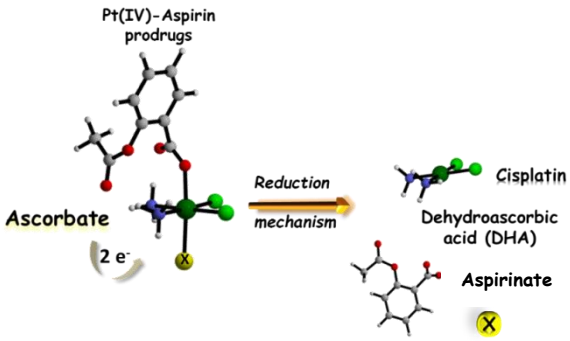

Scheme 1**.** Reduction Mechanism of Pt(IV)-Aspirin prodrugs by Ascorbate

Here, both the viable alternatives, that is inner- and outer-sphere mechanisms have been theoretically studied. In particular, for the first mechanism, where the electron transfer takes place through a bridging ligand, several mechanistic hypotheses have been considered.

- Platinum (IV) Prodrugs: new strategies for enhancing the efficacy

1) X-bridged electron transfer
2) Nucleophilic attack of the enolate β-carbon of the ascorbate on X-group
3) Pt(II) complex catalytic action

Our calculations show that the most favourable mechanism for Asplatin complex is the inner sphere "OH-bridged electron transfer" that required the formation of a bridge between the OH ligand and the reducing agent. For this mechanism, the energy barrier is the lowest than the energy barriers calculated for Asplatin analogues. These outcomes are in apparent disagreement with the bridging ability trend reported above.

The obtained results can be justified based on the fact the OH axial group can play two roles: acting as bridge and directly participating in the process leading to the formation of DHA, the oxidized form of ascorbic acid. Moreover, from the calculations of the standard reduction potentials it is clear that, in case an outer-sphere mechanism is assumed to be operative, the tendency towards the reduction increases in going from Asplatin to Asplatin-Cl to Asplatin-Br. Such trend respects the assumption known in the literature but does not reflect the trend in the rate of reduction by an inner-sphere mechanism.

From this study it is possible to infer how there is not a close correlation between the reduction rates and the reduction potentials.

3.2 A metadynamics perspective of the reduction mechanism of the Pt(IV) Asplatin prodrug

A detailed reduction study of Asplatin Pt(IV) complex has been, previously performed using functional density theory (DFT),[5] and in order to obtain further information about the activation key step of the complex, the metadynamics sampling technique has been applied. The adopted method allows simulating the different reduction pathways of the complex, giving information about the mechanism, and outlining the relative free energy surface.

In order to ensure the correct application of Metadynamics and then get successful simulations, it is required the selection of adequate degrees of freedom (collective variables, CVs).

To achieve such a goal, here, the new method named Multi Class Harmonic Linear Discriminant Analysis (MC-HLDA) has been used to build two one-dimensional collective variables (s_1^{HLDA} and s_2^{HLDA}).

The free energy surface reconstructed by metadynamics, as a function of two collective variables s_1 and s_2, shows the presence of 3 well separated minima related to the three metastable states (**React**, **Prod$_{red1}$** and **Prod$_{red2}$)**, as shown Figure 1**,** and the reduction mechanism which involves the formation of cisplatin and dehydroascorbic acid is the minimum energy path, in good agreement with the theoretical data obtained in static simulations.

In conclusion, the method can be successfully adopted for the study of complex redox reactions that involve several reaction pathways by properly choosing collective variables.

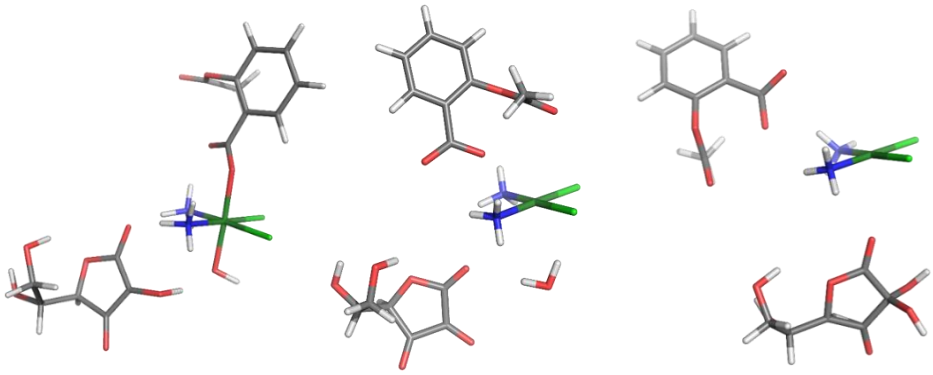

Figure 1. Structures of the React, $Prod_{red1}$ and $Prod_{red2}$

3.3 Antitumor Pt(IV) prodrugs: a systematic computational exploration of their reduction mechanism by L-ascorbic acid

Here have been reported the outcomes of a systematic computational analysis of the mechanism of activation, of different platinum complexes, with the aim of clarifying the mechanism of reduction, to establish the role played by the axial and equatorial ligands (both cisplatin and oxaliplatin complexes have been considered) and to advance conclusions about their activation and efficiency.

All the investigated system are reported in Scheme 2.

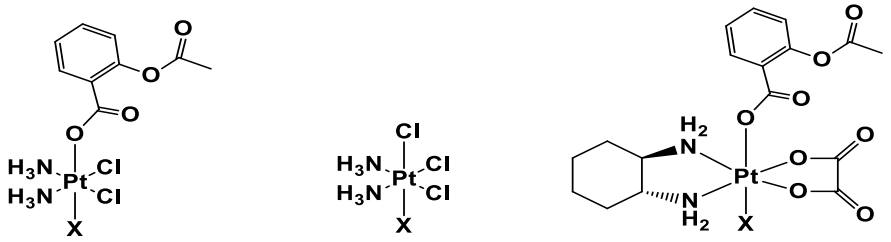

1 : X = OH
2 : X = Cl
3 : X = Br
4 : X = OAc

5 : X = OH
6 : X = Cl
7 : X = Br
8 : X = OAc

9 : X = OH
10 : X = Cl

Scheme 2. Pt(IV) complexes investigated for reduction

For some of the investigated complexes, the inner sphere mechanism seems to be the preferred mode of reduction because the reduction by ascorbate occurs overcoming very low energy barriers. Their ability to favour bridge formation lowers the energy barrier and increases the reduction rate. Moreover, the steric hindrance plays an important role for this mechanism.

Also the outer-sphere mechanism, following the procedure proposed by Baik and co-worker, has been explored. [6] The standard reduction potentials have been calculated for all the Pt(IV) complexes and such values indicate that if an outer-sphere mechanism is assumed to be operative the probability with which the redox reaction occurs depends principally on the nature of axial ligands and increases in the order: OH<OAc<Cl<Br and the rate of the reduction decreases in going from cisplatin derivatives to oxaliplatin ones.

For the complex with two chlorido ligands in axial position the mechanism named “base assisted outer-sphere” has been explored in detail. A two steps outer-sphere electron transfer leads the formation of metastable six-coordinate Pt(III) intermediate,[6] and it has been demonstrated to involve intersystem singlet-triplet crossings (the mechanism will be called as base-assisted outer sphere). This mechanism can become competitive with respect to the inner one.

It is possible to conclude that the tendency of Pt(IV) prodrugs toward the reduction can be properly modulated. Moreover, the obtained data show that when the activation by reduction for some of the investigated complexes of platinum(IV) is too fast, they can hardly reach the target before reduction and the reduction takes place extracellularly.

3.4 Elusive Intermediates in the Breakdown Reactivity Patterns of Prodrug Platinum(IV) Complexes

Since many years, the design of new drugs with improved pharmacokinetic properties is a challenge.

Literature data indicate that the properties of a Pt(IV) complex can be modulated by the nature of the ligand in both axial and equatorial positions.

Platinum (IV) Prodrugs: new strategies for enhancing the efficacy

For this reason, for a series of platinum Pt(IV) prodrugs with different ligands, the possible paths for the transformation that lead to Pt(II) species have been explored, employing mass spectrometric technique utilizing electrospray ionization (ESI-MS) in negative (deprotonated and negative ions) mode.

In particular, the technique that provides information about the ligand binding energies is the collision induced dissociation (CID), a mechanism of fragmentation of ions in the gas phase.

The fragmentation analysis of negative ions prove the presence of Pt(III) intermediates,[7,8] that are quite elusive in solution.

On the other hand, as ESI-MS studies are carried out on ionic species isolated in gas phase there is not direct connection with reaction dynamics in solution.

Here, the outcomes of a detailed ESI-MS study have been reported on a set of Pt(IV) complexes cisplatin and carboplatin based. In particular, DFT calculations have been employed to outline the free energy profile for the gas-phase fragmentation pattern of two sampled Pt(IV) complexes based on cisplatin and deprotonated on ammine ligand.(Figure 2)

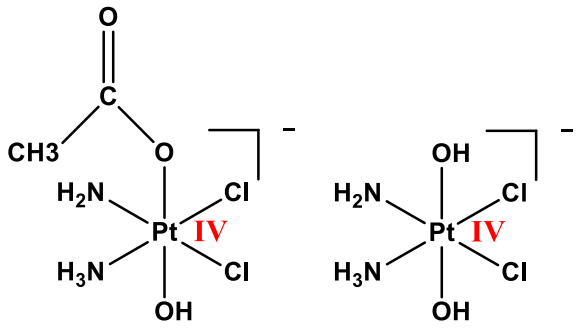

Figure 2. Chemical structure of the sampled Pt(IV) compounds theoretically studied.

The theoretical study of the free energy profiles of the presented complexes provide excellent support to the data obtained from CID experiments.

In particular, the formation of Pt(III) intermediates (isolated and characterized) has also been verified by DFT calculations. Moreover, during the reduction processes towards CID, the fragmentation paths show that complexes may have the possibility to lose both axial and equatorial ligands, confirmed also theoretically.

References Chapter 3

(1) Gramatica, P.; Papa, E.; Luini, M.; Monti, E.; Gariboldi, M. B.; Ravera, M.; Gabano, E.; Gaviglio, L.; Osella, D. Antiproliferative Pt(IV) Complexes: Synthesis, Biological Activity, and Quantitative Structure–Activity Relationship Modeling. *JBIC J. Biol. Inorg. Chem.* **2010**, *15* (7), 1157–1169. https://doi.org/10.1007/s00775-010-0676-4.

(2) Pathak, R. K.; Marrache, S.; Choi, J. H.; Berding, T. B.; Dhar, S. The Prodrug Platin-A: Simultaneous Release of Cisplatin and Aspirin. *Angew. Chem. Int. Ed.* **2014**, *53* (7), 1963–1967. https://doi.org/10.1002/anie.201308899.

(3) Cheng, Q.; Shi, H.; Wang, H.; Min, Y.; Wang, J.; Liu, Y. The Ligation of Aspirin to Cisplatin Demonstrates Significant Synergistic Effects on Tumor Cells. *Chem. Commun.* **2014**, *50* (56), 7427–7430. https://doi.org/10.1039/C4CC00419A.

(4) Lemma, K.; House, D. A.; Retta, N.; Elding, L. I. Kinetics and Mechanism for Reduction of Halo- and Haloam(m)Ine Platinum(IV) Complexes by l-Ascorbate. *Inorganica Chim. Acta* **2002**, *331* (1), 98–108. https://doi.org/10.1016/S0020-1693(01)00762-9.

(5) Ponte, F.; Russo, N.; Sicilia, E. Insights from Computations on the Mechanism of Reduction by Ascorbic Acid of PtIV Prodrugs with Asplatin and Its Chlorido and Bromido Analogues as Model Systems. *Chem. – Eur. J.* **2018**, *24* (38), 9572–9580. https://doi.org/10.1002/chem.201800488.

(6) McCormick, M. C.; Keijzer, K.; Polavarapu, A.; Schultz, F. A.; Baik, M.-H. Understanding Intrinsically Irreversible, Non-Nernstian, Two-Electron Redox Processes: A Combined Experimental and Computational Study of the Electrochemical Activation of Platinum(IV) Antitumor Prodrugs. *J. Am. Chem. Soc.* **2014**, *136* (25), 8992–9000. https://doi.org/10.1021/ja5029765.

(7) Ojha, R.; Boas, J. F.; Deacon, G. B.; Junk, P. C.; Bond, A. M. EPR Spectroscopic Characterization of a Monomeric PtIII Species Produced via Electrochemical Oxidation of the Anticancer Compound Trans-[PtII{(p-HC6F4)NCH2CH2NEt2}Cl(Py)]. *J. Inorg. Biochem.* **2016**, *162*, 194–200. https://doi.org/10.1016/j.jinorgbio.2016.01.015.

(8) Rivada-Wheelaghan, O.; Ortuño, M. A.; García-Garrido, S. E.; Díez, J.; Alonso, P. J.; Lledós, A.; Conejero, S. A Stable, Mononuclear, Cationic Pt(III) Complex Stabilised by Bulky N-Heterocyclic Carbenes. *Chem. Commun.* **2014**, *50* (11), 1299–1301. https://doi.org/10.1039/C3CC48553F.

- Platinum (IV) Prodrugs: new strategies for enhancing the efficacy

ChemPubSoc Europe

DOI: 10.1002/chem.201800488

CHEMISTRY
A European Journal
Full Paper

Drug Development

Insights from Computations on the Mechanism of Reduction by Ascorbic Acid of Pt^{IV} Prodrugs with Asplatin and Its Chlorido and Bromido Analogues as Model Systems

Fortuna Ponte, Nino Russo, and Emilia Sicilia*[a]

Abstract: The elucidation of the mechanism by which the reduction of coordinatively saturated Pt^{IV} prodrugs occurs, leading to the release of the two axial ligands, is of foremost importance, being the key step for the activation of these anticancer compounds, and addressing their synthetic strategies. A systematic DFT computational analysis of the reduction process by small biomolecules, which is supposed to occur by inner- or outer-sphere electron-transfer mechanisms, has been undertaken using the recently synthesised Asplatin Pt^{IV} complex, *c,c,t*-[$PtCl_2(NH_3)_2(OH)$(aspirin)], as model system and L-ascorbic acid as reducing agent. Further calculations have been carried out on Asplatin analogues that should be obtained replacing the OH^- ligand with Cl^- and Br^-. The most accredited inner-sphere mechanistic suggestions have been explored and a recently proposed computational methodology has been applied to estimate the corresponding standard redox potentials, which cannot be directly obtained from voltammetric experiments due to the irreversibility of the platinum(IV)-to-platinum(II) reduction process.

Introduction

The Pt drug that dominates medical oncology therapies cisplatin (*cis*-diamminedichloridoplatinum(II), $PtCl_2(NH_3)_2$), was synthesised by the Italian scientist Peyrone in 1845, but its anticancer properties were fortuitously discovered by Rosenberg 120 years later (1965).[1] Since then, cisplatin and platinum-based antitumor drugs, the use of which have been approved in medical protocols, continue to play a central role in the treatment of various types of cancer.[2] Despite the enormous success of cisplatin and related Pt^{II} complexes, severe toxic side effects together with acquired or intrinsic drug resistance have limited their use.[3] One promising alternative for decreasing side effects is to use much more inert low-spin d^6 Pt^{IV} octahedral complexes that, being coordinatively saturated, are more resistant to ligand substitution with respect to their Pt^{II} congeners.[4] Therefore, given that interactions of the prodrug and its degradation before arriving at the desired target are limited, unwanted side reactions and corresponding side effects are reduced. In addition, the two axial ligands can be chosen on the basis of tuneable properties such as increased cellular uptake, improved tumour cell targeting or enhanced cytotoxicity due to the incorporation of biologically active ligands, which may have synergistic effects with platinum therapy. Activation of Pt^{IV} prodrugs occurs inside the target cell where they are reduced, releasing the axial ligands and affording the active, four-coordinate, square-planar Pt^{II} analogues.[5] The reduction/activation step of the Pt^{IV} prodrugs is, therefore, of crucial importance in the mechanism of action of these compounds. Reduction can occur too rapidly, before the prodrug reaches the tumour, or too slowly if the prodrug resists the reductive nature of the reducing agents.[5d,6] Although there are many potential reducing agents in cells, L-ascorbic acid ($AscH_2$) and L-glutathione, which are present both in plasma and cells, are commonly believed to be the biological species responsible for the activation of Pt^{IV} prodrugs by reduction.[6a,7,8] Several mechanistic hypotheses have been formulated for the reductive elimination of axial ligands, and different mechanisms should be expected to be operative due to differences, for instance, in the nature of the involved substrate complexes. Thus, the mechanisms for the two-electron transfer have been classified as outer- and inner-sphere.[5d,7] In the latter case it is assumed that one of the axial ligands is able to form a bridge between the Pt^{IV} centre and the reductant, facilitating the electron-transfer process. The inner-sphere mechanism has also been suggested to involve the Pt^{II} complex catalytic action.[9] This latter mechanism, involving bridged Pt^{II}–Pt^{IV} dimers seems unlikely under cellular Pt^{II} complex concentrations. The most investigated axial ligands have been chlorides, hydroxides and carboxylates, but the data concerning both the mechanism and the ease of release is very controversial and a matter of debate.[5d,e,6a,8a–c] The information concerning the activation by reduction is usually obtained by cyclic voltammetry, which allows the reduction potential to be measured, but not the standard redox one because the platinum(IV)-to-platinum(II) reduction is irreversible. The standard

[a] F. Ponte, Prof. N. Russo, Prof. Dr. E. Sicilia
Department of Chemistry and Chemical Technologies
Università della Calabria
Ponte P. Bucci Cubo 14c, 87035 Arcavacata di Rende (CS) (Italy)
E-mail: emilia.sicilia@unical.it

Supporting information and the ORCID identification number(s) for the author(s) of this article can be found under: https://doi.org/10.1002/chem.201800488.

redox potential cannot be obtained as the midpoint potential from a typical cyclic voltammogram, and the peak potential for the cathodic wave obtained in cyclic voltammetric measurements is usually exploited. Some caution must be taken, however, because, besides the intrinsic irreversibility, the process involves two electrons and can be significantly influenced by the nature of the axial ligands and the ease with which they are released.[6b,10] Contrary to what would be expected, very often reduction potentials, measured by cyclic voltammetry, do not correlate with the reduction rate of Pt^{IV} complexes.[8b,11]

With the aim of contributing to the identification of the correct mechanism of this decisive step for the activation of Pt^{IV} prodrugs, in this study we have examined several mechanistic hypotheses using the recently proposed Asplatin[12] Pt^{IV} complex as prodrug model and L-ascorbic acid as reducing agent. Asplatin (or platin-A) is a novel Pt^{IV} prodrug of cisplatin, that is *c,c,t*-$[PtCl_2(NH_3)_2(OH)(aspirin)]$ (see Scheme 1), synthesised by tethering aspirin to oxoplatin and it is designed to release cisplatin and aspirin to modulate the apoptotic process and enhance the action of cisplatin.

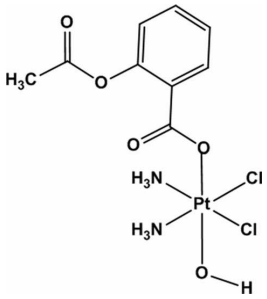

Scheme 1. The structure of Asplatin.

In addition, the same reduction mechanisms have been explored for Asplatin analogues that should be obtained by substituting the OH^- group with either Cl^- or Br^- to assess the assumption that better bridging ligands ($OH^- < Cl^- < Br^-$)[7b,12] should favour bridge formation, lowering the energy barrier and increasing the reduction rate. Finally, by following an approach recently proposed in the literature,[13] the reduction potentials for all the examined complexes have been quantum-mechanically calculated by using DFT.

Results and Discussion

Inner-sphere electron-transfer reduction of Asplatin investigations

The outcomes of our computational analysis of the inner-sphere reduction steps leading to the release of axial ligands in Asplatin (Asp) prodrug assisted by ascorbic acid are reported in Figures 1, 2 and 3 for all the explored mechanistic alternatives. A sketch of the stationary point structures is reported in the same figures, whereas complete Cartesian coordinate sets

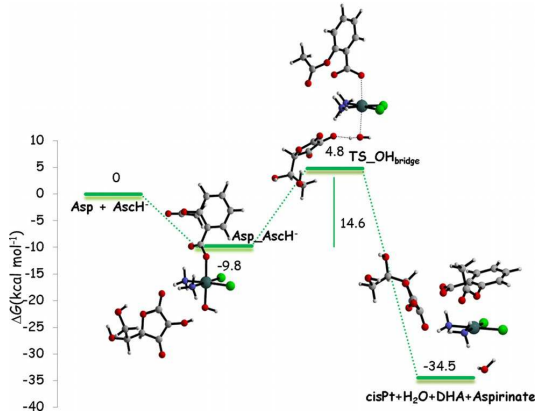

Figure 1. Calculated B3LYP-D3 free energy profile in water describing the OH-bridged electron transfer mechanism (a) for the Asplatin reduction by ascorbate. Energies are in kcal mol^{-1} and relative to separated reactants.

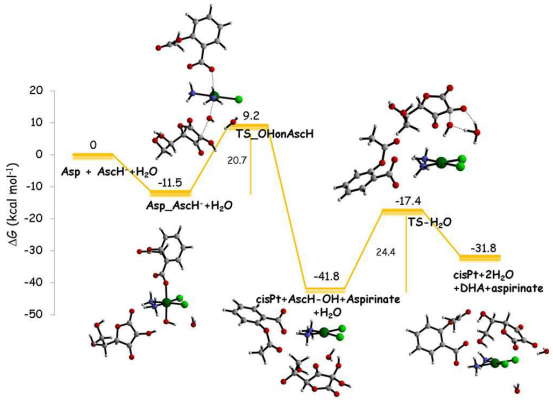

Figure 2. Calculated B3LYP-D3 free energy profile in water describing the enolate β-carbon attack on the axial OH- ligand mechanism (b) for the Asplatin reduction by ascorbate. Energies are in kcal mol^{-1} and relative to separated reactants.

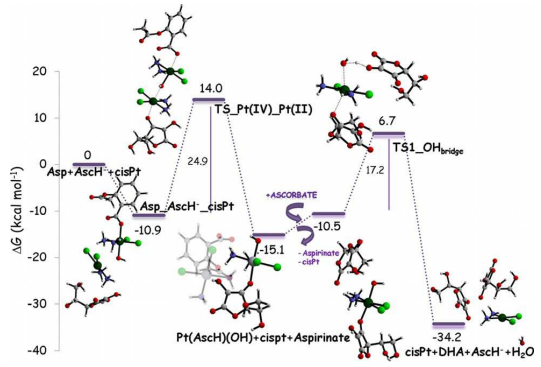

Figure 3. Calculated B3LYP-D3 free energy profile in water describing the Pt^{II}-assisted mechanism (c) for the Asplatin reduction by ascorbate. Energies are in kcal mol^{-1} and relative to separated reactants.

can be found in the Supporting Information in Table S1. Although recent theoretical investigations[14,15] have examined the possible participation of all the three forms, that is, neutral, monoanionic and dianionic, of ascorbic acid in the reduction process, here only the monodeprotonated form of ascorbic acid ($AscH^-$) has been assumed to be the reducing agent, with the concentration of such species, very likely, being the highest at physiological pH. Relative free energies, expressed in kcal mol^{-1}, have been calculated with respect to the sum of separated reactants free energies. All the intercepted transition states have been carefully checked by IRC calculations[16] to assess their proper connection with the corresponding minima. The mechanistic hypotheses taken into consideration are: a) OH-bridged electron transfer, b) the recently proposed nucleophilic attack of the enolate β-carbon[15] on the axial OH ligand and c) the Asc-Pt^{II}-X-Pt^{IV}-X dimer formation[9] due to the Pt^{II} catalytic action. The first examined mechanism (a), involving the hydroxido ligand as a bridge to facilitate the two-electron transfer, starts with the interaction between the reducing agent and the Asplatin Pt^{IV} complex. The adduct, named Asp_$AscH^-$, is formed, which is stabilised with respect to reactants by 9.8 kcal mol^{-1} due to the formation of a hydrogen bond between the ascorbate and the hydroxide ligand. The two-electron transfer occurs in one step through the shift of a H^- unit from the OH group of the ascorbate to the hydroxido ligand, leading to formation of a water molecule. Detachment of the water molecule occurs simultaneously with the release of the *trans* aspirinate ligand and dehydroascorbic acid (DHA) formation. The reduction of Pt^{IV} to Pt^{II} caused by such a rearrangement takes place, overcoming an energy barrier for the corresponding concerted transition state, TS_OH_{bridge}, of 14.6 kcal mol^{-1}. Separated products lie well below the energy at the entrance channel, as the process is calculated to be exergonic by 34.5 kcal mol^{-1}. The calculated activation energy barrier is low enough to assume that the reduction reaction could occur by following this mechanism. Nevertheless, the other two surmised alternative mechanisms have been also examined.

The free energy profile describing the nucleophilic attack to the OH^- ligand of the enolate β-carbon for the mechanism (b) is shown in Figure 2 together with the structures of the corresponding minima and transition states. Relative energies are calculated with respect to the sum of the energies of separated reactants, including a water molecule that plays an important role in the second part of the reaction. In analogy with the pathway described above, the Asp_$AscH^-$ adduct plus an explicit water molecule is formed. The next step, instead, is the enolate β-carbon attack to the OH ligand, leading to the formation of a new C–O bond simultaneously with the release of the *trans* aspirinate ligand. The height of the barrier for the corresponding concerted transition state, named TS_OHonAscH, is 20.7 kcal mol^{-1} and the products are cisplatin, aspirinate and the ascorbate with an additional OH moiety on the enolate β-carbon. Formation of such products is very favourable, being exergonic by 41.8 kcal mol^{-1}. The subsequent elimination of a water molecule from the two geminal hydroxo groups leads to the formation of the DHA oxidised species. This process occurs with the involvement of an additional water molecule that assists the elimination, working as a proton shuttle. The calculated height of the barrier for the corresponding transition state, TS_H_2O, is 24.4 kcal mol^{-1} and is significantly lower than that calculated in the absence of the auxiliary H_2O molecule, that is 39.1 (see Figure S1 in the Supporting Information). The whole process was calculated to be exergonic by 31.8 kcal mol^{-1}.

Finally, mechanism (c), involving Pt^{II} as catalyst for the reduction process, has also been explored, as shown in Figure 3, even if it is very unlikely that the reduction can occur following such a path due to the low cellular concentration of Pt^{II}. The postulated Pt^{II} catalysed reduction of Pt^{IV} complexes entails that the square planar Pt^{II} complex, coordinating an ascorbate, forms a square pyramidal five-coordinate Pt^{II} complex. This five-coordinate complex forms a ligand bridge to the Pt^{IV} centre to yield an AscH-Pt^{II}-X-Pt^{IV}-X dimer. Two electrons are transferred through the bridge, resulting in the formation of a Pt^{IV} ascorbato intermediate that is further reduced to yield the Pt^{II} complex. The mechanism we describe here, as is evident from Figure 3, does not involve all the hypothesised minima. Indeed, we have demonstrated[17] that the only formed intermediate is an adduct between the reducing agent and the Pt^{II} and Pt^{IV} complexes, which lies 10.9 kcal mol^{-1} below the energy of the entrance channel. The dimer is formed in only one step by overcoming an energy barrier of 24.9 kcal mol^{-1} for the concerted transition state TSPt(IV)–Pt^{II}. The intercepted transition state has been carefully checked by IRC calculations to establish whether it is connected to the correct minima. The normal mode associated with the imaginary frequency corresponds to the simultaneous coordination of the ascorbate to the platinum centre of cisplatin, detachment of the bridging OH^- ligand of the Pt^{IV} complex and its coordination to the Pt^{II} centre, and release of the aspirinate axial ligand. Formation of the corresponding products, that is cisplatin, aspirinate and the new Pt^{IV} complex with ascorbate and hydroxido ligands in axial positions, is calculated to be exergonic by 15.1 kcal mol^{-1}.

The formed ascorbate Pt^{IV} complex is further reduced by a second $AscH^-$ unit with the OH ligand that again accepts a H^- unit from the ascorbate, causing the oxidation to DHA of the reducing agent and the release of the ligand in *trans*. The height of the barrier that is necessary to overcome for such rearrangement to occur is 17.2 kcal mol^{-1}. It is worthwhile underlining that, in this examined case, the Pt^{II} complex does not play a catalytic role because the first and the second barrier heights are higher than and comparable to, respectively, the barrier calculated in its absence. The second step of the process occurs thanks to the bridging action of the hydroxido ligand and the barrier of 17.2 kcal mol^{-1} is about 3 kcal mol^{-1} higher than that along the analogous pathway for mechanism (a), with a different ligand, aspirinate in the former and ascorbate in the latter, in *trans* with respect to the OH ligand. Further investigations of such aspects are in progress to ascertain how the identity of the *trans* ligand might influence the rate of the process.

Inner-sphere electron-transfer reduction of *c,c,t*-[$PtCl_2(NH_3)_2(Cl)$(aspirin)] and *c,c,t*-[$PtCl_2(NH_3)_2(Br)$(aspirin)]

The inner-sphere reduction mechanisms (a) and (b) have been studied for the Asp Pt^{IV} analogous complexes in which we have substituted the OH^- ligand with chlorido and bromido ligands. Such complexes will be named from now on Asp–Cl and Asp–Br, respectively. The results of our investigation are reported in Figures 4 and 5, in which the structures of the intercepted stationary points are also sketched. Cartesian coordinates of minima and transition states can be found in Table S2 of the Supporting Information. Also in this case, the chlorido and bromido ligands should act as bridging ligands facilitating the electron transfer. Along the pathway for the Asp–Cl complex, the reaction starts with the formation of the first adduct that is stabilised by 8.6 kcal mol^{-1} with respect to separated reactants. Also in this case, the two-electron transfer from the $AscH^-$ reducing agent occurs in one step through the concerted TS_X_{bridge} transition state. The electrons are transferred thanks to the bridging Cl ligand that interacts with the deprotonated oxygen of the $AscH^-$ reducing species and simultaneously a proton shift occurs from the OH group to the *trans* aspirinate. As a result, the axial chloride and aspirin ligands are released and cisplatin and DHA are formed with a calculated energetic gain of 30.5 kcal mol^{-1}. The intercepted transition state has been carefully checked by IRC calculations, whereas all the attempts to locate minima and transition states along a stepwise pathway, in analogy with the results reported by Ejehi and Ariafard,[15] failed. The calculated height of the barrier for such rearrangement is 25.7 kcal mol^{-1}. Analogous calculations have been carried out on the complex named Asp–Br, bearing a Br ligand in axial position, and the results are also illustrated in Figure 4. The reaction proceeds in a similar manner by forming a first adduct lower in energy with respect to separated reactants by 12.5 kcal mol^{-1}. The concerted transition state that allows the transfer of the electrons from the ascorbate to the Pt^{IV} complex causing the detachment of the bromide and aspirinate ligands simultaneously to the shift of the proton from the OH group of $AscH^-$ to the aspirinate is higher in energy by 14.4 kcal mol^{-1} than separated reactants. An energy of 26.9 kcal mol^{-1} is required to surmount the transition state barrier and form the Pt^{II} cisplatin complex, DHA, aspirin and Br^-.

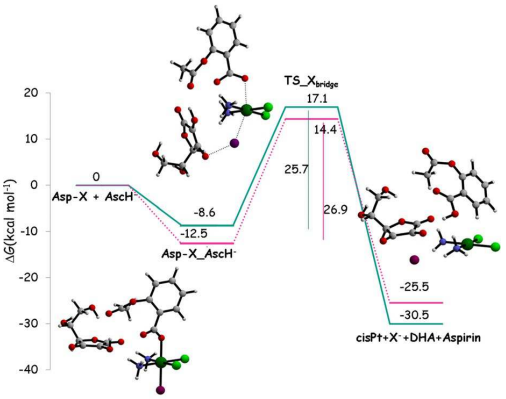

Figure 4. Calculated B3LYP-D3 free energy profile in water describing the X-bridged (X=Cl, Br) electron-transfer mechanism (a) for the Asp–Cl and Asp–Br complex reduction by ascorbate. Solid and dotted line profiles describe Asp–Cl and Asp–Br complexes, respectively. Energies are in kcal mol^{-1} and relative to separated reactants.

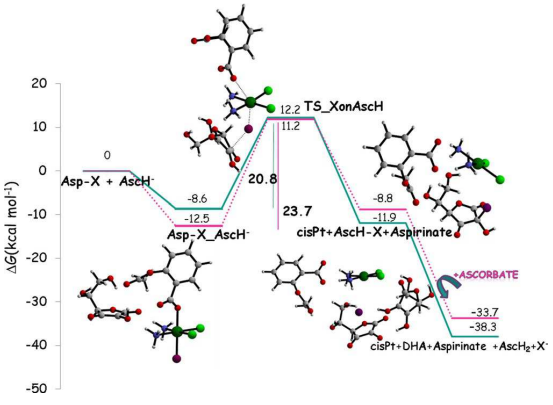

Figure 5. Calculated B3LYP-D3 free energy profiles in water describing the enolate β-carbon attack on the X (X=Cl, Br) axial ligand mechanism (b) for the Asp–Cl and Asp–Br complexes reduction by ascorbate. Solid and dotted line profiles are for Asp–Cl and Asp–Br complexes, respectively. Energies are in kcal mol^{-1} and relative to separated reactants.

It is worth underlining that the presence in the axial position of a ligand that is directly involved in the reduction process as a proton acceptor influences the course of the reaction; this is also evident from comparison of previous computational results.[15] On the basis of such results it is possible to draw the conclusion that, when the bridging ligand is a chloride or bromide ligand, the heights of the transition state barrier for the X-bridged electron transfer (a) mechanism are very similar and high enough to hypothesise that mechanism (b), involving the attack of the enolate β-carbon on the Cl or Br ligand, represents a viable alternative. The outcomes of the investigation of mechanism (b) for both Asp–Cl and Asp–Br are described in Figure 5.

After the first adduct, Asp-X_$AscH^-$, is formed, the nucleophilic attack of the enolate β-carbon on the X^- (X=Cl, Br) ligand occurs forming a new C–X bond and at the same time the *trans* aspirinate ligand is released. The concerted transition state is identified by a negative frequency that corresponds to such rearrangement and for the Asp–Cl complex lies 12.2 kcal mol^{-1} above the energy of separated reactants for a calculated barrier of 20.8 kcal mol^{-1}. The height of the analogous transition state for the Asp–Br complex is 23.7 kcal mol^{-1}. This step of the reaction is calculated to be exergonic by 11.9 and 8.8 kcal mol^{-1} for the Asp–Cl and Asp–Br, respectively, and leads to the release of the cisplatin complex, the free aspirinate ligand and the intermediate species in which the X atom is bonded to the enolate β-carbon in germinal position to the hydroxide. The addition of a second $AscH^-$ unit causes OH

group deprotonation to occur together with the formation of the final products in a process that does not involve any energy barrier to be overcome. Deprotonation of the OH group leads to the formation of the final DHA oxidized species and to the release of the X^- anions. The whole process is exergonic by 38.3 and 33.7 kcal mol^{-1} for Asp–Cl and Asp–Br, respectively. The exploration of the alternative mechanism (b) has shown that the whole process is thermodynamically more favourable than mechanism (a), involving an energy gain of about 8 kcal mol^{-1}, for both Asp–Cl and Asp–Br complexes. From a kinetic point of view, instead, the barrier is lower by about 5 kcal mol^{-1} for Asp–Cl and less than 3 kcal mol^{-1} for Asp–Br. Our computational analysis results show that, with respect to the behaviour of Asplatin, substitution of the hydroxido with chlorido and bromido ligands causes a decrease of the propensity to undergo reduction by monodeprotonated ascorbate, the active form of ascorbic acid at physiological pH, even when a different mechanism by which the reduction occurs is considered.

According to previous studies[5d,10b] demonstrating that reduction of Pt^{IV} pro-drugs might proceed not only by loss of the two axial ligands and equatorial ligands likewise could be involved, additional calculations have been performed on the Asp–Cl model to examine this hypothesis. Many unsuccessful attempts to check whether chlorido ligands in the equatorial position could assist the reduction process acting as bridging ligands have been carried out. Chorido axial ligands do not allow two-electron transfer to occur for the release of either cisplatin drug or reduction products maintaining the original axial ligands.

Summarising the reported results, it is worth underscoring the peculiarity of the hydroxo ligand in favouring the reduction process assisted by ascorbate. Indeed, as already emphasised above, it is generally assumed that inner-sphere electron-transfer requires the formation of a chemical bridge between the Pt^{IV} prodrug with halide or hydroxide ligands *trans* to a good leaving group. Electron transfer, therefore, is expected to be more favourable for chlorido and bromido ligands with respect to hydroxido as it is easier to form Cl^+ and Br^+ than OH^+. Previous results in contradiction[18] with this expected behaviour can be rationalised on the basis of what we report here, as we have demonstrated that the electron-transfer mechanism differs when the OH^- ligand is taken into consideration. Such a mechanism, indeed, involves formation and release of a water molecule due to the shift of an H^- unit from the OH group of the ascorbate to the hydroxido ligand. Therefore, the OH^- ligand not only plays the role of bridge to allow the transfer of the electrons, but directly participates in the reduction process leading to formation of the oxidised form of the ascorbic acid DHA. Moreover, even if chlorido and bromido can act as bridging ligands, the most favourable mechanism involves the enolate β-carbon attack on the Cl^- and Br^- axial ligands forming an intermediate that can be subsequently deprotonated by another $AscH^-$ to yield the final products. It is important to highlight the non-innocent role of the ligand in *trans* position, aspirinate in the present case, which can influence the course of the reaction as a proton acceptor.

Quantum chemically calculated reduction potentials for the two-electron reduction of Asp, Asp–Cl and Asp–Br Pt^{IV} complexes

As highlighted above, a convenient way to measure reduction of platinum(IV) to platinum(II) is the use of voltammetric experiments. However, since the reduction is an irreversible process, a standard redox potential cannot be obtained as the mid-point potential from a typical cyclic voltammogram. The peak potential of the irreversible cathodic response at a single scan rate is, therefore, used to approximate the ease of reduction of Pt^{IV} complexes. However, some caution has to be taken in interpreting these values because the cathodic peak potential of an irreversible process does not depend only on the thermodynamics of reduction, but is influenced by other factors such as the scan rate. Nevertheless, the relative cathodic peak potentials of structurally related complexes are generally correlated to the relative facility with which the metal centre is reduced and are utilised to estimate reduction rates in solution.[6b] Baik and co-workers[13] have demonstrated, with a series of electrochemical experiments, that the two-electron reduction process of Pt^{IV} produgs to their Pt^{II} analogues can be decomposed into electron transfers and Pt-ligand bond cleavage. DFT calculations have been employed to elucidate the mechanism and the calculated reduction potentials have been found to be in excellent agreement with experimentally determined values that are notably more positive than peak potentials previously reported in the literature. Baik and co-workers have adopted a decomposition scheme, sketched in Scheme 2, which has been shown to give reliable results for solution-phase redox processes[19–21] and allows chemical events to be separated from electrochemical events. As shown in Scheme 2, from the first six-coordinate Pt^{IV}-complex, adding an electron but not allowing the axial ligand to leave the coordination sphere of the metal centre, a Pt^{III} intermediate is obtained from which the two axial ligands are removed sequentially, with the second ligand released being a consequence of the

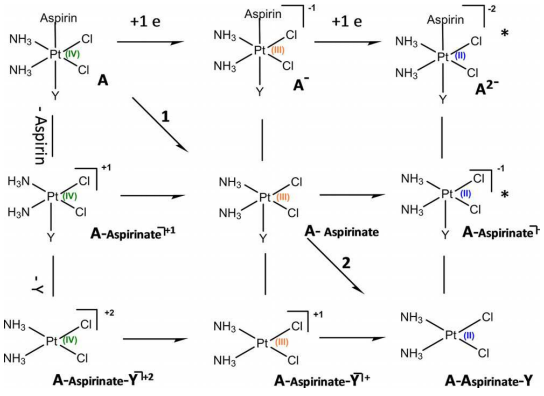

Scheme 2. Decomposition scheme for the electron transfer and ligand loss processes for the step-wise two-electron reduction of investigated Pt^{IV} complexes. Y=OH^-, Cl^-, Br^- in the present paper.

second electron addition. Structures labelled with an asterisk do not correspond to real minima because the ligands do not spontaneously remain in the coordination sphere of the Pt centre. The horizontal lines in Scheme 2 correspond to electron addition energies in eV and vertical lines represent ligand dissociation energies in eV. To separate the electron transfer energetics from the ligand loss chemical step, it has been assumed that, after the electron transfer, the anionic ligands are still bonded to the cationic Pt complex. By adopting such a scheme, all the energy changes corresponding to the formation of each of the species shown in Scheme 2 have been calculated. Cartesian coordinates for the species cited in the next paragraphs are collected in Table S3 of the Supporting Information.

Baik and co-workers have shown that addition of one electron to the first Pt^{IV} complex is more favourable than reduction of the five-coordinate Pt^{III} intermediate, named here **A**–**Asp**, whereas detachment of the first axial ligand from the anionic $\mathbf{A}^-$ intermediate is significantly less exergonic than detachment of the second axial ligand. As confirmed by comparison with the measured values obtained from their Savéant analysis,[22] they have demonstrated that the quantum-mechanically calculated reduction potential corresponds to the energy change that accompanies the one-electron transfer for the reduction of the six-coordinate Pt^{IV} to the six-coordinate Pt^{III} species. This trend is confirmed by the values of the analogous energy changes calculated for the Asplatin, Asp–Cl and Asp–Br complexes collected in Table 1. Consistent with previous calculations, minima corresponding to species indicated with an asterisk have not been located and their energies have been obtained from single-point energy calculations at the optimised geometries of their respective Pt^{III} analogues.

Full optimization of the structure of six coordinate, *c,c,t*-$[PtCl_2(NH_3)_2(Y)(aspirin)]$ (Y=OH, Cl, Br), Pt^{IV} anionic complexes was carried out in gas-phase without imposing any geometrical constraints. It is worth underlining a significant difference in behaviour between the Asplatin complex and the Asp–Cl and Asp–Br analogues. Indeed, for Asp–Cl and Asp–Br, after the addition of the first electron leading to the formation of the Pt^{IV} anionic intermediate $\mathbf{A}^-$, the detached ligands, according to the results reported by Baik and co-workers,[13] remain in the primary coordination sphere of the metal centre, forming hydrogen bonds with the equatorial ammonia ligands. Since these structures are realistic in gas-phase and unrealistic in solvent, as previously suggested, explicit water molecules, which have been removed for subsequent calculations in implicit solvent, have been added around the axial ligands. Fully optimised structures of such species with and without the inclusion of additional water molecules are shown in Figure S2 of the Supporting Information. When the Asplatin complex was examined, the addition of one electron, instead, did not cause the spontaneous release of the axial ligands. For such a chemical event to occur, in fact, it is necessary to surmount an activation energy barrier of 6.2 kcal mol^{-1}, as shown in Figure 6.

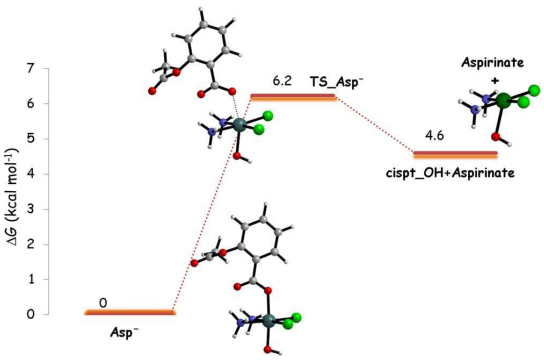

Figure 6. Calculated B3LYP-D3 free energy profile in water describing detachment of axial asprinate ligand from the anionic form of the Asplatin complex. Energies are in kcal mol^{-1} and relative to separated reactants.

The normal mode associated with the negative frequency that identifies the transition state **TS_Asp$^-$** corresponds to the elongation of the Pt–O bond, leading to the detachment of the ligand and to the formation of the corresponding products that are even destabilised with respect to the initial complex by 4.6 kcal mol^{-1}. This different behaviour highlights the low propensity of Asplatin drug to be reduced by an outer-sphere electron-transfer mechanism with respect to analogous Asp–Cl and Asp–Br complexes as it is mirrored by the values of the calculated reduction potentials reported below. To obtain calculated values of the standard redox potential for each of the examined complexes, the absolute potential of the standard hydrogen electrode (SHE), which has been determined to be 4.43 V in water,[23] has been used as a reference for the energy changes of Step 1. Thus, the relative potential is computed by using Equation (1):

Table 1. Free energy changes in eV for the electron transfer and ligand-Pt bond cleavage steps of the decomposition scheme describing the stepwise two-electron reduction of Asp, Asp–Cl and Asp–Br Pt^{IV} prodrugs. Values in italics are reported in kcal mol^{-1}.

X	First electron transfer	First ligand detachment	Step 1	Second electron transfer	Second ligand detachment	Step 2	ΔE
OH^-	−4.191	0.201	−3.990	−3.741	−0.895	−4.636	−0.646
	−96.6	*4.6*	*−92.0*	*−86.3*	*−20.6*	*−106.9*	*−14.9*
Cl^-	−4.559	−0.169	−4.728	−4.460	−1.029	−5.489	−0.761
	−105.1	*−3.9*	*−109.0*	*−102.8*	*−23.7*	*−126.6*	*−17.5*
Br^-	−4.709	−0.369	−5.078	−4.459	−0.930	−5.389	−0.311
	−108.6	*−8.5*	*−117.1*	*−102.8*	*−21.4*	*−124.3*	*−7.2*

$$E^{\circ} = -\Delta G_{(sol)} - 4.43\,V \quad (1)$$

Therefore, the calculated standard reduction potentials are −0.239, 0.129 and 0.279 eV for Asp, Asp–Cl and Asp–Br complexes, respectively. Such values, which allow an estimation of the probability with which the redox reaction occurs, indicate that the propensity to be reduced increases in going from Asp to Asp–Cl to Asp–Br, in case an outer-sphere mechanism is assumed to be operative. The trend in estimated values of the redox potentials does not reflect the trend in the rate of reduction by an inner-sphere mechanism that depends, instead, on the height of the energy barrier as illustrated above. This behaviour is consistent with the examples previously reported showing the lack of correlation between the rates of reaction and the reduction potentials.[5d,12] Moreover, if the calculated value of −0.239 eV of the standard reduction potential for the Asplatin drug is compared with the measured value −0.536 eV, versus the normal hydrogen electrode, it is confirmed that the peak potential is more negative than the normal potential, corresponding to a redox stability higher than the real one.

Conclusion

The elucidation of the mechanism by which P^{IV} pro-drugs are reduced to the corresponding platinum(II) drugs is of leading importance, being the key step for the activation of these anticancer compounds. On the basis of the information coming from experiments, many mechanistic hypotheses have been formulated that should depend on the identity of the equatorial and axial ligands and biological reducing agents. When assisted by small biological molecules, two are supposed to be viable alternatives; namely, inner- and outer-sphere mechanisms. Formation of a bridge between the ligand and the reducing agent is required in the former case. Therefore, an inner-sphere mechanism is favoured and the reduction rate increases as the ligand bridging ability increases. Vice versa, when such ability is low, an outer-sphere mechanism should prevail. A systematic detailed DFT theoretical investigation of the reduction mechanism has been carried out using the Pt^{IV} Asplatin complex, *c,c,t*-$[PtCl_2(NH_3)_2(OH)(aspirin)]$, as model system and ascorbic acid, in its mono-deprotonated form, as reductant. Reduction of analogous complexes obtained replacing the OH^- ligand with chlorido and bromido ligands have also been investigated. In addition, for all these complexes, the standard redox potential has been quantum-mechanically estimated by adopting an approach recently proposed as an alternative with respect to voltammetric experiments that cannot measure the redox potential due to the irreversibility of the reduction process. The outcomes reported here show how the mechanism for the Asplatin complex is different and involves a lower energy barrier than the corresponding Cl^- and Br^- containing complexes, in apparent disagreement with the behaviour expected on the basis of the bridging ability ($Br^- > Cl^- > OH^-$) of the involved ligands. Indeed, the OH^- ligand assists the electron transfer both acting as a bridge and directly participating in the process, leading to the formation of DHA, which is the oxidised form of ascorbic acid. Chlorido and bromido can play the role of bridging ligands, allowing the electron transfer from ascorbate, and calculations show that the possibility of the ligand in *trans* position, aspirinate in the present case, accepting protons can influence the rate of the reaction. The most favourable mechanism, however, entails the attack of the carbon atom in β-position of the enolate on Cl^- and Br^- ligands, forming an intermediate that is further deprotonated by another $AscH^-$ unit to yield the final products. The calculated standard reduction potentials are −0.239, 0.129 and 0.279 eV for Asp, Asp–Cl and Asp–Br complexes, respectively. Such values, which allow the probability that the redox reaction occurs to be estimated, indicate that the propensity to be reduced increases on going from Asp to Asp–Cl to Asp–Br, in case an outer-sphere mechanism is assumed to be operative. Further investigations are in progress to assess the role of the ligands both in *trans* and equatorial position and the nature of the reducing agent.

Computational Details

All calculations have been performed with the Gaussian 09 suite of programs,[24] in the framework of the density functional theory employing the hybrid Becke three-parameter exchange functional[25] and the Lee–Yang–Parr correlation functional,[26] B3LYP, including dispersion corrections for nonbonding interaction through the Grimme approach using atom pair-wise additive schemes,[27] denoted as DFT-D3 method. To describe the Pt atom, the relativistic compact Stuttgart/Dresden effective core potential[28] together with the split valence basis set has been used. Standard 6-311+G** Pople basis sets have been used to describe the rest of the atoms, except for peripheral atoms for which the 6-311G** basis sets have been employed to reduce the computational effort. Preliminary calculations have clearly shown that such basis set size saving does not provoke any significant change in geometrical structure and reactivity. Frequency calculations at the same level of theory have been performed to both calculate zero-point energy (ZPE) corrections and to identify all stationary points as minima (zero imaginary frequencies) or transition states (one imaginary frequency). The intercepted transition states have been carefully checked to be properly connected to the corresponding minima by IRC (intrinsic reaction coordinate) analysis[16] and to confirm that the vibrational mode associated with the imaginary frequency corresponds to the correct movement of the involved atoms. As underscored above, for the species indicated with an asterisk in the decomposition scheme proposed by Baik and co-workers,[13] full geometry optimization carried out without imposing any constraint did not allow proper minima to be located. The energies of these species have been obtained, in fact, from single-point energy calculations of the optimised geometries of the corresponding Pt^{III} analogues. Also for anionic forms of Asp–Cl and Asp–Br, obtained by one-electron transfer, unconstrained optimization gives unrealistic structures in solvent, as the released ligands interact with the ammonia ligands by forming hydrogen bonds. To include the effects of solvation during the optimization of the geometry, explicit water molecules have been added around the axial ligands. Such explicit solvent molecules, that do not allow the ligands to detach, have been removed for the subsequent calculations in implicit solvent. The influence of the aqueous environment has been taken into consideration by using the Tomasi's implicit Polarizable Continuum Model (PCM)[29] as implemented in Gaussi-

an 09. The UFF set of radii has been used to build-up the cavity in which solute molecules are accommodated. The solvation Gibbs free energies have been calculated in implicit water ($\varepsilon = 78.4$) at the same level, performing single-point calculations on all stationary point structures obtained from vacuum calculations. Enthalpies and Gibbs free energies have been obtained at 298 K at 1 atm from total energies, including zero-point, thermal and solvent corrections, using standard statistical procedures.[30] However, with the aim to more properly consider the entropic change, more relevant when association and dissociation steps are involved, that occurs when a solute is transferred from the gas- to the condensed-phase the following correction scheme has been adopted. Since the Gaussian's default standard state corresponds to an ideal gas at a standard pressure of 1 atm, the computed free energies have been converted[31] to yield Gibbs energies with a solution-phase standard state of 1 mol L^{-1} for all the species. For water molecules a standard state of 55.5 M has been used. That is, to the free energy of each species, as computed in Gaussian, a free energy correction term equal to $RT \ln (V_{\text{molar gas}}/V_{\text{molar solution}})$, ($R$ = gas constant, T = absolute temperature) has been added, where $V_{\text{molar gas}}$ is the volume occupied by one mole of ideal gas at the considered temperature, and $V_{\text{molar solution}}$ is the volume occupied by one mole of species in a standard solution of concentration 1 mol L^{-1}.

Acknowledgements

This research was supported by Università della Calabria.

Conflict of interest

The authors declare no conflict of interest.

Keywords: density functional calculations · drug delivery · drug development · prodrugs · redox chemistry

[1] a) B. Rosenberg, L. Van Camp, T. Krigas, *Nature* **1965**, *205*, 698 – 699; b) B. Rosenberg, L. Vancamp, J. E. Trosko, V. H. Mansour, *Nature* **1969**, *222*, 385 – 386.

[2] a) G. J. Bosl, R. J. N. Motzer, *N. Engl. J. Med.* **1997**, *337*, 242 – 253; b) M. Morris, P. J. Eifel, J. Lu, P. W. Grigsby, C. Levenback, R. E. Stevens, M. Rotman, D. M. Gershenson, D. G. N. Mutch, *N. Engl. J. Med.* **1999**, *340*, 1137 – 1143; c) J. H. Schiller, D. Harrington, C. P. Belani, C. Langer, A. Sandler, J. Krook, J. Zhu, D. H. N. Johnson, *N. Engl. J. Med.* **2002**, *346*, 92 – 98.

[3] a) N. Pabla, Z. Dong, *Kidney Int.* **2008**, *73*, 994 – 1007; b) R. W. Gregg, J. M. Molepo, V. J. Monpetit, N. Z. Mikael, D. Redmond, M. Gadia, D. J. Stewart, *J. Clin. Oncol.* **1992**, *10*, 795 – 803; c) Z. H. Siddik, *Oncogene* **2003**, *22*, 7265 – 7279; d) F. Zák, J. J. Turánek, A. Kroutil, P. Sova, A. Mistr, A. Poulová, P. Mikolin, Z. Žák, A. Kašná, D. Záluská, J. Nea, L. Šindlerová, A. Kozubík, *J. Med. Chem.* **2004**, *47*, 761 – 763.

[4] a) R. P. Feazell, N. Nakayama-Ratchford, H. Dai, S. J. Lippard, *J. Am. Chem. Soc.* **2007**, *129*, 8438 – 8439; b) S. Dhar, S. J. Lippard, *Proc. Natl. Acad. Sci. USA* **2009**, *106*, 22199 – 22204; c) C. M. Giandomenico, M. J. Abrams, B. A. Murrer, J. F. Vollano, M. I. Rheinheimer, S. B. Wyer, G. E. Bossard, J. D. Higgins, *Inorg. Chem.* **1995**, *34*, 1015 – 1021; d) M. D. Hall, H. R. Mellor, R. Callaghan, T. W. Hambley, *J. Med. Chem.* **2007**, *50*, 3403 – 34011; e) S. Dhar, N. Kolishetti, S. J. Lippard, O. C. Farokhzad, *Proc. Natl. Acad. Sci. USA* **2011**, *108*, 1850 – 1855.

[5] a) M. D. Hall, T. W. Hambley, *Coord. Chem. Rev.* **2002**, *232*, 49 – 67; b) E. Reisner, V. B. Arion, B. K. Keppler, A. J. L. Pombeiro, *Inorg. Chim. Acta* **2008**, *361*, 1569 – 1583; c) N. Graf, S. J. Lippard, *Adv. Drug Delivery Rev.* **2012**, *64*, 993 – 1004; d) E. Wexselblatt, D. Gibson, *J. Inorg. Biochem.* **2012**, *117*, 220 – 229; e) D. Gibson, *Dalton Trans.* **2016**, *45*, 12983 – 12991.

[6] a) S. Choi, C. Filotto, M. Bisanzo, S. Delaney, D. Lagasee, J. L. Whitworth, A. Jusko, C. Li, N. A. Wood, J. Willingham, A. Schwenker, K. Spaulding, *Inorg. Chem.* **1998**, *37*, 2500 – 2504; b) J. J. Wilson, S. J. Lippard, *Inorg. Chem.* **2011**, *50*, 3103 – 3115; c) M. D. Hall, S. Amjadi, M. Zhang, P. J. Beale, T. W. Hambley, *J. Inorg. Biochem.* **2004**, *98*, 1614 – 1624; d) P. Gramatica, E. Papa, M. Luini, E. Monti, M. Gariboldi, M. Ravera, E. Gabano, L. Gaviglio, D. Osella, *J. Biol. Inorg. Chem.* **2010**, *15*, 1157 – 1169.

[7] a) K. Lemma, A. M. Sargeson, L. I. Elding, *J. Chem. Soc. Dalton Trans.* **2000**, 1167 – 1172; b) K. Lemma, D. A. House, N. Retta, L. I. Elding, *Inorg. Chim. Acta* **2002**, *331*, 98 – 108.

[8] a) A. Nemirovski, I. Vinograd, K. Takrouri, A. Mijovilovich, A. Rompel, D. Gibson, *Chem. Commun.* **2010**, *46*, 1842 – 1844; b) J. Z. Zhang, E. Wexselblatt, T. W. Hambley, D. Gibson, *Chem. Commun.* **2012**, *48*, 847 – 849; c) M. Sinisi, F. P. Intini, G. Natile, *Inorg. Chem.* **2012**, *51*, 9694 – 9704; d) H. P. Varbanov, S. M. Valiahdi, C. R. Kowol, M. A. Jakupec, M. Galanski, B. K. Keppler, *Dalton Trans.* **2012**, *41*, 14404 – 14415; e) V. Pichler, S. Göschl, S. M. Meier, A. Roller, M. A. Jakupec, M. Galanski, B. K. Keppler, *Inorg. Chem.* **2013**, *52*, 8151 – 8162; f) C. K. J. Chen, J. Z. Zhang, J. B. Aitken, T. W. Hambley, *J. Med. Chem.* **2013**, *56*, 8757 – 8764; g) V. Pichler, S. Göschl, E. Schreiber-Brynzak, M. A. Jakupec, M. Galanski, B. K. Keppler, *Metallomics* **2015**, *7*, 1078 – 1090.

[9] E. L. Weaver, R. N. Bose, *J. Inorg. Biochem.* **2003**, *95*, 231 – 239.

[10] a) J. A. Platts, G. Ermondi, G. Caron, M. Ravera, E. Gabano, L. Gaviglio, G. Pelosi, D. Osella, *J. Biol. Inorg. Chem.* **2011**, *16*, 361 – 372; b) M. Ravera, E. Gabano, I. Zanellato, I. Bonarrigo, E. Escribano, V. Moreno, M. Font-Bardia, T. Calvetc, D. Osella, *Dalton Trans.* **2012**, *41*, 3313 – 3320.

[11] J. Dong, Y. Ren, S. Huo, S. Shen, J. Xu, H. Tian, T. Shi, *Dalton Trans.* **2016**, *45*, 11326 – 11337.

[12] a) R. K. Pathak, S. Marrache, J. H. Choi, T. B. Berding, S. Dhar, *Angew. Chem. Int. Ed.* **2014**, *53*, 1963 – 1967; *Angew. Chem.* **2014**, *126*, 1994 – 1998; b) Q. Cheng, H. Shi, H. Wang, Y. Min, J. Wang, Y. Liu, *Chem. Commun.* **2014**, *50*, 7427 – 7430.

[13] M. C. McCormick, K. Keijzer, A. Polavarapu, F. A. Schultz, M.-H. Baik, *J. Am. Chem. Soc.* **2014**, *136*, 8992 – 9000.

[14] F. Šebesta, J. V. Burda, *Eur. J. Inorg. Chem.* **2018**, 1481 – 1491.

[15] Z. Ejehia, A. Ariafard, *Chem. Commun.* **2017**, *53*, 1413 – 1416.

[16] a) K. Fukui, *J. Phys. Chem.* **1970**, *74*, 4161 – 4163; b) C. Gonzalez, H. B. Schlegel, *J. Chem. Phys.* **1989**, *90*, 2154 – 2161.

[17] I. Ritacco, G. Mazzone, N. Russo, E. Sicilia, *Inorg. Chem.* **2016**, *55*, 1580 – 1586.

[18] Y. Shi, S. A. Liu, D. J. Kerwood, J. Goodisman, J. C. Dabrowiak, *J. Inorg. Biochem.* **2012**, *107*, 6 – 14.

[19] M.-H. Baik, R. A. Friesner, *J. Phys. Chem. A* **2002**, *106*, 7407 – 7412.

[20] M.-H. Baik, C. K. Schauer, T. Ziegler, *J. Am. Chem. Soc.* **2002**, *124*, 11167 – 11181.

[21] S. Ghosh, M.-H. Baik, *Inorg. Chem.* **2011**, *50*, 5946 – 5957.

[22] C. Costentin, M. Robert, J.-M. Savéant, *Chem. Phys.* **2006**, *324*, 40 – 56 and references therein.

[23] H. Reiss, A. Heller, *J. Phys. Chem.* **1985**, *89*, 4207 – 4213.

[24] Gaussian 09, Revision D.01, M. J. Frisch, G. W. Trucks, H. B. Schlegel, G. E. Scuseria, M. A. Robb, J. R. Cheeseman, G. Scalmani, V. Barone, B. Mennucci, G. A. Petersson, H. Nakatsuji, M. Caricato, X. Li, H. P. Hratchian, A. F. Izmaylov, J. Bloino, G. Zheng, J. L. Sonnenberg, M. Hada, M. Ehara, K. Toyota, R. Fukuda, J. Hasegawa, M. Ishida, T. Nakajima, Y. Honda, O. Kitao, H. Nakai, T. Vreven, J. A. Montgomery, Jr., J. E. Peralta, F. Ogliaro, M. Bearpark, J. J. Heyd, E. Brothers, K. N. Kudin, V. N. Staroverov, T. Keith, R. Kobayashi, J. Normand, K. Raghavachari, A. Rendell, J. C. Burant, S. S. Iyengar, J. Tomasi, M. Cossi, N. Rega, J. M. Millam, M. Klene, J. E. Knox, J. B. Cross, V. Bakken, C. Adamo, J. Jaramillo, R. Gomperts, R. E. Stratmann, O. Yazyev, A. J. Austin, R. Cammi, C. Pomelli, J. W. Ochterski, R. L. Martin, K. Morokuma, V. G. Zakrzewski, G. A. Voth, P. Salvador, J. J. Dannenberg, S. Dapprich, A. D. Daniels, O. Farkas, J. B. Foresman, J. V. Ortiz, J. Cioslowski, and D. J. Fox, Gaussian, Inc., Wallingford CT, **2010**.

[25] A. D. Becke, *J. Chem. Phys.* **1993**, *98*, 5648 – 5652.

[26] C. Lee, W. Yang, R. G. Parr, *Phys. Rev. B* **1988**, *37*, 785 – 789.

[27] S. Grimme, J. Antony, S. Ehrlich, H. Krieg, *J. Chem. Phys.* **2010**, *132*, 154104 – 154122.

[28] D. Andrae, U. Häussermann, M. Dolg, H. Stoll, H. Preuss, *Theor. Chim. Acta* **1990**, *77*, 123 – 141.

[29] a) S. Miertuš, E. Scrocco, J. Tomasi, *Chem. Phys.* **1981**, *55*, 117 – 129; b) S. Miertuš, J. Tomasi, *Chem. Phys.* **1982**, *65*, 239 – 245; c) J. L. Pascual-Ahuir, E. Silla, I. Tuñón, *J. Comput. Chem.* **1994**, *15*, 1127 – 1138.
[30] D. A. McQuarrie, J. D. Simon, *Molecular Thermodynamics*, University Science Books, Sausalito, CA, **1999**.
[31] R. W. Ashcraft, S. Raman, H. W. Green, *J. Phys. Chem. B* **2007**, *111*, 11968 – 11983.

Manuscript received: January 30, 2018
Accepted manuscript online: May 2, 2018
Version of record online: June 10, 2018

A Metadynamics Perspective on the Reduction Mechanism of the Pt(IV) Asplatin Prodrug

Fortuna Ponte ,*[a] GiovanniMaria Piccini,[b,c] Emilia Sicilia ,[a] and Michele Parrinello[b,c,d]

Enhanced sampling molecular dynamics has been used to model the reduction mechanism of the antitumoral Asplatin Pt(IV) complex, c,c,t-[PtCl2(NH3)2(OH)(aspirin)] in the presence of L-ascorbic acid as reducing agent. In order to overcome the timescale problem, characteristic of many chemical reactions, we enhanced the sampling of the free energy landscape using Metadynamics. To achieve such a goal, the selection of adequate collective variables is crucial for the application of the method. Recently, a new method called Multi-Class Harmonic Linear Discriminant Analysis (MC-HLDA) has been proposed as a tool for constructing collective variables (CVs) for complex chemical processes. The method reduces the dimensionality of the variable space by generating appropriate linear combinations of several relevant chemical descriptors. The aim of this work is to assess the ability and performance of this method in describing the fundamental features of complex chemical reactions such as the Asplatin reduction mechanism in a compact, simple, and physically transparent manner. © 2019 Wiley Periodicals, Inc.

DOI: 10.1002/jcc.26100

Introduction

In recent years, the interest in the emerging class of inert and reasonably resistant Pt(IV) chemotherapeutic prodrugs, acting like potential alternative to the traditional Pt(II) drugs, has been growing. Their anticancer activity depends on the type of axial and equatorial ligands. In particular, actual research strategies propose the synthesis of new complexes in which the axial ligands may possess bio-pharmaceutical properties that improve their anticancer activity. Pt(IV) prodrugs are activated by reduction. Under particular conditions and in the presence of a reducing agent such as ascorbate, the reduction reaction involves the transfer of two electrons to the platinum center, the subsequent loss of the two ligands in axial position, and the formation of the Pt(II) active species. However, since the nature of the two axial ligands influences the course of the reduction process, the knowledge of the Pt(IV) activation mechanism is crucial for the development of new platinum-based anticancer drugs.

Aiming at elucidating the mechanism of reduction of Pt(IV) complexes, many theoretical[1–5] and experimental[6] studies have been carried out over the years. As a consequence of such efforts, many mechanistic details have been understood.[7]

Recently, a new cisplatin-based complex with aspirin and hydroxido ligands in axial position, named Asplatin, has been synthesized.[8] A computational investigation of the mechanism of the Asplatin prodrug reduction in the presence of the monodeprotonated form of L-ascorbic acid as a reducing agent has been carried out by means of density functional theory (DFT).[1] This study has demonstrated that for this complex the reduction reaction can take place following a mechanism different from those previously proposed and two different pathways, providing two different reduction products, have been suggested. These mechanistic alternatives have been selected using mechanistic hypotheses suggested in the recent[2,3] and less recent literature[9] together with a dose of chemical intuition.

The proposed mechanisms, as reported in Scheme 1, are (1) OH-bridged electron transfer, leading to the direct formation of the reduction products. These consist of dehydroascorbic acid (DHA), cisplatin, a water molecule, and the acetylsalicylate ion; (2) nucleophilic attack of the enolate β-carbon of the ascorbate on the OH ligand leading to the formation of a new C-OH bond on ascorbate and the consequent loss of the aspirinate axial ligand. The reduction product will be named $Prod_{red1}$ for mechanism (1) and $Prod_{red2}$ for mechanism (2). The latter mechanistic alternative has been previously suggested for a cisplatin derivative having a chlorido ligand in axial position,[3] whereas the former has not yet been proposed and is a viable path also for other ligands able to accept a proton when working as bridging ligands.[10]

Quantum-mechanical computations are powerful tools for the investigation of reaction mechanisms and can be applied to the characterization equally well of stable and short-life stationary points along the reaction paths. However, their application requires making use of assumptions based on experimental

[a] F. Ponte, E. Sicilia
Dipartimento di Chimica e Tecnologie Chimiche, Università della Calabria, Ponte P. Bucci, Cubo 14C, Arcavacata di Rende 87030, Italy
E-mail: fortuna.ponte@unical.it
[b] G. Piccini, M. Parrinello
Department of Chemistry and Applied Biosciences, ETH Zurich, c/o USI Campus, Via Giuseppe Buffi 13, Lugano 6900, Switzerland
[c] G. Piccini, M. Parrinello
Facoltà di Informatica, Istituto di Scienze Computazionali, Università della SvizzeraItaliana (USI), Via Giuseppe Buffi 13, Lugano 6900, Switzerland
[d] M. Parrinello
Istituto Italiano di Tecnologia, Via Morego 30, Genova 16163, Italy
Contract Grant sponsor: Università della Calabria; Contract Grant sponsor: European Union; Contract Grant number: ERC-2014-AdG-670227/VARMET

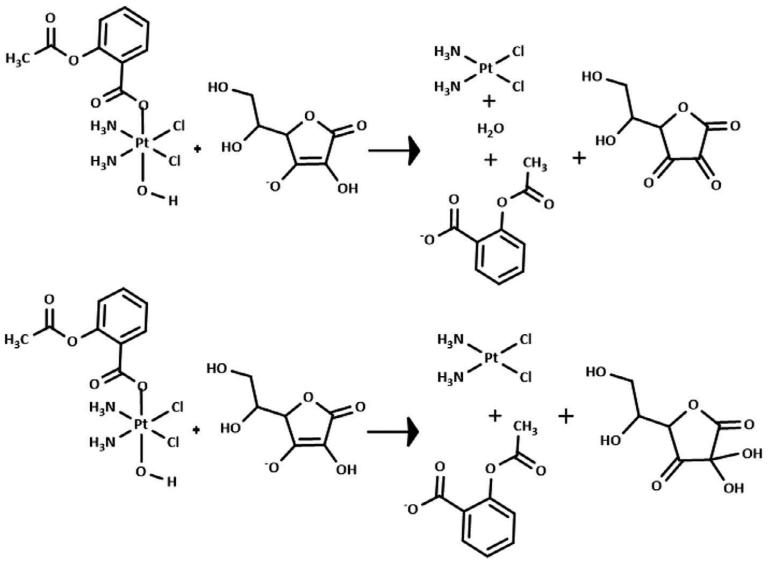

Scheme 1. Proposed Asplatin reduction mechanisms: (1) OH-bridged electron transfer and (2) enolate β-carbon.

information and/or chemical intuition. Therefore, in the course of the years, much effort has been devoted to the development of computational methods able to clarify reaction mechanisms even without using any prior information and chemical intuition.

Molecular dynamics (MD) is a versatile approach used for the study of chemical properties in atomistic detail. However, chemists are mainly interested in studying activated processes such as chemical reactions involving high free energy barriers and exhibiting complex energy landscapes. These events occur in a time scale for which the application of MD is not suitable. To circumvent this problem a wide variety of computational methods have been developed. Over the years, metadynamics has become a popular tool[11–13] for unraveling the mechanistic aspects of complex processes, rationalizing the experimental findings and predicting new results. Metadynamics adds a history-dependent bias potential, constructed as a sum of Gaussians, which facilitates sampling by increasing fluctuations between metastable states and allowing exploration of the reaction pathways. The bias potential acts on few parameters representing the slowest degrees of freedom involved in the reaction. These are functions, s, of the atomic coordinates R, $s(R)$, and are commonly referred to as collective variables (CVs). Selecting these degrees of freedom represents a key step for computing efficiently the free energy of an activated process. Thus, finding good CVs remains a challenge especially for complex transformations.

In order to select a proper set of CVs, some requirements must be fulfilled. The different metastable states have to be distinguished by the order parameters, the most relevant system slow modes have to be included and the CVs number has to be limited. Thus, to reduce the complexity of the problem a new approach, based on Fisher's linear discriminant analysis (LDA), named harmonic linear discriminant analysis (HLDA).[14] This technique, that has been originally used for dimensionality reduction, allows generating a lower-dimensional CV space reducing the complexity of the problem.

The procedure starts by choosing descriptors $d_i(R)$ that are able to distinguish the metastable states. Collecting the local fluctuations of these descriptors within the metastable states of interest, HLDA combines these descriptors into low-dimensional linear combination that can serve as CVs. The only information needed is the expectation values of the descriptors in the different states ad their covariance matrices.

This method has been tested so far for small chemically relevant systems[14,15] obtaining encouraging results. If more than two metastable states are relevant, the method can be extended to include multi-class (MC) problems,[16] where the classes correspond to the metastable states of interest. Therefore, for the study of chemical reactions, the combination of metadynamics and the MC-HLDA approach could be used to explore complex reaction free energy landscapes. The novelty is that this approach allows to study simultaneously in detail different reaction pathways without the guidance of any preliminary information, outlining the free energy profile and elucidating the minimum energy paths connecting reactants and products.

In this work, we report the ability of MC-HLDA in describing complex chemical free energy landscapes such as the one related to the Asplatin prodrug reduction in the presence of ascorbate. For computational convenience, we restricted our system to a model in which the prodrug and the ascorbic acid as isolated in the gas-phase. The aim of this work is to show how this approach can provide detailed mechanistic insights for complex reactions using a very limited amount of information and automating the process of chemical intuition.

Methods

Ab initio molecular dynamics

Ab initio molecular dynamics calculations have been performed using the CP2K-QuickStep code [17,18] at the semiempirical PM6

level.[19] The system has been kept at a temperature of 300 K through the velocity rescaling thermostat of Bussi et al.[20]

A time step of 1 fs has been used for the integration of the equations of motion and a wave function convergence of 10−5 a.u. has been set. The three metastable states have been equilibrated for 80 ps in the NVT ensemble.

Metadynamics

We use the well-tempered variant of metadynamics WT-MTD[13] as implemented in the PLUMED2 code .[21,22] Such a method allows sampling rare events during a MD simulation, while at the same time building the relative free energy landscape. Namely, it encourages the system to explore several configurations and different reaction pathways, through the addition of a history-dependent bias potential that grows whit time and acts on selected degrees of freedom. This potential is built as a sum of Gaussians. The WT-MTD run has been performed at 300 K for 2.5 ns adopting a bias factor γ of 50 and using a time step of 1 fs.[13]

Gaussian kernels of initial height of 5 kJ/mol were deposited every 50 fs. The Gaussians width was adapted to the underlying free-energy surface (FES) landscape using the dynamical approach of Branduardi et al. (https://pubs.acs.org/doi/10.1021/ct3002464).

In order to ensure the correct application of Metadynamics and then perform a successful simulation selection of adequate CVs is required. It is not easy to choose a reasonable number of CVs, especially for complex reactions in which many degrees of freedom are involved. The appropriate selection allows discriminating all system accessible configurations and building the free-energy surface as a function of the chosen CVs.

MC-HLDA

To study the reduction reaction in gas-phase, we applied the MC-HLDA method to extract chemically intuitive collective variables. The general formulation of the method permits to treat several metastable states simultaneously (multi-class problem) and in this case, the simultaneous study of both reaction paths.

For a system like the one under investigation, in which the metastable states (React, $Prod_{red1}$, $Prod_{red2}$) are three, MC-HLDA provides two CVs.

The first step for applying MC-HLDA is to choose good descriptors able to discriminate at best the three states of the reaction under examination. Four multiple coordination numbers CVs have been chosen as descriptors capable to describe the breaking and the formation of bonds in the three basins and to discriminate the states (a detailed definition of the utilized descriptors can be found in the Electronic Supplementary Information).

Thus, once selected the descriptors set for the three metastable states, 80 ps of unbiased simulation have been performed to compute average values and their variance.

Results and discussion

We are going to report the results of the study carried out by using MC-HLDA of reduction reaction of Asplatin assisted by mono-deprotonate ascorbic acid.

The outcomes of the MC-HLDA analysis provide the following linear combinations for the CVs that we report in Table 1.

It is noteworthy that important information about the Asplatin complex reduction mechanisms comes from analysis of the weight distributions. Indeed, for the first CV, the major contribution is given by the last coefficient d4, associated with the interaction between the ascorbate β-C and both the protonated ascorbate oxygen atom and the hydroxido ligand oxygen atom. This is indicative of the formation of a new C-O bond as a consequence of the attack of the enolate β-carbon to the OH ligand. In the second CV, the third coefficient d3 assumes the largest amplitude. This coefficient is representative of the interaction between the oxygen atoms of the OH ligand and the deprotonated one of the ascorbate with the H atoms of the OH groups of both ascorbate and hydroxido ligand. Therefore, the reducing agent, under these conditions, reacts by donating its H to the OH ligand leading to the formation of one water molecule.

The sign of the coefficients also contains precious information. For s1, the opposite signs of the d1, d2 and d3 descriptors with respect to d4, points out that they are associated with breaking of bonds. This detail confirms that the diol-product formation (Prodred2) occurs in a concerted fashion implicating the release of the ligands in axial position. The same information can be deduced for the s2 variable. The reaction occurs in one step by loss of the two axial ligands.

Thus, after the selection of the two collective variables s1 and s2, that are able to describe the entire process, a WT-MTD simulation has been run in the next step for 2.5 ns.

The free energy surface as a function of two CVs has been reconstructed and more insights into the reduction pathways have been obtained. The FES for the reduction of Asplatin has been reported in Figure 1.

It is possible to observe the presence of three channels that lead to the formation of three well-separated regions related to the three metastable states. The first state on the left is associated with the reactants state. Starting from it, a two-electron transfer can occur following two alternative mechanisms leading the formation of the reduction product Prodred1 (bottom left) and the second reduction product-intermediate Prodred2 (in the upper right), overcoming two different energy barriers.

The barrier for the first transition that leads to the formation of Prodred1 is estimated to be about 126 kJ mol^{-1}, while for the formation of Prodred2 the barrier is approximately 152 kJ mol^{-1}. Since the transitions between the metastable states occur with a probability proportional to the exponential of the free energy, the first reduction mechanism which involves the formation of cisplatin and dehydroascorbic acid is the most likely one from a kinetic point of view.

Table 1. MC-HLDA coefficients for the reaction collective variable

sHLDA	d1	d2	d3	d4
s1	−0.243	−0.083	−0.220	0.941
s2	0.546	0.188	−0.808	0.118

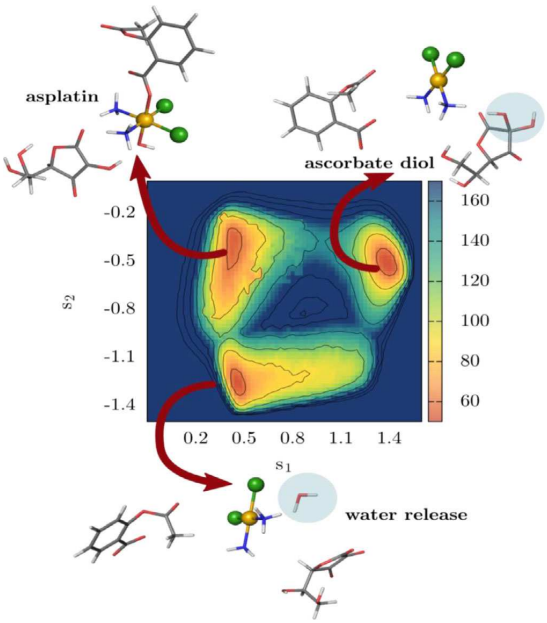

Figure 1. Free energy surface showing three basins. To each basin, the corresponding structure was associated. [Color figure can be viewed at wileyonlinelibrary.com]

This result is in good agreement with the theoretical data obtained in static simulations.

In addition, the two basins, corresponding to the two reduction products, Prodred1 and Prodred2, are interconnected by an energy barrier of 160 kJ mol^{-1}. Moreover, from the transition zones of the three channels, the configurations corresponding to the transition states have been extracted (Figure 2).

The configurations associated with the first concerted transition state correspond to hydrogen transfer from the hydroxido group of the Ascorbate to the OH ligand, leading to the formation of a water molecule and simultaneous release of an Aspirinate. This transition state well connects the two metastable states of reactant and the first reduction product. The second transition state links the reactant metastable state to the second reduction product. The associated configurations show the OH transfer from platinum center to the β-Carbon of AscH. Finally, the third transition state is related to the highest energy path and, as it is shown by the configurations, involves the elimination of a water molecule from the two germinal hydroxido moieties.

The free energy surface reconstructed by metadynamics gives the possibility to show how this method is able to well describe these complex transitions using only two CVs and identify the exact mechanism of this important reduction reaction in a compact and instructive form.

The two one-dimensional CVs obtained by MC-HLDA analysis provides a very satisfactory solution to the problem under investigation, describing in appropriate way the two different reaction mechanisms.

Conclusions

The reduction reaction of the Pt(IV) prodrug Asplatin can be classified as a rare event. We presented the outcomes of a computational investigation involving a combination of Metadynamics and MC-HLDA. The two collective variables obtained by using the MC-HLDA method allow a deep insight into the nature of this complicated process. This method provides reliable results on the reaction mechanisms and allows a full investigation of multidimensional free energy landscapes. The analysis of the barrier connected to the three reaction pathways allows to identify the minimum free energy path.

It is worth mentioning that the application of this method only requires the knowledge of the fluctuations in the basins of the three metastable states and no prior information on the reaction pathways is necessary.

In conclusion, the present investigation demonstrates that the new MC-HLDA approach can be successfully adopted, by properly choosing collective variables, for the study of redox reactions that involve several reaction pathways.

Work is in progress to take into account the influence the solvent can have on the description of the reduction mechanism and to apply this tool for the exploration of new anticancer drug mechanisms of action.

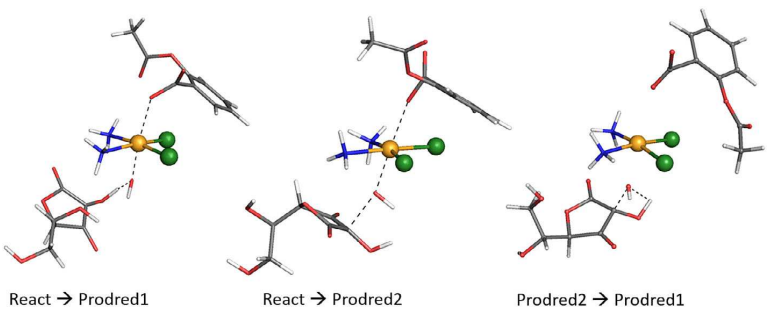

Figure 2. Configurations transition states extracted from the barrier top region. [Color figure can be viewed at wileyonlinelibrary.com]

Acknowledgments

This research was supported by the European Union Grant No. ERC-2014-AdG-670227/VARMET. The authors also thank the Università della Calabria.

Keywords: Asplatin · Pt(IV)-prodrugs · metadynamics simulation · MC-HLDA · reduction mechanism

How to cite this article: F. Ponte, G. M. Piccini, E. Sicilia, M. Parrinello. *J. Comput. Chem*. **2019**, 9999, 1–5. DOI: 10.1002/jcc.26100

Additional Supporting Information may be found in the online version of this article.

[1] F. Ponte, N. Russo, E. Sicilia, *Chem. A Eur. J.* **2018**, *24*, 9572.
[2] F. Šebesta, J. V. Burda, *Eur. J. Inorg. Chem.* **2018**, *2018*, 1481.
[3] Z. Ejehia, A. Ariafard, *Chem. Commun.* **2017**, *53*, 1413.
[4] E. L. Weaverand, R. N. Bose, *J. Inorg. Biochem.* **2003**, *95*, 231.
[5] I. Tolbatov, C. Coletti, A. Marrone, N. Re, *Inorg. Chem.* **2018**, *57*, 3411.
[6] M. C. McCormick, K. Keijzer, A. Polavarapu, F. A. Schultz, M. Baik, *J. Am. Chem. Soc.* **2014**, *136*, 8992.
[7] J. Z. Zhang, E. Wexselblatt, T. W. Hambley, D. Gibson, *Chem. Commun.* **2012**, *48*, 847.
[8] R. K. Pathak, S. Marrache, J. H. Choi, T. B. Berding, S. Dhar, *Angew. Chem. Int. Ed.* **2014**, *53*, 1963.
[9] E. Wexselblatt, D. Gibson, *J. Inorg. Biochem.* **2012**, *117*, 220.
[10] E. Dabbish, F. Ponte, N. Russo, E. Sicilia, *Inorg. Chem.* **2019**, *58*, 3851.
[11] A. Laio, M. Parrinello, *Proc. Natl. Acad. Sci. U. S. A.* **2002**, *99*, 12562.
[12] J. F. Dama, M. Parrinello, G. A. Voth, *Phys. Rev. Lett.* **2014**, *112*, 240602.
[13] A. Barducci, G. Bussi, M. Parrinello, *Phys. Rev. Lett.* **2008**, *100*, 020603.
[14] D. Mendels, G. Piccini, M. Parrinello, *J. Phys. Chem. Lett.* **2018**, *9*, 2776.
[15] D. Mendels, G. Piccini, Z. F. Brotzakis, Y. I. Yang, M. Parrinello, *J. Chem. Phys.* **2018**, *149*, 194113.
[16] G. Piccini, D. Mendels, M. Parrinello, *J. Chem. Theory Comput.* **2018**, *14*, 5040.
[17] CP2K website. http://www.cp2k.org.
[18] J. VandeVondele, M. Krack, F. Mohamed, M. Parrinello, T. Chassaing, J. Hutter, *Comput. Phys. Commun.* **2005**, *167*, 103.
[19] J. J, *J. Mol. Model.* **2007**, *13*, 1173.
[20] G. Bussi, D. Donadio, M. Parrinello, *J. Chem. Phys.* **2007**, *126*, 014101.
[21] M. Bonomi, D. Branduardi, G. Bussi, C. Camilloni, D. Provasi, P. Raiteri, D. Donadio, F. Marinelli, F. Pietrucci, R. A. Broglia, *Comput. Phys. Commun.* **2009**, *180*, 1961.
[22] G. A. Tribello, M. Bonomi, D. Branduardi, C. Camilloni, G. Bussi, *Comput. Phys. Commun.* **2014**, *185*, 604.

Received: 3 July 2019
Revised: 16 October 2019
Accepted: 17 October 2019

Inorganic Chemistry
Cite This: Inorg. Chem. 2019, 58, 3851−3860
Article
pubs.acs.org/IC

Antitumor Platinium(IV) Prodrugs: A Systematic Computational Exploration of Their Reduction Mechanism by L-Ascorbic Acid

Eslam Dabbish, Fortuna Ponte, Nino Russo, and Emilia Sicilia*

Department of Chemistry and Chemical Technologies, Università della Calabria, 87036, Arcavacata di Rende, CS, Italy

ABSTRACT: The reduction mechanism of Pt(IV) anticancer prodrugs, still today a matter of debate, assisted by one of the dominant reductants in human plasma, that is L-ascorbic acid in its monodeprotonated form, has been computationally examined in this work. In order to check what should be the influence on the reduction rate of the identity of the ligands in axial and equatorial position, both cisplatin and oxaliplatin derivatives have been studied, varying the ligands in axial position in connection with the role they should play as bridges, *trans* leaving species, and proton acceptors. OH, OAc, Cl, and Br ligands have been tested as bridging/leaving ligands, whereas Cl and aspirin have been used as *trans* labile and less labile ligands, respectively. The most recent theoretical and experimental investigations have demonstrated that the generally adopted grouping of reduction mechanisms into inner- and outer-sphere does not properly take into account all the viable alternatives. Therefore, inner-sphere mechanisms, classified as ligand-bridged, ligand-bridged-H transfer and enolate β-carbon attack, have been explored for all the complexes under investigation. Concerning the outer-sphere mechanism, redox potentials have been calculated adopting a recently proposed procedure based on the separation between electrochemical and chemical events to evaluate their propensity to be reduced. Moreover, according to the hypothesis that the outer-sphere reduction mechanism involves the sequential addition of two electrons causing the formation of a Pt(III) intermediate, the possibility that singlet and triplet pathways can cross for the Pt(IV) cisplatin derivative having two chlorido ligands in axial position has been explored in detail. Results show that the mechanism indicated as base-assisted outer sphere can become competitive with respect to the inner one if two singlet−triplet spin inversions occur. Results presented here are helpful in addressing synthetic strategies as they show that Pt(IV) prodrugs propensity to be reduced can be properly tuned and give indications on how this aim can be accomplished.

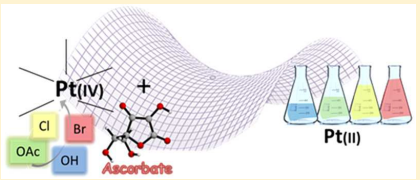

1. INTRODUCTION

Platinum complexes, notwithstanding the fact that only a relatively small number of metal-containing drugs are currently in clinical use, have proven to be invaluable and are the pillars of cancer chemotherapy.[1] Only three Pt(II)-based anticancer drugs are approved by the FDA and used worldwide: cisplatin, carboplatin, and oxaliplatin, which are square-planar d^8 Pt(II) complexes, whose mechanism of action (MoA) involves water substitution of ligands for the formation of the corresponding "aquated" complexes acting as transcription inhibitors by binding to nuclear DNA and distorting its structure.[2−4] Although very efficacious, cisplatin and related Pt(II) complexes suffer from side-effects. Furthermore, bioavailability is limited and oral administration is precluded, since a large amount of Pt(II) drugs is lost in the bloodstream before arriving at the ultimate target.[5] Aiming at overcoming such shortcomings new strategies have emerged including the use of six-coordinate Pt(IV) complexes, as inert prodrugs, which are shown to release the corresponding four-coordinate active Pt(II) species upon reduction by cellular reducing agents or by photoactivation.[6]

Pt(IV) complexes are relatively inert to substitution.[7] Reactions with biological nucleophiles, therefore, are disfavored and lifetime in biological fluids is expected to increase making even oral administration feasible. The administration of nontoxic Pt(IV) prodrugs might reduce unwanted reactions with biomolecules and consequently minimize undesired side-effects. In addition, axial ligands can be designed to improve in different ways the pharmacological properties of the prodrug. Intracellular reductive elimination represents the critical and decisive step of the MoA of such compounds and, as a consequence, a great amount of attention has been focused on aspects such as the identity of the reducing agents, the ease, the rate and mainly the mechanism of the reduction process. Although many potential reducing agents are present both in plasma and cells and several hypotheses have been formulated,[8] L-ascorbic acid ($AscH_2$) and L-glutathione are commonly believed to be the biological species responsible for the reduction of Pt(IV) prodrugs and continue to be used for *in vitro* experiments.[9−13]

Several hypotheses on the mechanism by which Pt(IV) prodrugs are reduced have been formulated mainly on the basis of the information coming from kinetic measurements. Electron transfer mechanisms are generally classified as ligand-bridged inner-sphere, assuming that one of the axial ligands is able to form a bridge between the Pt(IV) center and the reductant mediating the flow of the electrons, and outer-sphere.[6a,11c,14] However, such classification does not properly account for all the proposed mechanistic alternatives. The

Received: December 14, 2018
Published: March 7, 2019

DOI: 10.1021/acs.inorgchem.8b03486
Inorg. Chem. 2019, 58, 3851−3860

inner-sphere mechanism could involve the Pt(II) complex catalytic action[15] or the enolate β-carbon of the monodeprotonated form of L-ascorbic acid ($AscH^-$) attack to the axial ligands.[16] Outer-sphere reduction can take place through a two steps electron transfer encompassing formation of a metastable six-coordinate Pt(III) intermediate,[17] and intersystem singlet−triplet crossings.[16] Very recently, we have shown that when one of the axial ligands is an OH group and $AscH^-$ is the reducing agent, the inner-sphere electron transfer proceeds by the direct participation of the ligand, leading to the release of a water molecule and formation of dehydroascorbic acid (DHA), the oxidized form of L-ascorbic acid.[18]

Experimental information on the ease of reduction is usually obtained by cyclic voltammetry, which allows to measure the peak potential for the irreversible reduction, but not the standard redox potential. Since the electron transfer is accompanied by the release of the two axial ligands, the measured peak potentials do not necessarily correlate with the rate of the reduction process[19] that depends both on the rate of the electron transfer and on strength of the bonds between the ligands and the metal center. Theoretical procedures for the elucidation of the reduction mechanism and calculation of redox potential have been proposed.[17,20] Baik and coworkers[17] have demonstrated that reduction occurs in two steps. The first step involves one electron transfer accompanied by the formation of a six-coordinate Pt(III) complex and, being less exergonic than the second one, determines the magnitude of the redox potential as it has been confirmed by computations.[18,21]

Motivated by the attention devoted to the design of novel antineoplastic agents based on Pt(IV) prodrugs and the contradictory information coming from experimental and theoretical investigations, we have undertaken a thorough computational analysis of the chief reduction step using several platinum complexes and L-ascorbic acid as reducing agent. The Pt(IV) model complexes have been selected to check what is the influence on the reduction rate of the nature of the equatorial and, mostly, axial ligands owing to the role they should play as bridges, *trans* leaving species and proton acceptors.

2. RESULTS AND DISCUSSION

A systematic examination of the inner- and outer-sphere reduction mechanisms for all the Pt(IV) complexes, shown in Scheme 1 has been carried out. Ascorbic acid, in its monoanic form, $AscH^-$, at physiological pH (pK_a ca. 3.8), has been used as reducing agent. The reduction mechanism of Asplatin complex, *c,c,t*-$[PtCl_2(NH_3)_2(OH)(aspirin)]$, a dual-action drug with the ability to release cisplatin and aspirin for their respective biological actions,[6b,c] has been recently investigated by us.[18] For comparison with the outcomes of our study on Asplatin and its analogues, obtained by substituting the OH (**1**) group with either Cl (**2**) or Br (**3**), the corresponding acetate (OAc) complex (**4**) has been examined. Furthermore, in order to check the influence on the reaction rate of the nature of the ligand in *trans* with respect to bridging/leaving ligands, the behavior of the Pt(IV) complexes *c,c,t*-$[PtCl_2(NH_3)_2(X)(Cl)]$ (X = OH^- (**5**), Cl^- (**6**), Br^-(**7**), Ac^- (**8**)) has been analyzed, with the chlorido ligand being both a better leaving ligand than aspirinate and unable to accept a proton. The influence of the nature of the ligands in equatorial position has been examined by considering Pt(IV) derivatives of oxaliplatin, that is [Pt(dach)(Ox)] (dach = (1*R*,2*R*)-1,2-diaminocyclohexane, Ox = oxalate). Calculations have been carried out for two complexes in which one of the axial ligands is the aspirinate having in the *trans* position a hydroxido (**9**) and a chlorido (**10**) ligand.

Scheme 1. Pt(IV) Complexes Investigated for Reduction

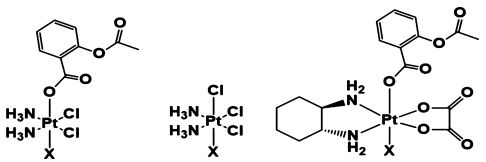

1 : X = OH
2 : X = Cl
3 : X = Br
4 : X = OAc

5 : X = OH
6 : X = Cl
7 : X = Br
8 : X = OAc

9 : X = OH
10 : X = Cl

The explored alternatives are shown in Scheme 2. The inner-sphere mechanistic alternative involving Pt(II) as catalyst has not been explored because of both the previously calculated[18] high energy barriers for the reduction and the low viability of this path as a consequence of the low cellular concentration of Pt(II).

Scheme 2. Inner-Sphere Mechanistic Alternatives

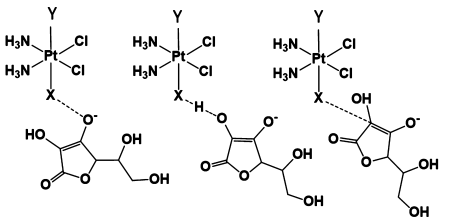

a) Ligand-bridged **b) Ligand-bridged-H transfer** **c) Enolate β-carbon attack**

2.1. Inner-Sphere Reduction of *c,c,t*-$[PtCl_2(NH_3)_2(X)(aspirin)]$, X = OH^-, Cl^-, Br^-, OAc^-. The detailed investigation of the inner-sphere reduction reaction of Asplatin (**1**) and its chlorido (**2**) and bromido (**3**) derivatives in the presence of $AscH^-$ has highlighted[18] the peculiar behavior of the OH^- ligand. Indeed, for the (**1**) complex, the reduction mechanism involves formation and release of a water molecule due to the shift of a H^- unit from the OH group of the ascorbate to the hydroxido ligand. Therefore, the hydroxido ligand not only plays the role of bridge to allow the transfer of the electrons, but directly participates in the reduction process leading to formation of the oxidized form of the ascorbic acid DHA. Simultaneously, the *trans* aspirinate ligand detaches and the cisplatin drug is formed. When the reduction mechanism of **2** and **3** complexes is taken into consideration, the electrons are transferred thanks to the bridging Cl and Br ligands that interact with the deprotonated oxygen of the $AscH^-$ reducing species and concurrently a proton shift occurs from the OH group of the ascorbate to the *trans* aspirinate. As a result, the chlorido or bromido, ligands are released along with aspirin. Cisplatin and DHA are formed. However, for (**2**) and (**3**) complexes the most favorable mechanism is that involving the nucleophilic attack of the enolate β-carbon of ascorbate on the X (X = Cl, Br) ligand leading to the formation of a new C−X bond and the release of the ligand in *trans* position. Since many

DOI: 10.1021/acs.inorgchem.8b03486
Inorg. Chem. 2019, 58, 3851−3860

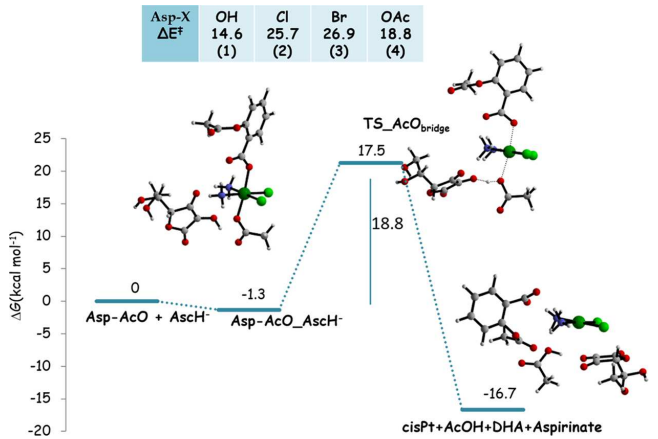

Figure 1. Calculated B3LYP-D3 free energy profile in water describing the OAc-bridged-H electron transfer mechanism for the reduction of complex **4** by ascorbate. Energies are in kcal·mol^{-1} and relative to separated reactants.

Pt(IV) cisplatin and oxaliplatin derivatives have been prepared by tethering carboxylate axial ligands to the metal center, also the behavior of a possible Asplatin derivative obtained by substituting the OH ligand with an acetate (OAc) (**4**) one has been investigated. The calculated energy profile together with the structures of intercepted stationary points describing the ascorbate assisted reduction of complex **4** is reported in Figure 1.

In the same figure, for the sake of comparison, the heights of the analogous free energy barriers for complexes **1**, **2**, and **3** are reported. The interaction between the reducing agent and complex **4** leads to the formation of the adduct named **Asp-OAc_AscH$^-$**, which is slightly more stable than the reactants by 1.3 kcal mol^{-1}. In analogy with the mechanism operative for the hydroxido ligand and as already suggested,[22] the two-electron transfer occurs in one step through the shift of a H$^-$ unit from the OH group of the ascorbate to the acetate oxygen coordinated to the metal center. Formed acetic acid detaches and, simultaneously, the *trans*-aspirinate ligand is released and dehydroascorbic acid is formed. The Pt(IV) to Pt(II) reduction caused by such rearrangement takes place overcoming on an energy barrier of 18.8 kcal mol^{-1} for the corresponding concerted transition state, **TS_OAc$_{bridge}$**, characterized by an imaginary frequency of 142*i* cm^{-1}. Formation of separated products is calculated to be exergonic by 16.7 kcal mol^{-1}.

The possibility that the reduction reaction can occur by a nucleophilic attack of the enolate *β*-carbon of ascorbate (mechanism c in Scheme 2) on the acetate ligand has been also unsuccessfully explored, very likely due to steric hindrance of the acetate ligand.

2.2. Inner-Sphere Reduction of *c,c,t*-[PtCl$_2$(NH$_3$)$_2$(X)(Cl)], X = OH, Cl, Br, OAc. Aiming at analyzing what should be the role played by the ligands in *trans* with respect to the bridging ligands that allow the Pt(IV) reduction to occur, Pt(IV) cisplatin derivatives *c,c,t*-[PtCl$_2$(NH$_3$)$_2$(X)(Cl)] (X = OH (**5**), Cl (**6**), Br (**7**), OAc (**8**)) have been examined. With respect to aspirin, chlorido ligand both is a better leaving ligand and is not able to accept protons. It is worth underlining that for complex (**6**), recently, Dong et al.[19b] have studied the reduction process by ascorbic acid in a wide range of pH and proposed a halide-bridged inner-sphere electron transfer mode for the rate-determining steps. The outer-sphere electron transfer mode practically has been excluded and activation parameters have been measured at physiological pH. The energy profiles describing the reduction of complexes **5**−**8** by ascorbate are depicted in Figure 2.

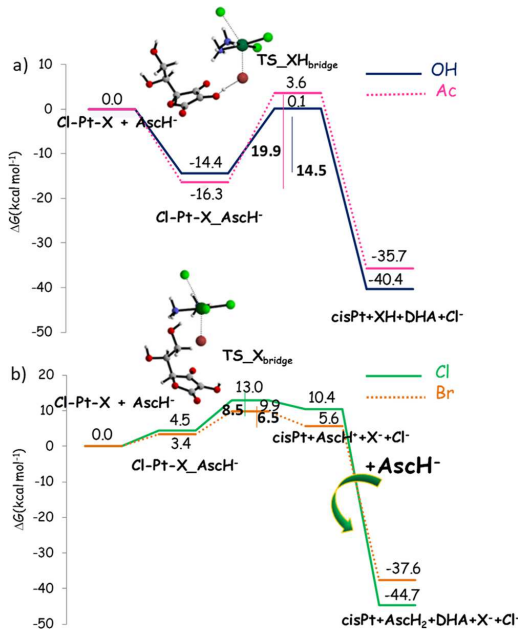

Figure 2. Calculated B3LYP-D3 free energy profiles in water describing the X-bridged electron transfer mechanism in the presence of ascorbate as reducing agent for (a) **5** (X = OH), solid line, and **8** (X= OAc), dotted line, and (b) **6** (X = Cl), solid line, and **7** (X = Br), dotted line. Energies are in kcal·mol^{-1} and are relative to separated reactants.

DOI: 10.1021/acs.inorgchem.8b03486
Inorg. Chem. 2019, 58, 3851−3860

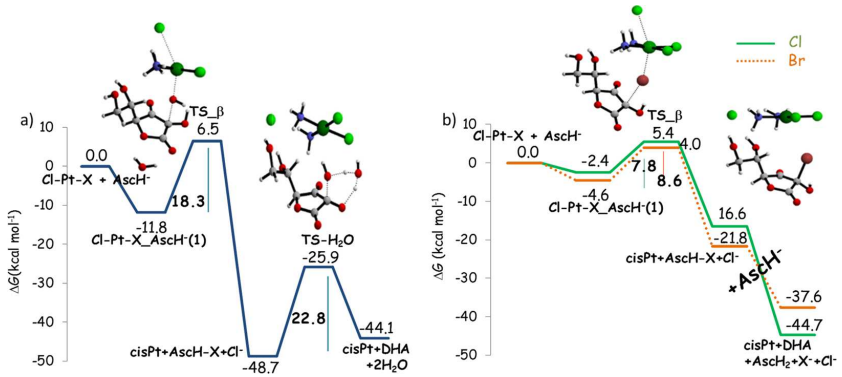

Figure 3. Calculated B3LYP-D3 free energy profiles in water describing the enolate β-carbon attack mechanism in the presence of ascorbate as reducing agent for (a) **5** (X = OH) and (b) **6** (X = Cl), solid line, and 7 (X = Br), dotted line. Energies are in kcal mol^{-1} and are relative to separated reactants.

The two (**5** and **8**) cisplatin derivatives undergo the two-electrons reduction reaction following a mechanism that, in analogy with complexes **1** and **4**, involves the transfer of a H$^-$ unit from the OH group of the ascorbate to the bridging hydroxido and acetato ligands, respectively, to form the oxidized form of ascorbic acid, DHA. Formed water and acetic acid molecules detach from the platinum center inducing the simultaneous detachment of the *trans* chlorido ligand. After the exergonic formation of the first adduct (−14.4 and −16.3 kcal mol^{-1} for OH and OAc, respectively), for the subsequent rearrangement to take place it is required that a barrier of 14.5 kcal mol^{-1} for the OH ligand and 19.9 kcal mol^{-1} for the OAc ligand is overcome. The corresponding transition states are characterized by 94*i* and 172*i* cm^{-1} imaginary frequencies, respectively.

The whole process is calculated to be exergonic by 40.4 and 35.7 kcal mol^{-1} for complexes **5** and **8**, respectively. Comparison with the results obtained for complexes **1** and **4**, shows that the reduction process is not greatly affected by the identity of the *trans* ligand. When the reduction behavior of **6** and **7** complexes is examined, Cl and Br only act as bridging ligands allowing two-electron transfer after the endergonic formation of the initial adducts (4.5 and 3.4 kcal mol^{-1} for Cl and Br, respectively). In the subsequent transition state, chlorido and bromido ligands interact with the deprotanated oxygen of the ascorbate reducing agent causing the detachment of the *trans* chlorido ligand. The imaginary frequencies are 65*i* and 68*i* cm^{-1} for chlorido and bromido, respectively. Such rearrangement has an energetic cost of 8.5 kcal mol^{-1} for Cl and 6.5 kcal mol^{-1} for Br and leads to the release of the anionic axial ligands, the reduced platinum complex and protonated dehydroascorbate. Products lie 10.4 and 5.6 kcal mol^{-1}, respectively above the zero reference energy.

The Pt(IV) to Pt(II) reduction is completed by the intervention of a species, that we have imagined to be a second AscH$^-$ unit, capable to accept the proton from the OH group of the dehydroascorbate. DHA together with the cisplatin complex and the detached axial ligands are afforded. Such step is barrierless and exergonic by 44.7 kcal mol^{-1} for the **6** complex and 37.6 kcal mol^{-1} for the **7** one. With respect to our previous investigation,[18] the presence in *trans* position of the chlorido ligand, which is a good leaving group unable to accept the proton from the ascorbate, has a beneficial effect on the kinetics of the process as the calculated activation barriers significantly lower. Moreover, the assistance of an additional basic species is required in order to accomplish the reduction process.

The main conclusion of such analysis is that when the *trans* living ligand is the labile chlorido the rate of the reaction depends on the bridging ability that follows the expected trend (Br > Cl > OAc > OH) even if the role played by hydroxido and acetato is different with respect to that of chlorido and bromido ligands.

The outcomes of the examination of the alternative β-carbon inner-sphere mechanism involving the attack of the enolate β-carbon on the X = OH, Cl, Br ligands, of complexes **5**−**7**, are shown in Figure 3. Once again the β-carbon attack does not take place when X = OAc.

In the first step the adduct, **Cl−Pt-X_AscH$^-$** (**1**), which favorably orients the ascorbate to facilitate the nucleophilic attack of the enolate β-carbon on the X (X = OH, Cl, Br) ligand, is formed. All the intermediates lie lower in energy with respect to reactants: −11.8, −2.4, and −4.8 kcal mol^{-1} for OH, Cl and Br, respectively. As a consequence of the attack a new C−X bond is formed and simultaneously the *trans* chlorido ligand is released. The intercepted concerted transition states, are identified by a negative frequency (120*i* cm^{-1} for the hydroxido and 85*i* cm^{-1} for both chlorido and bromido ligands) corresponding to such rearrangement and the calculated barriers are 18.3 kcal mol^{-1} for the hydroxido complex and 7.8 and 8.6 kcal mol^{-1} for the chlorido and bromido ones, respectively. The reaction is calculated to be exergonic for all the examined complexes, as shown in Figure 3, and leads to the release of the cisplatin complex, the free chlorido *trans* ligand and the intermediate species in which the X atom is bonded to the enolate β-carbon in geminal position to the OH. In the case of the hydroxido complex (**5**), elimination of a water molecule requires an auxiliary water molecule that assists the process acting as a proton shuttle. The calculated barrier height for the corresponding transition state is 22.8 kcal mol^{-1} and leads to the exergonic formation of the final products. For the chlorido and bromido complexes (**6** and **7**), instead, the action of a second AscH$^-$ unit causes the OH group deprotonation and the final products formation in a

DOI: 10.1021/acs.inorgchem.8b03486
Inorg. Chem. 2019, 58, 3851−3860

barrierless process. The whole process results to be exergonic by 44.7 and 37.6 kcal mol^{-1} for the chlorido and bromido complexes, respectively.

The height of the calculated barriers for both inner sphere ligand-bridging and β-carbon mechanisms for complex **6**, even if lower than the value which can be obtained using the activation parameters measured by Dong et al.[19b] ($\Delta H^{\ddagger}$ = 46.7 ± 1.5 kJ mol^{-1}, $\Delta S^{\ddagger}$ = −34 ± 9 J K^{-1} mol^{-1}), support the hypothesis that the electron transfer occurs in an inner-sphere fashion.

2.3. Inner-Sphere Reduction of [Pt(dach)(Ox)(X)-(aspirin)], X = OH, Cl. As anticipated above, in order to understand how the nature of the ligands in equatorial position can influence the Pt(IV) complexes reduction, two possible oxaliplatin derivatives have been considered: with one aspirinate and one hydroxido ligand (**9**), with one aspirinate and one chlorido ligand (**10**). For each complex, both inner bridging and β-carbon mechanisms have been examined. Outcomes for the bridging mechanism are shown in Figure 4.

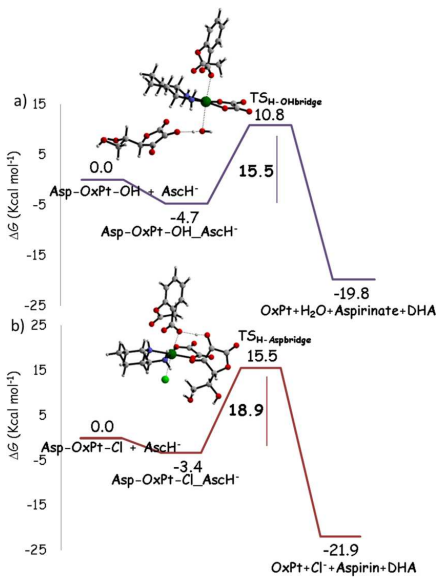

Figure 4. Calculated B3LYP-D3 free energy profiles in water describing the bridging reduction mechanism in the presence of ascorbate as reducing agent for (a) **9** (X = OH) and (b) **10** (X = Cl), complexes. Energies are in kcal·mol^{-1} and relative to separated reactants.

Along the calculated pathways the structures of the intercepted transition states are sketched. For the oxaliplatin derivative (**9**) having a hydroxido group in *trans* position to the aspirinate ligand, the reaction proceeds following the same steps already illustrated above, and the drawn energy profile strictly mirrors those of **1** and **5** complexes. After the formation of the first adduct (ΔG = −4.7 kcal mol^{-1}), reduction takes place by the transfer of a H$^-$ unit to the OH group causing the contemporaneous detachment of a water molecule and the *trans* aspirinate ligand. The active Pt(II) species and the DHA oxidized form of ascorbic acid are formed. The intercepted transition state lies 10.8 kcal mol^{-1} above the zero reference energy of reactants for a calculated barrier of 15.5 kcal mol^{-1}, and is characterized by an imaginary frequency of 75*i* cm^{-1}. The whole reaction is exergonic by 19.8 kcal mol^{-1}. The behavior of complex (**10**), having in axial position a chlorido in *trans* position to the aspirinate, significantly differs with respect to the similar situations already examined.

Indeed, many unsuccessful attempts have been carried out to locate a transition state for the formation of a bridge between the negatively charged ascorbate oxygen atom and the Cl ligand to allow two-electron transfer. Due to the steric hindrance of the ligands in equatorial position, the two-electron transfer through the Cl bridging ligand accompanied by the proton shift from the OH group of the ascorbate to the *trans* aspirinate cannot occur. The only intercepted transition state, named $\mathbf{TS_{H\text{-}Aspbridge}}$, involves the shift of a H$^-$ unit from the OH group of the ascorbate to the aspirinate ligand leading to the detachment of an aspirin molecule. The *trans* chlorido ligand is released and oxaliplatin and DHA reduction products are formed. The height of the energy barrier that is necessary to overcome is 18.9 kcal mol^{-1}. The imaginary frequency that confirms the nature of this stationary point is 59*i* cm^{-1}.

The pathways describing the alternative inner-sphere mechanism comprising the nucleophilic attack of the enolate β-carbon to the OH and Cl ligand are shown in Figure 5. Once again the two (**9** and **10**) complexes behave differently as a consequence of the presence of a hydroxido and chlorido ligand in *trans* to the aspirinate. Indeed, after the slightly exergonic formation of the first adduct (−0.4 kcal mol^{-1} for OH and −3.3 kcal mol^{-1} for Cl), the reaction proceeds with the β-carbon attack of the ascorbate on the living ligand forming new C−O and C−Cl bonds and causing the *trans* aspirinate ligand release. The calculated barrier is 21.5 kcal mol^{-1} for both complexes, whereas the reaction is exergonic by 18.9 and 1.9 kcal mol^{-1} for the **Asp-OxPt−OH** and **Asp-OxPt-Cl**, respectively. The oxaliplatin complex, the free aspirinate ligand and the intermediate species in which the OH and Cl moieties are bonded to the enolate β-carbon in germinal position to the OH are formed. The imaginary frequencies characterizing these TSs are 247*i* for **Asp-OxPt−OH** and 122*i* cm^{-1} for **Asp-OxPt-Cl**. The reaction is completed by the release of a water molecule for complex (**9**) assisted by an additional water molecule and surpassing a barrier of 20.0 kcal mol^{-1}. The transition state structure is characterized by an imaginary frequency of 1177*i* cm^{-1}. Detachment of the Cl$^-$ ion and deprotonation of the OH group to yield the oxidized DHA product occurs in the presence of a second AscH$^-$ unit in a barrierless fashion according to what observed in all analogous situations.

2.4. Calculated Two-Electron Reduction Potentials of Complexes 1−10. Although standard cyclic voltammetry has been routinely used to characterize redox behavior of Pt(IV) antitumor compounds, the study of the reduction process involving transfer of two electrons and release of the two axial ligands is challenging owing to the intrinsic irreversibility of the reduction and the influence that the rate of the ligand loss can have on the thermodynamics and kinetics of the process. The two-electron redox process is commonly observed as a single irreversible reduction event, and the peak potential for the cathodic wave obtained in cyclic voltammetric measurements is usually used to measure the ease of reduction instead of the standard redox potential. Peak potentials, however, strongly depend on the experimental conditions. Therefore, it is matter

DOI: 10.1021/acs.inorgchem.8b03486
Inorg. Chem. 2019, 58, 3851−3860

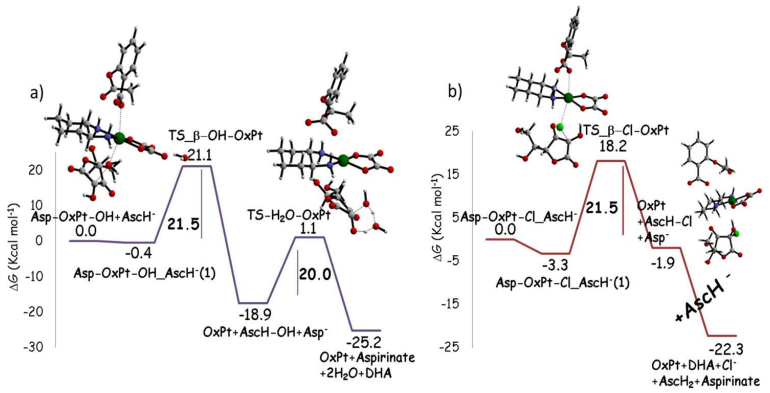

Figure 5. Calculated B3LYP-D3 free energy profiles in water describing the enolate β-carbon attack mechanism in the presence of ascorbate as reducing agent for (a) **9** (X = OH) and (b) **10** (X = Cl) complexes. Energies are in kcal·mol^{-1} and relative to those of separated reactants.

of debate the possibility to extract information about the redox behavior of Pt(IV) prodrugs from such measurements.

Baik and co-workers in a recent study,[17] have carried out a series of electrochemical experiments to study the mechanism of the two-electron reduction of Pt(IV) cisplatin derivatives demonstrating that electron transfer and Pt−ligand bond cleavage occur in a stepwise fashion, thus leading to the formation of a metastable six-coordinate Pt(III) intermediate upon the first electron addition. From this intermediate the two axial ligands are removed sequentially, being the second ligand released as a consequence of the second electron addition. Furthermore, density functional calculations have been performed to elucidate the reduction mechanism and estimate standard reduction potentials. Indeed, on the basis of the adopted decomposition scheme the reduction potential can be calculated as the energy change that accompanies the one electron transfer for the reduction of the six-coordinate Pt(IV) complex to the corresponding six-coordinate Pt(III) (see Scheme 3) species with the axial ligand remaining in the coordination sphere of the metal center as it is illustrated in the Computational Details section.

Scheme 3. First Step of the Decomposition Scheme Proposed by Baik et al. for the First Electron Transfer

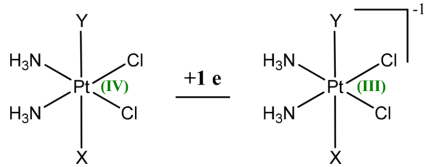

The reduction potential is computed as $E_{first}^{\circ} = -\Delta G_{(sol)} - 4.43$ V, where $\Delta G_{(sol)}$ is the Gibbs free energy change in solution for the one electron transfer to the Pt(IV) complex and 4.43 V is the absolute potential of the standard hydrogen electrode (SHE) in water used as a reference. The values of the calculated redox potential for all the examined complexes are collected in Table 1. The difference in behavior between the Asplatin complex (**1**) and its Asp-Cl (**2**) and Asp-Br (**3**) derivatives has been already underlined.[18] Indeed, the addition of one electron to **2** and **3** complexes causes the spontaneous release of the aspirinate ligand that, according to the results reported by Baik and co-workers,[17] remains in the primary coordination sphere of the metal center forming hydrogen bonds with the equatorial ammonia ligands.

As formation of such bonds is unrealistic in solvent, explicit water molecules have to be included for a more realiable simulation. Aspirinate detachment from complex **1**, instead, takes place, overcoming an energy barrier. In analogous way, full optimization of the structure of six coordinate Pt(III) anionic complexes obtained by adding an electron to neutral (**4**−**10**) complexes has been carried out in gas-phase without imposing any geometrical constrain. Spontaneous release of the first ligand as a consequence of one electron addition has been observed for **6**, **7**, and **8** cisplatin derivatives. Thus, explicit water molecules, which have been removed for subsequent calculations in implicit solvent, have been added around the axial ligands. For the rest of complexes, the electrochemical and chemical events occur in two separate steps.

The calculated standard reduction potentials allow to estimate the propensity of the examined complexes to be reduced. Therefore, the possibility that the reduction occurs, if an outer-sphere mechanism is assumed to be operative, depends principally on the nature of axial ligands and increases

Table 1. Standard Reduction Potentials, in eV, Calculated as the Energy Change That Accompanies the First Step One-Electron Transfer for the Reduction of the Six-Coordinate Pt(IV) Complexes in the Proposed by Baik et al.[17] Decomposition Scheme

E_{first}°	(**1**) Asp-OH −0.241	(**2**) Asp-Cl 0.127	(**3**) Asp-Br 0.279	(**4**) Asp-OAc −0.051
E_{first}°	(**5**) Cl−Pt−OH −0.163	(**6**) Cl−Pt−Cl 0.374	(**7**) Cl−Pt−Br 0.439	(**8**) Cl−Pt−OAc 0.431
E_{first}°	(**9**) Asp-Oxpt−OH −0.536	(**10**) Asp-Oxpt-Cl 0.132		

DOI: 10.1021/acs.inorgchem.8b03486
Inorg. Chem. 2019, 58, 3851−3860

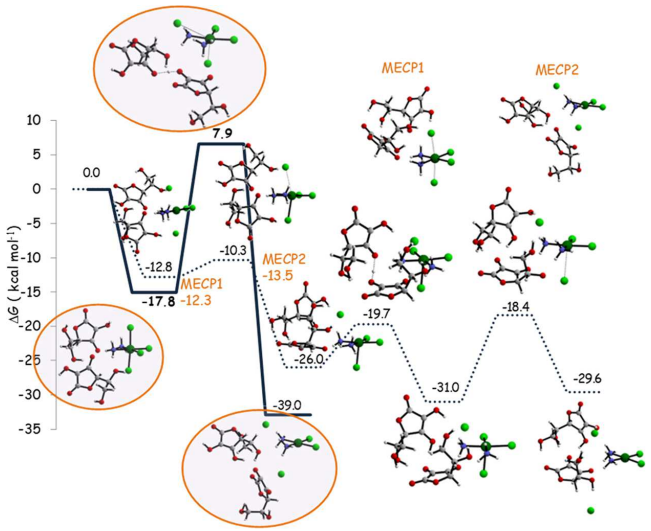

Figure 6. Singlet (solid) and triplet (dotted) crossing free energy profiles for the Cl−Pt−Cl (**6**) complex describing the "base-assisted" outer-sphere electron transfer mechanism in presence of ascorbate as reducing agent. Energies are in kcal mol^{-1} and relative to separated reactants.

in the order: OH < OAc < Cl < Br. Moreover, the tendency to be reduced increases when in cisplatin derivatives the aspirinate ligand is substituted by the chlorido one. Concerning the influence of the nature of the equatorial ligands, it appears that the rate of the reduction for cisplatin derivatives is generally higher than oxaliplatin ones. The trend in the tendency to be reduced by an outer-sphere mechanism does not necessarily correspond to the trend in the rate of reduction by an inner-sphere mechanism. This disagreement can explain the observed lack of correlation between the measured rates of reaction and the reduction potentials.[10b,11c]

The calculated valued of 0.374 eV of the standard reduction potential for complex (**6**) compared with the measured value −0.206 eV,[23] versus the normal hydrogen electrode, confirms the already reported trends.[17,18] That is, redox potentials calculated adopting such procedure are considerably different from those reported in the literature, corresponding to a redox-stability higher than the real one.

2.5. Potential Energy Surface Description of the Outer-Sphere Electron Transfer Mechanism. According to the hypothesis that the outer-sphere reduction mechanism involves the sequential addition of two electrons causing the formation of a Pt(III) intermediate, the possibility that singlet and triplet pathways can cross has been recently computationally examined for the [Pt(dach)Cl$_4$] (dach = diaminocyclohexane) model complex.[16] Here, the results of an analogous calculation carried out for complex (**6**) having two axial chlorido ligands are reported. Free energy profiles for both singlet and triplet multiplicities are drawn in Figure 6. Relative free energies in solution have been calculated with respect to the ground-state singlet reactants' asymptote (**6**) + 2AscH$^-$. The adduct formed by the Cl−Pt−Cl (**6**) complex and two ascorbate molecules has been optimized in both singlet and triplet multiplicities. The singlet and triplet adducts lie 17.8 and 12.8 kcal mol^{-1}, respectively below the entrance channel. The reduction reaction, along the singlet pathway directly leads to the formation of the products: cisplatin, two chlorido ligands, ascorbic acid and dehydroascorbic acid. The concerted transition state, that is necessary to overcome for the reduction to occur, lies 7.9 kcal mol^{-1} above the reactants' reference energy for a barrier of 25.7 kcal mol^{-1}. The imaginary frequency is 59.2i cm^{-1}. The rearrangement of the reactants involves the elimination of the two axial chlorido ligands as a consequence of the outer-sphere two-electrons transfer and the proton shift from one of the ascorbates to the other, leading to the formation of both ascorbic and dehydroascorbic acids. The reaction is calculated to be exergonic by 39.0 kcal mol^{-1}. The presence of two ascorbate units is required for the proton shift to occur simultaneously with the electron transfer. Indeed, a very huge number of attempts carried out in presence of only one ascorbate unit all failed. It is worth underlining that such mechanism corresponds to the mechanism classified as "base assisted outer-sphere" by Ejehi and Ariafard, found to be the preferred one for the reduction of the [Pt(dach)Cl$_4$] complex.[16] Along the triplet surface the reaction takes place going through several intermediates. Once the first adduct is formed the reaction proceeds with the transfer of one electron leading to the release of one chlorido ligand and formation of a penta-coordinated intermediate more stable than the previous one by 13.2 kcal mol^{-1}. The barrier for the corresponding transition state is only 2.5 kcal mol^{-1} and the imaginary frequency is 38.5i cm^{-1}. In the next step the transfer of the proton from one ascorbate to the other occurs surmounting an energy barrier of 6.3 kcal mol^{-1}, and forming a stable intermediate at −31.0 kcal mol^{-1}. The TS is characterized by an imaginary frequency of 391.0i cm^{-1}.

In the last step the second electron is transferred causing the detachment of the second axial Cl ligand and therefore the exergonic (ΔG = −29.6 kcal mol^{-1}) formation of the final products.

A careful search of the minimum energy crossing points (MECPs) has allowed to identify the structure and the energy of the points where the singlet and triplet PESs cross along

DOI: 10.1021/acs.inorgchem.8b03486
Inorg. Chem. 2019, 58, 3851−3860

with the calculation of the frequencies within the seam of crossing for both MECPs.

The reaction starts in a singlet state and, immediately after, a crossing occurs avoiding the high energy barrier for the singlet transition state. In going from the singlet state adduct to the triplet transition state it is necessary to overcome a barrier of 7.5 kcal mol^{-1}. As it is evident from both geometry and energy of this point, the crossing occurs in the vicinity of the triplet minimum with the MECP1 structure that lies only 0.5 kcal mol^{-1} higher in energy. In the framework of the two-state reactivity (TSR) paradigm, this kind of spin crossing occurring before formation of the transition state has to be considered a rate-limiting factor.[24] The second surface spin crossing occurs after the triplet transition state is surpassed and due to the spin change the reaction finishes with the formation of the products in a singlet spin multiplicity. Looking at the energy of the MECP2 reported in Figure 6, it appears that it is closer to the triplet transition state and, as it is located after the transition states, does not play a key role. This process is a typical example of the TSR paradigm[24] as a reaction that is not viable becomes accessible thanks to a spin change and products formation arises from an interplay of spin inversion and the respective barrier heights on both spin surfaces. Moreover, the reaction is formally spin conserving as reactants and products ground states have the same spin multiplicity. Along the reaction path, the reaction starts in a singlet state, the spin is changed to triplet to avoid the very high energy singlet transition state and continues to form the final products in a singlet state. It is worth mentioning that only if the spin inversions are taken into consideration do the so-called base-assisted outer-sphere path become viable and competitive with respect to the described inner-sphere alternatives.

3. SUMMARY AND CONCLUSIONS

In this paper, the outcomes of a systematic investigation of the key reduction step of Pt(IV) antiproliferative complexes have been illustrated. In order to obtain information on the influence of the identity of ligands in axial and equatorial position, both cisplatin and oxaliplatin derivatives have been examined and compared varying involved ligands. Mono-deprotonated ascorbic acid has been used as reducing agent model. The usually invoked classification of Pt(IV) into Pt(II) complexes reduction mechanisms as inner- and outer-sphere does not properly account for all the possible alternatives. Indeed, beside the possible involvement of Pt(II) as catalyst that has been considered to be not viable, the inner-sphere mechanisms have been classified as (a) ligand-bridged, (b) ligand-bridged-H transfer, and (c) enolate β-carbon attack. Results reported here show that (i) for both OH and OAc ligands the inner sphere two-electron transfer, classified as ligand-bridged-H transfer, is the preferred mechanism. The rate of the process is not influenced by the identity of the ligands in both axial and equatorial positions. The enolate β-carbon attack can occur for the OH group but overcoming higher energy barriers, whereas it does not take place when the OAc ligand is involved. (ii) For Cl and Br ligands, the preferred mechanism is a function of the nature of the ligands in *trans*-axial and equatorial positions. When cisplatin derivatives are taken into consideration and the *trans* ligand is Cl the inner-sphere ligand-bridged is the most favorable mechanism. When the ligand in *trans* is the aspirinate, the calculated barriers become significantly higher and the enolate β-carbon attack becomes the preferred mechanism. (iii) For the Cl oxaliplatin derivative having aspirinate in *trans* axial position, the reduction occurs by the ligand-bridged-H transfer mechanism involving the aspirinate ligand. Very likely the mechanism changes due to the equatorial ligands steric hindrance. The enolate β-carbon attack can occur, but it is not competitive.

The exploration of the so-called base-assisted outer-sphere mechanism shows that both singlet and triplet multiplicities are involved. The apparently spin conserving process starts in a singlet state, the spin is changed to triplet to avoid the very high energy singlet transition state and continues along the singlet energy profile, due to a second spin crossing, to form the final products. The spin inversions allow the base-assisted outer-sphere mechanism to be accessible and competitive with respect to inner-sphere alternatives.

Finally, redox potentials calculated for all the Pt(IV) complexes under examination by separating the steps for the electron transfer from those for the axial ligand release, show that the propensity to be reduced by an outer-sphere mechanism depends principally on the nature of axial ligands. Such propensity increases in the order: OH < OAc < Cl < Br and the rate of the reduction decreases in going from cisplatin derivatives to oxaliplatin ones. Calculated values for the cisplatin derivative (**6**) having two chlorido ligands in axial position confirms that generally used peak potentials are significantly more negative than redox potentials computed adopting this method.

In conclusion, results demonstrate that the propensity of Pt(IV) prodrugs to be reduced can be appropriately modulated. The inner-sphere, in its different mechanistic alternatives, is the preferred mode of reduction, when monoanionic ascorbate is the reducing agent, for some of the examined cases. Very low calculated energy barriers strongly support the thesis, already formulated, that these prodrugs can hardly reach the target before reduction and the reduction takes place extracellularly.

4. COMPUTATIONAL DETAILS

All molecular geometry optimizations have been carried out with the Gaussian09 software package,[25] at density functional level of theory employing the B3LYP functional[26,27] and including dispersion corrections for nonbonding interaction through the Grimme approach[28] that uses an atom pairwise additive scheme denoted as DFT-D3.

For the Pt atom, the relativistic compact Stuttgart/Dresden effective core potential has been used[29] in conjunction with the split valence basis set. For the atoms directly participating in the process the standard triple-ζ quality 6-311+G** basis sets of Pople and co-workers have been used, while to reduce the computational effort, for peripheral atoms, the 6-311G** basis sets have been employed.

Calculation of vibrational frequencies at the same level of theory has been carried out to both establishing the nature of intercepted stationary points as minima and transition states and calculating both zero-point energy (ZPE) and Gibbs free energy corrections. The involved transition states have been carefully checked to be properly connected to the correct minima by IRC (intrinsic reaction coordinate) analysis.[30]

With the purpose of characterizing the MECPs, geometries and corresponding frequencies have been calculated with the help codes developed for the localization of MECPs[31] and the vibrational frequency analysis at these points (GlowFreq).[32,33]

DOI: 10.1021/acs.inorgchem.8b03486
Inorg. Chem. 2019, 58, 3851−3860

In the decomposition scheme proposed by Baik and coworkers,[17] it is assumed that electron transfer occurs separately with respect to ligand release. However, it can happen that in Pt(III) anionic intermediates ligands are released and remain in the metal coordination sphere as a consequence of the bonding interactions with the equatorial ligands. As these structures are unrealistic in solvent, explicit water molecules in proximity of the axial ligands have been included for the gas-phase optimizations and removed for subsequent calculations in implicit solvent.

The effects due to the presence oft he solvent have been taken into consideration by using the Tomasi's implicit polarizable continuum model (PCM)[34] as implemented in Gaussian09. The UFF set of radii has been used to build-up the cavity in which solute molecules are accommodated. Single-point calculations on all stationary points structures obtained in vacuum have been carried out in implicit water (ε = 78.4) at the same level for obtaining solvation Gibbs free energies. Using standard statistical procedures,[35] enthalpies and Gibbs free energies have been obtained at 298 K at 1 atm from total energies, including zero-point, thermal and solvent corrections. However, mainly when association and dissociation steps are involved, the entropic change that occurs when a solute is transferred from the gas- to the condensed-phase is not properly taken into consideration the following correction scheme has been adopted. Since the Gaussian's default standard state corresponds to an ideal gas at a standard pressure of 1 atm, the computed free energies have been converted[36] to yield Gibbs energies with a solution phase standard state of 1 mol L^{-1} for all the species. For water molecules a standard state of 55.5 M has been used. That is, to the free energy of each species, as computed in Gaussian, a free energy correction term equal to $RT \ln(V_{\text{molar gas}}/V_{\text{molar solution}})$, ($R$ = gas constant, T = absolute temperature) has been added, where $V_{\text{molar gas}}$ is the volume occupied by one mole of ideal gas at the considered temperature, and $V_{\text{molar solution}}$ is the volume occupied by one mole of species in a standard solution of concentration 1 mol L^{-1}.

AUTHOR INFORMATION

Corresponding Author

*(E.S.) E-mail: emilia.sicilia@unical.it.

ORCID

Emilia Sicilia: 0000-0001-5952-9927

Notes

The authors declare no competing financial interest.

REFERENCES

(1) (a) Johnstone, T. C.; Suntharalingam, K.; Lippard, S. J. The Next Generation of Platinum Drugs: Targeted Pt(II) Agents, Nanoparticle Delivery, and Pt(IV) Prodrugs. *Chem. Rev.* **2016**, *116*, 3436−3486. (b) Dilruba, S.; Kalayda, G. V. Platinum-based drugs: past, present and future. *Cancer Chemother. Pharmacol.* **2016**, *77*, 1103−1124.

(2) (a) Klein, A. V.; Hambley, T. W. Platinum Drug Distribution in Cancer Cells and Tumors. *Chem. Rev.* **2009**, *109*, 4911−4920. (b) Benedetti, M.; Ducani, C.; Migoni, D.; Antonucci, D.; Vecchio, V. M.; Ciccarese, A.; Romano, A.; Verri, T.; Ciccarella, G.; Fanizzi, F. P. Experimental evidence that a DNA polymerase can incorporate N7-platinated guanines to give platinated DNA. *Angew. Chem.* **2008**, *120*, 517−520. (c) Carrisi, C.; Romano, A.; Lunetti, P.; Antonucci, D.; Verri, T.; De Benedetto, G. E.; Dolce, V.; Fanizzi, F. P.; Benedetti, M.; Capobianco, L. Platinated nucleotides are substrates for the human mitochondrial deoxynucleotide carrier (DNC) and DNA polymerase. Relevance for the development of new platinum based drugs. *Chemistry SELECT* **2016**, *1*, 4633−4637. (d) Benedetti, M.; Romano, A.; De Castro, F.; Girelli, C. R.; Antonucci, D.; Migoni, D.; Verri, T.; Fanizzi, F. P. N7-platinated ribonucleotides are not incorporated by RNA polymerases. New perspectives for a rational design of platinum antitumor drugs. *J. Inorg. Biochem.* **2016**, *163*, 143−146.

(3) Gibson, D. The mechanism of action of platinum anticancer agents—what do we really know about it? *Dalton Trans* **2009**, 10681−10689.

(4) Bugarčić, Ž. D.; Bogojeski, J.; Petrović, B.; Hochreuther, S.; van Eldik, R. Mechanistic studies on the reactions of platinum(II) complexes with nitrogen- and sulfur-donor biomolecules. *Dalton Trans* **2012**, *41*, 12329−12345.

(5) (a) Galluzzi, L.; Senovilla, L.; Vitale, I.; Michels, J.; Martins, I.; Kepp, O.; Castedo, M.; Kroemer, G. Molecular mechanisms of cisplatin resistance. *Oncogene* **2012**, *31*, 1869−1883. (b) Wexselblatt, E.; Yavin, E.; Gibson, D. Cellular interactions of platinum drugs. *Inorg. Chim. Acta* **2012**, *393*, 75−83.

(6) (a) Graf, N.; Lippard, S. J. Redox activation of metal-based prodrugs as a strategy for drug delivery. *Adv. Drug Delivery Rev.* **2012**, *64*, 993−1004. (b) Pathak, R. K.; Marrache, S.; Choi, J. H.; Berding, T. B.; Dhar, S. The Prodrug Platin-A: Simultaneous Release of Cisplatin and Aspirin. *Angew. Chem., Int. Ed.* **2014**, *53*, 1963−1967. (c) Cheng, Q.; Shi, H.; Wang, H.; Min, Y.; Wang, J.; Liu, Y. The ligation of aspirin to cisplatin demonstrates significant synergistic effects on tumor cells. *Chem. Commun.* **2014**, *50*, 7427−7430. (d) Gabano, E.; Ravera, M.; Osella, D. Pros and cons of bifunctional platinum(IV) antitumor prodrugs: two are (not always) better than one. *Dalton Trans* **2014**, *43*, 9813−9820. (e) Butler, J. S.; Sadler, P. J. Targeted delivery of platinum-based anticancer complexes. *Curr. Opin. Chem. Biol.* **2013**, *17*, 175−188.

(7) (a) Wexselblatt, E.; Yavin, E.; Gibson, D. Platinum(IV) Prodrugs with Haloacetato Ligands in the Axial Positions can Undergo Hydrolysis under Biologically Relevant Conditions. *Angew. Chem., Int. Ed.* **2013**, *52*, 6059−6062. (b) Ritacco, I.; Mazzone, G.; Russo, N.; Sicilia, E. Investigation of the Inertness to Hydrolysis of Platinum(IV) Prodrug. *Inorg. Chem.* **2016**, *55*, 1580−1586. (c) Bradáč, O.; Zimmermann, T.; Burda, J. V. Can Satraplatin be hydrated before the reduction process occurs? The DFT computational study. *J. Mol. Model.* **2013**, *19*, 4669−4680.

(8) (a) Nemirovski, A.; Kasherman, Y.; Tzaraf, Y.; Gibson, D. Reduction of cis,trans,cis-[PtCl2(OCOCH3)2(NH3)2] by aqueous extracts of cancer cells. *J. Med. Chem.* **2007**, *50*, 5554−5556. (b) Jungwirth, U.; Kowol, C. R.; Keppler, B. K.; Hartinger, C. G.; Berger, W.; Heffeter, P. Anticancer activity of metal complexes: involvement of redox processes. *Antioxid. Redox Signaling* **2011**, *15*, 1085−1127. (c) Lasorsa, A.; Stuchlikova, O.; Brabec, V.; Natile, G.; Arnesano, F. Activation of Platinum(IV) Prodrugs by Cytochrome c and Characterization of the Protein Binding Sites. *Mol. Pharmaceutics* **2016**, *13*, 3216−3223.

(9) Choi, S.; Filotto, C.; Bisanzo, M.; Delaney, S.; Lagasee, D.; Whitworth, J. L.; Jusko, A.; Li, C. R.; Wood, N. A.; Willingham, J.; Schwenker, A.; Spaulding, K. Reduction and Anticancer Activity of Platinum(IV) Complexes. *Inorg. Chem.* **1998**, *37*, 2500−2504.

(10) (a) Lemma, K.; Sargeson, A. M.; Elding, L. I. Kinetics and mechanism for reduction of oral anticancer platinum(IV) dicarboxylate compounds by L-ascorbate ions. *J. Chem. Soc., Dalton Trans.* **2000**, 1167−1172. (b) Lemma, K.; House, D. A.; Retta, N.; Elding, L. I. Kinetics and mechanism for reduction of halo- and haloam(m)ine platinum(IV) complexes by L-ascorbate. *Inorg. Chim. Acta* **2002**, *331*, 98−108.

(11) (a) Nemirovski, A.; Vinograd, I.; Takrouri, K.; Mijovilovich, A.; Rompel, A.; Gibson, D. New reduction pathways for ctc-[PtCl2-(CH3CO2)2(NH3)(Am)] anticancer prodrugs. *Chem. Commun.* **2010**, *46*, 1842−1844. (b) Zhang, J. Z.; Wexselblatt, E.; Hambley, T. W.; Gibson, D. Pt(IV) analogs of oxaliplatin that do not follow the expected correlation between electrochemical reduction potential and rate of reduction by ascorbate. *Chem. Commun.* **2012**, *48*, 847−849.

DOI: 10.1021/acs.inorgchem.8b03486
Inorg. Chem. 2019, 58, 3851−3860

(c) Wexselblatt, E.; Gibson, D. What do we know about the reduction of Pt(IV) pro-drugs? *J. Inorg. Biochem.* **2012**, *117*, 220−229.
(12) Sinisi, M.; Intini, F. P.; Natile, G. Dependence of the reduction products of platinum(IV) prodrugs upon the configuration of the substrate, bulk of the carrier ligands, and nature of the reducing agent. *Inorg. Chem.* **2012**, *51*, 9694−9704.
(13) (a) Varbanov, H. P.; Valiahdi, S. M.; Kowol, C. R.; Jakupec, M. A.; Galanski, M.; Keppler, B. K. Novel tetracarboxylatoplatinum(IV) complexes as carboplatin prodrugs. *Dalton Trans* **2012**, *41*, 14404−14415. (b) Pichler, V.; Göschl, S.; Meier, S. M.; Roller, A.; Jakupec, M. A.; Galanski, M.; Keppler, B. K. Bulky N(,N)-(di)alkylethane-1,2-diamineplatinum(II) Compounds as Precursors for Generating Unsymmetrically Substituted Platinum(IV) Complexes. *Inorg. Chem.* **2013**, *52*, 8151−8162. (c) Chen, C. K. J.; Zhang, J. Z.; Aitken, J. B.; Hambley, T. W. Influence of Equatorial and Axial Carboxylato Ligands on the Kinetic Inertness of Platinum(IV) Complexes in the Presence of Ascorbate and Cysteine and within DLD-1 Cancer Cells. *J. Med. Chem.* **2013**, *56*, 8757−8764. (d) Pichler, V.; Göschl, S.; Schreiber-Brynzak, E.; Jakupec, M. A.; Galanski, M.; Keppler, B. K. Influence of reducing agents on the cytotoxic activity of platinum(IV) complexes: induction of G_2/M arrest, apoptosis and oxidative stress in A2780 and cisplatin resistant A2780cis cell lines. *Metallomics* **2015**, *7*, 1078−1090.
(14) (a) Hall, M. D.; Hambley, T. W. Platinum(IV) antitumour compounds: their bioinorganic chemistry. *Coord. Chem. Rev.* **2002**, *232*, 49−67. (b) Reisner, E.; Arion, V. B.; Keppler, B. K.; Pombeiro, A. J. L. Electron-transfer activated metal-based anticancer drugs. *Inorg. Chim. Acta* **2008**, *361*, 1569−1583.
(15) Weaver, E. L.; Bose, R. N. Platinum(II) catalysis and radical intervention in reductions of platinum(IV) antitumor drugs by ascorbic acid. *J. Inorg. Biochem.* **2003**, *95*, 231−239.
(16) Ejehi, Z.; Ariafard, A. A computational mechanistic investigation into the reduction of Pt(IV) prodrugs with two axial chlorides by biological reductants. *Chem. Commun.* **2017**, *53*, 1413−1416.
(17) McCormick, M. C.; Keijzer, K.; Polavarapu, A.; Schultz, F. A.; Baik, M. H. Understanding Intrinsically Irreversible, Non-Nernstian, Two-Electron Redox Processes: A Combined Experimental and Computational Study of the Electrochemical Activation of Platinum-(IV) Antitumor Prodrugs. *J. Am. Chem. Soc.* **2014**, *136*, 8992−9000.
(18) Ponte, F.; Russo, N.; Sicilia, E. Insights from Computations on the Mechanism of Reduction by Ascorbic Acid of Pt^{IV} Prodrugs with Asplatin and Its Chlorido and Bromido Analogues as Model Systems. *Chem. - Eur. J.* **2018**, *24*, 9572−9580.
(19) (a) Zhang, J. Z.; Wexselblatt, E.; Hambley, T. W.; Gibson, D. Pt(IV) analogs of oxaliplatin that do not follow the expected correlation between electrochemical reduction potential and rate of reduction by ascorbate. *Chem. Commun.* **2012**, *48*, 847−849. (b) Dong, J.; Ren, Y.; Huo, S.; Shen, S.; Xu, J.; Tian, H.; Shi, T. Reduction of ormaplatin and cis-diamminetetrachloroplatinum(iv) by ascorbic acid and dominant thiols in human plasma: kinetic and mechanistic analyses. *Dalton Trans* **2016**, *45*, 11326−11337.
(20) Šebesta, F.; Baxová, K.; Burda, J. V. Redox Potentials for Tetraplatin, Satraplatin, Its Derivatives and Ascorbic Acid; Computational Study. *Inorg. Chem.* **2018**, *57*, 951−962.
(21) Tolbatov, I.; Coletti, C.; Marrone, A.; Re, N. Insight into the Electrochemical Reduction Mechanism of Pt(IV) Anticancer Complexes. *Inorg. Chem.* **2018**, *57*, 3411−3419.
(22) Šebesta, F.; Burda, J. V. Interactions of Ascorbic Acid with Satraplatin and Its Trans Analog JM576; DFT Computational Study'. *Eur. J. Inorg. Chem.* **2018**, *2018*, 1481−1491.
(23) Gramatica, P.; Papa, E.; Luini, M.; Monti, E.; Gariboldi, M. B.; Ravera, M.; Gabano, E.; Gaviglio, L.; Osella, D. Antiproliferative Pt(IV) complexes: synthesis, biological activity, and quantitative structure-activity relationship modeling. *JBIC, J. Biol. Inorg. Chem.* **2010**, *15*, 1157−1169.
(24) Schröder, D.; Shaik, S.; Schwarz, H. Two-State Reactivity as a New Concept in Organometallic Chemistry. *Acc. Chem. Res.* **2000**, *33*, 139−145.
(25) Frisch, M. J.; Trucks, G. W.; Schlegel, H. B.; Scuseria, G. E.; Robb, M. A.; Cheeseman, J. R.; Scalmani, G.; Barone, V.; Mennucci, B.; Petersson, G. A.; Nakatsuji, H.; Caricato, M.; Li, X.; Hratchian, H. P.; Izmaylov, A. F.; Bloino, J.; Zheng, G.; Sonnenberg, J. L.; Hada, M.; Ehara, M.; Toyota, K.; Fukuda, R.; Hasegawa, J.; Ishida, M.; Nakajima, T.; Honda, Y.; Kitao, O.; Nakai, H.; Vreven, T.; Montgomery, Jr., J. A.; Peralta, J. E.; Ogliaro, F.; Bearpark, M.; Heyd, J. J.; Brothers, E.; Kudin, K. N.; Staroverov, V. N.; Keith, T.; Kobayashi, R.; Normand, J.; Raghavachari, K.; Rendell, A.; Burant, J. C.; Iyengar, S. S.; Tomasi, J.; Cossi, M.; Rega, N.; Millam, J. M.; Klene, M.; Knox, J. E.; Cross, J. B.; Bakken, V.; Adamo, C.; Jaramillo, J.; Gomperts, R.; Stratmann, R. E.; Yazyev, O.; Austin, A. J.; Cammi, R.; Pomelli, C.; Ochterski, J. W.; Martin, R. L.; Morokuma, K.; Zakrzewski, V. G.; Voth, G. A.; Salvador, P.; Dannenberg, J. J.; Dapprich, S.; Daniels, A. D.; Farkas, O.; Foresman, J. B.; Ortiz, J. V.; Cioslowski, J.; Fox, D. J. *Gaussian 09*, Revision D.01; Gaussian, Inc.: Wallingford CT, 2010.
(26) Becke, A. D. Density-functional thermochemistry. III. The role of exact exchange. *J. Chem. Phys.* **1993**, *98*, 5648−5652.
(27) Lee, C.; Yang, W.; Parr, R. G. Development of the Colle-Salvetti correlation-energy formula into a functional of the electron density. *Phys. Rev. B: Condens. Matter Mater. Phys.* **1988**, *37*, 785−789.
(28) Grimme, S.; Antony, J.; Ehrlich, S.; Krieg, H. A consistent and accurate ab initio parameterization of density functional dispersion correction (DFT-D) for the 94 elements H-Pu. *J. Chem. Phys.* **2010**, *132*, 154104−154122.
(29) Andrae, D.; Häussermann, U.; Dolg, M.; Stoll, H.; Preuss, H. Energy-adjusted ab initio pseudopotentials for the second and third row transition elements. *Theor. Chim. Acta* **1990**, *77*, 123−141.
(30) (a) Fukui, K. Formulation of the reaction coordinate. *J. Phys. Chem.* **1970**, *74*, 4161−4163. (b) Gonzalez, C.; Schlegel, H. B. An improved algorithm for reaction path following. *J. Chem. Phys.* **1989**, *90*, 2154−2161.
(31) Harvey, J. N.; Aschi, M.; Schwarz, H.; Koch, W. The Singlet and Triplet States of Phenyl Cation. A Hybrid Approach for Locating Minimum Energy Crossing Points between Non-interacting Potential Energy Surfaces. *Theor. Chem. Acc.* **1998**, *99*, 95−99.
(32) Gannon, K. L.; Blitz, M. A.; Liang, C.-H.; Pilling, M. J.; Seakins, P. W.; Glowacki, D. R.; Harvey, J. N. An experimental and theoretical investigation of the competition between chemical reaction and relaxation for the reactions of 1CH2 with acetylene and ethene: implications for the chemistry of the giant planets. *Faraday Discuss.* **2010**, *147*, 173−188.
(33) Plane, J. M. C.; Whalley, C. L.; Frances-Soriano, L.; Goddard, A.; Harvey, J. N.; Glowacki, D. R.; Viggiano, A. A. $O_2(a^1\Delta g)$ + Mg, Fe, and Ca: Experimental kinetics and formulation of a weak collision, multiwell master equation with spin-hopping. *J. Chem. Phys.* **2012**, *137*, 014310−20.
(34) (a) Miertuš, S.; Scrocco, E.; Tomasi, J. Electrostatic interaction of a solute with a continuum. A direct utilizaion of AB initio molecular potentials for the prevision of solvent effects. *Chem. Phys.* **1981**, *55*, 117−129. (b) Miertuš, S.; Tomasi, J. Approximate evaluations of the electrostatic free energy and internal energy changes in solution processes. *Chem. Phys.* **1982**, *65*, 239−245. (c) Pascual-Ahuir, J. L.; Silla, E.; Tuñón, I. GEPOL: An improved description of molecular surfaces. III. A new algorithm for the computation of a solvent-excluding surface. *J. Comput. Chem.* **1994**, *15*, 1127−1138.
(35) McQuarrie, D. A.; Simon, J. D. *Molecular Thermodynamics*; University Science Books: Sausalito, CA, 1999.
(36) Ashcraft, R. W.; Raman, S.; Green, H. W. Ab initio aqueous thermochemistry: application to the oxidation of hydroxylamine in nitric acid solution. *J. Phys. Chem. B* **2007**, *111*, 11968−11983.

DOI: 10.1021/acs.inorgchem.8b03486
Inorg. Chem. 2019, 58, 3851−3860

J. Am. Soc. Mass Spectrom. (2019) 30:1881–1894
DOI: 10.1007/s13361-019-02186-7

FOCUS: HONORING HELMUT SCHWARZ'S ELECTION TO THE NATIONAL ACADEMY OF SCIENCES: RESEARCH ARTICLE

Elusive Intermediates in the Breakdown Reactivity Patterns of Prodrug Platinum(IV) Complexes

Davide Corinti,[1] Maria Elisa Crestoni,[1] Simonetta Fornarini,[1] Fortuna Ponte,[2] Nino Russo,[2] Emilia Sicilia,[2] Elisabetta Gabano,[3] Domenico Osella[3]

[1]Dipartimento di Chimica e Tecnologie del Farmaco, Università di Roma "La Sapienza", P.le A. Moro 5, 00185, Rome, Italy
[2]Department of Chemistry and Chemical Technologies, Università della Calabria, Ponte P. Bucci Cubo 14c, 87036, Arcavacata di Rende, Italy
[3]Dipartimento di Scienze e Innovazione Tecnologica, Università del Piemonte Orientale, Viale T. Michel 11, 15121, Alessandria, Italy

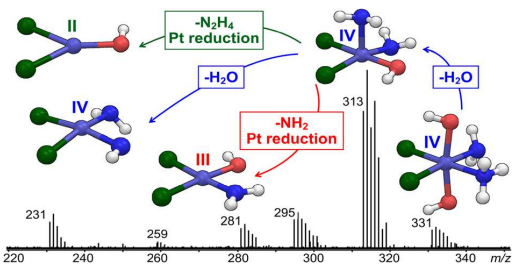

Abstract. Kinetically inert platinum(IV) complexes are receiving growing attention as promising candidates in the effort to develop safe and valid alternatives to classical square-planar Pt(II) complexes currently used in antineoplastic therapy. Their antiproliferative activity requires intracellular Pt(IV)–Pt(II) reduction (activation by reduction). In the present work, a set of five Pt(IV) complexes has been assayed using mass spectrometry–based techniques, i.e., collision-induced dissociation (CID), and IR multiple photon dissociation (IRMPD) spectroscopy, together with ab initio theoretical investigations. Breakdown and reduction mechanisms are observed that lead to Pt(II) species. Evidence is found for typically transient Pt(III) intermediates along the dissociation paths of isolated, negatively charged (electron-rich) Pt(IV) prodrug complexes.

Keywords: Collision-induced dissociation, IRMPD spectroscopy, FT-ICR mass spectrometry, Reduction processes, Cisplatin

Received: 1 February 2019/Revised: 1 March 2019/Accepted: 5 March 2019/Published Online: 12 April 2019

Introduction

The redox behavior of transition metal complexes has represented an important topic since the dawn of coordination chemistry [1]. In particular, the mechanism of reduction of six-coordinate octahedral d^6 Pt(IV) complexes to the corresponding four-coordinate square planar d^8 Pt(II) congeners has been intensely studied by Basolo and coworkers [2]. This process has gained renewed interest since evidence indicated that Pt(IV) anticancer prodrugs are reduced in the hypoxic tumor cells to the pharmacologically active Pt(II) counterparts (Scheme 1) [3–6]. The interpretation of the experimental data concerning such process is not conclusive though [7].

Electrochemical investigations have been hampered by the chemically irreversible character of such a reduction that impedes the evaluation of a meaningful thermodynamic potential [8], as well as by the quick poisoning of the working electrode surface [9]. A number of computational studies at density functional theory (DFT) level have been recently carried out in order to estimate the electrochemical potentials and to suggest a reliable pathway of reduction [10–12]. Interestingly, most of these studies suggested a metastable six-coordinate Pt(III) intermediate. A Pt(III)-containing polymeric material has been indeed described as "platinblau" (platinum blue)

Electronic supplementary material The online version of this article (https://doi.org/10.1007/s13361-019-02186-7) contains supplementary material, which is available to authorized users.

Correspondence to: Simonetta Fornarini;
e-mail: simonetta.fornarini@uniroma1.it, Emilia Sicilia;
e-mail: emilia.sicilia@unical.it, Domenico Osella;
e-mail: domenico.osella@uniupo.it

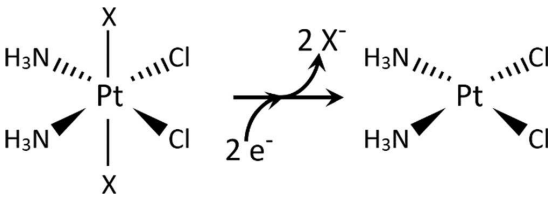

Scheme 1. A cisplatin-based Pt(IV) derivative bearing two axial X ligands. The $2e^-$ reduction produces the active cisplatin metabolite with loss of two X^- anions

because of its characteristic dark blue color. Thus, Pt(III) does exist at least in solid state [13].

Several kinetic experiments on the reduction of Pt(IV) derivatives have been carried out using biological reductants such as ascorbic acid (H_2Asc, or more properly at physiologic pH its mono-anion $HAsc^-$), glutathione, cysteine, or methionine [14]. Depending on the kind of the six ligands around the Pt(IV) core and on the nature of the reducing agent, inner-sphere (attack of the reductant especially on hydroxido or chlorido ligands) or outer-sphere redox processes have been suggested [7]. However, it was shown that reduction of Pt(IV) derivatives is mainly carried out by high molecular weight cellular components [15], and Arnesano et al. [16] proved that cytochrome c is indeed able to promote such activation by reduction. Although this mechanism is not fully elucidated in its intimate details, QSAR studies [17] indicated that appropriate reduction potential and lipophilicity are the key factors for designing efficient Pt(IV) anticancer prodrugs. Thus, it is clearly a challenge to ascertain the role of the ligands around the Pt(IV) core and to design new prodrugs with better pharmacokinetics performances.

In view of this highly active interest, a study has been undertaken on possible pathways for the transformation from six-coordinate Pt(IV) to four-coordinate Pt(II) complexes following the evolution of ions sampled by electrospray ionization mass spectrometry (ESI-MS) in negative (deprotonated species) mode. In particular, in the fragmentation scheme of negative ions (electron-rich species, potentially prone to undergo reduction), evidence for intermediates (in particular species formally containing Pt(III)) that are quite elusive in solution [18, 19] is specifically searched, also taking advantage of the long-lived conditions that may be attained by a naked ion in the gas phase. Clearly, this study refers to ionic species isolated in the gas phase rather than to solvated ions or neutrals stabilized by non-covalent interactions in a dielectric medium. It will therefore definitely not provide any direct connection with reaction dynamics in solution or, even less, in vivo. ESI-MS-based methods have been already largely exploited, allowing in-depth studies on the gas phase chemistry of platinum(II) complexes and enabling the determination of ligand binding energies through the measurement of energy-resolved collision-induced dissociation (CID) experiments [20]. In another area, ESI-MS combined with kinetic studies has allowed to establish that cationic platinum(II) complexes are catalytically active in H/D exchanges involving benzene [21]. ESI-MS coupled with density functional theory (DFT) calculations have shown the occurrence of gas-phase carbon–carbon bond forming reactions catalyzed by Pt(II) and other group 10 metal complexes [22]. Positively charged cisplatin adducts with primary and secondary alcohols have shown C–H bond activation and unexpected dissociation pathways when activated in a linear ion trap [23]. More recently, kinetic and mechanistic features of the ligand exchange reactions of cisplatin-derived aqua complexes have been assayed by ESI coupled with Fourier transform ion cyclotron resonance (FT-ICR) MS [24, 25]. ESI has succeeded in delivering the encounter complexes that play a key role in the ligand displacement reaction in solution, to the gas phase where they have been characterized by both reactivity and spectroscopy [25, 26]. With regard to platinum(IV) complexes, a detailed study has addressed the degradation paths of protonated satraplatin (*trans*,*cis*,*cis*-bis(acetato)ammine-cyclohexylaminedichloridoplatinum(IV)), platinum anticancer agent suitable for oral administration [27]. Results based on ESI-MS and DFT calculations have shown that protonation, as verified in the gastric acidic environment, facilitates the loss of the axial ligand, a key step towards the formation of the platinum(II) effective drug. Energy-resolved CID experiments have proven valuable in disclosing the C–C coupling rate-limiting step in alkane reductive elimination from Pt(IV) complexes in the gas phase [28].

While the development of new anticancer drugs has involved the design and synthesis of numerous Pt(IV) compounds [29–32], the present study is focused on a set of compounds characterized by two NH_3 molecules in *cis* position in the equatorial plane. Pt(IV) complexes typically display octahedral coordination and react slowly in ligand substitution reactions. The remaining positions in the equatorial plane bear either two chlorido or 1,1-cyclobutanedicarboxylato ligands, and the sampled compounds are shown in Scheme 2. They can be reduced readily to their Pt(II) counterparts, thus behaving as prodrugs, and reactivity can be tuned by the nature of the axial ligands.

High-resolution MS (based on the use of a 7T FT-ICR mass spectrometer in France) and infrared multiple photon dissociation (IRMPD) spectroscopy are employed to gain precise detail on the ion compositions and indication on their structures. The proposed pathways and intermediates are corroborated by means of theoretical calculations at the DFT level.

Methods

Sample Preparation

The complexes under investigation, namely (SP-6-33)-diamminedichloridodihydroxidoplatinum(IV) (oxoplatin, EP32, *cis*,*trans*,*cis*-$PtCl_2(OH)_2(NH_3)_2$), (SP-6-33)-diacetatodiamminedichloridoplatinum(IV) (EP416, *cis*,*trans*,*cis*-$PtCl_2(CH_3COO)_2(NH_3)_2$), (SP-6-44)-acetatodiamminedichloridohydroxidoplatinum(IV) (EP417, *cis*,*trans*,*cis*-$PtCl_2(CH_3COO)(OH)(NH_3)_2$), (SP-6-33)-diammine(cyclobutane-1,1-dicarboxylato)

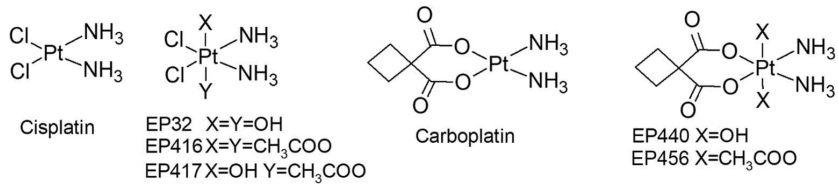

Scheme 2. Schematic representation of the sampled Pt(IV) compounds either cisplatin- (EP32, EP416, EP417) or carboplatin-based (EP440, EP456). The structures of the related Pt(II) drugs are also displayed

dihydroxidoplatinum(IV) (EP440, *cis*,*trans*,*cis*-Pt$(C_6H_6O_4)(OH)_2(NH_3)_2$), and (SP-6-33)-diacetatodiammine(cyclobutane-1,1-dicarboxylato)platinum(IV) (EP456, *cis*,*trans*,*cis*-Pt$(C_6H_6O_4)(CH_3COO)_2(NH_3)_2$), have been prepared according to previously published procedures. In particular, EP32 [17, 33] and EP440 [34] have been synthesized by oxidation of cisplatin or carboplatin with hydrogen peroxide in water.

EP416 [17, 35] and EP456 [36] have been synthesized by the reaction between the corresponding dihydroxido complex and acetic anhydride.

EP417 [37, 38] has been prepared by oxidation of cisplatin with hydrogen peroxide in acetic acid, but the same method has been only partially successful in the case of (SP-6-44)-acetatodiammine(cyclobutane-1,1-dicarboxylato)hydroxidoplatinum(IV), because the synthesis seemed to result in two isomeric products. In fact, HPLC-MS analysis indicated the presence of two chromatographic peaks (in different ratios depending on the reaction time), corresponding to the same MS signal, possibly due to *cis*/*trans* isomers. The formation of the *cis* isomer has been rarely reported, but it has been already observed for a similar Pt(II) compound containing cyclobutane-1,1-dicarboxylato and 2,2-dimethyl-1,3-propanediamine, in the case of its oxidation with hydrogen peroxide in acetic acid (to *cis*-diacetato Pt(IV) product), with respect to the use of acetic anhydride (*trans*-diacetato Pt(IV) product) [39, 40]. Because the two isomers could not be easily separated and might have different reduction behavior, the (SP-6-44)-acetatodiammine(cyclobutane-1,1-dicarboxylato)hydroxidoplatinum(IV) derivative has been excluded from the present investigation.

All the complexes employed have been washed several times with cold water, methanol, and diethyl ether, and their purity has been checked with HPLC-MS and elemental analysis (within ± 0.4% of the calculated value) as reported elsewhere [41, 42]. This point is particularly important because impurities might give rise to undesired mass signals (above all, when they are easily ionized).

The samples for ESI-MS experiments have been prepared starting from stock solutions of the selected complexes 10^{-3} M in water. The solutions have been subsequently diluted in MeOH/H_2O (1:1 *v*/*v*) to 5×10^{-5} M to be directly infused in the ESI source of the MS platforms described in the following section. In order to enhance the abundance of the deprotonated species, an ammonia solution 0.1 M in aqueous methanol has been used as a solvent system.

Mass Analysis and CID Experiments

Three different mass spectrometry platforms have been employed.

Preliminary MS analyses were conducted in a Paul ion-trap (Esquire 6000, Bruker) through direct infusion of the solutions, prepared as stated above, in the ESI source at a flow rate of 180 μL h^{-1}. Typical parameters were a capillary voltage at 3.8 kV and drying gas (N_2) fluxed at 7 L/min^{-1} at 300 °C. Soft conditions were needed to avoid unwanted dissociation of the complexes in the ESI process. Therefore, low voltage settings have been used for the capillary exit and the skimmer, respectively, − 60 V and − 45 V. CID experiments have been performed on mass-selected ions using an activation amplitude comprised between 0.20 V and 0.35 V and an activation time of 0.50 ms.

High-resolution mass spectra have been recorded on a hybrid FT-ICR tandem MS (APEX-Qe Bruker Daltonics) sited at the Université Paris-Sud, Orsay. The samples have been directly infused in the ESI source of the mass spectrometer whose capillary voltage has been set to ca. 4 kV. The instrument comprises a quadrupole-hexapole interface to mass select and accumulate ions before the FT-ICR analyzer, equipped with 7.0 T actively shielded cryomagnet. In particular, the Pt(IV) complexes have been mass-selected in the quadrupole and subsequently accumulated for 1 s in the hexapole pressurized with argon. Finally, the ions have been mass-analyzed in a broadband mode using a 2-M data set. Mass spectra result from the accumulation of 30 scans. The elemental composition has been determined comparing the experimentally obtained accurate masses with the exact ones calculated using the isotope list of the National Institute of Standards and Technology (https://physics.nist.gov/cgi-bin/Compositions/stand_alone.pl). The ions have been assigned to their chemical formula with a tolerance below 3 ppm. Accurate masses of the fragments generated by CID of deprotonated EP32, EP416, and EP417 have been also recorded, by performing a mass selection of the precursor ion in the quadrupole sector of the instrument and activation in the hexapole. The accurate masses have been compared with the calculated ones, as previously

described, to assess the chemical composition of the product ions of interest.

CID experiments varying the collision energy (CE) have been carried out using a hybrid triple quadrupole linear ion trap ($Q1q2Q_{LIT}$) instrument (Applied Biosystems API 2000 Q-Trap). The presence of a quadrupole linear ion trap (Q_{LIT}) as the third sector of the instrument permits to accumulate the fragments obtained by CID in the second sector (q2) and to increase sensitivity and resolution. The MS parameters used for the experiments are the following: curtain gas at 50.0 psi, ion source gas at 20.0 psi, declustering potential at 30 V, and entrance potential at 5 V. Nitrogen has been used as collision gas at a nominal pressure of 2.7×10^{-5} mbar.

IRMPD Experiments

IR multiple photon dissociation (IRMPD) spectra have been obtained in the 3000–3700 cm^{-1} range (pertinent to X–H (X = C, N, O) stretching modes) employing an optical parametric oscillator/amplifier (OPO/OPA) laser system (LaserVision) pumped by a 10-Hz Nd:YAG laser coupled with a Paul ion-trap (Bruker Esquire 6000) mass spectrometer. The apparatus has been already described in detail [43]. The mass-selected ions have been trapped for 10–40 ms, depending on their abundance, and irradiated for 1 s or 2 s, depending on their ease to undergo fragmentation. The typical output energy from the OPO/OPA laser was 15 mJ $pulse^{-1}$ with a spectral width of 5 cm^{-1}. In a few instances, IRMPD has been assisted by a continuous wave CO_2 laser [44]. A train of CO_2 pulses at 25 Hz has been generated and synchronized with the tunable laser to enhance the fragmentation yield. The CO_2 laser pulse length was adjusted so as to avoid IRMPD by the CO_2 laser radiation alone. The IR action spectra are obtained by plotting the photofragmentation yield $R = -\ln[I_p/(I_p + \Sigma I_f)]$, where I_p and ΣI_f are the parent and sum of the fragment ion intensities, respectively, as a function of the radiation wavenumber [45].

Computational Details

Geometry optimizations have been performed with the Gaussian09 software package [46], at DFT level using the hybrid Becke three parameter exchange functional [47] and the Lee-Yang-Parr correlation functional [48], B3LYP. To describe the Pt atom, the relativistic compact Stuttgart/Dresden effective core potential [49] in combination with the split valence basis set has been employed. For the rest of the atoms, the standard triple-ζ quality 6-311++G** basis sets of Pople have been used. Calculation of vibrational frequencies at the same level of theory has been performed to both establish the nature of intercepted stationary points as minima and transition states and get zero point energy (ZPE) corrections. Enthalpies and Gibbs free energies have been obtained at 298 K at 1 atm from total energies, including zero-point and thermal corrections, using standard statistical procedures [50]. The involved transition states have been carefully checked to be properly connected to the correct minima by IRC (intrinsic reaction coordinate) analysis [51, 52].

Results and Discussion

Breakdown Behavior of Prodrug Pt(IV) Complexes

The mass spectra of the selected set of compounds, recorded by ESI in negative ion mode, display the pattern of ionic species formed in solution. Common features as well as distinctive trends are observed, depending on individual structures. The mass spectrum of the prototypical complex in the series, namely EP32, is reported in Figure S1 in the Supplementary Material (SM). The major ion cluster in the spectrum corresponds to the deprotonated species $[EP32\text{-}H]^-$, confirming the stability of the complex and its resistance to hydrolysis. The isotopic pattern reflects the natural abundances of Pt and Cl isotopes giving rise to the distribution well identified in high-resolution FT-ICR MS. The insert in Figure S1 shows the isotopic cluster while the exact mass measurements on the individual peaks confirm the expected elemental composition. Henceforth, anionic complexes will be associated to and named after the *m/z* value of the first significant ion in the isotopic cluster. For example, $[EP32\text{-}H]^-$ is represented by *m/z* 331, corresponding to the $[\{^{194}Pt(OH)_2(^{35}Cl)_2(NH_3)_2\}\text{-}H]^-$ isotopic composition. Other ions appearing in the mass spectrum are related to $[EP32\text{-}H\text{-}H_2O]^-$ and $[EP32+Cl]^-$, the former due to H_2O loss and the second one to the attachment of chloride, a ubiquitous ion in solution. The mass spectra of the other compounds in the series conform to a similar pattern and are displayed in Figures S2–S5. The minor presence of an ion due to water loss is observed also in the mass spectra of EP417 and EP440, while the only negligible loss of acetic acid is found in the mass spectra of EP416, EP417, and EP456.

The naked negatively charged complexes $[EPX\text{-}H]^-$ (X = 32, 416, 417, 440, and 456) have been submitted to collision-induced dissociation (CID) aiming to point out fragmentation products discriminating any tendency towards a reduction in oxidation state and ligation number. In these experiments, the energy released on the activated ion may be varied to provide a relative trend of energy thresholds in dissociation processes. When submitted to CID, $[EPX\text{-}H]^-$ ions display a complex scheme of parallel and consecutive fragmentation paths. The first step, common to all species, involves loss of an axial ligand and is typically followed by either a direct cleavage of one of the equatorial ligands or a fragmentation process involving reduction of the remaining ionic species. In the following paragraph, the fragmentation of $[EP32\text{-}H]^-$ is described in detail and used as a reference for the behavior of other sampled Pt(IV) complexes.

Figure 1 shows the CID mass spectra of selected $[EP32\text{-}H]^-$ ions recorded at high resolution in FT-ICR MS. The analogous CID experiments performed on $[EPX\text{-}H]^-$ (X = 416, 417, 440) are illustrated in Figures S6–S8 in the SM. Mass spectra are collected in the FT-ICR cell after CID in the quadrupole sector of the instrument run at two different values of collision energy (CE, in the laboratory frame). The main fragment formed from $[EP32\text{-}H]^-$ at low CE (4 V) is the product ion at *m/z* 313 due to loss of water.

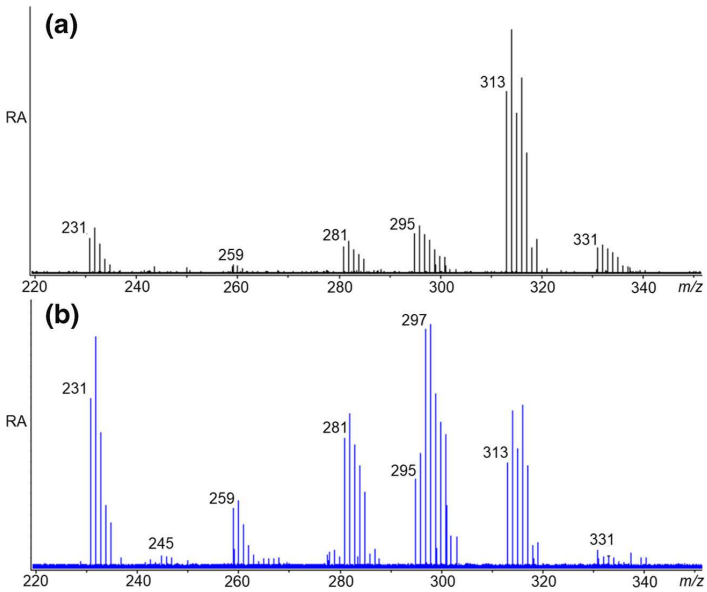

Figure 1. CID mass spectrum of $[EP32\text{-}H]^-$ (*m/z* 331–337) recorded with a collision energy of 4 V (panel (**a**), black profile) and 8 V (panel (**b**), blue profile). Relative abundances (RAs) are in arbitrary units

Increasing the collision energy to 8 V, the abundance of the precursor ion $[EP32\text{-}H]^-$ at *m/z* 331 becomes negligible and also the relative fraction of $[EP32\text{-}H\text{-}H_2O]^-$ at *m/z* 313 decreases in favor of lower mass ions. A complete fragmentation scheme linking all the observed species is obtained by MS^n experiments, in which each individual product ion from $[EP32\text{-}H]^-$ is submitted to activation and subsequent mass analysis.

The complete frame linking the observed fragments is summarized in Scheme 3, showing that all lower mass fragments are generated from the ion *m/z* 313. As also shown by the CID mass spectrum of $[EP32\text{-}H]^-$ at 4 V (Figure 1), two main product ions are formed by the subsequent fragmentation of $[EP32\text{-}H\text{-}H_2O]^-$ at *m/z* 313, namely an ion at *m/z* 295 corresponding to loss of a second water molecule and an ion at *m/z* 281 involving a neutral loss of 32 Da, possibly accounted for by either NHOH or N_2H_4 as neutral fragment. The former possibility involves a single-electron reduction, leading to a formal Pt(III)–containing species, while in the second one, a 2-electron redox process yields a Pt(II) complex $[PtCl_2(OH)]^-$. Other fragments also observed in Figure 1 pertain to dissociation paths from the ion at *m/z* 295. In particular, the species at *m/z* 259 derives from HCl loss yielding in turn the ion at *m/z* 231 by loss of N_2. Moving to higher CE (Figure 1b), a novel feature regards the formation of an ion at *m/z* 297 with an isotopic cluster overlaying the ion at *m/z* 295. This dissociation channel involves a 16-Da loss that can be ascribed to either NH_2 loss, concomitant with a one-electron reduction of the complex, or an O atom loss implying a two-electron reduction.

In order to solve the ambiguities regarding fragments at *m/z* 297 and 281, their accurate mass obtained by high-resolution (HR) FT-ICR mass spectrometry has been compared with the calculated exact mass for potential candidates. An example of these measurements is provided in Figure 2, an enlargement of the HR mass spectrum of Figure 1b showing that four elemental compositions are contributing to *m/z* 297.

The most abundant peak at *m/z* 296.92210 is assigned to $[^{194}Pt^{35}Cl_2(NH_2)(OH)]^-$ with a confidence of 0.8 ppm, thus confirming the presence of a formal Pt(III)–containing complex generated by a neutral NH_2 loss from the *m/z* 313 ion (as displayed in Scheme 3). No signal complying with the elemental composition of a candidate Pt(II) complex $[PtCl_2(NH_2)(NH_3)]^-$ has been found, while the *m/z* signals at 296.92734 and 296.93257 are consistent with the presence of the ions $[^{194}Pt^{35}Cl^{37}Cl(NH_2)(NH)]^-$ and $[^{196}Pt^{35}Cl_2(NH_2)(NH)]^-$, respectively, which are part of the isotopic cluster of the fragment generated by water loss from the complex at *m/z* 313. Finally, the ion *m/z* 296.91630 conforms to the formula $[^{195}Pt^{35}Cl_2(NH)(OH)]^-$ arguably obtained from a tiny fraction of secondary NH_3 loss (not reported in Scheme 3 due to negligible intensity). The whole set of fragments reported in Scheme 3 has been confirmed comparing the high-resolution experimental mass with the calculated exact mass (Table S2), also assessing the nature of the ion at *m/z* 281, which has been assigned to a formal Pt(II)–containing complex, $[PtCl_2(OH)]^-$, generated by N_2H_4 loss from $[PtCl_2(NH_2)_2(OH)]^-$.

The same procedure has been employed to establish breakdown schemes for $[EP416\text{-}H]^-$, $[EP417\text{-}H]^-$, $[EP440\text{-}H]^-$, and $[EP456\text{-}H]^-$ (Schemes S1–S4 and Tables S3–S5 in the SM). The schemes display increasing complexity. For example, the dissociation pattern of $[EP416\text{-}H]^-$ (Scheme S1) entails the

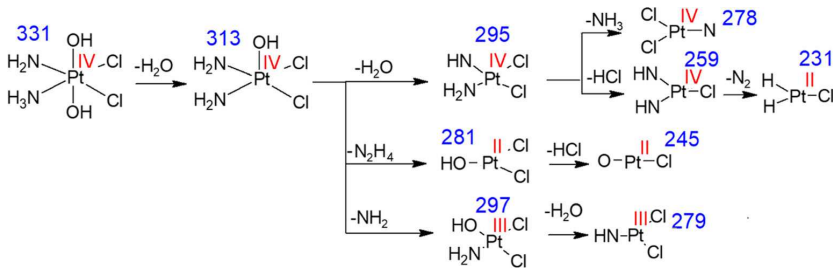

Scheme 3. Schematic representation of the dissociation pattern generated by CID of $[EP32\text{-}H]^-$. The *m/z* ratio of each species is indicated in blue and the formal oxidation state of platinum in red. Every complex is negatively charged; charges are not made explicit

presence of more than 25 different product ions. For the sake of simplicity, we will refer to the primary channels generated from the precursor ion, noting two dissociation paths related to the axial ligands, acetic acid loss and CH_2COO loss, and two fragmentations involving the equatorial ligands, loss of ammonia, and NH_2Cl loss. Interestingly, loss of CH_2COO has been already observed in the degradation of polynuclear platinum complexes bearing acetato ligands, and this fragment has been ascribed to oxacyclopropanone [53]. In this study, a formal Pt(III) dinuclear cluster has been obtained in the gas phase by degradation of a tetrameric compound in the ESI source [53]. The CH_2COO loss channel leads to the formation of a Pt(II) complex, $[PtCl_2(NH_3)_2(CH_3CO_2)]^-$, presenting the base structure of cisplatin with an additional acetato ligand, likely placed in an external coordination sphere [10]. It represents the only dissociation channel involving a redox reaction associated with cleavage of an axial ligand in the whole set of examined Pt(IV) species. The dissociation path involving NH_2Cl loss also requires a redox step generating a Pt(II) complex in which the two axial ligands are still bound to platinum. In contrast, the redox process in water is considered to involve mainly the axial ligands [3, 7, 54, 55], while leaving the equatorial ones untouched. However, a few evidences are reported supporting possible participation of the equatorial ligands in some redox process [30], rather in line with the gas-phase reaction where the equatorial ligands are acting in the reduction reaction of platinum(IV).

In the endeavor to provide a comprehensive description of the breakdown behavior of the sampled complexes, Figure 3 summarizes the normalized intensities of the major dissociation channels of $[EPX\text{-}H]^-$ (X = 32, 416, 417, 440, 456) at a common CE value.

The behavior of $[EP416\text{-}H]^-$, compared with that of $[EP32\text{-}H]^-$, shows less extensive dissociation and the contribution of an important ammonia loss. Moving to $[EP417\text{-}H]^-$, possessing different axial ligands, the behavior under CID condition reflects its mixed nature showing an intermediate extent of precursor ion fragmentation to yield fragments pertaining to both $[EP32\text{-}H]^-$ and $[EP416\text{-}H]^-$, as reported in Scheme 4 (and more thoroughly illustrated in Scheme S2 of the SM). However, the primary water loss is the most prominent channel (Figure 3), confirming it to be the easiest dissociation path.

Concerning $[EP440\text{-}H]^-$, it presents the same hydroxido axial ligands as EP32 but differs for the equatorial ligands, where the two chlorido are substituted by a chelating 1,1-cyclobutanedicarboxylato ligand. The low percentage of intact precursor ion makes it similar to $[EP32\text{-}H]^-$ suggesting the crucial factor that eases the water loss path to be the presence of two hydroxido ligands in axial positions. In addition, one may note the presence of a small fraction of anionic ligand, 1,1-cyclobutanedicarboxylate, dissociating from the complex. Scheme S3 in the SI displays the

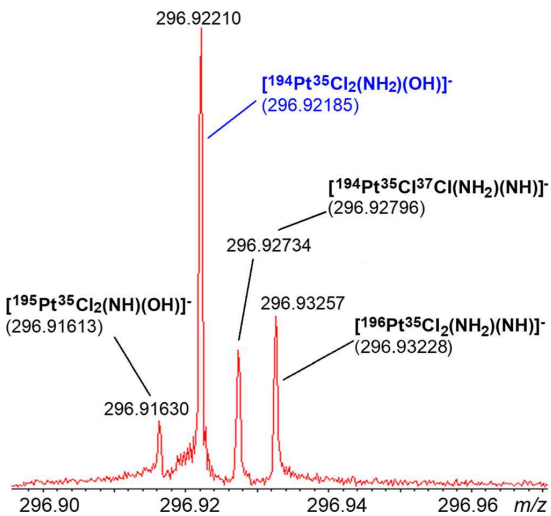

Figure 2. Excerpt of the CID mass spectrum of $[EP32\text{-}H]^-$. The assigned elemental composition is reported for each ion together with the corresponding calculated exact mass in Da (in brackets). The ion corresponding to the Pt(III)-containing complex (in blue) is the most abundant species, while all other species are formal Pt(IV) complexes. Table S1 in the SM provides a comprehensive list of experimental and calculated *m/z* values and associated error

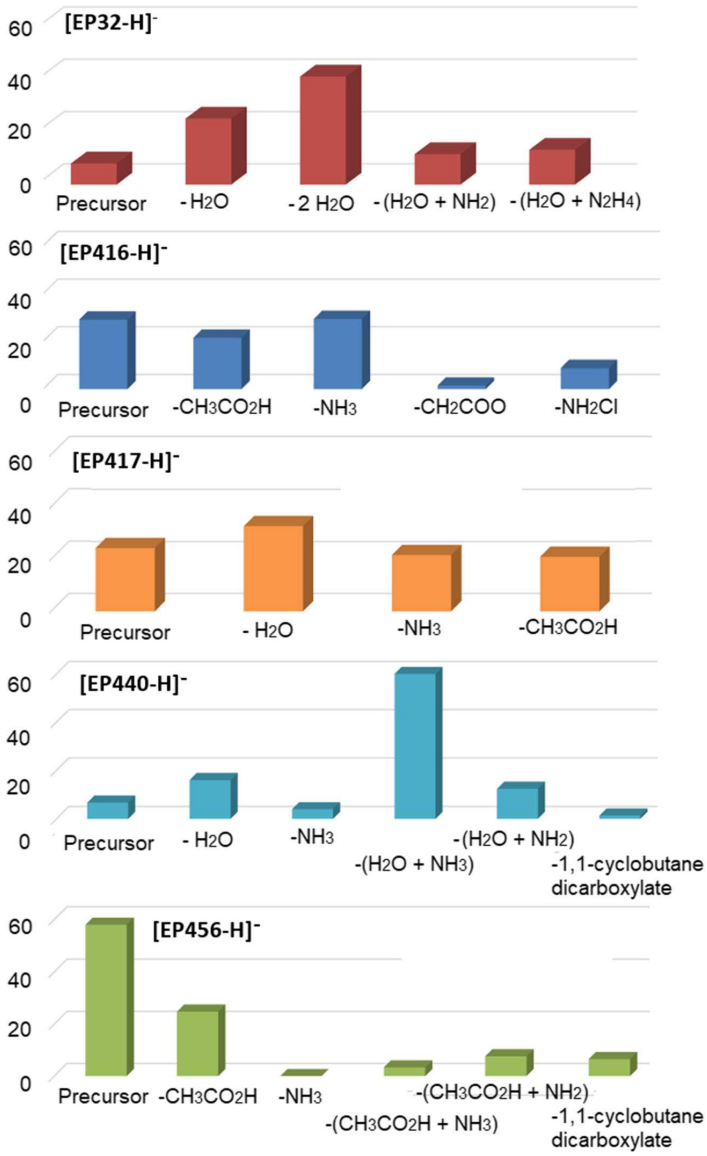

Figure 3. Major breakdown channels from deprotonated EPX (X = 32, 416, 417, 440, 456) and their normalized ratio in the CID mass spectrum at CE = 5 V

complete fragmentation pattern of $[EP440\text{-}H]^-$ showing the presence of a channel producing a formal Pt(III)–containing complex by loss of NH_2 following the primary dissociation of water. This channel is instead missing in the CID of $[EP416\text{-}H]^-$ suggesting the hydroxido ligand to have a major role in the reaction mechanism along the EP32/EP416/EP417 series. The process is conceivably bound to the possibility for the OH to swap from axial to equatorial position, thus replacing the NH_2 group in the pentacoordinated complexes formed by the primary water loss, as further illustrated in the following section. This evidence is limited to the cisplatin prodrugs EP32/EP416/EP417 though. In fact, in the case of EP456, the fragmentation pattern of the deprotonated species, reported in Scheme 5 and, more comprehensively, in Scheme S4, shows the formation of an ion corresponding to $[Pt(1,1\text{-cyclobutanedicarboxylato})(CH_3COO)(NH_2)]^-$ formally containing Pt(III) despite the absence of any OH ligand. Interestingly, this is also the major secondary channel as shown in Figure 3.

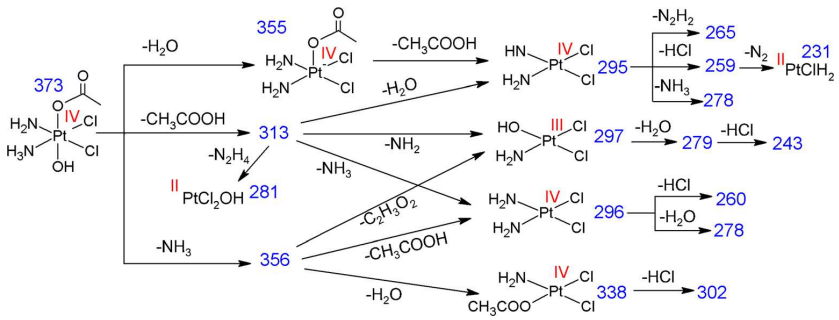

Scheme 4. Schematic representation of the dissociation pattern generated by CID of $[EP417\text{-}H]^-$. The *m/z* ratio of each species is indicated in blue and the formal oxidation state of platinum in red. Every complex is negatively charged; charges are not made explicit

The $[Pt(1,1\text{-cyclobutanedicarboxylato})(CH_3COO)(NH_2)]^-$ complex at *m/z* 411 fragments once again by loss of NH_2 forming a Pt(II) complex. This two-step sequence, corresponding to a stepwise reduction from Pt(IV) to Pt(II), is characteristic of EP456 and unusual with respect to the otherwise prevailing direct dissociation of N_2H_4. The $[EP456\text{-}H]^-$ complex is also the most resistant towards fragmentation, as demonstrated by the high fraction of intact parent ion reported in Figure 3. In this respect, EP456 conforms to the already mentioned lower ease to undergo dissociation shown by complexes presenting two acetato ligands in axial positions.

Structural Assay of Selected Deprotonated Complexes by IRMPD Spectroscopy

Two species in the set of deprotonated complexes have been selected for an assay by vibrational spectroscopy in the X–H (X = C, N, O) stretching range, namely $[EP32\text{-}H]^-$ and $[EP417\text{-}H]^-$, in order to gain direct, experimental evidence on the structure of these species which may be ascertained by comparing experimental IRMPD features with IR spectra of computed structures.

The experimental spectrum of $[EP32\text{-}H]^-$ in the 3000–3700 cm^{-1} region is reported in Figure 4 together with the calculated IR spectra for two candidate isomers, EP32_1 and EP32_2.

The first species is obtained from EP32 neutral complex by abstraction of a proton from one of the ammine ligands. This isomer is lower in energy. The search for a local minimum corresponding to deprotonation from the OH group has failed in spite of sustained effort. In the second isomer, EP32_2, a proton has moved from NH_3 to one of the hydroxido ligands. The ensuing species is higher in free energy by 10.0 kcal mol^{-1}. It is thus not surprising that the comparison between experimental and theoretical spectra points to EP32_1 as the major species representing the gas-phase population. The IRMPD spectrum is dominated by a broad and asymmetric feature around 3400 cm^{-1} comprising two signals at 3410 and 3332 cm^{-1} (see gray profile in Figure 4 and Table S6 in the SM) which may be ascribed to the asymmetric stretching modes of the intact ammine ligand calculated at 3440 and 3394 cm^{-1}. The sharp feature at 3625 cm^{-1} can be assigned to the OH stretching mode that is calculated at 3670 cm^{-1} for EP32_1. Thus, in the experimental spectrum, the OH stretching mode is shifted to a lower value with respect to the calculated

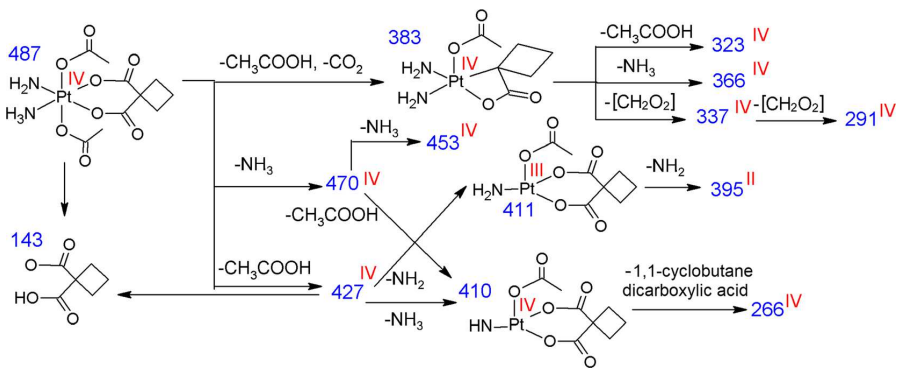

Scheme 5. Schematic representation of the dissociation pattern generated by CID of $[EP456\text{-}H]^-$. The *m/z* ratio of each species is indicated in blue and the formal oxidation state of platinum in red. Every complex is negatively charged; charges are not made explicit

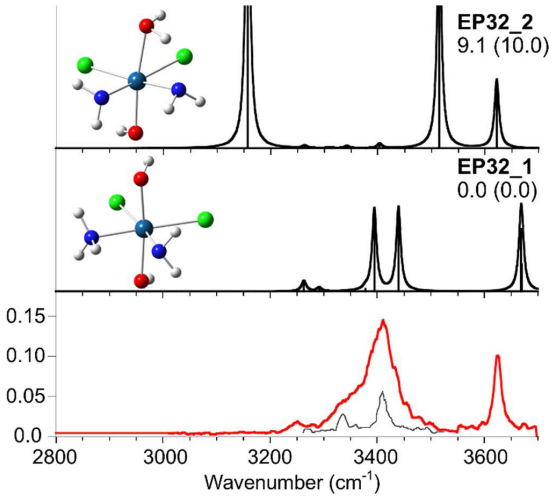

Figure 4. IRMPD spectrum of $[EP32\text{-}H]^-$ (red profile and gray profile recorded at lower laser power) compared with calculated IR spectra for EP32_1 and EP32_2 (black profiles). Optimized geometries are reported together with relative enthalpies and free energies (in brackets) at 298 K in kcal mol^1. A factor of 0.957 is used to scale the calculated harmonic frequencies

IR frequency. This kind of discrepancy is, however, a common finding for the OH stretching mode in related platinum complexes assayed by IRMPD spectroscopy [25]. A small band around 3247 cm^{-1} in the IRMPD spectrum can be assigned to the N–H symmetric stretching calculated at 3263 cm^{-1} for the NH_3 ligand in EP32_1. The contribution of EP32_2 to the sampled gas-phase population is unlikely, in view of the absence of any IRMPD activity in the 3500–3550 and 3100–3200 cm^{-1} ranges. In fact, isomer EP32_2 is expected to present strong absorptions near 3515 and 3158 cm^{-1}, related to the H_2O asymmetric and symmetric stretching modes, respectively. Their relatively low wavenumber in the calculated spectrum is due to the interaction of the water hydrogen atoms with nitrogen of equatorial NH_2. This isomer is rather likely to play a role as intermediate in the water loss path, the largely prevailing dissociation process in the breakdown chemistry of $[EP32\text{-}H]^-$.

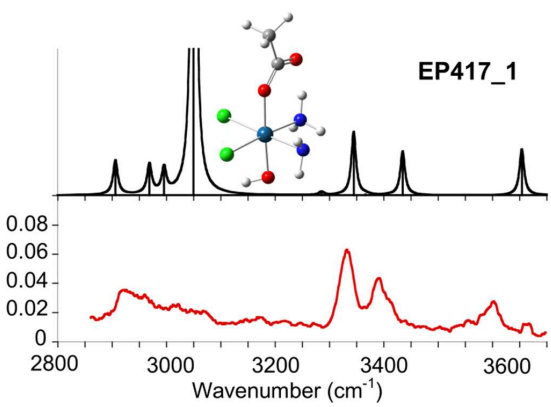

Figure 5. IRMPD spectrum of $[EP417\text{-}H]^-$ (red profile) compared with the IR spectrum of EP417_1 (black profile). The optimized geometry is reported. A factor of 0.957 is used to scale the calculated harmonic frequencies

IRMPD spectroscopy has also been used to inquire about the structural and vibrational features of $[EP417\text{-}H]^-$. Figure 5 shows the experimental spectrum (red profile) to be compared with the IR spectrum (black profile) for the optimized geometry of the lowest lying conformer of $[EP417\text{-}H]^-$, namely EP417_1. Once again, the deprotonation site is an ammine ligand. No other isomers have been found exploring possible prototropic rearrangements. A few other conformers of EP417_1 have been also considered, involving modifications in the Pt-O-C angle and rotations around the O-Pt-O axis. The optimized geometries and their relative enthalpies and free energies are reported in Figure S9 together with their calculated IR spectra. However, the presence of these higher lying conformers in the sampled gas-phase population is unlikely on the basis of both their high relative free energy compared to the global minimum ($G_{rel}(298\ K) \geq 6.4$ kcal mol^{-1}) and the comparison of calculated and experimental spectroscopic features. We will therefore refer to the lowest lying conformer EP417_1 in discussing the experimental IR features.

The IRMPD spectrum (Figure 5 and Table S7) shows a signal at 3605 cm^{-1}, matching the OH stretching frequency calculated at 3654 cm^{-1} [25], which is followed by two features at 3397 and 3330 cm^{-1} fairly well accounted for by the NH_3 asymmetric stretching modes calculated at 3435 and 3345 cm^{-1}. In the spectral range below 3100 cm^{-1}, one may recognize a broad asymmetric absorption with maximum around 2920 cm^{-1} that can be attributed to a combination of the asymmetric and symmetric stretching modes of the methyl group (2996, 2969, and 2906 cm^{-1}, respectively) with the symmetric stretching of ammonia at 3050 cm^{-1}. This latter vibrational mode is red-shifted due to H-bonding between a positively polarized hydrogen of NH_3 oriented towards the carbonyl oxygen of the acetato ligand. This stabilizing interaction undoubtedly contributes to this geometry being the lowest lying in energy. It also explains the low activity of the experimental feature and its broad width, as extensively reported in the literature [56–59].

Computed Paths for the Gas-Phase Breakdown Pattern

DFT calculations have been employed to outline the free energy profile for the gas-phase fragmentation pattern of two sampled Pt(IV) complexes. Figure 6 presents the potential energy surface (PES) for the $[EP32\text{-}H]^-$ complex. IRMPD evidence has pointed to the EP32_1 structure for $[EP32\text{-}H]^-$ involving deprotonation at an ammine ligand.

Water loss is the common first event, prior to subsequent dissociation steps as depicted in Scheme 3. The water loss process in the dissociation pathway of $[EP32\text{-}H]^-$ occurs in two steps, namely proton transfer from the remaining NH_3

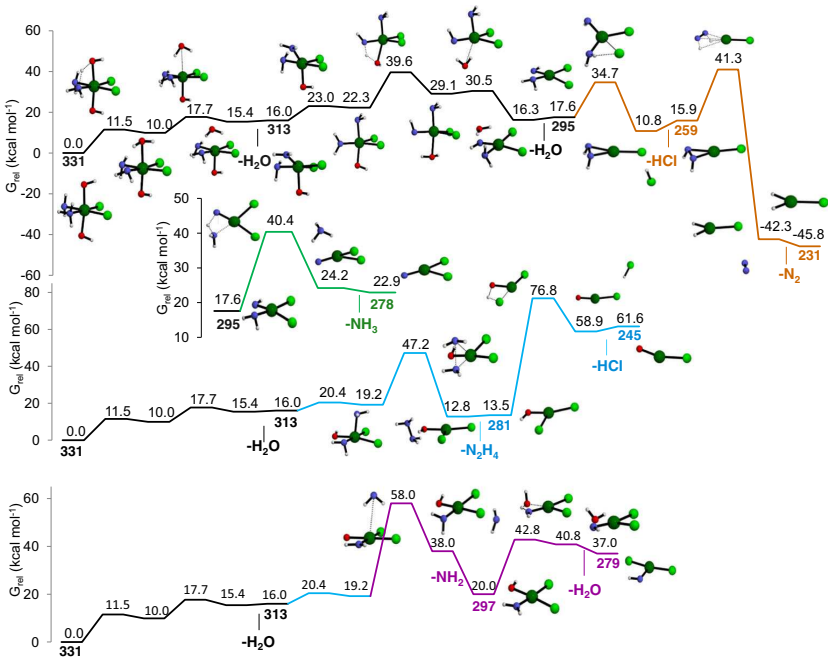

Figure 6. PES for the breakdown pattern of $[EP32\text{-}H]^-$. The black trace, common to all profiles, regards the common water loss process. The neutral losses for all dissociation paths are indicated below the colored lines. Relative free energies at 298 K in kcal mol^{-1} are reported in black. The *m/z* value for each species is reported in color

ligand within EP32_1 to an axial OH (forming EP32_2) and detachment of the so-formed water molecule. The two corresponding intercepted transition states lie at 11.5 and 17.7 kcal mol^{-1} for the former and the latter step, respectively. These relatively low values are in agreement with the observed ease for fragmentation even at low CE (Figures 1a and 3). The overall process for dissociation of water from $[EP32\text{-}H]^-$ yielding the product ion at *m/z* 313 results to involve a ΔG value of 16.0 kcal mol^{-1}. Subsequent fragmentation paths entail competing losses of a second H_2O molecule, N_2H_4, and NH_2. For the second water loss, it is necessary to overcome three transition states involving motion of one of the NH_2 groups from equatorial to axial position, transfer of one hydrogen from the NH_2 group in equatorial position to OH, and detachment of the so-formed water. The three transition states lie at 23.0, 39.6, and 30.5 kcal mol^{-1}, respectively (black profile, Figure 6). For N_2H_4 and NH_2 release, the corresponding transitions states lie at 47.2 (blue profile, Figure 6) and 58.0 (purple profile, Figure 6) kcal mol^{-1}, respectively. The data are consistent with the behavior of $[EP32\text{-}H]^-$ which shows a preferential second-step fragmentation involving water loss (*m/z* 295) and loss of N_2H_4 (*m/z* 281) at 4 V CE (Figure 1a). At this CE value, hardly any product involving NH_2 loss is formed while it becomes a prevailing species at 8 V CE (Figure 1b). At this same CE, the product at *m/z* 295 undergoes subsequent dissociation yielding ions at *m/z* 259, *m/z* 231, and *m/z* 278. The last one is the least abundant (Figure 1b) in agreement with the higher activation free energy (40.4 kcal mol^{-1}, green profile of Figure 6) compared to the 34.7 kcal mol^{-1} needed to activate the loss of HCl from *m/z* 295 (orange profile, Figure 6). Finally, the ion *m/z* 259 generates the fragment at *m/z* 231 in a process involving N_2 loss as shown in Scheme 3. This latter dissociation channel presents a calculated transition state energy of 16.7 kcal mol^{-1}, lower than the one involved in the secondary channel involving loss of NH_2, as shown in the orange and purple profiles of Figure 6, respectively.

Overall, the computational survey offers a reliable description and interpretation of the experimentally observed phenomena. A few details regarding the reaction mechanism can be underlined, focusing in particular on the processes generating the reduced platinum species. There are three paths leading to either Pt(II) (*m/z* 231 and 281) or Pt(III) (*m/z* 297) species that are formed via a redox process involving the former ammonia molecules bound to the metal. Indeed, it is a different landscape when compared with the reactivity pattern in solution where reduction of platinum(IV) is accompanied by oxidation and dissociation of the axial ligands [7, 17, 30, 32]. However, in the naked gaseous platinum(IV) complex, water molecules are largely lost by direct cleavage concomitant with proton transfer from the ammine ligand, whose acidity is enhanced by ligation to the metal. The so-formed *cis* NH_2 groups react upon CID by donating two electrons to the electron-poor Pt(IV) atom to generate a N–N bond leading to dissociation (blue profile in Figure 6). In contrast, the reaction producing the Pt(III)

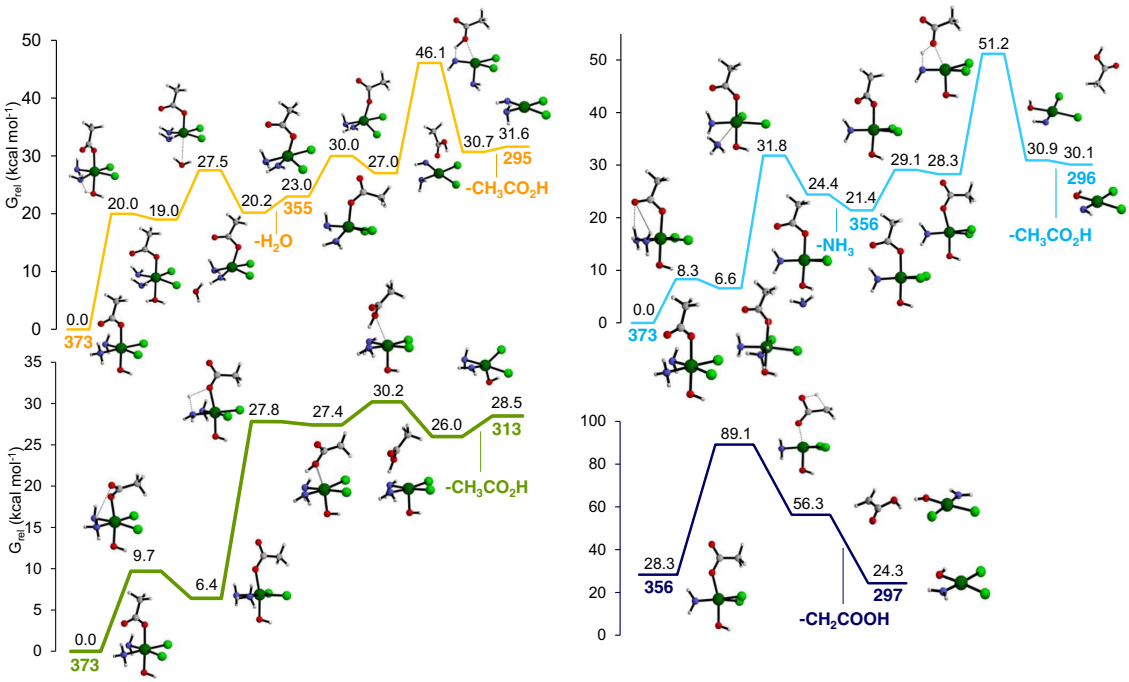

Figure 7. PES for the breakdown pattern of $[EP417\text{-}H]^-$. The neutral losses for all dissociation events are indicated below the colored lines. Relative free energies at 298 K in kcal mol^{-1} are reported in black. The *m/z* value for each species is reported in color

complex proceeds by a direct cleavage of NH_2 with a preliminary swapping of the hydroxido axial group to the equatorial position forming a complex where the NH_2 group is in axial position. The so-formed Pt(III) complex $[PtCl_2(OH)(NH_2)]^-$ is stable enough and can be isolated and subsequently assayed in the gas phase in spite of there being no clearcut evidence for the formation of Pt(III) species in the reaction paths of Pt(IV) complexes in solution.

The second Pt(IV) complex sampled by DFT calculations is $[EP417\text{-}H]^-$, where deprotonation has once again interested one of the NH_3 ligands, as shown by the IRMPD spectroscopic assay. The different ligands in the axial position open a larger variety of breakdown paths as reported in Scheme 4 and Scheme S2. The calculated PES for the early steps in the dissociation pattern is depicted in Figure 7 and shows the first competing processes involving loss of either water (orange profile), acetic acid (green profile), or ammonia (pale blue profile). The pathway for water cleavage illustrated in the yellow profile comprises two steps. Starting from the most stable structure, corresponding to EP417_1, the transition state for proton shift from NH_3 to the axial OH group lies at 20.0 kcal mol^{-1}. The subsequent event of H_2O cleavage involves a barrier at 27.5 kcal mol^{-1}. The magnitude of the overall activation barrier for water loss is thus significantly higher than the one affecting the departure of water from EP32_1, which is in agreement with the comparatively limited dissociation of $[EP417\text{-}H]^-$ relative to $[EP32\text{-}H]^-$ (Figure 4).

As already noticed, the hydrogen bond between a proton belonging to NH_3 and the carbonyl group of the acetato ligand exerts a stabilizing influence. However, this interaction needs to be released in order to activate the NH_3 cleavage process, which occurs by way of a transition state at 8.3 kcal mol^{-1} relative to EP417_1 (see pale blue profile in Figure 7) to achieve a higher energy structure at 6.6 kcal mol^{-1} relative energy (named EP417_3 in the survey of $[EP417\text{-}H]^-$ geometries collected in Figure S9). EP417_3 then releases NH_3 after passing a barrier at 31.8 kcal mol^{-1} in an overall 21.4 kcal mol^{-1} endoergonic process. The third possible primary cleavage of $[EP417\text{-}H]^-$ ions concerns acetic acid loss. Once again, a proton migration event is required which needs a rotational rearrangement of EP417_1 to be activated. As shown in the green profile of Figure 7, EP417_1 isomerizes to a structure (EP417_2 in Figure S9) lying at 6.4 kcal mol^{-1}, whereby the methyl hydrogens are oriented towards the two chlorido ligands. From this configuration, a transition state for proton shift from NH_3 to acetate is reached at 27.8 kcal mol^{-1}, and finally, overcoming a barrier at 30.2 kcal mol^{-1}, acetic acid is released in an overall 28.5 kcal mol^{-1} endoergonic process. One may notice that the highest lying transition state for acetic acid loss (at 30.2 kcal mol^{-1}) is rather close to the one for NH_3 departure (31.8 kcal mol^{-1}). This nearly negligible difference may account for the similar ease for acetic acid vs. NH_3 loss that results from the data displayed in Figure 3.

It may be underlined that also the breakdown pattern of $[EP417\text{-}H]^-$ shows the formation of products where the metal has formally undergone reduction. Thus, the ion at *m/z* 313, corresponding to $[Pt(OH)Cl_2(NH_2)_2]^-$, a common species in the fragmentation landscape of $[EP32\text{-}H]^-$, confirms here the reduction to a Pt(II) product, $[Pt(OH)Cl_2]^-$, concomitant with cleavage of N_2H_4. Also, the formal Pt(III) complex already observed in the breakdown pattern of $[EP32\text{-}H]^-$, $[Pt(OH)Cl_2(NH_2)]^-$, is formed along the pathway depicted in dark blue in Figure 7 involving loss of CH_2COOH, an oxidation product of acetic acid. In this case, the reduction is accompanying the cleavage of a former axial ligand, occurring, however, only after the release of NH_3. The process is reminiscent of the fragmentation pathway by loss of an acetyloxyl radical from a gaseous uranyl complex, thus undergoing reduction from $U^{VI}O_2^{2+}$ to $U^{V}O_2^{+}$ [60]. The formation of reduced species after CID activation has indeed been reported in the breakdown behavior of deprotonated uranyl-containing complexes [61–63], while the corresponding protonated species showed no tendency to undergo reduction reactions [62].

Conclusions

The ESI-MS study of the breakdown pattern of negatively charged ions corresponding to deprotonated platinum(IV) complexes EPX (X = 32, 416, 417, 440, 456), prodrugs for the widely used cisplatin and carboplatin anticancer agents, has revealed a highly varied landscape, modulated by the nature of the axial ligands as well as by the equatorial ones. The deprotonated, negatively charged ions have been purposely assayed, aiming to verify reduction processes leading to platinum(II) species. To this end, a detailed survey of CID schemes has been accomplished, whereas IRMPD spectroscopy has provided the means to ascertain the structure of the starting sampled ions. The ammine ligand has thus been found to be the preferred deprotonation site. When interrogated by CID, the deprotonated species show a complex dissociation pattern, involving axial ligand as well as ammonia loss and dissociation channels eventually leading to reduction of the metal. Interestingly, the reduction processes observed upon activation towards CID have been always accompanied by equatorial ligand loss, either ammine or chlorido. In contrast, reduction reactions from Pt(IV) complexes in condensed phase are considered to be concomitant with axial ligand loss. In this regard, the reduced species characterized using ESI and high-resolution mass spectrometry present alternative paths in the reduction mechanism of platinum(IV) complexes.

Noteworthyly, the gas-phase activation of $[EP32\text{-}H]^-$, $[EP417\text{-}H]^-$, $[EP440\text{-}H]^-$, and $[EP456\text{-}H]^-$ has permitted to isolate and characterize platinum complexes with formal metal oxidation state of +3. Platinum(III)-containing species have been seldom observed in solution and only theoretically postulated in the reaction mechanism of Pt(IV) prodrugs. However, as shown in the present work, the mononuclear Pt(III) complexes generated by dissociation in the gas phase have been found to be stable enough to be isolated and further activated. Finally, DFT calculations on the free energy paths for the observed fragmentation reactions have provided theoretical support for the CID dissociation patterns, viewed in the light of thermodynamic reasons.

As an ending note, one may restate that the observed breakdown reactivity patterns describe high energy paths as available to isolated ionic species activated to undergo CID. However, high-resolution FT-ICR mass spectrometry is highly efficient in uncovering the potentially cytotoxic reactivity properties of platinum(IV) complexes, as comprehensively described in a recent report on light-driven platination of neuropeptides having a role in some types of cancer [5].

Acknowledgements

This work has been supported by Università della Calabria, Università del Piemonte Orientale, and Università di Roma "La Sapienza" (DR n. 3210/16), by the European Union's Horizon 2020 research and innovation program under grant agreement no. 731077, and by the French FT-ICR network (FR3624CNRS). We are indebted to Inter-University Consortium for Research on the Chemistry of Metals in Biological Systems (CIRCMSB, Bari, Italy) for providing opportunities of stimulating discussion during the annual meetings.

References

1. Taube, H.: Electron Transfer Reactions of Complex Ions in Solution. Academic Press, New York (1970)
2. Basolo, F., Morris, M.L., Pearson, R.G.: Bridged mechanism for the platinum(II) catalysis of chloride exchange in chloroammine-platinum(IV) complexes. Disc. Faraday Soc. **29**, 80–91 (1960)
3. Hall, M.D., Hambley, T.W.: Platinum(IV) antitumour compounds: their bioinorganic chemistry. Coord. Chem. Rev. **232**, 49–67 (2002)
4. Venkatesh, V., Sadler, P.J.: Platinum(IV) prodrugs in metal ions in life sciences, Volume 18. In: Sigel, A., Sigel, H., Freisinger, E., Sigel, R.K.O. (eds.), Metallo-Drugs: Development and Action of Anticancer Agents, pp. 69–108. de Gruyter GmbH, Berlin, DE (2018)
5. Wootton, C.A., Sanchez-Cano, C., Lopez-Clavijo, A.F., Shaili, E., Barrow, M.P., Sadler, P.J., O'Connor, P.B.: Sequence-dependent attack on peptides by photoactivated platinum anticancer complexes. Chem. Sci. **9**, 2733–2739 (2018)
6. Hall, M.D., Mellor, H.R., Callaghan, R., Hambley, T.W.: Basis for design and development of platinum(IV) anticancer complexes. J. Med. Chem. **50**, 3403–3411 (2007)
7. Wexselblatt, E., Gibson, D.: What do we know about the reduction of Pt(IV) pro-drugs? J. Inorg. Biochem. **117**, 220–229 (2012)
8. Platts, J.A., Ermondi, G., Caron, G., Ravera, M., Gabano, E., Gaviglio, L., Pelosi, G., Osella, D.: Molecular and statistical modeling of reduction peak potential and lipophilicity of platinum(IV) complexes. J. Biol. Inorg. Chem. **16**, 361–372 (2011)
9. McCormick, M.C., Schultz, F.A., Baik, M.-H.: Glassy carbon electrodes deliver unpredictable reduction potentials for platinum(IV) antitumor prodrugs. Polyhedron. **103**, 28–34 (2016)
10. McCormick, M.C., Keijzer, K., Polavarapu, A., Schultz, F.A., Baik, M.H.: Understanding intrinsically irreversible, non-nernstian, two-electron redox processes: a combined experimental and computational study of the electrochemical activation of platinum(IV) antitumor prodrugs. J. Am. Chem. Soc. **136**, 8992–9000 (2014)
11. Šebesta, F., Baxová, K., Burda, J.V.: Redox potentials for tetraplatin, satraplatin, its derivatives, and ascorbic acid: a computational study. Inorg. Chem. **57**, 951–962 (2018)

12. Tolbatov, I., Coletti, C., Marrone, A., Re, N.: Insight into the electrochemical reduction mechanism of Pt(IV) anticancer complexes. Inorg. Chem. **57**, 3411–3419 (2018)
13. Gillard, R.D., Wilkinson, G.: Platinum blue and related compounds. J. Chem. Soc. 2835–2837 (1964)
14. Jovanović, S., Petrović, B., Bugarčić, Ž.D., van Eldik, R.: Reduction of some Pt(IV) complexes with biologically important sulfur-donor ligands. Dalt. Trans. **42**, 8890–8896 (2013) and references therein
15. Nemirovski, A., Kasherman, Y., Tzaraf, Y., Gibson, D.: Reduction of cis,trans,cis-$[PtCl_2(OCOCH_3)_2(NH_3)_2]$ by aqueous extracts of cancer cells. J. Med. Chem. **50**, 5554–5556 (2007)
16. Lasorsa, A., Stuchlíková, O., Brabec, V., Natile, G., Arnesano, F.: Activation of platinum(IV) prodrugs by cytochrome c and characterization of the protein binding sites. Mol. Pharm. **13**, 3216–3223 (2016)
17. Gramatica, P., Papa, E., Luini, M., Monti, E., Gariboldi, M.B., Ravera, M., Gabano, E., Gaviglio, L., Osella, D.: Antiproliferative Pt(IV) complexes: synthesis, biological activity, and quantitative structure–activity relationship modeling. J. Biol. Inorg. Chem. **15**, 1157–1169 (2010)
18. Ojha, R., Boas, J.F., Deacon, G.B., Junk, P.C., Bond, A.M.: EPR spectroscopic characterization of a monomeric Pt^{III} species produced via electrochemical oxidation of the anticancer compound trans-$[Pt^{II}\{(p\text{-}HC_6F_4)NCH_2CH_2NEt_2\}cl(Py)]$. J. Inorg. Biochem. **162**, 194–200 (2016)
19. Rivada-Wheelaghan, O., Ortuño, M.A., García-Garrido, S.E., Díez, J., Alonso, P.J., Lledós, A., Conejero, S.: A stable, mononuclear, cationic Pt(III) complex stabilised by bulky N-heterocyclic carbenes. Chem. Commun. **50**, 1299–1301 (2014)
20. Hammad, L.A., Gerdes, G., Chen, P.: Electrospray ionization tandem mass spectrometric determination of ligand binding energies in platinum(II) complexes. Organometallics. **24**, 1907–1913 (2005)
21. Gerdes, G., Chen, P.: Cationic platinum(II) carboxylato complexes are competent in catalytic arene C−H activation under mild conditions. Organometallics. **23**, 3031–3036 (2004)
22. Woolley, M., Ariafard, A., Khairallah, G.N., Kwan, K.H.-Y., Donnelly, P.S., White, J.M., Canty, A.J., Yates, B.F., O'Hair, R.A.J.: Decarboxylative-coupling of allyl acetate catalyzed by group 10 organometallics, $[(Phen)M(CH_3)]^+$. J. Org. Chem. **79**, 12056–12069 (2014)
23. Springer, A., Bürgel, C., Böhrsch, V., Mitrić, R., Bonačić-Koutecký, V., Linscheid, M.W.: The gas-phase chemistry of cis-diammineplatinum(II) complexes: a joint experimental and theoretical study. ChemPhysChem. **7**, 1779–1785 (2006)
24. Corinti, D., Coletti, C., Re, N., Piccirillo, S., Giampà, M., Crestoni, M.E., Fornarini, S.: Hydrolysis of Cis- and transplatin: structure and reactivity of the aqua complexes in a solvent free environment. RSC Adv. **7**, 15877–15884 (2017)
25. Corinti, D., Coletti, C., Re, N., Chiavarino, B., Crestoni, M.E., Fornarini, S.: Cisplatin binding to biological ligands revealed at the encounter complex level by IR action spectroscopy. Chem. Eur. J. **22**, 3794–3803 (2016)
26. Corinti, D., Coletti, C., Re, N., Paciotti, R., Maître, P., Chiavarino, B., Crestoni, M.E., Fornarini, S.: Short-lived intermediates (encounter complexes) in cisplatin ligand exchange elucidated by infrared ion spectroscopy. Int. J. Mass Spectrom. **435**, 7–17 (2019)
27. Ritacco, I., Al Assy, M., Abd El-Rahman, M.K., Fahmy, S.A., Russo, N., Shoeib, T., Sicilia, E.: Hydrolysis in acidic environment and degradation of satraplatin: a joint experimental and theoretical investigation. Inorg. Chem. **56**, 6013–6026 (2017)
28. Couzijn, E.P.A., Kobylianskii, I.J., Moret, M.-E., Chen, P.: Experimental gas-phase thermochemistry for alkane reductive elimination from Pt(IV). Organometallics. **33**, 2889–2897 (2014)
29. Johnstone, T.C., Suntharalingam, K., Lippard, S.J.: The next generation of platinum drugs: targeted Pt(II) agents, nanoparticle delivery, and Pt(IV) prodrugs. Chem. Rev. **116**, 3436–3486 (2016)
30. Gibson, D.: The mechanism of action of platinum anticancer agents—what do we really know about it? Dalt. Trans. **0**, 10681–10689 (2009)
31. Gabano, E., Ravera, M., Osella, D.: Pros and cons of bifunctional platinum(IV) antitumor prodrugs: two are (not always) better than one. Dalt. Trans. **43**, 9813–9820 (2014)
32. Petruzzella, E., Sirota, R., Solazzo, I., Gandin, V., Gibson, D.: Triple action Pt(IV) derivatives of cisplatin: a new class of potent anticancer agents that overcome resistance. Chem. Sci. **9**, 4299–4307 (2018)
33. Gabano, E., Ravera, M., Trivero, F., Tinello, S., Gallina, A., Zanellato, I., Gariboldi, M.B., Monti, E., Osella, D.: The cisplatin-based Pt(IV)-diclorofibrato multi-action anticancer prodrug exhibits excellent performances also under hypoxic conditions. Dalt. Trans. **47**, 8268–8282 (2018)
34. Varbanov, H.P., Valiahdi, S.M., Kowol, C.R., Jakupec, M.A., Galanski, M., Keppler, B.K.: Novel tetracarboxylatoplatinum(IV) complexes as carboplatin prodrugs. Dalt. Trans. **41**, 14404–14415 (2012)
35. Zanellato, I., Bonarrigo, I., Colangelo, D., Gabano, E., Ravera, M., Alessio, M., Osella, D.: Biological activity of a series of cisplatin-based aliphatic bis(carboxylato) Pt(IV) prodrugs: how long the organic chain should be? J. Inorg. Biochem. **140**, 219–227 (2014)
36. Giandomenico, C.M., Abrams, M.J., Murrer, B.A., Vollano, J.F., Barnard, C.F.J., Harrap, K.R., Goddard, P.M., Kelland, L.R., Morgan, S.E.: Synthesis and reactions of a new class of orally active Pt(IV) antitumour complexes. In: Howell, S.B. (ed.) Platinum and Other Metal Coordination Compounds in Cancer Chemotherapy, pp. 93–100. Plenum, New York (1991)
37. Ravera, M., Gabano, E., Zanellato, I., Fregonese, F., Pelosi, G., Platts, J.A., Osella, D.: Antiproliferative activity of a series of cisplatin-based Pt(IV)-acetylamido/carboxylato prodrugs. Dalt. Trans. **4**, 5300–5309 (2016)
38. Ravera, M., Gabano, E., Tinello, S., Zanellato, I., Osella, D.: May glutamine addiction drive the delivery of antitumor cisplatin-based Pt(IV) prodrugs? J. Inorg. Biochem. **167**, 27–35 (2017)
39. Wilson, J.J., Lippard, S.J.: Synthetic methods for the preparation of platinum anticancer complexes. Chem. Rev. **114**, 4470–4495 (2014)
40. Lee, Y.-A., Yoo, K.H., Jung, O.-S., et al.: Bull. Chem. Soc. Jpn. **76**, 107–110 (2003)
41. Alessio, M., Zanellato, I., Bonarrigo, I., Gabano, E., Ravera, M., Osella, D.: Antiproliferative activity of Pt(IV)-bis(carboxylato) conjugates on malignant pleural mesothelioma cells. J. Inorg. Biochem. **129**, 52–57 (2013)
42. Ravera, M., Gabano, E., Pelosi, G., Fregonese, F., Tinello, S., Osella, D.: A new entry to asymmetric platinum(IV) complexes via oxidative chlorination. Inorg. Chem. **53**, 9326–9335 (2014)
43. Sinha, R.K., Maître, P., Piccirillo, S., Chiavarino, B., Crestoni, M.E., Fornarini, S.: Cysteine radical cation: a distonic structure probed by gas phase IR spectroscopy. Phys. Chem. Chem. Phys. **12**, 9794–9800 (2010)
44. Sinha, R.K., Nicol, E., Steinmetz, V., Maître, P.: Gas phase structure of micro-hydrated $[Mn(ClO_4)]^+$ and $[Mn_2(ClO_4)_3]^+$ ions probed by infrared spectroscopy. J. Am. Soc. Mass Spectrom. **21**, 758–772 (2010)
45. Prell, J.S., O'Brien, J.T., Williams, E.R.: IRPD spectroscopy and ensemble measurements: effects of different data acquisition and analysis methods. J. Am. Soc. Mass Spectrom. **21**, 800–809 (2010)
46. Frisch, M.J., Trucks, G.W., Schlegel, H.B., Scuseria, G.E., Robb, M.A., Cheeseman, J.R., Scalmani, G., Barone, V., Mennucci, B., Petersson, G.A., Nakatsuji, H., Caricato, M., Li, X., Hratchian, H.P., Izmaylov, A.F., Bloino, J., Zheng, G., Sonnenberg, J.L., Hada, M., Ehara, M., Toyota, K., Fukuda, R., Hasegawa, J., Ishida, M., Nakajima, T., Honda, Y., Kitao, O., Nakai, H., Vreven, T., Montgomery Jr., J.A., Peralta, J.E., Ogliaro, F., Bearpark, M., Heyd, J.J., Brothers, E., Kudin, K.N., Staroverov, V.N., Keith, T., Kobayashi, R., Normand, J., Raghavachari, K., Rendell, A., Burant, J.C., Iyengar, S.S., Tomasi, J., Cossi, M., Rega, N., Millam, J.M., Klene, M., Knox, J.E., Cross, J.B., Bakken, V., Adamo, C., Jaramillo, J., Gomperts, R., Stratmann, R.E., Yazyev, O., Austin, A.J., Cammi, R., Pomelli, C., Ochterski, J.W., Martin, R.L., Morokuma, K., Zakrzewski, V.G., Voth, G.A., Salvador, P., Dannenberg, J.J., Dapprich, S., Daniels, A.D., Farkas, Ö., Foresman, J.B., Ortiz, J.V., Cioslowski, J., Fox, D.J.: Gaussian 09, revision D.01. Gaussian, Inc., Wallingford (2010)
47. Becke, A.D.: Density-functional thermochemistry. III. The role of exact exchange. J. Chem. Phys. **98**, 5648–5652 (1993)
48. Lee, C., Yang, W., Parr, R.G.: Development of the Colle-Salvetti correlation-energy formula into a functional of the electron density. Phys. Rev. B. **37**, 785–789 (1988)
49. Andrae, D., Häussermann, U., Dolg, M., Stoll, H., Preuss, H.: Energy-adjusted ab initio pseudopotentials for the second and third row transition elements. Theor. Chim. Acta. **77**, 123–141 (1990)
50. McQuarrie, D.A., Simon, J.D.: Molecular Thermodynamics. University Science Books, Sausalito (1999)
51. Fukui, K.: Formulation of the reaction coordinate. J. Phys. Chem. **74**, 4161–4163 (1970)
52. Gonzalez, C., Schlegel, H.B.: An improved algorithm for reaction path following. J. Chem. Phys. **90**, 2154–2161 (1989)
53. Butschke, B., Schwarz, H.: The "missing link": the gas-phase generation of platinum-methylidyne clusters Pt_nCH^+ (N=1, 2) and their reactions with hydrocarbons and ammonia. Chem. Eur. J. **17**, 11761–11772 (2011)

54. Choi, S., Filotto, C., Bisanzo, M., Delaney, S., Lagasee, D., Whitworth, J.L., Jusko, A., Li, C., Wood, N.A., Willingham, J., Schwenker, A., Spaulding, K.: Reduction and anticancer activity of platinum(IV) complexes. Inorg. Chem. **37**, 2500–2504 (1998)
55. Ravera, M., Gabano, E., Zanellato, I., Bonarrigo, I., Escribano, E., Moreno, V., Font-Bardia, M., Calvet, T., Osella, D.: Synthesis, characterization and antiproliferative activity on mesothelioma cell lines of bis(carboxylato)platinum(IV) complexes based on picoplatin. Dalt. Trans. **41**, 3313–3320 (2012)
56. Oomens, J., Steill, J.D., Redlich, B.: Gas-phase IR spectroscopy of deprotonated amino acids. J. Am. Chem. Soc. **131**, 4310–4319 (2009)
57. Roithovà, J.: Characterization of reaction intermediates by ion spectroscopy. Chem. Soc. Rev. **41**, 547–559 (2012)
58. Corinti, D., De Petris, A., Coletti, C., Re, N., Chiavarino, B., Crestoni, M.E., Fornarini, S.: Cisplatin primary complex with L-histidine target revealed by IR multiple photon dissociation (IRMPD) spectroscopy. ChemPhysChem. **18**, 318–325 (2017)
59. Leavitt, C.M., Deblase, A.F., Johnson, C.J., Van Stipdonk, M., McCoy, A.B., Johnson, M.A.: Hiding in plain sight: unmasking the diffuse spectral signatures of the protonated N-terminus in isolated dipeptides cooled in a cryogenic ion trap. J. Phys. Chem. Lett. **4**, 3450–3457 (2013)
60. Perez, E., Hanley, C., Koehler, S., Pestok, J., Polonsky, N., Van Stipdonk, M.: Gas phase reactions of ions derived from anionic uranyl formate and uranyl acetate complexes. J. Am. Soc. Mass Spectrom. **27**, 1989–1998 (2016)
61. Dau, P.D., Gibson, J.K.: Halide abstraction from halogenated acetate ligands by actinyls: a competition between bond breaking and bond making. J. Phys. Chem. A. **119**, 3218–3224 (2015)
62. Van Stipdonk, M.J., Chien, W., Anbalagan, V., Bulleigh, K., Hanna, D., Groenewold, G.S.: Gas-phase complexes containing the uranyl ion and acetone. J. Phys. Chem. A. **108**, 10448–10457 (2004)
63. Van Stipdonk, M., Bubas, A., Tatosian, I., Perez, E., Polonsky, N., Metzler, L., Somogyi, A.: Formation of $[U^{V}OF_4]^-$ by collision-induced dissociation of a $[U^{VI}O_2(O_2)(O_2C\text{-}CF_3)_2]^-$ precursor. Int. J. Mass Spectrom. **424**, 58–64 (2018)

4

A NEW CLASS OF ANTICANCER DRUGS: ORGANO IRIDIUM, RUTHENIUM AND OSMIUM COMPLEXES

A new class of anticancer drugs: Organo Iridium, Ruthenium and Osmium complexes

Introduction

In the development of new anticancer drugs, it is of great interest the class of organometallic complexes containing metals other than platinum.

The organometallic complexes reactivity is strongly dependent on the ligand set. Therefore, the discovery of new metallodrugs with different structure and mechanism of action plays an important role in cancer drug research.

Promising alternatives, concomitantly with platinum based metallodrugs, are Ru, Ir, Os and Rh organometallodrugs. In particular, half-sandwich iridium(III) cyclopentadienyl, ruthenium (II) arene and osmium(II) arene complexes containing chelating ligands are a new and promising generation of anticancer drugs. These complexes, based on structural modifications in ligands around the metal center, can bind to DNA and/or also perturb the redox status of cells.

Here, the attention has been focused on two categories of complexes that present polyvalent ligands and represent an innovative strategy in the development and design of new metallodrugs with diverse and simultaneous functions. In particular, the investigation of the mechanism of activation of novel C,N-cyclometalated benzimidazole complexes and organo-metal complexes containing azo-aromatic ligands has been carried out.

The iridium(III) and ruthenium(II) compounds containing a benzimidazole ligand (a widely used pharmacophore) linked with a phenyl ring, exhibit a promising cytotoxic activity against several cancer cell lines.[1] These complexes can undergo hydrolysis, to be activated in cancer cells. Their reactivity depends on the type of ligands. In particular, the benzimidazole ligand and the phenyl ring allow a simple functionalization through the binding of different substituents to modulate several chemical properties and anticancer activity. So, the study of their structure-activity relationship (SAR) opens new perspectives on cancer drugs development.

In vitro tests have also shown that osmium and iridium complexes containing an azopyridine chelating ligand exhibit promising anticancer activity[2,3] and a novel activation mechanisms with respect to that of platinum complexes. These new complexes could therefore be potential candidates to overcome platinum resistance.

These azopyridine complexes are hypothesized to be activated in the cancer cells by the most important biological reducing agent glutathione (GSH), probably through the redox mediation of the azo group.

A proposed mechanism for the organo-Ir complex involves the glutathione attack to the azo bond, formation of the GSSG species and the regeneration of the azo bond. For the osmium complex, the glutathione can promote intracellular activation by hydrolysis

reactions via redox mediation of the azo group. Both drug-candidates are capable of increasing dramatically the production of reactive oxygen species (ROS) and perturb the oxidative status in cancer cells.

Aim of the work

A theoretical study with the aid of density functional theory (DFT) has been carried out to investigate the hydrolysis reactions of two novel half-sandwich organo-iridium and organo-ruthenium complexes containing benzimidazole ligands, recently synthetized and proposed as antitumor agents (**Paper 5**).

Moreover, a theoretical investigation, performed at density functional level of theory has been carried out, with the purpose of elucidating the activation mechanism of the iodido Os(II) azopydine complex **(Paper 6)** and Ir(III) azopyridine complex **(Paper 7**), and rationalizing experimental data provided by the Sadler's group.

Here, are reported the outcomes to prove that the hydrolytic activation of the iodido Os(II) and Ir(III) complexes under investigation involves catalytic attack by the intracellular tripeptide glutathione (GSH) on the azo bond of the chelating ligand in the complexes.

4.1 Theoretical determination of the aquation reaction mechanism of cyclometalated benzimidazole Ru(II) and Ir(III) anticancer complexes

For many anticancer drugs, the activation step coincides with hydrolysis step. Over the years, several experimental and theoretical studies established a relationship between the hydrolysis rate and anticancer activity.[4,5] So, the exploration of factors that control the aqueous chemistry of organometallic compounds could lead to design of more efficient anticancer drugs.

Here, the hydrolysis reaction of novel C,N-cyclometalated benzimidazole ruthenium(II) and iridium(III) complexes of the type [(η^5-C_5Me_5)IrCl(methyl 1-butyl-2-arylbenzimidazolecarboxylate), named 1A, and[(η^6-pcymene)-RuCl(methyl1-butyl-2-rylbenzimidazolecarboxylate)], named 2A, with various substituents (H, CF_3) in the R4 position of the phenyl ring of the 2-phenylbenzimidazole chelating ligand has been theoretically explored.

The structures of the two neutral benzimidazole C,N cyclometalated complexes are reported in Scheme 1.

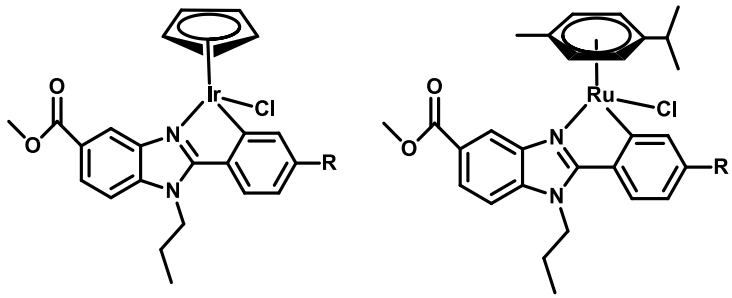

Scheme 1. Chemical structure of cyclometalated Ru and Ir complexes

The reaction, for all the complexes investigated here, proceeds by one step second-order nucleophilic substitution (SN2) mechanism, that involves the exchange of leaving group, the chlorido anion, with the water molecule to generate the aqua complexes Ir/Ru-H_2O.

In order to test the influence of the monodentate ligand on the rate of aquation, the hydrolysis mechanism of the complexes in which the chlorido ligand has been replaced with pyridine, has been studied. Also in this case, the hydrolysis reaction occurs following a SN2 mechanism, which leads to the formation of the corresponding aqua complex.

Such studies have shown as the presence of the strongly bound pyridine ligand slows down the rate of hydrolysis reaction compared to that of its chlorido analogue. The more electron withdrawing CF_3 group in R4 position of the phenyl ring decreases lability of the monodentate ligand with a consequent increment of the energy barriers.

From this theoretical investigation it is possible to assume that the reactivity of all the investigated complexes is ligand-dependent.

4.2 Glutathione activation of an organometallic half-sandwich anticancer drug candidate by ligand attack

The organometallic complexes belonging to the family of Os(II) arene complexes [Os(η^6-*p*-cym)(5-R^1-pyridylazo-4-R^2-phenyl))I]$^+$ (where *p*-cym = para-cymene), 1-I (R^1 = H, R^2 = NMe_2), show promising anticancer activity as they are capable of overcoming platinum resistance problems and cause fewer side-effects, [3,6] very likely due to the novel mechanism of action (MoA) [7,8] they exhibit.

Another potent drug-candidate in anticancer treatment, the [Os(η^6-*p*-cymene)(4-(2-pyridylazo)-*N*,*N*-dimethylaniline)I]$^+$ complex, also known as FY26 and here reported as **1-I** (Figure 1) has been the focus of the attention of Sadler's group. This osmium complex is 49× more active than cisplatin in 800 cancer cell lines.[7]

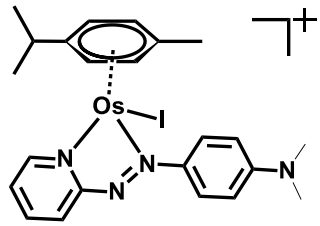

Figure 1.Chemical structure of FY26

The drug-candidate reported in Figure 1 increases oxidative stress in treated cells through the production of reactive oxygen species (ROS) and target mitochondrial metabolism rather than DNA.[3,9]

Experimental data provided by Sadler and co-workers show that the osmium complex is relatively inert in solution, over long period is

stable in blood serum, but appears to be activated by GSH (γ-L-Glu-L-Cys-Gly) in cancer cells and generates ROS.

The hydrolysis reaction seems to be the key step in the complex activation and it is promoted by the tripeptide glutathione to generate the hydroxido 1-OH more reactive complex. 1-OH organo-complex, in turn, can react with other molecules/ions present in cells, such as hydrogen peroxide generating hydroxido radicals in the process.[3]

In addition, obtained experimental results suggest the possible catalytic nature of the reaction and that the hydrolysis of the complex occurs only in presence of glutathione and, in particular, through its direct interaction with the azo bond of the chelating ligand in the complex.

In collaboration with Sadler's group, combined theoretical and experimental approaches have been used to study the hydrolysis of the organo-osmium complex in presence of GSH.

Three different possible hydrolysis mechanisms, in presence of deprotonated glutathione (GS^-), have been proposed and explored:

1. Direct hydrolysis of the Os-I bond
2. Direct interaction of the metal with GS^- and subsequent hydrolysis
3. Attack of GS^- to the –N=N- bond followed by hydrolysis reaction.

DFT computational analysis shows that the most favourable hydrolysis pathway involves the redox mediation by the azo group.

The proposed attack of the glutathione on the azo bond (-N=N-) in Os-I during the hydrolysis process has been further probed using X-ray absorption spectroscopy (XAS) and chromatographic experiments, to provide structural information.

Analogous calculations have been carried out for the complex obtained by the binding to the pyridine ring the electron-donating ethoxy group.

Very similar results have been obtained, but lower energy barriers have been calculated when compared with 1-I according to experimental findings.

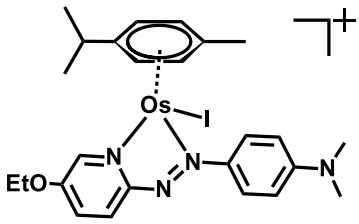

Figure 2.Chemical structure of 2-I.

It is possible to conclude that GSH plays an important role in the activation of the osmium complex. Specifically, the redox mediation by the azo group has an important role in the hydrolysis and intracellular activation.

Overall, these results provide new insights into the novel mechanism of activation of 1-I and will be of fundamental importance in the development of future generations of anticancer agents.

4.3 Ligand-centred redox activation of inert organo-iridium(III) anticancer complexes

Half-sandwich iridium(III) cyclopentadienyl complexes containing azopyridine ligands exhibit promising *in vitro* antiproliferative activity and novel mechanism of action that differ from Pt(II) complexes.

Experimental data provided by the group of Sadler, probe that they are inert towards hydrolysis reactions, but are activated by GSH, under physiologically relevant conditions, forming Ir-thiolate complexes.

It is worth of attention the catalytic action of these azopyridine complexes in the reduction reaction that involves the oxidation of the most important biological reducing agent glutathione (GSH) to glutathione disulphide (GSSG). A proposed redox cycle involves the attack to the azo bond, the formation of GSSG species and the regeneration of the azo bond.

The reactivity of the Ir(III)-iodido complex, $[(Cp^{ph})Ir(azpy\text{-}OH)I]^{+}$, named 2-I (Figure 3) with the aid of density functional theory (DFT) has been studied with the purpose of elucidating the activation mechanism and rationalizing experimental data. The possible involvement of O_2 in reactive oxygen species (ROS) generation has been also taken into consideration.

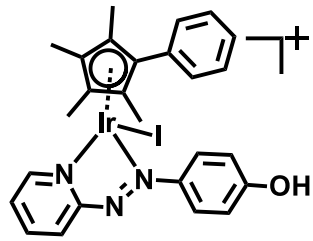

Figure 3.Chemical structure of 2-I.

Three different possible reaction mechanisms have been explored for the iridium complex. The first studied mechanism involves the hydrolysis of the Ir-I bond. The second mechanism involves the displacement of iodide by SG^-. The third investigated mechanism, instead, occurs by the GS^- attack on the N atom of the double bond. Subsequent hypothesized steps lead to the formation of the GSSG oxidized product, in presence of O_2.

The energy barrier for the attack to the azo bond by GSH is much lower than the direct replacement of iodide by GSH from the Ir center (20.2 kcal·mol-1), and it is 5.6 kcal·mol^{-1}. Moreover, it is important to underline that the Ir center preferably binds with GS^- to form the Ir-SG complex rather than bind with H_2O. Finally, it is important to note that the product of the whole reaction, which includes the formation of superoxide anion and GSSG, is largely exergonic with final energy of -59.4 kcal·mol^{-1}.

From a detailed analysis of the explored reaction paths, it can be concluded that GSH plays a role in the activation and ROS generation and that the activation of the Ir-I complex occurs through attack of GS^- on the azo bond.

Outcomes from computations are in good agreement with the experimental evidence.

References Chapter 4

(1) Yellol, G. S.; Donaire, A.; Yellol, J. G.; Vasylyeva, V.; Janiak, C.; Ruiz, J. On the Antitumor Properties of Novel Cyclometalated Benzimidazole Ru(II), Ir(III) and Rh(III) Complexes. *Chem. Commun.* **2013**, *49* (98), 11533–11535. https://doi.org/10.1039/C3CC46239K.

(2) Liu, Z.; Sadler, P. J. Organoiridium Complexes: Anticancer Agents and Catalysts. *Acc. Chem. Res.* **2014**, *47* (4), 1174–1185. https://doi.org/10.1021/ar400266c.

(3) Needham, R. J.; Sanchez-Cano, C.; Zhang, X.; Romero-Canelón, I.; Habtemariam, A.; Cooper, M. S.; Meszaros, L.; Clarkson, G. J.; Blower, P. J.; Sadler, P. J. In-Cell Activation of Organo-Osmium(II) Anticancer Complexes. *Angew Chem Int Ed Engl* **2017**, *56* (4), 1017–1020. https://doi.org/10.1002/anie.201610290.

(4) Zhang, Y.; Guo, Z.; You, X.-Z. Hydrolysis Theory for Cisplatin and Its Analogues Based on Density Functional Studies. *J. Am. Chem. Soc.* **2001**, *123* (38), 9378–9387. https://doi.org/10.1021/ja0023938.

(5) Wang, F.; Habtemariam, A.; van der Geer, E. P. L.; Fernández, R.; Melchart, M.; Deeth, R. J.; Aird, R.; Guichard, S.; Fabbiani, F. P. A.; Lozano-Casal, P.; et al. Controlling Ligand Substitution Reactions of Organometallic Complexes: Tuning Cancer Cell Cytotoxicity. *Proc. Natl. Acad. Sci. U.S.A.* **2005**, *102* (51), 18269–18274. https://doi.org/10.1073/pnas.0505798102.

(6) Organometallic osmium arene complexes with potent cancer cell cytotoxicity. - PubMed - NCBI https://www.ncbi.nlm.nih.gov/pubmed/20977192 (accessed Sep 17, 2019).

(7) Hearn, J. M.; Romero-Canelón, I.; Munro, A. F.; Fu, Y.; Pizarro, A. M.; Garnett, M. J.; McDermott, U.; Carragher, N. O.; Sadler, P. J. Potent Organo-Osmium Compound Shifts Metabolism in Epithelial Ovarian Cancer Cells. *Proc. Natl. Acad. Sci. U.S.A.* **2015**, *112* (29), E3800-3805. https://doi.org/10.1073/pnas.1500925112.

(8) Romero-Canelón, I.; Mos, M.; Sadler, P. J. Enhancement of Selectivity of an Organometallic Anticancer Agent by Redox Modulation. *J. Med. Chem.* **2015**, *58* (19), 7874–7880. https://doi.org/10.1021/acs.jmedchem.5b00655.

(9) Afrasiabi, Z.; Sinn, E.; Padhye, S.; Dutta, S.; Padhye, S.; Newton, C.; Anson, C. E.; Powell, A. K. Transition Metal Complexes of Phenanthrenequinone Thiosemicarbazone as Potential Anticancer Agents:

Synthesis, Structure, Spectroscopy, Electrochemistry and in Vitro Anticancer Activity against Human Breast Cancer Cell-Line, T47D. *J Inorg Biochem* **2003**, *95* (4), 306–314. https://doi.org/10.1016/S0162-0134(03)00131-4.

A new class of anticancer drugs: Organo Iridium, Ruthenium and Osmium complexes

Inorganica Chimica Acta 470 (2018) 325–330

Contents lists available at ScienceDirect

Inorganica Chimica Acta

journal homepage: www.elsevier.com/locate/ica

Research paper

Theoretical determination of the aquation reaction mechanism of cyclometalated benzimidazole Ru(II) and Ir(III) anticancer complexes

Fortuna Ponte, Ida Ritacco, Gloria Mazzone, Nino Russo, Emilia Sicilia *

Dipartimento di Chimica e Tecnologie Chimiche, Università della Calabria, 87036 Rende (CS), Italy

ARTICLE INFO

Article history:
Received 11 April 2017
Received in revised form 30 May 2017
Accepted 1 June 2017
Available online 1 June 2017

Special Volume: Protagonists in Chemistry
Dedicated to Professor Carlo Mealli

Keywords:
DFT
Ir(III) complexes
Ru(II) complexes
Hydration process
PES

ABSTRACT

The free energy profiles for the hydrolysis reaction mechanism of two synthesized C,N-cyclometalated benzimidazole chorido-Ir(III) and Ru(II) anticancer complexes, which have shown promising anticancer activity, have been explored theoretically employing density functional theory (DFT). Analogous calculations have been carried out for the complexes obtained by the substitution of either the H atom in R4 position of the phenyl ring of the 2-phenylbenzimidazole chelating ligand with the electron-withdrawing CF_3 group or the chloride ligand with pyridine with the purpose to probe the influence of such substitutions on the hydrolysis profiles. Results show that for the unsubstituted complexes displacement of the labile chloride ligand by water requires that low energy barriers are surmounted for the aquation process to occur. Substitution with either the CF_3 group in peripheral position or chloride with pyridine causes an increase of barriers heights. The only complex with an hydrolysis barrier comparable with that of cisplatin is the pyridine leaving ligand ruthenium complex.

1. Introduction

Cisplatin (*cis*-diamminedichloridoplatinum(II), $PtCl_2(NH_3)_2$), the most used drug in anticancer therapy, was synthesized by the Italian scientist Peyrone in 1845, but its ability to inhibit cell division has been serendipitously discovered by Rosenberg after 120 years (1965) [1]. Over the past decades it has been used with some success in the treatment of testicular and ovarian tumors and, consequently, its use has been extended to other types of cancer (e.g. in bladder, cervical, head and neck). Despite this intensive use, this drug presents severe limitations due to its serious side effects and the resistance that some cancers develop towards its use. These limitations have to a great extent stimulated the search for new metal-containing anticancer drugs able to circumvent cisplatin resistance and reduce its toxicity [2]. To date, amongst thousands of proposed and tested compounds, only two, carboplatin [3] and oxaliplatin [4], have obtained the necessary approvals in most of the world for their use in medical protocols and, besides the classical Pt(II) compounds, also Pt(IV) prodrugs, that release Pt(II) anticancer agents, have been the subject of intensive studies [2,5–10]. Particularly promising is the Pt(IV) drug satraplatin designed with ligands ensuring lipophilicity and stability that allow oral administration [9]. The latest strategies for finding new antineoplastic agents, however, focus on organometallic compounds containing metals other than platinum and, to this aim the potential of many metal based compounds has been widely explored. Ruthenium-based complexes, designed on the model of cisplatin, have shown favorable antineoplastic activity and lower systemic toxicity than platinum(II) compounds, both in vitro and in vivo, towards a number of cancers [11–18]. One of these, the [Him]trans-[$RuCl_4$(DMSO-S)Im] has passed the preclinical tests and entered in phase I clinical trial [11]. A series of half-sandwich cyclopentadienyl Iridium (III) complexes has been synthesized and characterized as potential anticancer agents [19–21]. In the recent literature many examples of half-sandwich metal complexes of general formula [(η^6-arene)Me(YZ)(X)]$^{0/+}$, where YZ is typically a chelating ligand and X is a halide, have been reported [20,22–27]. Such compounds have demonstrated their potential as anticancer agents due the presence of the hydrophobic arene ligand that seems to enable the diffusion through the cell membrane, and of various ligands around the metal centre capable to properly tune biological and pharmacological properties.

It is well known that the anticancer activity of platinum-containing compounds is essentially due to their binding ability to DNA with consequent inhibition of the replication process, even if other targets such as mitochondrial membranes, thiol-containing proteins, enzymes, metal transport protein and RNA can be

* Corresponding author.
E-mail address: siciliae@unical.it (E. Sicilia).

http://dx.doi.org/10.1016/j.ica.2017.06.001
0020-1693/

involved [28–33]. The interaction with these target is also responsible of the strong site effects of cisplatin, while the resistance is due to the possible repair of platinated DNA that can be conferred by a number of mechanisms [34,35]. While the DNA is the main biological target of cisplatin, its widely accepted mechanism of action includes a first phase for the cellular uptake followed by the drug activation through the hydrolysis reaction, the subsequent interaction of the aquated complex with DNA and, as a last step, the cellular processing of DNA lesions that lead to cell death [36,37]. The hydrolysis process plays an important role since if the ligand substitution is fast, a high amount of activated drug enters the cellular environment reducing its effectiveness and contributing to the increase of side effects. Previous studies have demonstrated as the chloride/water ligand exchange does not occur in blood, where the Cl^- concentration is about 100 mM, but into the cell where the Cl^- ion concentration is less than 20 mM and requires about 2 h to occur [2]. The superior activity of carboplatin and oxaliplatin has been related to the slow kinetics of the aquation process that occurs in more than a week. In this scenario, accurate qualitative and quantitative studies of the hydrolysis mechanism become important and allow for a rational design of new metal-bases anticancer drugs. Computational investigations, able to locate and characterize stationary points along potential energy surfaces, have allowed the elucidation at atomistic level of the hydrolysis reaction of cisplatin, carboplatin, oxaliplatin and other anticancer complexes as well as the binding with DNA highlighting the role of the ligands in the exchange process [14,38–45]. In this paper we present a detailed theoretical study, performed at density functional level of theory, of the hydrolysis reactions of two novel half-sandwich organo-iridium and organo-ruthenium complexes recently synthetized and proposed as antitumor agents [46,47]. The structures of the two neutral benzimidazole C,N-cyclometalated investigated complexes, [(η^5-C_5Me_5)IrCl(methyl 1-butyl-2-arylbenzimidazolecarboxylate), named **1A**, and [(η^6-*p*-cymene)-RuCl(methyl 1-butyl-2-arylbenzimidazolecarboxylate)], named **2A**, are sketched in Scheme 1. With the purpose to reduce the computational cost, the methyl groups of the pentamethylcyclopentadienyl ligand have been substituted with hydrogen atoms and preliminary calculations have been performed to probe that such substitution does not affect the course of the hydrolysis reactions. Additional calculations have been carried out on the same complexes substituting either the H atom in the R4 position of the phenyl ring of the 2-phenylbenzimidazole chelating ligand with the more electron-withdrawing CF_3 group or the chloride ligand with pyridine, as shown in Scheme 1, aiming at probing the influence of such substitutions on the hydrolysis profiles.

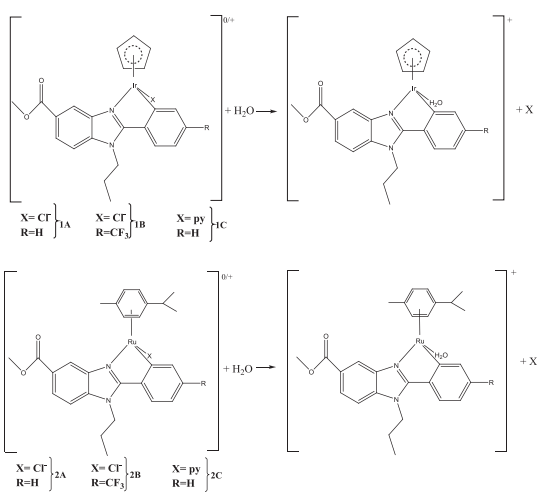

Scheme 1.

2. Computational details

Geometry optimizations have been performed at DFT level using the Truhlar's meta-GGA functional M06-L [48], whose use is suggested for the study of organometallic systems [49], employing the relativistic compact Stuttgart/Dresden effective core potentials [50] for Ir and Ru centers in combination with the split valence basis set. The standard triple-ζ quality 6-311G** basis sets of Pople and co-workers have been used for the rest of the atoms except peripheral atoms, not directly influencing the behavior of the complexes, for which the smaller 6-31G basis sets have been employed. It is worth mentioning that for Cl atom the 6-311+G** basis set has been employed to take into consideration the formation of an anion. All calculations have been carried out with the Gaussian09 software package [51]. Calculation of vibrational frequencies has been performed for both establishing the nature of intercepted stationary points as minima and transition states and including unscaled zero point energy corrections. The involved transition states have been checked to connect the correct minima by IRC (intrinsic reaction coordinate) analysis [52,53]. In order to estimate the impact of solvation effects on the energy profiles the Tomasi's implicit polarizable continuum model (PCM) in its Integral-Equation-Formalism (IEF) [54–56] formulation as implemented in Gaussian09 has been adopted and the UFF set of radii has been chosen to build up the cavity. The solvation Gibbs free energies have been calculated in implicit water (ε = 78.4) at the same level of theory by performing single-point calculations on all stationary points structures optimized in vacuum. Enthalpies and Gibbs free energies have been obtained at standard (298 K and 1 atm) from total energies, including zero-point, thermal, and solvent corrections, using standard statistical procedures [57]. However, since the Gaussian's default standard state corresponds to an ideal gas at a standard pressure of 1 atm, the computed free energies have been converted [58] to yield Gibbs energies with a solution phase standard state of 1 mol L^{-1} for all the species. For water molecules a standard state of 55.5 M has been used. That is, to the free energy of each species as computed in Gaussian has been added a free energy correction term equal to RT $\ln(V_{molar\ gas}/V_{molar\ solution})$, (R = gas constant, T = absolute temperature) where $V_{molar\ gas}$ is the volume occupied by one mole of ideal gas at the considered temperature, and $V_{molar\ solution}$ is the volume occupied by one mole of species in a standard solution of concentration 1 mol L^{-1}.

3. Results and discussion

Fully optimized structure of the investigated C,N-cyclometalated benzimidazole iridium(III), labeled **1A**, and ruthenium(II), labeled **2A**, complexes are depicted in Fig. 1, where the experimental and theoretical values of the most significant geometrical parameters are compared. The adopted classical pseudo-octahedral piano-stool arrangement is properly reproduced, with the arene ring displaying the common π-bonded η^6-coordination mode and the arylbenzimidazole-type ligand assuming a bidentate chelating coordination mode. The comparison between calculated and experimental, extracted from the crystallographic characterization, geometrical parameters shows a good modeling of the investigated systems.

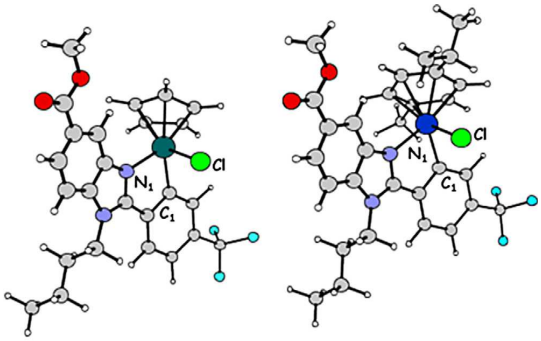

Ir-Cl=2.434 (2.406)	Ru-Cl=2.441(2.419)
Ir-N_1=2.107(2.060)	Ru-N_1=2.115(2.0666)
Ir-C_1=2.046(2.059)	Ru-C_1=2.066(2.0508)
Ir-Cp(centroid)=1.898(1.81)	Ru-Cym(centroid)=1.725(1.712)
C_1-Ir-N1=76.64 (76.8)	C_1-Ru-N_1=76.23(76.64)
C_1-Ir-Cl=86.45(88.7)	C_1-Ru-Cl=85.61(87.68)
N_1-Ir-Cl=82.82(85.6)	N_1-Ru-Cl=83.23(86.77)
Cp(centroid)-Ir-Cl=125.00(125.6)	Cym(centroid)-Ru-Cl=125.67(128.26)
Cp(centroid)-Ir-N_1=137.15(133.1)	Cym(centroid)-Ru-N_1=133.41(131.30)
Cp(centroid)-Ir-C_1=130.79(130.4)	Cym(centroid)-Ru-C_1=133.86(129.02)

Fig. 1. Fully optimized structures of **1A** and **2A** complexes. Selected bond lengths (in Å) and angles (degrees) are compared with available experimental values (in parentheses).

As metal aqua complexes are generally more reactive than the corresponding non-aqua complexes and the hydrolysis might represent a key step of the activation process of the proposed anticancer drugs, in analogy with a wide number of previously examined metal-containing anticancer compounds [2,38–45], the hydrolysis reaction mechanism of the M–Cl bond has been investigated (see Scheme 1) for the half-sandwich **1A** and **2A** complexes. According to the substitution patterns experimentally carried out at the peripheral R4 position of the phenyl ring of 2-phenylbenzimidazole chelating ligand [47], the effect of the substitution with the electron-withdrawing CF_3 group on the hydrolysis pathways has been also investigated. The corresponding Ir(III) and Ru(II) complexes have been named **1B** and **2B**, respectively. Furthermore, as a result of our previous experience with iridium complexes [59] we have considered to be of interest to study the effect of the substitution of the chloride ligand with the less labile pyridine ligand. As shown in Scheme 1, the pyridine substituted complexes have been indicated as **1C** and **2C**. The hydration process consists of only one step in which a water molecule approaches the complex and going throughout the transition state it replaces the X ligand in an associative way. The potential energy surfaces for the hydrolysis of the studied complexes are reported in Fig. 2. The optimized structures of the intermediates and transition states intercepted along the hydrolysis pathways are depicted in Fig. 3a for **1A**, **1B** and **1C** complexes and in Fig. 3b for **2A**, **2B** and **2C** complexes. For the Ir(III) **1A**, **1B** and **1C** complexes the approach of water leads to the formation of three adducts with energies that lie below that of separated reactants and the more stable one is $\mathbf{INT_{1A}}$ (at −3.4 kcal mol^{-1}) followed by $\mathbf{INT_{1B}}$ (at −2.7 kcal mol^{-1}) and $\mathbf{INT_{1C}}$ (at −0.7 kcal mol^{-1}). In all three intermediates, the incoming water molecule is located at relatively long distance (about 4 Å), while the bond distances of the Cl^- leaving group are close to those of the corresponding starting complexes. The entering water molecule, in all cases, appears to occupy a position that does not allow establishing interactions with both metal and leaving Cl^- and py ligands. The respective transition state relative energies result to be 11.9 kcal mol^{-1} ($\mathbf{TS_{1A}}$), 14.8 kcal mol^{-1} ($\mathbf{TS_{1B}}$) and

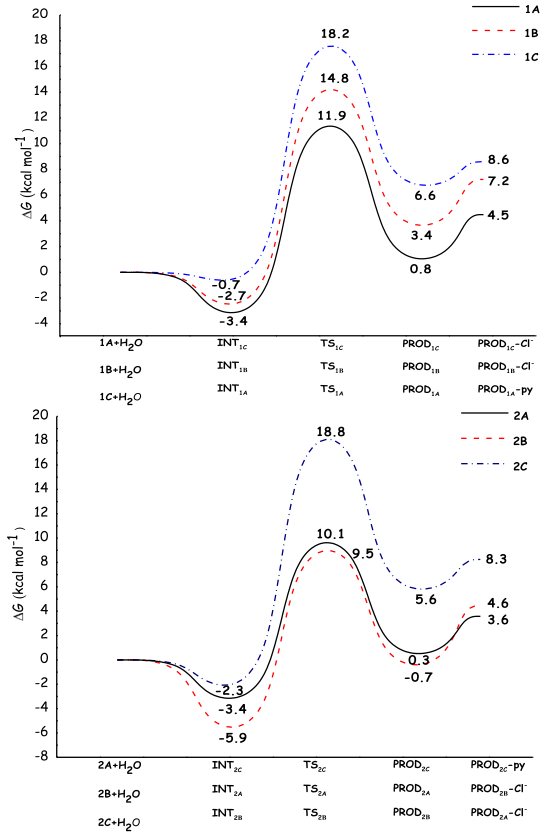

Fig. 2. Calculated free energy profiles in water for the hydrolysis of (a) Ir(III) **1A**, **1B** and **1C** and (b) Ru(II) **2A**, **2B** and **2C** complexes. Energies are in kcal mol^{-1} and relative to separated reactants for $\mathbf{TS_{1A}}$, $\mathbf{TS_{1B}}$ and $\mathbf{TS_{1C}}$, respectively and the vibrational mode properly corresponds to the simultaneous Ir-Cl/Ir-N bond breaking and Ir-O bond formation. Proper connection of intercepted transition states with corresponding minima has been verified by IRC calculations.

18.2 kcal mol^{-1} ($\mathbf{TS_{1C}}$). Thus, as expected, the formation of the aquated complexes requires the overcoming of an energy barrier that depends on the nature of the ligands. In fact, for the **1A** chloride complex the barrier is 15.3 kcal mol^{-1} while, introducing the withdrawing CF_3 group in the ancillary ligand (**1B**) the barrier increases (17.5 kcal mol^{-1}). The replacement of the chloride with pyridine (**1C**) leads to an even higher barrier (18.9 kcal mol^{-1}). All the structures of the intercepted TSs (Fig. 3) correspond to the associative X ligand displacement by water and are characterized by imaginary frequencies of 102*i*, 128*i* and 70*i* cm^{-1}.

Formation of the adducts $\mathbf{PROD_{1A}}$, $\mathbf{PROD_{1B}}$ and $\mathbf{PROD_{1C}}$ in which the released ligands are weakly bonded to the aquated complexes is calculated to be endothermic in all cases, even if for the **1A** complex is almost thermoneutral. Finally, definitive release from the formed adducts of the displaced Cl^- and py ligands requires 3.7, 3.8 and 2.0 kcal mol^{-1} to occur for **1A**, **1B** and **1C** complexes, respectively.

The Ru(II) corresponding complexes, **2A**, **2B** and **2C**, (see Fig. 1b), show very similar behaviors with the formation of first intermediates and adducts between released ligands and aquated complexes calculated to be exothermic and endothermic, respectively. The barriers heights are 13.5 kcal mol^{-1} for **2A**,

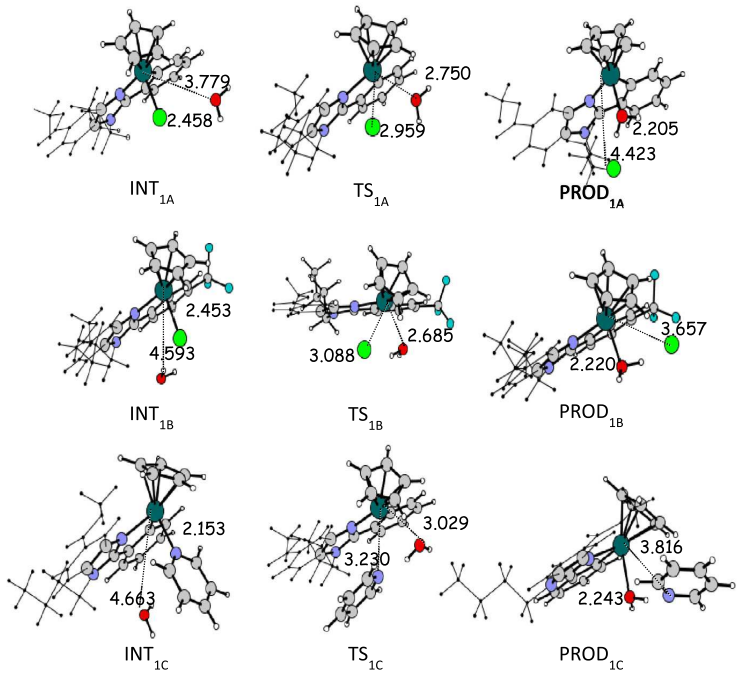

Fig. 3. Fully optimized structures of stationary points intercepted along the hydration pathways of the **1A**, **1B** and **1C** Ir(III) complexes. The breaking (Cl^- and py) and forming (H_2O) bond lengths (in Å) are reported.

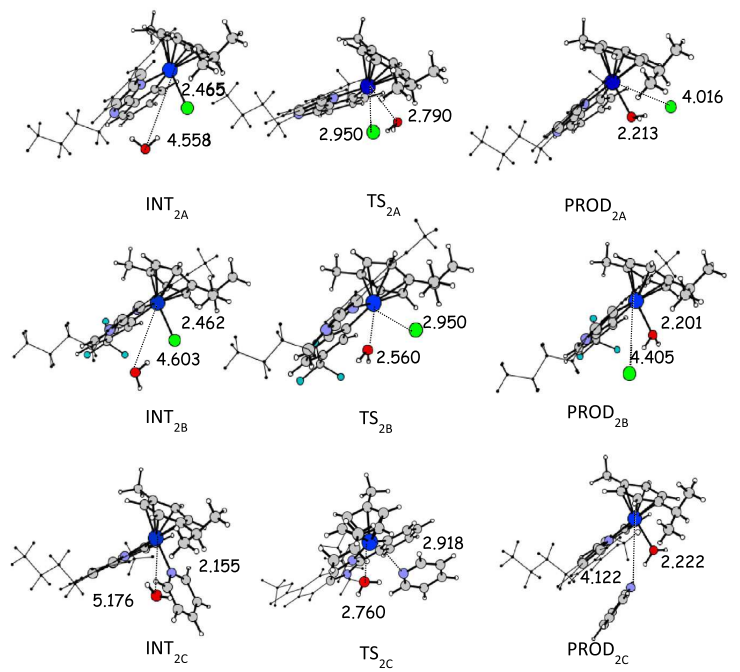

Fig. 4. Fully optimized structures of stationary points intercepted along the hydration pathways of the **2A**, **2B** and **2C** Ru(II) complexes. The breaking (Cl^- and py) and forming (H_2O) bond lengths (in Å) are reported.

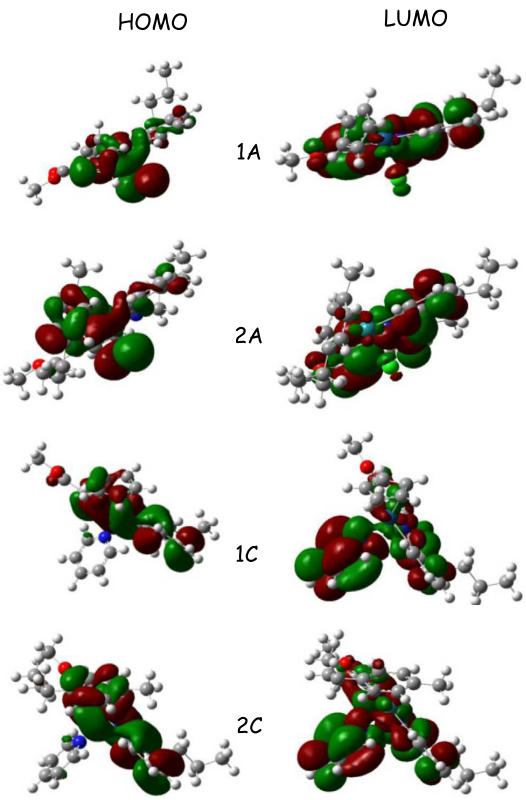

Fig. 5. HOMO and LUMO plots for chloride **1A** and **2A**, and pyridine **1C** and **2C** complexes.

15.4 kcal mol^{-1} for **2B** and 21.1 kcal mol^{-1} for **2C**. Also in this case the highest barrier is obtained for the pyridine complex. Loss of the released Cl^- and py ligands requires 3.3, 5.3 and 2.7 kcal mol^{-1} to occur from the formed **PROD$_{2A}$**, **PROD$_{2B}$** and **PROD$_{2C}$** adducts, respectively. As shown in Fig. 4, the structural changes in stationary points intercepted along the hydrolysis pathways show similar trends to those observed for the iridium complexes. Comparison with cisplatin, for which the calculated barrier for the first aquation process is 23.8 kcal mol^{-1} [60] (24.1 kcal mol^{-1}) [61], reveals that the hydrolysis process for the examined complexes require less energy to occur with a consequent increase of the reaction rate. As mentioned above and demonstrated by Sadler et al. for Ru(II) arene complexes [14,21], a relationship exists between hydrolysis rate and cytotoxic activity. Therefore, aquation kinetics might play a key role since fast aquation causes the release of high amounts of activated drug reducing, consequently, its activity and increasing the side effects. Comparable kinetics with cisplatin can be obtained only if the chloride ligand is substituted by pyridine in Ru complex **2A**.

In order try to rationalize the reported results and better characterize the complexes we have examined the energy and the composition of HOMO and LUMO frontier orbitals. The HOMO to LUMO energy gaps of complexes **1A** and **2A** are comparable being 2.69 and 2.72 eV, respectively. When the pyridine complexes are examined the values of the gap become 3.02 and 2.97 eV for **1C** and **2C**, respectively. The values for the pyridine complexes account for the higher kinetic stability and lower chemical reactivity of these species as revealed by the calculated energy barriers. The analysis of the molecular frontier orbitals, shown in Fig. 5, for chloride and pyridine complexes **1A**, **2A**, **1C** and **2C**.

In both **1A** and **2A** HOMO a high contribution of chloride is present, while the contribution of the π system is larger for the Ru complex due the participation of η^6-p-cymene ligand. The LUMOs of **1A** and **2A** systems show similar composition. The **1C** and **2C** complexes are characterized by a large participation of the pyridine ligand in the LUMO while the HOMOs' compositions are similar.

4. Conclusions

In this work we have investigated the hydrolysis pathways of two recently synthesized and characterized cyclometalated benzimidazole Ru(II) and Ir(III) anticancer compounds and of the corresponding complexes obtained by substitution of the H atom in R4 position of the phenyl ring of the 2-phenylbenzimidazole chelating ligand with the more electron-withdrawing CF_3 group. In addition, other two complexes in which the leaving chloride ligand has been replaced by pyridine have been examined with the aim to prove whether this substitution can slow down the aquation kinetics. The investigation has been carried out at density functional level of theory accounting for solvent effects and employing a computational protocol previously and successfully used in a series of metal-containing anticancer systems. The outcomes of our computational analysis show that the one-step hydrolysis reaction proceeds, in all cases, going through a transition state for the associative replacement of the labile ligand and for the ruthenium complexes calculated barriers are higher than those for the corresponding iridium ones. The presence of an electron withdrawing CF_3 group in R4 position of the phenyl ring of the phenyl-benizimidazole ancillary ligand causes an increase of the activation barriers, which are further raised by the substitution of the Cl- labile ligand with pyridine. We hope the results reported here can stimulate further experimental investigations on these promising complexes for their potential anticancer activity.

Acknowledgments

This work is supported by Università della Calabria.

Appendix A. Supplementary data

Cartesian coordinates, absolute energies and zero-point corrected energies for all the stationary points intercepted along the hydration pathways. Supplementary data associated with this article can be found, in the online version, at http://dx.doi.org/10.1016/j.ica.2017.06.001.

References

[1] B. Rosenberg, L. Van Camp, T. Krigas, Nature 205 (1965) 698–699.
[2] J.C. Timothy, K. Suntharalingam, S.J. Lippard, Chem. Rev. 116 (2016) 3436–3486.
[3] M.J. Cleare, J.D. Hoeschele, Bioinorg. Chem. 2 (1973) 187–210.
[4] J. Graham, M. Muhsin, P. Kirkpatrick, Nat. Rev. Drug Discovery 3 (2004) 11–12.
[5] G.R. Gibbons, S. Wyrick, S.G. Chaney, Cancer Res. 49 (1989) 1402–1407.
[6] L. Pendyala, J.W. Cowens, G.B. Chheda, S.P. Dutta, P.J. Creaven, Cancer Res. 48 (1988) 3533–3536.
[7] L. Pendyala, A.V. Arakali, P. Sansone, J.W. Cowens, P.J. Creaven, Cancer Chemother. Pharmacol. 27 (1990) 248–250.
[8] L.R. Kelland, G. Abel, M.J. McKeage, M. Jones, P.M. Goddard, M. Valenti, B.A. Murrer, K.R. Harrap, Cancer Res. 53 (1993) 2581–2586.
[9] A. Bhargava, U.N. Vaishampayan, Expert Opin. Invest. Drugs 18 (2009) 1787–1797.
[10] I. Ritacco, G. Mazzone, N. Russo, E. Sicilia, Inorg. Chem. 55 (2016) 1580–1586.

[11] J.M. Rademaker-Lakhai, D. van den Bongard, D. Pluim, J.H. Beijnen, J.H.M. Schellens, Clin. Cancer Res. 10 (2004) 3717–3727.
[12] M.A. Jakupec, M. Galanski, V.B. Arion, C.G. Hartinger, B.K. Keppler, Dalton Trans. (2008) 183–194.
[13] R. Trondl, P. Heffeter, C.R. Kowol, M.A. Jakupec, W. Berger, B.K. Keppler, Chem. Sci. 5 (2014) 2925–2932.
[14] F. Wang, A. Habtemariam, E.P.L. van der Geer, R. Fernandez, M. Melchart, R.J. Deeth, R. Aird, S. Guichard, F.P.A. Fabbiani, P. Lozano-Casal, I.D.H. Oswald, D.I. Jodrell, S. Parsons, P.J. Sadler, PNAS 102 (2005) 18269–18274.
[15] G. Sava, R. Gagliardi, A. Bergamo, E. Alessio, G. Mestroni, Anticancer Res. 19 (1999) 969–972.
[16] E. Alessio, G. Mestroni, A. Bergamo, G. Sava, Curr. Top. Med. Chem. 4 (2004) 1525–1535.
[17] N. Bešker, C. Coletti, A. Marrone, N. Re, J. Phys. Chem. B 112 (2008) 3871–3875.
[18] A.V. Vargiu, A. Robertazzi, A. Magistrato, P. Ruggerone, P. Carloni, J. Phys. Chem. B 112 (2008) 4401–4409.
[19] Z. Liu, P.J. Sadler, Acc. Chem. Res. 47 (2014) 1174–1185.
[20] Z. Liu, L. Salassa, A. Habtemariam, A.M. Pizarro, G.J. Clarkson, P.J. Sadler, Inorg. Chem. 50 (2011) 5777–5783.
[21] Z. Liu, I. Romero-Canelón, B. Qamar, J.M. Hearn, A. Habtemariam, N.P.E. Barry, A.M. Pizarro, G.J. Clarkson, P.J. Sadler, Angew. Chem. Int. Ed. 53 (2014) 3941–3946.
[22] W. Liu, R. Gust, Chem. Soc. Rev. 42 (2013) 755–773.
[23] L. Oehninger, R. Rubbiani, I. Ott, Dalton Trans. 42 (2013) 3269–3284.
[24] Y. Fu, M.J. Romero, A. Habtemariam, M.E. Snowden, L. Song, G.J. Clarkson, B. Qamar, A.M. Pizarro, P.R. Unwin, P.J. Sadler, Chem. Sci. 3 (2012) 2485–2493.
[25] H. Huang, P. Zhang, B. Yu, Y. Chen, J. Wang, L. Ji, H.J. Chao, Med. Chem. 57 (2014) 8971–8983.
[26] J. Hearn, I. Romero-Canelón, B. Qamar, Z. Liu, I. Hands-Portman, P.J. Sadler , ACS Chem. Biol. 8 (2013) 1335–1343.
[27] C.M. Clavel, E. Păunescu, P. Nowak-Sliwinska, A.W. Griffioen, R. Scopelliti, P.J. Dyson, J. Med. Chem. 57 (2014) 3546–3558.
[28] L. Boselli, I. Ader, M. Carraz, C. Hemmert, O. Cuvillier, H. Gornitzka, Eur. J. Med. Chem. 85 (2014) 87–94.
[29] R.A. Haquea, S.Y. Chooa, S. Budagumpi, M.A. Iqbal, A.A.-A. Abdullah, Eur. J. Med. Chem. 90 (2015) 82–92.
[30] H.Z. Zulikha, R.A. Haque, S. Budagumpi, A.M.S.A. Majid, Inorg. Chim. Acta 411 (2014) 40–47.
[31] A.D. Tinoco, C.D. Incarvito, A.M. Valentine, J. Am. Chem. Soc. 129 (2007) 3444–3454.
[32] A.D. Tinoco, E.V. Eames, A.M. Valentine, J. Am. Chem. Soc. 130 (2008) 2262–2270.
[33] M. Pavlaki, K. Debeli, I.E. Triantaphyllidou, N. Klouras, E. Giannopoulou, A.J. Aletras, J. Biol. Inorg. Chem. 14 (2009) 947–957.
[34] C.A. Rabik, M.E. Dolan, Cancer Treat. Rev. 33 (2007) 9–23.
[35] N. Graf, W.H. Ang, G. Zhu, M. Myint, S.J. Lippard, ChemBioChem 12 (2011) 1115–1123.
[36] M. Zaki, F. Arjmand, S. Tabassum, Inorg. Chim. Acta 444 (2016) 1–22.
[37] Y. Yoshiia, T. Furukawad, Y. Kiyonoa, R. Watanabeb, A. Wakia, T. Moria, H. Yoshiic, M. Ohc, T. Asaia, H. Okazawaa, M.J. Welche, Y. Fujibayashi, Nucl. Med. Biol. 37 (2010) 395–404.
[38] C. Zhu, J. Raber, L.A. Eriksson, J. Phys. Chem. B 109 (2005) 12195–12205.
[39] D.V. Deubel, J. Am. Chem. Soc. 128 (2006) 1654–1663.
[40] M. Pavelka, M.F. Lucas, N. Russo, Chem. Eur. J. 13 (2007) 10108–10116.
[41] M.E. Alberto, M.F. Lucas, M. Pavelka, N. Russo, J. Phys. Chem. B 112 (2008) 10765–10768.
[42] M.E. Alberto, M.F. Lucas, M. Pavelka, N. Russo, J. Phys. Chem. B 113 (2009) 14473–14479.
[43] M.F. Lucas, M. Pavelka, M.E. Alberto, N. Russo, J. Phys. Chem. B 113 (2009) 831–838.
[44] M.E. Alberto, N. Russo, Chem. Commun. 47 (2011) 887–889.
[45] M.E. Alberto, C. Cosentino, N. Russo, Struct. Chem. 23 (2012) 831–837.
[46] G.S. Yellol, A. Donaire, J.G. Yellol, V. Vasylyev, C. Janiak, J. Ruiz, Chem. Commun. (2013) 11533–11535.
[47] J. Yellol, S.A. Pérez, A. Buceta, G. Yellol, A. Donaire, P. Szumlas, P.J. Bednarski, G. Makhloufi, C. Janiak, A. Espinosa, J. Ruiz, J. Med. Chem. 58 (2015) 7310–7327.
[48] Y. Zhao, D.G. Truhlar, J. Chem. Phys. 125 (2006) 194101–194118.
[49] Y. Zhao, D.G. Truhlar, Theor. Chem. Acc. 120 (2008) 215–241.
[50] D. Andrae, U. Hüßermann, M. Dolg, H. Stoll, H. Preuß, Theor. Chim. Acta 77 (1990) 123–141.
[51] M.J. Frisch, G.W. Trucks, H.B. Schlegel, G.E. Scuseria, M.A. Robb, J.R. Cheeseman, G. Scalmani, V. Barone, G.A. Petersson, H. Nakatsuji, X. Li, M. Caricato, A. Marenich, J. Bloino, B.G. Janesko, R. Gomperts, B. Mennucci, H.P. Hratchian, J.V. Ortiz, A.F. Izmaylov, J.L. Sonnenberg, D. Williams-Young, F. Ding, F. Lipparini, F. Egidi, J. Goings, B. Peng, A. Petrone, T. Henderson, D. Ranasinghe, V.G. Zakrzewski, J. Gao, N. Rega, G. Zheng, W. Liang, M. Hada, M. Ehara, K. Toyota, R. Fukuda, J. Hasegawa, M. Ishida, T. Nakajima, Y. Honda, O. Kitao, H. Nakai, T. Vreven, K. Throssell, J.A. Montgomery Jr., J.E. Peralta, F. Ogliaro, M. Bearpark, J.J. Heyd, E. Brothers, K.N. Kudin, V.N. Staroverov, T. Keith, R. Kobayashi, J. Normand, K. Raghavachari, A. Rendell, J.C. Burant, S.S. Iyengar, J. Tomasi, M. Cossi, J.M. Millam, M. Klene, C. Adamo, R. Cammi, J.W. Ochterski, R. L. Martin, K. Morokuma, O. Farkas, J.B. Foresman, D.J. Fox, Gaussian 09, Revision D.01, Gaussian, Inc., Wallingford CT, 2016.
[52] K.J. Fukui, Phys. Chem. 74 (1970) 4161–4163.
[53] C. Gonzalez, H.B. Schlegel, J. Chem. Phys. 90 (1989) 2154–2161.
[54] Miertuš, E. Scrocco, J. Tomasi, Chem. Phys. 55 (1981) 117–129.
[55] S. Miertuš, J. Tomasi, Chem. Phys. 65 (1982) 239–245.
[56] J.L. Pascual-Ahuir, E. Silla, I. Tuñón, J. Comput. Chem. 15 (1994) 1127–1138.
[57] D.A. McQuarrie, J.D. Simon, Molecular Thermodynamics, University Science Books, Sausalito, CA, 1999.
[58] R.W. Ashcraft, S. Raman, H.W. Green, J. Phys. Chem. B 111 (2007) (1983) 11968–11983.
[59] I. Ritacco, N. Russo, E. Sicilia, Inorg. Chem. 54 (2015) 10801–10810.
[60] J.S. Coe, MTP Int. Rev. Sci. Inorg. Chem. Ser. 2 (1974) 45.
[61] J.R. Perumareddi, A.W. Adamson, J. Phys. Chem. 72 (1978) 414–425.

ChemComm

COMMUNICATION

View Article Online
View Journal

Cite this: DOI: 10.1039/c9cc06725f

Received 29th August 2019,
Accepted 28th October 2019

DOI: 10.1039/c9cc06725f

rsc.li/chemcomm

Glutathione activation of an organometallic half-sandwich anticancer drug candidate by ligand attack†

Xin Zhang,‡[a] Fortuna Ponte,‡[b] Elisa Borfecchia,[c] Andrea Martini,[c] Carlos Sanchez-Cano,§*[a] Emilia Sicilia*[b] and Peter J. Sadler*[a]

In contrast to the clinical drug cisplatin, the anticancer complex [Os(η⁶-*p*-cymene)(4-(2-pyridylazo)-*N*,*N*-dimethylaniline)I]⁺ [1-I] is inert towards hydrolysis and targets cancer cell metabolism rather than DNA. A combination of DFT calculations and X-ray absorption spectroscopy (XAS) suggests that hydrolytic activation of 1-I involves catalytic attack by the intracellular tripeptide glutathione (GSH) on the azo bond of the chelating ligand in the complex.

[Os(η⁶-*p*-cymene)(4-(2-pyridylazo)-*N*,*N*-dimethylaniline)I]⁺ [**1-I**] and its analogues (Chart 1), are inert prodrugs activated by the reducing environment in cancer cells.[1] **1-I**, is a promising drug candidate capable of overcoming Pt resistance,[2] with a novel mechanism of action.[3] **1-I** increases oxidative stress in cancer cells through mitochondrial and other pathways, and exploits an inherent weakness in cancer cell energy generation.[3]

Prodrugs hypothesised to be activated by intracellular reduction include Pt^{IV} complexes which are reduced to active Pt^{II} species.[3] A number of Ru^{III} anticancer complexes are also thought to be prodrugs activated in a similar way,[4] but recent experiments have not detected reduction of Ru^{III} compounds in tumours.[5] However, activation of **1-I** and its analogues does not appear to involve changes in the oxidation state of Os^{II} in cells. On the contrary, initial experiments suggest that hydrolysis of the Os–I bond is promoted by the tripeptide glutathione (GSH). This generates the more reactive hydroxido adduct **1-OH**, which can react with other molecules in cells, such as H_2O_2 (generating hydroxyl radicals).[1] The aim of the present work was to establish both experimental and theoretical (density functional theory, DFT) evidence for this proposed highly unusual mechanism of activation of a metallo-prodrug.

DFT computational analysis can provide insights into reaction mechanisms for metal coordination compounds.[6] Hence we probed the most favourable mechanism, involving deprotonated glutathione (GS^-), for the hydrolysis of **1-I** using quantum-mechanical DFT calculations. First, the direct replacement of the iodido ligand by water (pathway **a**), a process observed under physiological conditions for many Os^{II}, Ru^{II}, or Ir^{III} half-sandwich complexes $[M(arene)(L)X]^+$,[7] was explored. Our calculations suggested an overall energy barrier of 25.4 kcal mol^{-1} and an endergonic (by 9.8 kcal mol^{-1}) exchange by second-order nucleophilic substitution (SN2) (pathway **a**; Fig. S1a, ESI†). An alternative, direct replacement of the iodide ligand by GS^-, to form an Os-SG adducts, followed by replacement of the thiolate ligand by water was also studied (pathway **b**). Such a reaction has been reported for other complexes, *e.g.* $[Ru(arene)(en)Cl]^+$ and its analogues.[8] In this case, the energy barrier to generate the stable **1-SG** complex was 23.2 kcal mol^{-1}, and the substitution product lies 18.9 kcal mol^{-1} below the entrance channel. However, hydrolysis of **1-SG** to form the experimentally observed **1-OH** required surmounting a very high energy barrier of 30.3 kcal mol^{-1} (pathway **b**, Fig. S1b, ESI†). Finally, we explored ligand-based attack on the complex by GSH resulting in hydrolysis of the Os–I bond through redox mediation involving the N=N double bond (pathway **c**).

Some organic azo compounds are known to catalyse oxidation of GSH in presence of O_2,[9] reactions also possible for azo-containing ligands in Ru^{II} or Ir^{III} complexes.[10] The reported mechanism can involve addition of GSH to the diazene double bond and subsequent

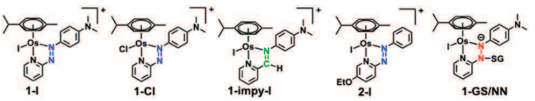

Chart 1 Structures of complexes and captured intermediate (**1-GS/NN**).

[a] Department of Chemistry, University of Warwick, Coventry, CV4 7AL, UK. E-mail: p.j.sadler@warwick.ac.uk
[b] Dipartimento di Chimica e Tecnologie Chimiche, Università della Calabria, Ponte P. Bucci, Cubo 14cI-87030, Arcavacata di Rende, Italy. E-mail: emilia.sicilia@unical.it
[c] Department of Chemistry, NIS Center and INSTM Reference Center, University of Turin, via Giuria 7, 10125, Turin, Italy

† Electronic supplementary information (ESI) available. See DOI: 10.1039/c9cc06725f

‡ These authors contributed equally to the manuscript.

§ Current address: CIC biomaGUNE, Parque Científico y Tecnológico de Gipuzkoa, Paseo Miramón 182, 20014 San Sebastian, Spain. E-mail: csanchez@cicbiomagune.es

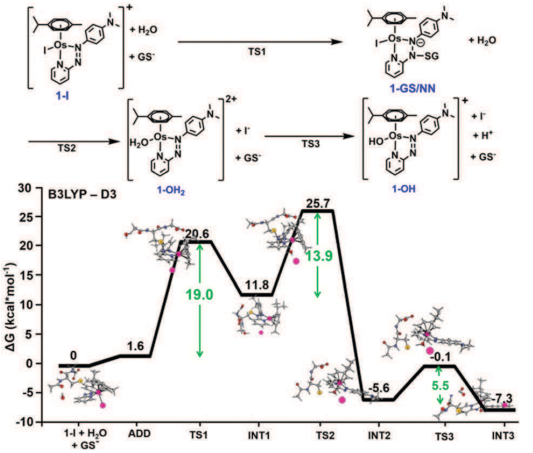

Fig. 1 DFT free energy profile describing the most favourable pathway for the reaction of **1-I** with GS$^-$ (pathway **c**). Calculated energies are in kcal mol^{-1} and relative to reference energy of separated reactants. Alternative higher energy pathways **a** and **b** are in Fig. S1 (ESI†).

reduction to an hydrazo group.[9] However, the free azo ligand in **1-I** does not react with GSH.[11]

We probed azo bond attack by GSH using DFT, but the most favourable energy barrier for the only viable reaction mechanism was high (40.2 kcal mol^{-1} Fig. S2, ESI†). Nevertheless, the attack by GS$^-$ on the azo N atom bound to the pyridine ring, preluding hydrolysis of **1-I**, yielded the lowest barrier (19.0 kcal mol^{-1}). This led to intermediate **1-GS/NN** (pathway **c**, Fig. 1), that lies 11.8 kcal mol^{-1} above the reactant reference energy, and accumulated electronic density near Os, causing the weakening of the Os–I bond. This facilitates displacement of the I$^-$ ligand by water (13.9 kcal mol^{-1}), which occurred simultaneously with detachment of the GS$^-$ and regeneration of the azo bond. Further deprotonation of the coordinated water (requiring 5.5 kcal mol^{-1}) yielded **1-OH**, which was stabilised by 7.3 kcal mol^{-1} (with respect to entrance channel). Computational analysis of the activation of **2-I**, an analogue with an electron donating ethoxy group on the pyridine ring gave similar results, but with lower energy barriers (Fig. S3, ESI†). This paralleled experimental data showing faster hydrolysis of **2-I** compared to **1-I**.[1]

Interestingly, our calculations proposed thermodynamically favoured hydrolysis pathways in the presence of glutathione, and kinetic control favouring the azo-based mechanism. This was confirmed by following the hydrolysis of chlorido [Os(η^6-*p*-cymene)(4-(2-pyridylazo)-*N*,*N*-dimethylaniline)Cl]$^+$ [**1-Cl**] and imino [Os(η^6-*p*-cymene)(4-(2-iminopyridine)-*N*,*N*-dimethyl-aniline)I]$^+$ [**1-impy-I**] analogues in presence or absence of GSH using HPLC (the solvent gradient used is on page S11 of the ESI†). As for **1-I**, **1-Cl** is stable in aqueous solution, but treatment with GSH promotes faster hydrolysis than **1-I** (Fig. S18, ESI†). However, both **1-Cl** and **1-I** hydrolysed in the presence of GSH following the same mechanism, generating first **1-OH** (Fig. S19, S20 and Tables S3, S4, ESI†), which can be attacked by GSH or Cl$^-$ to form **1-Cl** or **1-SG**. **1-SG** can be further oxidised to the sulfenate complex **1-SOG** (Fig. S21 and S22, ESI†). Notably, similar pathways were observed when different thiols induce hydrolysis of **1-I** (Fig. S23, S24 and Table S5, ESI†). In contrast, the iminopyridine complex **1-impy-I** readily hydrolysed in the absence of GSH, generating both hydroxido **1-impy-OH** and chlorido **1-impy-Cl** species. Incubation with GSH did not increase the extent of hydrolysis, but generated the thiolato adduct **1-impy-SG** (Fig. S18 and S25, ESI†), even when **1-impy-I** was in large excess. This confirmed that the azo bond in the azopyridine complexes is the likely target site for GS$^-$ (as it is the only difference between the chemical structure of **1-I** and **1-impy-I**). Hydrolysis of **1-I** was *ca.* 3× faster at pH 10 compared to pH 7, attributable to the higher proportion of GS$^-$ present (p$K_{a(SH)}$: 9.42),[12] whereas hydrolysis was inhibited at pH 2.4 (Fig. S26 and Table S6, ESI†). No **1-OH** was observed in the absence of thiol at basic pH (Fig. S27, ESI†).

The proposed attack of GSH on the –N=N– bond in **1-I** during the hydrolysis was further probed using X-ray absorption spectroscopy (XAS), to provide structural information.[13] We acquired XAS spectra at the Os L_3-edge for solid reference compounds **1-I**, **1-Cl**, **1-OH** and **1-SG** (for synthesis and characterisation see ESI†), and an aqueous solution (pH 7 buffer) of **1-I** on beamline BM23 at ESRF.[14] Discrimination between the different references could not rely on analysis of the XANES region (Fig. 2a and Fig. S28, ESI†).[15] However, there were distinguishing differences in the EXAFS oscillations for **1-I**, when compared with **1-Cl**, **1-OH** and **1-SG** especially from

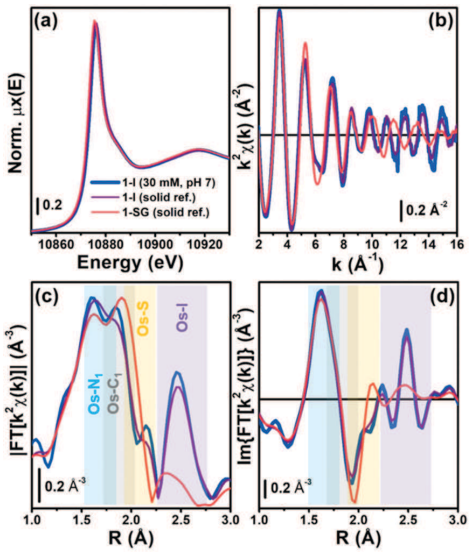

Fig. 2 (a) Os L_3-edge XANES spectra of aqueous **1-I** (30 mM, pH 7; blue), and solid **1-I** (purple) and **1-SG** (orange). (b) $k^2\chi(k)$ EXAFS functions for samples in (a). Phase-uncorrected (c) magnitude, and (d) imaginary part of the FT-EXAFS functions for the same samples, obtained by transforming the $k^2\chi(k)$ functions (b) in the 2.0–15.5 Å^{-1} range. R-space ranges of major contributions from the different EXAFS components arising from the coordination spheres around Os centres are highlighted by coloured rectangles.

k = 10 Å^{-1} upward (Fig. 2b–d and Fig. S29, S30, ESI†). In contrast, the spectra of **1-Cl** and **1-SG** were similar (due to similar size and atomic number of Cl and S). XAS spectra from the reference compounds were also used to validate structural models generated by our DFT calculations (Fig. S31, ESI†). Based on these data, we simulated an EXAFS signature corresponding to the DFT model of the intermediate **1-GS/NN** (Fig. S31, see ESI† for details). This allowed us to probe the presence of **1-GS/NN** in reactions between **1-I** and GSH followed *in situ* by EXAFS.

The kinetics for the hydrolysis of **1-I** in presence of GSH was further monitored *in situ* by acquiring consecutive EXAFS spectra (Fig. 3). Data analysis used the structural models obtained from EXAFS spectra of the experimental standards and DFT calculations for the **1-GS/NN** intermediate. Initially, an *in situ* XAS experiment was carried at pH 7, at an Os : GSH mol ratio of 1 : 2 (Fig. 3a). Under these conditions (30 mM **1-I**, 60 mM GSH; pH 7) Os–I hydrolysis was much faster than in HPLC experiments, and the reaction was complete after *ca.* 40 min, with only minor further spectral modifications up to 220 min. Linear combination fits (LCF) indicated the dominant presence of **1-SG** and **1-Cl** after 80 min, accounting for >80% of the Os species in the reaction mixture, together with contributions of <10% from **1-I** and **1-OH** (Table S9 and Fig. S33, ESI†). LCF provided estimates of the combined % of chlorido and thiolato adducts (Table S9, ESI†) since **1-Cl** and **1-SG** could not be readily discriminated by EXAFS analysis. In contrast, when the same experiment (30 mM **1-I**, 60 mM GSH) was repeated at pH 3, EXAFS spectra were almost identical to **1-I** standards, and remained unchanged over the duration of study (Fig. 3b). This suggested that it is possible to capture the dynamics of some steps in these reactions from XAS measurements by careful tuning of the reaction conditions.

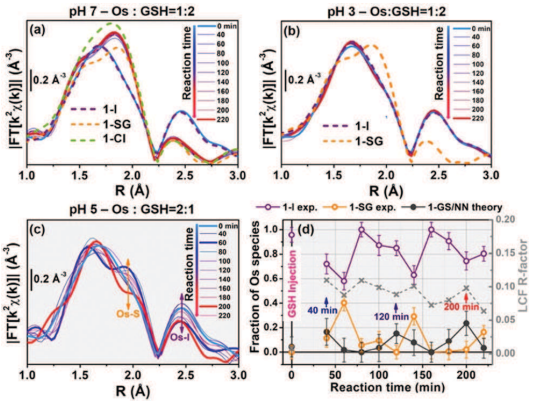

Fig. 3 Time-resolved *in situ* FT-EXAFS during reaction between **1-I** (30 mM) and GSH in buffered aqueous solutions at (a) pH 7, Os : GSH = 1 : 2, (b) pH 3, Os : GSH = 1 : 2 and (c) pH 5, Os : GSH = 2 : 1. (d) LCF analysis of the time-resolved $k^2\chi(k)$ curves resulting in the EXAFS spectra in (c), yielding concentration profiles for reactant **1-I**, product **1-SG**, and proposed intermediate **1-GS/NN**, which all appear to oscillate but with different phases. LCF R-factors (grey x) are also given (right axis). In (a and b) FT-EXAFS spectra of solid-state references are dashed lines, for comparison. All FT-EXAFS spectra have been transformed in the 2.0–12.5 Å^{-1} range.

The reaction of **1-I** (30 mM) with GSH was further studied at pH = 5, at an Os : GSH ratio of 2 : 1, in an attempt to moderate the reaction rate (as the [GS$^-$] at pH 5 is two orders of magnitude lower than at pH 7, according to the Henderson–Hasselbalch equation;[16] Fig. 3c and Fig. S34, ESI†). Remarkably, EXAFS spectra in the 40–220 min reaction time range, showed an oscillatory behaviour. Periodic and opposite changes in the intensities of the peaks at *ca.* 2.5 Å (Os–I single scattering [SS] contribution from **1-I**), and the shoulder at *ca.* 2.0 Å (Os–S SS contribution from **1-SG**) in the phase-uncorrected spectra were observed (Fig. 3c). Yet, certain time points showed dampened contributions from Os–I SS without an increase in the characteristic Os–S SS (*e.g.* after 200 min; red curve in Fig. 3c), suggesting the presence within the reaction of additional unknown Os species. Furthermore, the cyclic behaviour might arise from alternating periods dominated by cleavage or formation of Os–I bonds. To check this, Os-speciation as a function of the reaction time was evaluated by applying EXAFS LCF analysis in k-space (Fig. 3d). Based on our observations, three different components were used to generate the LCF model: the reference compounds **1-I** and **1-SG** and the simulated EXAFS signature for the **1-GS/NN** intermediate predicted by theory. The model adopted reproduced the experimental data well (Fig. S35, ESI†). Inclusion in the LCF model of the **1-GS/NN** component resulted in a significant improvement of the fitting quality for the time points with high concentrations of such species (coloured arrows in Fig. 3d) with respect to a two-component model of only **1-I** and **1-SG** (Fig. S36, ESI†). Crucially, the maxima in the relative abundance of **1-GS/NN** (16–24% total Os) systematically preluded increases in the concentration of **1-SG**. These data supported the presence of the **1-GS/NN** species during the reaction, in line with its intermediate character defined by DFT. LCF results highlighted the oscillating character of the reaction. **1-I** was cyclically converted into **1-SG** (with a period of 60–80 min), which then was transformed again to **1-I**. This may be related to fluctuations in the concentrations of free I$^-$ ions and free GSH as a result of the hydrolysis of Os–I bonds, and the formation of new Os–SG species. Indeed, our chromatographic experiments have shown previously that the presence of high concentrations of Cl$^-$ ions in the medium can alter the amount of **1-Cl** detected during the hydrolysis of **1-I** in the presence of GSH. Moreover, a more complex four-component LCF model (with **1-I**, **1-SG** and **1-OH** and simulated **1-GS/NN** references) suggested negligible presence of **1-OH** in the reaction mixture (Fig. S37, ESI†). This might indicate the presence of high concentrations of free I$^-$ ions and free GSH. By calculating the concentrations of free I$^-$ ions and free GSH (from amounts of **1-I** and **1-SG** species indicated by LCF), we observed an alternation between long periods of low I$^-$/GSH ratios and short periods of high I$^-$/GSH ratios (every 60–80 min). Remarkably, the highest concentrations of free I$^-$ ions were always just before periods dominated by the formation of Os–I bonds (Fig. S38, ESI†), providing a possible explanation for the regeneration of **1-I**. The presence of fluctuations in GSH, together with complete hydrolysis of Os–I bonds (31.2 mM in total, calculated from amounts of **1-I** and **1-SG** indicated by LCF) by 15 mM of GSH suggested a catalytic reaction, with the thiol being regenerated. This was

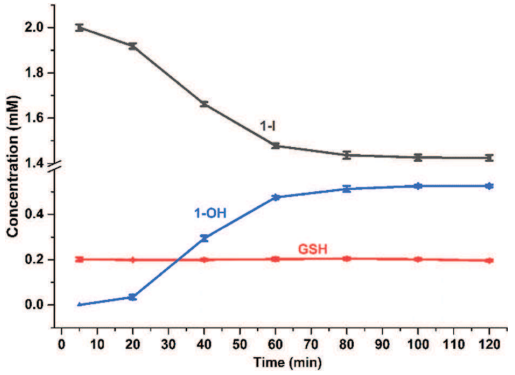

Fig. 4 Time-dependent concentration changes for GSH, **1-I** and **1-OH** in the reaction of **1-I** (2 mM) with GSH (200 μM), 75 mM phosphate buffer (pH 7.4), 298 K, for 2 h based on integration of ^{1}H NMR peak areas (Table S10 and Fig. S40, ESI†).

confirmed by the almost total conversion of **1-Cl** to **1-OH** after 12 h incubation with sub-stoichiometric quantities of GSH (0.5, 0.25 or 0.125 mol equiv.; Fig. S39, ESI†). Furthermore, significant amounts of **1-OH** (525 μM) were generated with little consumption of GSH when **1-I** (2 mM) reacted with 0.1 mol equiv. of the thiol (200 μM) for 2 h (Fig. 4) under N_2 (protecting GSH from oxidation). ^{1}H NMR spectra provided a turnover frequency (TOF) number of 1.97 h^{-1} for the reaction under such conditions.

In summary, DFT calculations suggested that substitution of bound iodide by water in the inert organo-osmium anticancer complex **1-I** is dependent on high energy kinetic barriers, but revealed a favourable reaction pathway involving attack of GS^{-} on the –N=N– azo bond in the chelating ligand, giving a **1-GS/NN** intermediate (Fig. S31, ESI†) containing an N–SG bond.

Experimental chromatographic analysis of the GSH-induced hydrolysis then confirmed the importance of the azo ligand in the mechanism of the hydrolysis, and demonstrated enhanced rates at high pH and inhibition at low pH (importance of GS^{-} in the attack). Time resolved XAS data provided evidence for the proposed **1-GS/NN** intermediate during the hydrolysis reaction. Our experiments also revealed the possible catalytic nature of the reaction (TOF *ca.* 2 h^{-1}). Overall, these investigations reveal a novel activation pathway for a metallodrug in which an inert metal–ligand bond is activated towards hydrolysis, and subsequent interactions with biomolecules, by the attack of the abundant intracellular thiol glutathione on a chelating ligand. Such findings have implications for the design of new generations of anticancer metallodrugs.

XAS spectra were acquired in the frame of the ESRF proposal CH-5212. We thank M. Monte Caballero and E. M. Bolitho for the support during experiments at BM23. We thank CRUK/EPSRC (Grant No. C53561/A19933), EPSRC (Grant No. EP/F034210/1) and Wellcome Trust (Grant No. 107691/Z/15/Z) for financial support.

Conflicts of interest

There are no conflicts to declare.

References

1 R. J. Needham, C. Sanchez-Cano, X. Zhang, I. Romero-Canelón, A. Habtemariam, M. S. Cooper, L. Meszaros, G. J. Clarkson, P. J. Blower and P. J. Sadler, *Angew. Chem., Int. Ed.*, 2017, **56**, 1017.
2 J. M. Hearn, I. Romero-Canelon, A. F. Munro, Y. Fu, A. M. Pizarro, M. J. Garnett, U. McDermott, N. O. Carragher and P. J. Sadler, *Proc. Natl. Acad. Sci. U. S. A.*, 2015, **112**, E3800.
3 N. Graf and S. J. Lippard, *Adv. Drug Delivery Rev.*, 2012, **64**, 993; R. G. Kenny, S. W. Chuah, A. Crawford and C. J. Marmion, *Eur. J. Inorg. Chem.*, 2017, 1596; Z. Wang, Z. Deng and G. Zhu, *Dalton Trans.*, 2019, **48**, 2536.
4 A. Levina, A. Mitra and P. A. Lay, *Metallomics*, 2009, **1**, 458; R. Trondl, P. Heffeter, C. R. Kowol, M. A. Jakupec, W. Berger and B. K. Keppler, *Chem. Sci.*, 2014, **5**, 2925.
5 A. Blazevic, A. A. Hummer, P. Heffeter, W. Berger, M. Filipits, G. Cibin, B. K. Keppler and A. Rompel, *Sci. Rep.*, 2017, **7**, 40966; E. Alessio, *Eur. J. Inorg. Chem.*, 2017, 1549; E. Alessio and L. Messori, *Molecules*, 2019, **24**, 1995.
6 I. Ritacco, N. Russo and E. Sicilia, *Inorg. Chem.*, 2015, **54**, 10801.
7 C. Scolaro, A. Bergamo, L. Brescacin, R. Delfino, M. Cocchietto, G. Laurenczy, T. J. Geldbach, G. Sava and P. J. Dyson, *J. Med. Chem.*, 2005, **48**, 4161; W. F. Schmid, R. O. John, V. B. Arion, M. A. Jakupec and B. K. Keppler, *Organometallics*, 2007, **26**, 6643; H. Zhang, L. Guo, Z. Tian, M. Tian, S. Zhang, Z. Xu, P. Gong, X. Zheng, J. Zhao and Z. Liu, *Chem. Commun.*, 2018, **54**, 4421.
8 F. Wang, J. Xu, A. Habtemariam, J. Bella and P. J. Sadler, *J. Am. Chem. Soc.*, 2005, **127**, 17734.
9 E. M. Kosower and T. Miyadera, *J. Med. Chem.*, 1972, **15**, 307; E. M. Kosower and H. Kanety-Londner, *J. Am. Chem. Soc.*, 1976, **98**, 3001; C. Boulègue, M. Löweneck, C. Renner and L. Moroder, *ChemBioChem*, 2007, **8**, 591.
10 G. Li, Y. Chen, J. Wu, L. Ji and H. Chao, *Chem. Commun.*, 2013, **49**, 2040; Q.-X. Zhou, Y. Zheng, T.-J. Wang, Y.-J. Chen, K. Li, Y.-Y. Zhang, C. Li, Y.-J. Hou and X.-S. Wang, *Chem. Commun.*, 2015, **51**, 10684.
11 S. J. Dougan, A. Habtemariam, S. E. McHale, S. Parsons and P. J. Sadler, *Proc. Natl. Acad. Sci. U. S. A.*, 2008, **105**, 11628.
12 S. G. Tajc, B. S. Tolbert, R. Basavappa and B. L. Miller, *J. Am. Chem. Soc.*, 2004, **126**, 10508.
13 S. Bordiga, E. Groppo, G. Agostini, J. A. van Bokhoven and C. Lamberti, *Chem. Rev.*, 2013, **113**, 1736; C. Garino, E. Borfecchia, R. Gobetto, J. A. van Bokhoven and C. Lamberti, *Coord. Chem. Rev.*, 2014, **277–278**, 130; M. L. Baker, M. W. Mara, J. J. Yan, K. O. Hodgson, B. Hedman and E. I. Solomon, *Coord. Chem. Rev.*, 2017, **345**, 182; S. N. MacMillan and K. M. Lancaster, *ACS Catal.*, 2017, **7**, 1773.
14 O. Mathon, A. Beteva, J. Borrel, D. Bugnazet, S. Gatla, R. Hino, I. Kantor, T. Mairs, M. Munoz, S. Pasternak, F. Perrin and S. Pascarelli, *J. Synchrotron Radiat.*, 2015, **22**, 1548.
15 C. Sanchez-Cano, D. Gianolio, I. Romero-Canelon, R. Tucoulou and P. J. Sadler, *Chem. Commun.*, 2019, **55**, 7065.
16 L. B. Poole, *Free Radical Biol. Med.*, 2015, **80**, 148.

For submission to ***Chemical Science***

Ligand-centred redox activation of inert organo-iridium(III) anticancer complexes

Wen-Ying Zhang,[a] Samya Banerjee,[a] George M. Hughes,[a] Hannah Bridgewater,[a] Ji-Inn Song,[a] Ben Breeze,[b] Guy J. Clarkson,[a] James P. C. Coverdale,[a] Carlos Sanchez-Cano,[a] Fortuna Ponte[c], Emilia Sicilia,[c] and Peter J. Sadler*[a]

[a] W.-Y. Zhang, Dr. S. Banerjee, Dr. G. M. Hughes, H. Bridgewater, J.-I. Song, Dr. G. J. Clarkson, Dr. J. P. C. Coverdale, Dr. C. Sanchez-Cano and Prof. P. J. Sadler

Department of Chemistry, University of Warwick, Coventry, CV4 7AL (UK)

Email: p.j.sadler@warwick.ac.uk

[b] Dr. B. Breeze

Spectroscopy Research Technology Platform, University of Warwick, Coventry, CV4 7AL (UK)

[c] F. Ponte and Prof. E. Sicilia

Department of Chemistry and Chemical Technologies, University of Calabria, via Pietro Bucci 87036 Arcavacata di Rende, Cs (Italy)

Abstract

We report the synthesis and characterization of 10 novel half-sandwich phenylazopyridine Ir(III) complexes, $[(\eta^5\text{-}Cp^X)Ir(5\text{-}R_1\text{-pyridylazo-}4\text{-}R_2\text{-phenyl})X]PF_6$ where Cp^X is pentamethylcyclopentadienyl (Cp*) or 1-phenyl-2,3,4,5-tetramethyl cyclopentadienyl (Cp^{ph}), R_1 = -Br, $-CF_3$ or -H, R_2 = -OH or -H, X = Cl or I, including eight x-ray crystal structures. The iodido complexes, in contrast to chlorido analogues, are remarkably inert towards aquation or reaction with nucleobases. Most of the complexes are more active against A549 human lung cancer cells than cisplatin with IC_{50} values (half maximal inhibitory concentration) ranging from 0.33 (ca. 10x more active) to 1.59 μM. Also iodido complex **1** has a lower resistance factor (RF ≈ 0.20) towards cisplatin-resistant human ovarian cancer cells (A2780*cis*R) as well as lower toxicity in zebrafish (*Danio rerio*) embryos than its chlorido analogue complex **9** (RF ≈ 0.95). Iodido complexes **1**-**6** exhibit a zwitterionic character due to deprotonation of the ligand phenol group at physiological pH 7.4, which increases their cellular accumulation and cytotoxicity. These inert iridium iodido complexes are activated by forming Ir-thiolate complexes with GSH under physiologically relevant conditions. DFT calculations suggest that release of iodide is preceded by attack of GS^- on the azo bond in the chelated ligand. Cyclic voltammetry showed that the 2-step reduction of the azo bond is more facile for the complexes compared to free azopyridine ligands. In the presence of O_2, this redox reaction leads to the formation of hydroxyl radicals (detected by EPR), and GSSG. Complex **7,** induced a dramatic increase in the level of reactive oxygen species (ROS) in A549 lung cancer cells. These ligand-centered redox reactions of an inert organo-iridium iodido prodrug induced by an abundant cellular

metabolite (GSH), represent a novel mechanism of action for an anticancer metal coordination complex.

Introduction

Three key platinum drugs, cisplatin, carboplatin, and oxaliplatin are administered in approximately 50% of worldwide cancer chemotherapies. However, platinum resistance and undesirable side effects are now limiting their future use.[1] Therefore, it is important to discover non-classical metal complexes with different modes of action compared with platinum drugs.[2, 3] Third-row $5d^6$ iridium(III) complexes offer potential structural diversity of octahedral coordination geometry and slow ligand exchange kinetics, as well as facile synthesis.[4-6] For example, Meggers and co-workers have reported kinetically inert octahedral iridium pyridicarbazole scaffolds as selective protein kinase inhibitors,[7] and Sheldrick et al. have investigated extensively the anticancer activity of inert iridium polypyridine complexes which might have targets other than DNA.[8] Inert bis-cyclometalated iridium complexes are promising photosensitizers for singlet oxygen production,[9, 10] and the diselenobenzoquinone-based iridium complex reported by Amouri et al. exhibits comparable potency to cisplatin and appears to target cytochrome P450 reductase.[11] Here we report a novel activation mechanism for potent kinetically-inert organo-iridium(III) anticancer complexes.

Half-sandwich organometallic iridium cyclopentadienyl complexes $[(\eta^5\text{-}Cp^A)Ir(L\text{^}L')X]^{n+/0}$, where $Cp^* = Cp^*$ (pentamethyl-cyclopentadienyl), Cp^{ph} (tetramethyl(phenyl)-cyclopentadienyl), or Cp^{biph} (tetramethyl(biphenyl)-cyclopentadienyl), can bind to DNA, but also perturb the redox status of cells and target lysosomes.[12-14] The chelated ligand L^L′, the ancillary leaving group X and the π-bound Cp^A ligand together modulate the overall electronic structures and chemical reactivity of such iridium complexes. Reported half-sandwich iridium anticancer complexes with X=Cl are labile and most likely to be activated in the cancer cells through fast hydrolysis (minutes) of the chlorido ligand.[5] Extension of the Cp* ring to Cp^{ph} or Cp^{biph} can slow down the hydrolysis rate, and increase the extent of hydrolysis.[15] Rapid hydrolysis sometimes compromises the anticancer activity due to rapid deactivation by side reactions in advance of reaching targets. For example, compared to pyridine analogue $[(\eta^5\text{-}Cp^{biph})Ir(ppy)py]^+$ (ppy = 2-phenylpyridine), the chlorido complex $[(\eta^5\text{-}Cp^{biph})Ir(ppy)Cl]$ is more reactive, hydrolyzes rapidly, and reacts readily with the abundant (*ca.* 0.5-10 mM) cellular thiol glutathione (GSH), but has only one third the potency of the pyridine analogue toward cancer cells.[12] Hence, a major aim is to design potent iridium(III) anticancer agents by rational control of their reactivity.

In this work, two complementary approaches are explored to potentially optimise the anticancer activity. Firstly, iodide is used as the monodentate ancillary leaving group since based on the distinctly 'soft' nature of iridium(III) and the steric bulk and softer character of iodide compared to chloride, it is expected to be more strongly bond and a poorer leaving

group.[16] Only a few biologically active half-sandwich iodido iridium complexes appear to have been reported, namely, $[Cp^*Ir(dpa)I]^+$ (dpa = 2, 2'-dipyridylamine),[17] $[Cp^{biph}Ir(tolbig)I]^+$ (tolbig = 1-(o-Tolyl)biguanide),[18] and $[Cp^*Ir(pp)I]^+$ (pp = pyridylphosphinate)[19]. Secondly, due to the low-lying π* orbitals of the azo bond, the chelated azopyridine ligand provides a pathway for electron transfer and redox reactions. Previously we have found that phenylazopyridine ligands in half-sandwich arene Ru(II) and Os(II) complexes can bring about intriguing reactivities with glutathione.[20, 21] Interestingly the combination of azopyridine ligand $azpyNMe_2$ (N,N-dimethylphenylazopyridne) with Cp^{ph} Ir(III) chloride gives a markedly different pattern of antiproliferative activity in over 800 cancer cell lines compared with 253 standard drugs, suggesting a novel multi-targeting mechanism of action which can overcome resistance.[22]

Here we report the design of ten novel half-sandwich organoiridium(III) iodido complexes bearing variously substituted bidentate phenylazopyridine ligands, as shown in **Chart 1**. Their toxicity *in vivo* as well as anticancer activity in a variety of cancer cell lines are compared to chlorido complexes. Correlations between the anticancer activity of the iodido complexes and stability in aqueous solution, lipophilicity, cellular accumulation and generation of reactive oxygen species (ROS) are investigated. The mechanism of reactions with GSH is elucidated by density functional theory (DFT) calculations. This work reveals new metal and ligand-based activation mechanisms for potent inert half-sandwich iridium(III) iodido complexes which provide a strategy for overcoming resistance to current clinical drugs.

Chart 1. Synthetic route to and structures of iodido iridium(III) complexes.

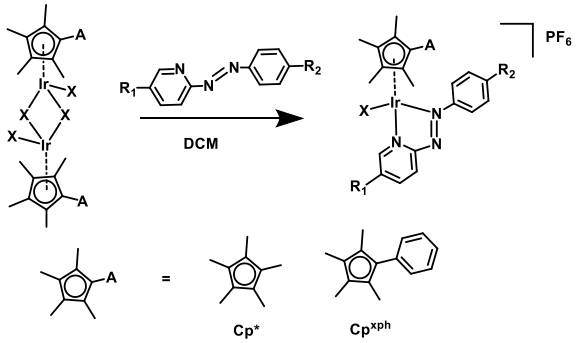

Complex	R_1	R_2	X
$[(Cp^*)Ir(azpy\text{-}OH)I]PF_6$ (**1**)	H	OH	I
$[(Cp^{ph})Ir(azpy\text{-}OH)I]PF_6$ (**2**)	H	OH	I
$[(Cp^*)Ir(Br\text{-}azpy\text{-}OH)I]PF_6$ (**3**)	Br	OH	I
$[Cp^{ph})Ir(Br\text{-}azpy\text{-}OH)I]PF_6$ (**4**)	Br	OH	I
$[(Cp^*)Ir(CF_3\text{-}azpy\text{-}OH)I]PF_6$ (**5**)	CF_3	OH	I
$[(Cp^{ph})Ir(CF_3\text{-}azpy\text{-}OH)I]PF_6$ (**6**)	CF_3	OH	I
$[(Cp^*)Ir(azpy)I]PF_6$ (**7**)	H	H	I
$[(Cp^{ph})Ir(azpy)I]PF_6$ (**8**)	H	H	I
$[(Cp^*)Ir(azpy\text{-}OH)Cl]PF_6$ (**9**)	H	OH	Cl
$[(Cp^{ph})Ir(azpy\text{-}OH)Cl]PF_6$ (**10**)	H	OH	Cl

Results

Synthesis and characterization

Ten novel iridium(III) azopyridine complexes were synthesized in good yields by vigorously stirring mixtures of 1 mol equiv. iridium chlorido/iodido dimer precursor and 2 mol equiv. of the appropriate chelating azopyridine ligand in dichloromethane (**Chart 1**). All the complexes were characterized by NMR spectroscopy (^{1}H, ^{1}H-^{1}H COSY, ^{13}C, HSQC, HMBC), elemental analysis and ESI-MS.

The complexes have a chiral Ir(III) centre. ^{1}H NMR spectra of cationic complexes **1** and **2** in d_4-MeOD after addition of the chiral anionic shift regent Δ-trisphat at 298 K (Figs. **S1, S2**) show splitting of the aromatic proton signals in 1:1 ratios, indicating the presence of two stable enantiomers in equal abundance, consistent with previously reported chiral osmium/ruthenium arene picolinamide and iminopyridine anticancer complexes.[23, 24]

Single crystals suitable for x-ray diffraction of **1-I**·MeOH, **2**, **3**·MeOH, **5**·MeOH, **7-I**, **8-I**, **9-Cl**·MeOH and **10** as PF_6^- salts (except **1-I**, **7-I**, **8-I**, and **9-Cl** as iodide/chloride salts) were obtained at ambient temperature by slow diffusion of Et_2O into saturated methanol or dichloromethane (**8-I**) solutions. X-ray crystal structures for complexes **1-I** and **9-Cl** are shown in **Fig. 1**, and for the other six complexes in **Fig. S3**. In the unit cells of these complexes, there are two mirror-image enantiomers, for example shown in **Fig. S4** for complex **7-I**. X-ray crystallographic data are listed in **Tables S1, S2**, and selected bond lengths and bond angles in **Tables S3**, **S4**. All complexes adopt a typical pseudo-octahedral geometry with a "piano-stool" shape. The Ir-I bond lengths in the Cp^* structures range from 2.6799(5)-2.6851(2) Å, a little shorter than 2.69042(16)-2.6943(3) Å for complexes with the Cp^{ph} ring. Interestingly, in the Cp^* complexes **1-I**·MeOH and **7-I**, the Ir-N1 bond length is slightly longer than Ir-N8, while in their Cp^{ph} analogues **2** and **8-I**, these

bond lengths are similar. The azo N=N bond lengths are within the range of 1.27-1.29 Å, consistent with the normal N=N double bond length (1.20-1.28 Å)[25]. The distances from the Cp^A ring centroid to iridium are within 1.820 ± 0.009 Å, except for complex **5** (1.870 Å), similar to the C^N chelated complex [(η^5-Cp^*)Ir(ppy)Cl] (1.82 Å) (ppy = 2-phenylpyridine) while slightly longer than the N^N chelated complex [(η^5-Cp^*)Ir(bpy)Cl]Cl (1.78 Å) (bpy = 2,2'-bipyridine).[15, 26, 27] The crystal structures of all 6 phenolic complexes (**1**, **2**, **3**, **5**, **9**, **10**) contained protonated phenolic groups.

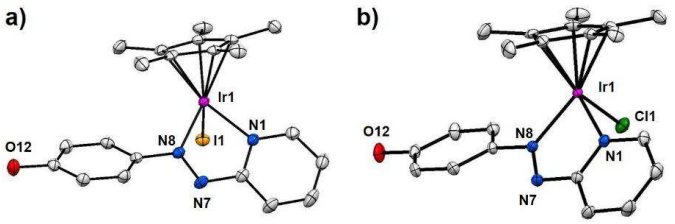

Fig. 1. X-ray crystal structures of (a) [(η^5-Cp^*)Ir(azpy-OH)I]I·MeOH (**1-I**·MeOH), (b) [(η^5-Cp^*)Ir(azpy-OH)Cl]Cl·MeOH (**9-Cl**·MeOH). The hydrogen atoms, counter anions and solvent molecules have been omitted for clarity.

UV-visible spectra and pK_a of the phenolic group

Complexes [(Cp^*)Ir(azpy-OH)I]PF_6 (**1**), [(Cp^*)Ir(Br-azpy-OH)I]PF_6 (**3**) and [(Cp^*)Ir(CF_3-azpy-OH)I]PF_6 (**5**) containing a phenolic group on the ligand showed pH-dependent UV-vis spectra in aqueous solution, illustrated in **Fig. 2a**. At pH = 3.0, the spectra of **1**, **3**, and **5**, display a MLCT (metal-to-ligand charge-transfer) absorption band at 439-464 nm (ε= 8000-23000 $M^{-1}\cdot cm^{-1}$). Raising the pH to 11.5 led to a dramatic red-shift of this MLCT band to 558-586 nm with a much higher extinction coefficient (26900-57200 $M^{-1}\cdot cm^{-1}$). The maximum absorption wavelengths and the corresponding molar extinction coefficients of phenolic complexes **1**-**6** at pH = 3.0 ± 0.1 and pH = 11.5 ± 0.3 are listed in **Table S5**.

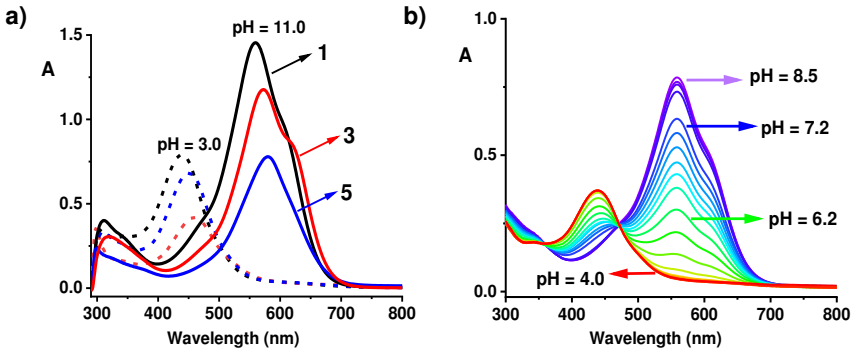

Fig. 2. (a) UV-vis spectra of aqueous solutions of complexes **1** (41 μM, black), **3** (33 μM, red) and **5** (29 μM, blue) at pH = 3.0 ± 0.3 (dash lines) and pH = 11.0 ± 0.3 (solid lines); (b) UV-vis changes for complex **1** from pH 4 to 8.5.

The changes of UV-vis absorbance with pH allowed determination of the pK_a values of the phenolic groups in complexes **1**-**6** and **9**-**10** (**Figs. 2b** and **S5**) as 5.90-6.50, with the exception of the more acidic [(Cp^{ph})Ir(CF$_3$-azpy-OH)I]PF$_6$ (**6**), pK_a 3.90 (**Chart 2**). Compared to the pK_a values of Cp* analogues, all the iodido Cp^{ph} complexes have lower pK_a values. For example, ΔpK_a = -0.22 from **1** to **2** (R$_1$ = H), -0.35 from **3** to **4** (R$_1$ = Br), -2.55 from **5** to **6** (R$_1$ = CF$_3$). The chlorido Cp* complex **9** and its Cp^{ph} analogue complex **10** have the same pK_a value of 5.88, much lower than their respective iodido analogues **1** and **2**.

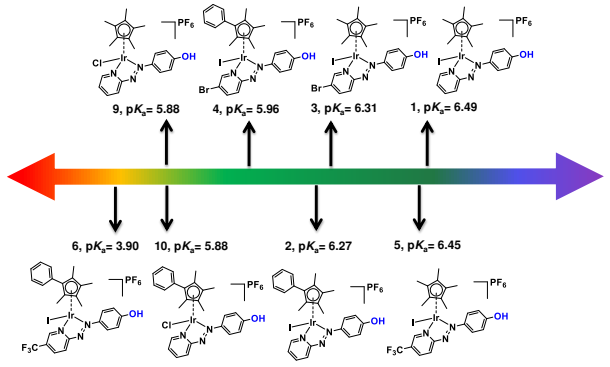

Chart 2. pK_a values of phenolic groups of iodido complexes **1**-**6** and chlorido complexes **9**-**10**.

Electrochemistry of iodido iridium complexes

Electrochemical reduction of complexes **1**, **3**, **7** in comparison with unbound azpy (phenylazopyridine), azpy-OH (4-OH-phenylazopyridine) ligands and iridium dimeric precursor [(Cp*)Ir(μ-I)I]$_2$, was studied by cyclic voltammetry (CV) under N$_2$ versus a Ag$^+$/Ag reference electrode. Complexes **1**, **3**, **7** exhibited more facile sequential reduction potentials than the corresponding free azopyridine ligands as well as the iridium precursor [(Cp*)Ir(μ-I)I]$_2$. The first reduction step is quasi-reversible, ranging from -0.07 to -0.28 V and the second is irreversible, ranging from -0.58 to -0.79 V (**Table 1,** cyclic voltammograms shown in **Fig.S6**).

Table 1. Electrochemical reduction potentials of selected ligands and complexes.

Ligand/Complex[a]	E_{red} (V)	Complex[a]	E_{red} (V)
Azpy	-1.07, -1.93	**1**	-0.28, -0.79
Azpy-OH	-0.94, -1.76	**3**	-0.13, -0.58
$[Cp^*Ir(\mu\text{-}I)I]_2$	-1.21, -1.69	**7**	-0.07, -0.63

[a] Conditions: 1 mM free ligand or iridium complexes with 0.1 M Bu_4NPF_6 as supporting electrolyte in acetonitrile under N_2 at ambient temperature, $E_{1/2}$ (ferrocene/ferrocenium) = 0.063 V, scan rate = 100 $mV \cdot s^{-1}$.

Hydrolysis of chlorido and iodido complexes

^{1}H NMR spectra of iodido complexes **1-8** were recorded in d_4-MeOD/D_2O (1/5 v/v) at 310 K at various time intervals up to 24 h. No changes in the spectra were observed after 24 h. Over this time the ESI-MS analysis of the NMR solutions showed only peaks assignable to cation $[M\text{-}PF_6]^+$ of the intact iodido complexes. To verify that the ^{1}H NMR spectrum contained only peaks for the intact complexes, and therefore no hydrolysis had occurred, complex $[(Cp^*)Ir(Br\text{-}azpy\text{-}OH)I]PF_6$ (**3**) was reacted with 1.2 molar equiv. $AgNO_3$ at 310 K to remove the coordinated iodide in MeOD/D_2O (1/1, v/v). The resulting NMR peaks for the aqua adduct **3-H_2O** were assigned (**Fig. S7a**) and contrasted with the hydrolysis-inert complex **3** (**Fig. S7b**).

In contrast, chlorido complexes **9** and **10** hydrolyzed rapidly to the extent of 53% (**Fig. S8**) and 66% (**Fig. S9**), respectively, after 24 h.

Stability in aqueous NaCl and DMSO

The stability of the iodido complex $[(Cp^*)Ir(Br\text{-}azpy\text{-}OH)I]PF_6$ (**3**) (1.0 mM) in MeOD/D_2O (1/1, v/v, pH^* 7.0) in the presence of 4.0 mM, 23.0 mM, or 103.0 mM NaCl over 24 h at 310 K was evaluated by integration of the methyl ^{1}H NMR peaks for Cp^* at δ 1.73 ppm (**3**) and δ 1.59 ppm (**3-Cl**, the chlorido analogue of **3**), **Fig. S10**. The amount of **3-Cl** formed by I^-/Cl^- ligand exchange at these three NaCl concentrations was 2.7%, 7.8%, and 16.5%, respectively, **Fig. S10**. LC-MS for complex **3** at micromolar concentrations with the three different NaCl concentrations showed a positive-ion peak for the chlorido analogue with a shorter retention time of ca. 17.6 min (ca. 21.0 min for **3**, **Fig. S11**).

In addition, ^{1}H NMR spectra of iodido complex $[(Cp^{ph})Ir(CF_3\text{-}azpy\text{-}OH)I]PF_6$ (**6**) as well as the chlorido complexes $[(Cp^*)Ir(azpy\text{-}OH)Cl]PF_6$ (**9**) in d_6-DMSO were monitored for 27 d at 298 K to investigate their stability, since DMSO was used as a solvent in cell growth inhibition assays. However, no changes to any ^{1}H NMR peaks was observed (**Fig. S12, S13**). ESI-MS data showed peaks only for the original complexes, providing evidence for the inertness of these complexes toward solvolysis in DMSO.

Interaction with nucleobase models and amino acids

Reactions of complexes [(Cp^{ph})Ir(azpy-OH)I]PF_6 (**2**) and [(Cp^*)Ir(Br-azpy-OH)I]PF_6 (**3**) with 3.0 molar equiv. nucleotide guanosine 5'-monophosphate (5'-GMP) or nucleobase 9-ethylguanine (9-EtG) (**Fig. S14**) in 0.1 M phosphate buffer D_2O/d_4-MeOD (1/1, v/v, pH^* 7.8) were investigated by monitoring ^{1}H NMR spectra and ESI-MS over 24 h at 310 K. However, no adducts were observed by NMR or ESI-MS.

Reactions of complex **3** (1 mM) with 3.0 mol equiv. of amino acids L-histidine, N-acetyl-L-methionine, L-tryptophan, and L-arginine were studied by ^{1}H NMR at pH 7.4 at 310 K over 24 h. Only trace formation (<5%) of adducts of **3** with with N-acetyl-L-methionine or L-histidine was observed (**Fig. S15**), and no reaction with L-Trp or L-Arg.

Reactions with N-acetyl-L-cysteine (NAC)

Reactions of highly potent complexes **1** and **3** as well as moderately potent complex **7** with N-acetyl-L-cysteine (NAC) as an example of a biologically important thiol, were initially studied by ^{1}H NMR spectroscopy. Time-dependent ^{1}H NMR spectra of [(Cp^*)Ir(azpy-OH)I]PF_6 (**1**) (1 mM) with 3 mol equiv. NAC in d_4-MeOD/0.1 M phosphate buffer D_2O (3/7 v/v, pH^* 7.4) were recorded up to 24 h at 310 K (**Fig.S16**). In the aromatic region, a new set of ligand-based peaks appeared with the set of ligand peaks of iodido complex **1** decaying during the first hour (**Fig. S16**). While in the aliphatic area, the peak for Cp^* protons of complex **1** shifted completely from δ 1.71 ppm to 1.59 ppm within the first hour, and two new sets of peaks in a 1:1 ratio for acetyl methyl protons of NAC appeared at δ 1.88 ppm and 1.77 ppm.

LC-MS analysis of **1** (100 μM) after reaction with 3 mol equiv. NAC for 1 h showed one new ESI-MS peak at a shorter retention time of ca. 12.5 min with *m/z* $[689.26]^+$ assignable as [(**1**-I^-)+NAC]$^+$ (calcd 689.18, NAC is $[CH_3CONHCH(COOH)(CH_2S)]^-$ with a bound deprotonated thiolate group; **Fig. S17**). This confirmed that the new sets of NMR peaks for ligand, Cp* and NAC were from **1-NAC** adducts. The two sets of acetyl methyl peaks for the bound NAC can be assigned to the diastereomers of **1-NAC** (**Fig. S16**) due to the chirality of the iridium centre and the chiral nature of NAC. Diastereomers were more explicitly observed in the ^{1}H NMR spectra for the adducts of complex **7** (**Fig. 3**) and **3** (**Fig. S18**) with NAC, which had been isolated and characterized. Similarly, all the ^{13}C NMR signals showed equally duplicated peaks for **7-NAC** (see assignments of ^{13}C NMR for **7-NAC** in the Synthesis and Characterization part of the Supporting Information). This appears to be the first report of characterised half-sandwich iridium NAC adducts.

In contrast, no adduct was observed by LC-MS upon incubation of complex **7** with 10 mol equiv. of the amino acid β-alanine under the same reaction conditions. Hence the thiol group of NAC appears to be a critical reaction site for reaction with these iodido iridium complexes.

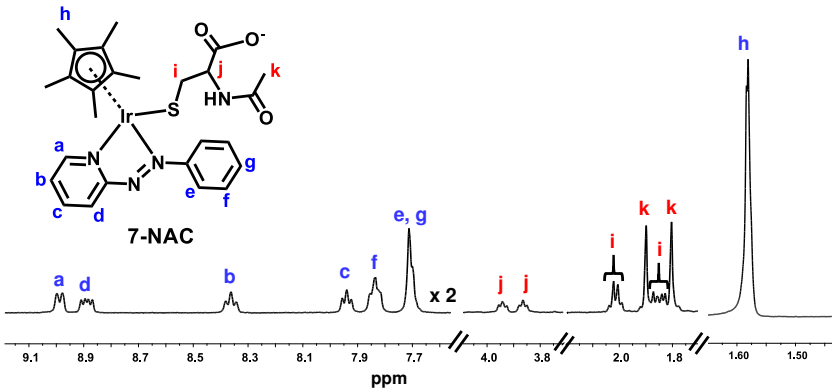

Fig. 3. ^{1}H NMR spectrum (400 MHz, d_4-MeOD/0.1 M phosphate buffer D_2O, 3/7, v/v, pH* 7.4, 298 K) of isolated **7-NAC** adduct. The bound NAC has two sets of peaks (assigned as red i, j, k) due to the presence of diastereomers of **7-NAC**.

Reactions with glutathione (GSH)

In the ^{1}H NMR spectrum of [(Cp*)Ir(azpy)I]PF_6 (**7**) (1 mM) within 15 min of reaction with GSH (20 mM) in d_4-MeOD/0.1 M phosphate buffer D_2O, 3/7, v/v, pH* 7.4 at 310 K, a new set of aromatic ligand peaks as well as a new set of GSH protons appeared, and the Cp* methyl peak shifted from 1.70 ppm to 1.53 ppm and split into two peaks (**Fig. 4**).

Meanwhile, HPLC separation on the NMR solution revealed a new peak with a shorter retention time (ca. 12 min) compared with the parent complex **7** (ca. 21.5 min, **Fig. S19a**). The new peak was identified by ESI-MS with *m/z* 817.4 (**Fig. S19b**) as the glutathione thiolato adduct [(**7-SG**)+H$^+$] (calcd *m/z* 817.2).

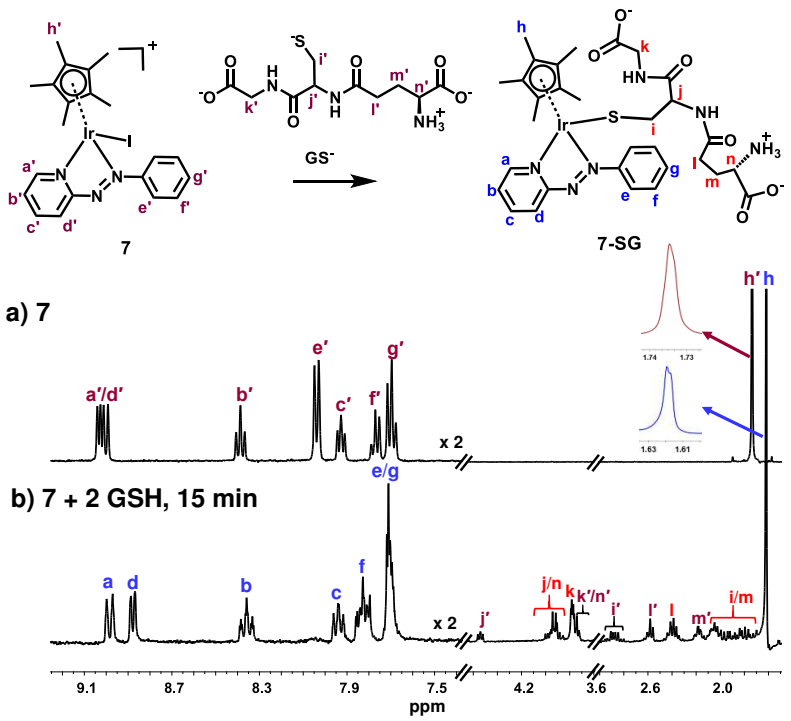

Fig. 4. ^{1}H NMR spectra (400 MHz, d_4-MeOD/0.1 M phosphate buffer D_2O, 3/7, v/v, pH* 7.4, 298 K) of (a) free complex **7**; (b) 15 min after addition of 2 mol equiv. GSH (2 mM) to complex **7** (1 mM) at 310 K. **7-SG** adduct formed within 15 min of addition of GSH to solution of complex **7**; the doublet peak for Cp* in **7-SG** indicates the diastereomers of **7-SG**.

When the reaction of **7** was repeated with 10 mol equiv. GSH under similar conditions, there was a dramatic loss in intensity of peaks in the aromatic region of the ^{1}H NMR spectrum after 15 min, together with broadening of several peaks in the aliphatic region shown in **Fig. 5b**. After 3 h, a new set of peaks appeared in the aromatic region combined with double peaks at 1.79 /1.82 ppm in 1:1 ratio as well as peaks assignable to GSSG, shown in **Fig. 5c**.

The main species in the final NMR mixture were subsequently separated by HPLC and analyzed by LC-MS. The MS peak at *m/z* 183.65 was assigned as unbound azpy ligand [(azpy)+H$^+$] (calcd 183.08), and the peak at *m/z* 185.64 as the two-electron-reduced azpy ligand phenylhydrazopyridine [(Hazpy)+H$^+$] (calcd 186.10) (**Fig. S20**). In addition, an observed MS peak at *m/z* 786.96 was assigned as binuclear $[(Cp^*)_2Ir_2(\mu\text{-SG})_3+H^+]^{2+}$ (calcd 787.19; **Fig. S20**). These species indicate that after 3 h the new set of aromatic peaks in the ^{1}H NMR (**Fig. 5c**) is phenylhydrazopyridine which is formed due to the reduction and release of azpy ligand, and the symmetrical doublet peak at 1.79 /1.82 ppm is assignable to the Cp* methyls of $[(Cp^*)_2Ir_2(\mu\text{-SG})_3]^+$.

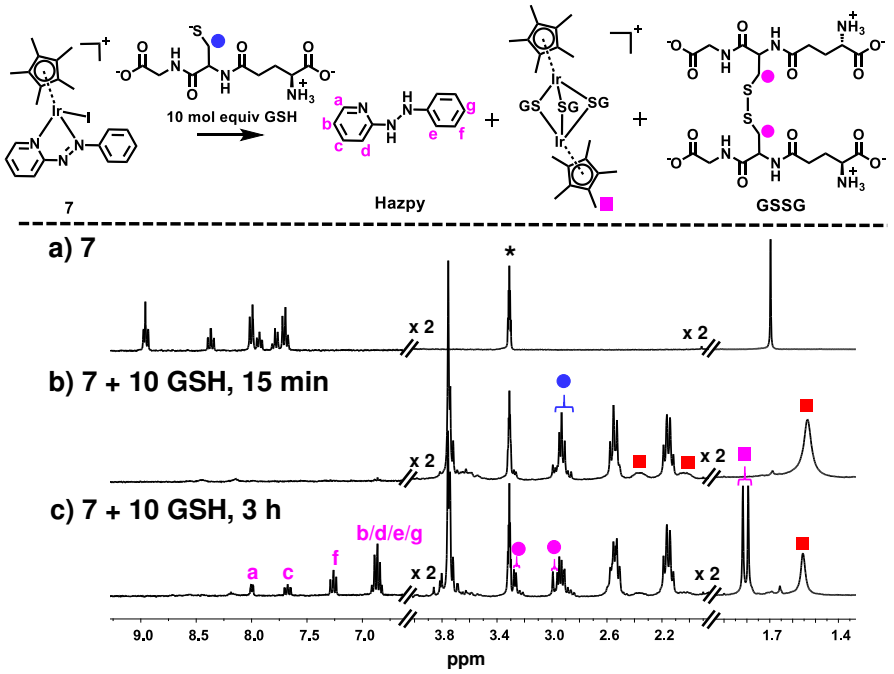

Fig. 5. ^{1}H NMR spectra (400 MHz, d_4-MeOD/0.1 M phosphate buffer D_2O, 3/7, v/v, pH* 7.4, 298 K) of (a) complex **7**, (b) 15 min, and (c) 3 h after reaction of complex **7** (1 mM) with 10 mol equiv. GSH at 310 K. The broadening of peaks in (b) can be ascribed to either exchange or (more likely –see text) paramagnetic effects, and the new set of peaks in (c) assigned to the formed phenylhydrazopyridine (Hazpy) and tri-SG bridged iridium dimer $[(Cp^*)_2Ir_2(\mu\text{-}SG)_3]^+$. * denotes residual $CHCD_2OD$.

Radical trapping by EPR

Next we investigated whether the NMR peak broadening **(Fig. 5b**) might be due to the presence of radicals and attempted to detect them by electron paramagnetic resonance (EPR) using a spin trap. EPR spectra of solution containing **7** (1 mM) with 20 mol equiv. GSH in 0.1 M phosphate buffer pH 7.4 and a spin trap DEPMPO (**Fig. 6**) or DMPO (**Fig. S21)** showed a strong doublet of quartets of 1: 2: 2: 1 peak ratio within the first 1.45 h (**Fig. 6**), which decreased in intensity thereafter. As expected, the control sample of GSH alone in 0.1 M phosphate buffer without complex **7** was EPR-silent. The EPR signals are assignable by simulation to trapped hydroxyl radicals (**Fig. 6**).

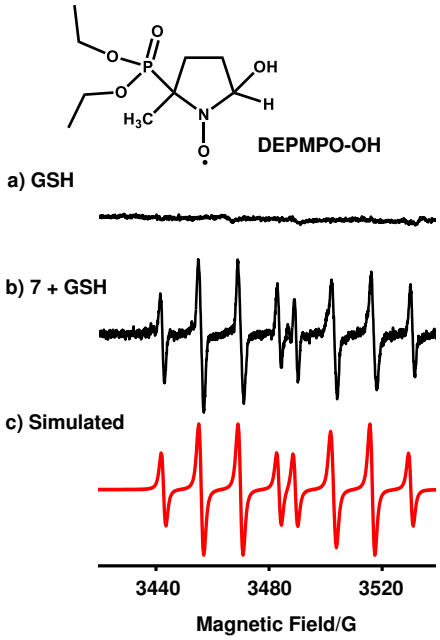

Fig. 6. EPR spectra of (a) GSH alone;(b) radicals trapped by DEPMPO (100 mM) in the reaction mixture of complex **7** (1 mM) with GSH (20 mM) in 0.1 M phosphate buffer, pH 7.4, in the initial 87 min at 298 K; (c) simulated spectrum for trapped hydroxyl radicals DEPMPO-OH (a^N = 14.0 G, a^H = 13.2 G, and a^P = 47.3 G).[28]

DFT simulation of aquation and GSH reactions

Direct attack of GSH on Ir

The x-ray crystal structure of the [(Cp^{ph})Ir(azpy-OH)I]PF_6 complex (**2**) was used as a starting point for DFT calculations on the attack of H_2O or glutathione GSH, on the Ir centre with the displacement of the iodide ligand. DFT calculations suggested that all the investigated pathways involve deprotonated GSH.

After initial formation of the slightly less stable adducts between **2** and H_2O or GS^-, the reactions proceed by a second-order nucleophilic substitution (SN2). The activation barriers to form the transition states for the associative attack by water or GS^- are similar (19.9 vs 20.2 kcal·mol^{-1}, **Fig. 7**). In contrast, the thermodynamics for the displacement of iodide by H_2O or GS^- are calculated to be different, being endergonic by 10.7 kcal·mol^{-1} for H_2O, and exergonic by -30.3 kcal·mol^{-1} to form Ir-SG.

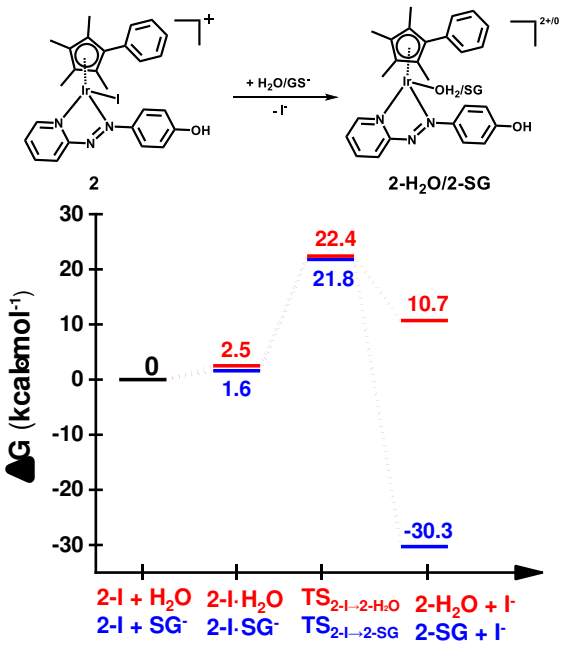

Fig. 7. DFT calculated free energy profiles for direct substitution of iodide in complex **2** by water (aquation) or GS^-**.** Relative energies are in kcal·mol^{-1} and calculated with respect to separated reactants.

Attack of GSH to the azo bond.

DFT exploration of possible, less energy-demanding, alternative pathways for the substitution of iodide by GS^- or H_2O shows that the reversible attack of GS^- on the N=N double bond of the azopyridine ligand can assist the process (**Scheme 1**).

The attack of GS^- to the non-coordinated N atom of the azo double bond, that can precede water coordination, involves a barrier of only 9.2 kcal·mol^{-1}, and causes the contemporaneous release of I^- (**Fig. 8a**). Along pathway **I**, water coordination to the vacant site on Ir occurs by surmounting an energy barrier of 8.7 kcal·mol^{-1}. Detachment of GS^- from the N atom corresponds to a very low energy barrier of only 0.2 kcal·mol^{-1}, and completes the substitution of I^- by water. The whole reaction is almost thermoneutral.

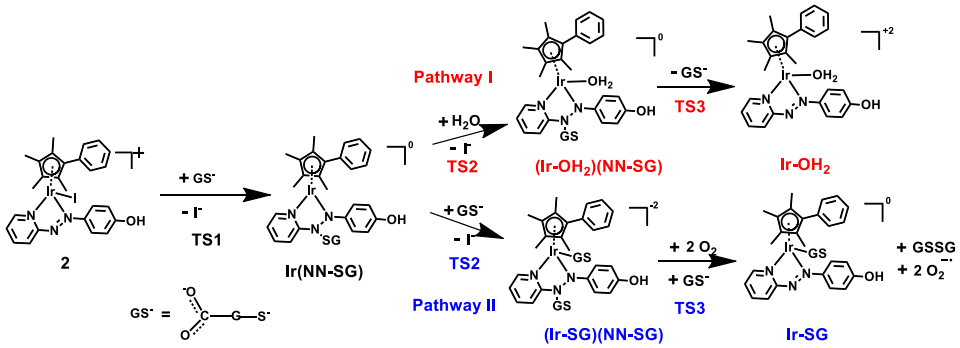

Scheme 1. Pathways **I** and **II** for the formation of Ir-H_2O and Ir-SG substitution products assisted by the attack of GS^- on the azo bond, as investigated by DFT calculations.

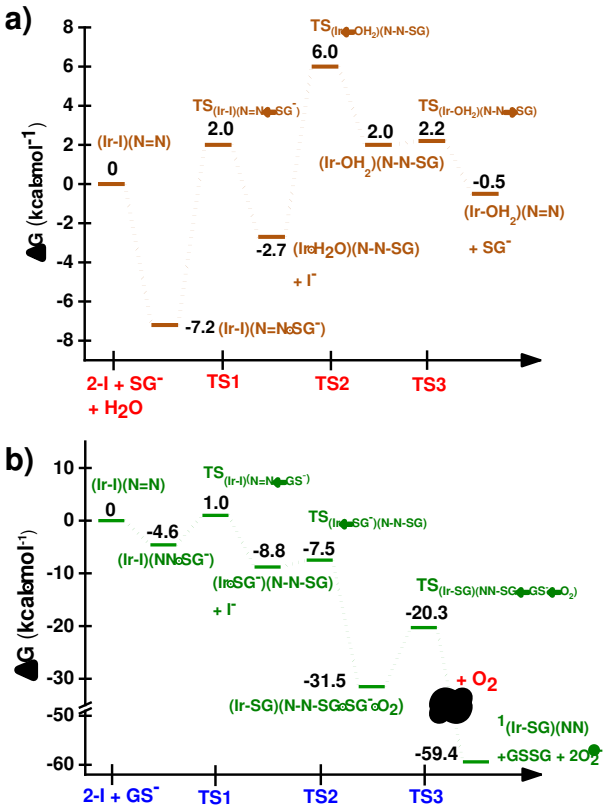

Fig. 8. Calculated free energy profiles describing iodide substitution by (a) water (pathway **I**), and (b) GS^- (pathway **II**). Relative energies are in kcal·mol^{-1} and calculated with respect to separated reactants.

Along pathway **II** (**Fig. 8b**), the first step of attack by GS^- on the N atom of the azo bond and the simultaneous release of the iodide ligand occur by surmounting a low energy

barrier of 5.6 kcal·mol^{-1}. The free energy profile for the next step, that is the coordination of GS$^-$ to iridium is very flat with a barrier of only 1.3 kcal·mol^{-1} to form the transitional state of [(Ir-SG)(N-N-SG)]. With respect to the pathway illustrated above describing attack by water in Figure **8a**, the GS$^-$ bound to the N atom of the azo group in pathway **II** is not spontaneously released. Instead, in the presence of a third GS$^-$, the detachment of GS$^-$ from the N atom occurs to form oxidized glutathione, GSSG. The latter step, therefore, involves the transfer of two electrons from the two released GS$^-$ molecules. Computations suggest that ground state triplet-O_2 can act as an electron acceptor for this step. The O-O bond elongates consistent with formation of superoxide $O_2^{\cdot-}$, whereas the second electron is localized on the N atom previously bound to GS$^-$ (N-N single bond). The whole system is in a triplet state again, and the spin is conserved. The singlet multiplicity of the complex can be recovered in several ways, for example, due to the presence of a second O_2 molecule. In Scheme 2 pathway **II**, the reported final products are the singlet state complex, GSSG, and two $O_2^{\cdot-}$ radicals to conserve the triplet multiplicity. Overall, this reaction is largely exergonic.

pH-dependent formation of Ir-SG

When complex **7** (1 mM) reacted with 5 mol equiv. GSH at 310 K over 24 h, at pH* 3.6, 75% formed **7-SG,** while in the presence of 100 mM KI, only 20% formed **7-SG**, **Fig. S22**. At pH* 8.0, the reaction of complex **7** with GSH to form **7-SG** was complete within 10 min, even in the presence of 100 mM KI, **Fig. S23**.

Anticancer activity of iridium azopyridine complexes

The antiproliferative activity of complexes **1**-**10** towards human lung A549 cancer cells in comparison with cisplatin (CDDP) was determined using the SRB assay[29], **Fig. 9**. Iodido complexes **1**-**6** and chlorido complexes **9-10** sharing the common feature of a phenolic substituent on the phenylazo-pyridine ligand are highly potent, with IC_{50} values (the concentration that inhibits cell growth by 50%) within the range of 0.3-1.6 μM. Particularly, complex **3** (R_2 = OH, R_1 = Br), with an IC_{50} value of 0.33 μM towards A549 cancer cells, is 10x more active than cisplatin. By contrast, complexes **7** and **8** with unsubstituted phenyl-azopyridine ligands are less active than **1**-**6** and **9**-**10**. The substitution of one methyl group on Cp* by a phenyl substituent to give Cp^{ph} does not enhance the anticancer activity of iodido complexes **1**-**8**, while the Cp^{ph} chlorido complex **10** with is slightly more active than its Cp* analogue **9**.

To study the influence of the halido ligand on anticancer activity, representative iodido complex **1** and its chlorido analogue complex **9** bearing the same phenylazopyridine ligand were screened against four human cancer cell lines, A549 (lung), CNE2 (nasopharyngeal), A2780 (ovarian), and A2780*cis*R (cisplatin-resistant ovarian), **Table 2**. A2780*cis*R is resistant through reduced drug transport, enhanced DNA repair/tolerance and elevated GSH levels.[30] Iodido complex **1** exhibited similar potency to chlorido analogue **9** against

A549, CNE2, and A2780 cell lines (IC_{50} values in **Table 2**), although both are much more potent than cisplatin. Iodido complex **1** was ca. 2x more potent than the chlorido complex **9** towards the A2780*cis*R resistant ovarian cell line, and notably neither complex was not cross resistant with cisplatin (resistance factor = IC_{50}(A2780*cis*R)/IC_{50}(A2780*)* = 0.2 for **1** and 0.95 for **9**).

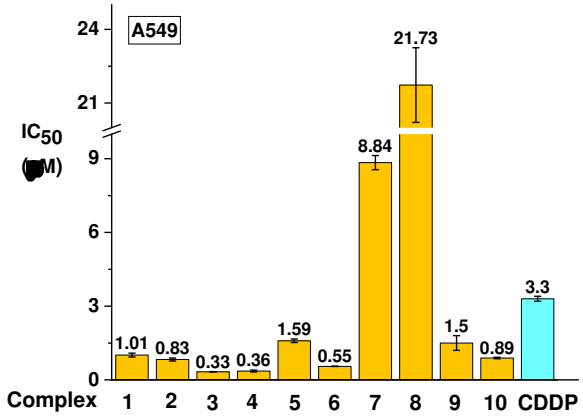

Fig. 9. Inhibition of growth of A549 human lung cancer cells *in vitro* by complexes **1**-**10** in comparison with cisplatin (CDDP). The values of half maximal growth inhibitory concentration (IC_{50}) are given as the mean ± standard deviations for three independent experiments.

Table 2. Cytotoxicity of iodido complex **1** and chlorido analogue **9** towards human A549 lung, CNE2 nasopharyngeal, A2780 ovarian, and A2780*cis*R cisplatin-resistant ovarian cancer cells.

Complex	A549	CNE2	A2780	A2780*cis*R (RF)[a]
[(Cp*)Ir(azpy-OH)I]PF_6 (**1**)	1.01 ± 0.08	1.26 ± 0.3	0.25 ± 0.02	0.049 ± 0.001[b] (0.20)
[(Cp*)Ir(azpy-OH)Cl]PF_6 (**9**)	1.5 ± 0.3	2.3 ± 0.3	0.12 ± 0.04	0.114 ± 0.003 (0.95)
Cisplatin	11.5 ± 0.3	3.3 ± 0.1	1.2 ± 0.2	7.7 ± 0.3 (6.41)

[a] resistance factor RF = IC_{50} resistant/ IC_{50} sensitive; [b] IC_{50} for complex **9** with chloride as counter anion.

Toxicity *in vivo*

The toxicity of iodide complex **1** in comparison with its chlorido analogue **9** was determined in zebrafish (*Danio rerio*) embryos, a high-throughput vertebrate model often used as a predictor for drug toxicity in humans.[31-34] The iodido complex **1** (LC_{50} = 0.26 ±

0.08 μM) was ca. 25x less toxic to zebrafish than its chlorido analogue **9** (LC_{50} = 0.010 ± 0.003 μM).

Partition coefficients (log P) and cell accumulation

Anticancer activity of metal complexes often correlates with cellular uptake and lipophilicity.[35] Partition coefficients (log P values) provide measurements of the lipophilicity of compounds. We compared the lipophilicity of complexes **3** and **7** by determining their octanol-phosphate buffer (pH 7.4) partition coefficients using the "shake-tube" method. [21] Phosphate buffer was used instead of water on account of the tendency of the phenolate complexes to deprotonate at physiological pH, which would affect their partition. As shown in **Table 3**, phenolic complex **3** [(Cp*)Ir(Br-azpy-O⁻)I]PF_6 which would exist as a neutral zwitterion at pH 7.4, has a larger partition coefficient and is much more lipophilic than cationic complex **7** [(Cp*)Ir(azpy)I]PF_6. Accumulation of iridium in A549 lung cancer cells was determined by ICP-MS after treatment with 0.5x, 1.0x, and 2.0x IC_{50} concentrations of complexes of **3** or **7** for 24 h. A linear correlation of Ir accumulation with the dose of complex **3** or **7** was observed (**Fig. S24**). The cellular Ir accumulation of [(Cp*)Ir(Br-azpy-O⁻)I]PF_6 (**3**) is over 2x that of [(Cp*)Ir(azpy)I]PF_6 (**7**) (101 ± 1.3 ng of Ir vs 51 ± 10.1 ng of Ir per 10^6 cells) at their equipotent IC_{50} concentrations, shown in **Table 3**. This difference correlates well with their cytotoxicity (IC_{50} = 0.33 μM for **3** vs 8.84 μM for **7**).

Table 3. Partition coefficients between octanol and phosphate buffer (2 mM, pH 7.4) at 298 K for complexes **3** and **7**, and their cellular iridium accumulation (at equipotent IC_{50} concentrations) in A549 lung cancer cells.

Complex	$logP_{7.4}$	IC_{50} (μM)	Ir Accumulation (ng/10^6 A549 cells)
[(Cp*)Ir(Br-azpy-O⁻)I]PF_6 (**3**)	-0.08	0.33 ± 0.01	101 ± 1.3
[(Cp*)Ir(azpy)I]PF_6 (**7**)	-0.59	8.84 ± 0.29	51.3 ± 10.1

ROS detection

The levels of reactive oxygen species (ROS) in A549 human lung cancer cells treated with complexes **3** and **7** were determined at 2x IC_{50} concentrations (**Fig. 10**) by flow cytometry fluorescence analysis through the total ROS/Superoxide (SO) Detection Kit. The superoxide production was monitored by the orange channel FL1, and total ROS species, including H_2O_2, peroxy and hydroxyl radicals, peroxynitrile and NO, were monitored by the green channel FL2, respectively. After 24 h drug exposure, an increase in ROS/SO levels in cells treated with complexes **3** and **7** compared to untreated cells was observed. Meanwhile, a burst of superoxide production by complex **7** was also observed, while complex **3** produced a negliable level of superoxide.

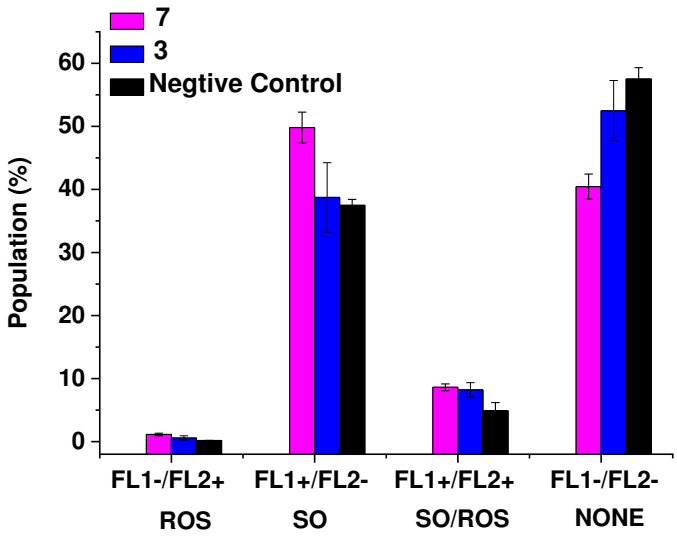

Fig. 10. ROS induction in A549 cancer cells exposed to complexes **3** and **7** at 2x IC_{50} concentrations for 24 h compared with the untreated cells (negative control). FL1 channel detects superoxide production, and FL2 channel detects total oxidative stress. Normalized population data are presented as the mean ±SD of triplicate samples for one experiment. *p*-Values were calculated after t-test against the negative control data, **p*< 0.05, ***p*<0.01.

Discussion

Aquation and stability

Transition metal anticancer complexes containing chlorido ligands can undergo activation by hydrolysis, including cisplatin and Ru(II) arene complexes, which are more reactive in the form of aqua adducts.[36] The Ir(III) analogue of the Ru(III) clinic trial drug NAMI-A, *trans*-[$IrCl_4$(DMSO)(Im)][ImH], (DMSO = dimethyl sulfoxide, Im = imidazole), exhibits low cytotoxic activity, attributable to its inertness towards hydrolysis.[37] Potent half-sandwich $5d^6$ Ir(III) chlorido complexes with N,N chelating bidentate ligands often undergo rapid hydrolysis.[38] Similarly, the chlorido iridium complexes **9** and **10** studied here bearing azopyridine-OH ligands were ca. 53% and 66% hydrolyzed after 24 h at 310 K. However, their iodido analogues complexes **1** and **2** are inert towards hydrolysis, consistent with the expected softer character of iodide and stronger covalency of Ir^{III}-I bonds. Similarly, the higher stability of iodido Ru(II) and Os(II) arene azopyridine complexes compared to chlorido analogues has also been observed.[39]

In addition, these iodido complexes are not readily converted into the chlorido analogues even at high blood plasma NaCl concentrations (103 mM), **Fig. S10e**, suggesting that intact iodido complexes can enter cells. Although lack of hydrolysis or interaction with nucleobases (9-EtG or 5'-GMP), the most active iodido complex [(Cp^*)Ir(Br-azpy-OH)I]PF_6 (**3**) is 10x more active than cisplatin, suggesting that other factors play

important roles in the mechanism of action of these iridium azopyridine complexes. This is distinct from other iridium anticancer agents,[40] which undergo hydrolysis first before reacting with possible targets, such as coenzyme NADH. The extension of Cp* to Cp^{ph} in the iridium complexes studied did not improve the anticancer activity significantly, contrary to expectations if DNA is a target.

Anticancer activity for chlorido and iodido complexes

Despite its substitutional inertness, iodido complex **1** still exhibits similar potency to its chlorido analogue against A549, CNE2, and A2780 cancer cell lines, and even higher potency and a lower resistance factor towards cisplatin resistant A2780*cis*R ovarian cancer cells. Firstly, the hydrolysis might readily lead to unwanted side-reactions before reaching target sites. On the other hand, if hydrolysis is not essential for potent anticancer activity, these inert iodido complexes might be activated in cancer cells by an alternative mechanism as is the case for iodido Os(II) arene complexes.[41]

Organometallic iodido Ru(II) and Os(II) anticancer complexes with azo/imino-pyridine ligands are more selective for cancer cells versus normal cells than the corresponding chlorido analogues.[39] Halide replacement of chloride in complex **9** by iodide in complex **1** greatly reduces the toxicity *in vivo* as assessed in zebrafish embryos. Whereas the iodido complex has a similar toxicity to cisplatin (LC_{50} = 0.6 μM),[42] the chlorido complex is 25x more toxic than the iodido complex. Meanwhile, the iodido complex **1** retains high potency (**Table 2**) in cancer cells.

Structure-activity relationship for iodido complexes

The iodido complexes **1-6** were isolated with protonated phenolic substituents, but their pH-dependent UV-vis absorption shows that at pH 7.4, under biological screening conditions, they will exist largely as deprotonated forms (pK_a values 3.90-6.49, **Fig. 2**, **Table S5**).

The deprotonated phenolate ligands (**Fig. 11**) decrease the π-acidity of the azo group,[43] thus shifting the Ir $5d^6$ orbitals to higher energy, and narrowing the energy gap between Ir $5d^6$ and azo π* orbitals, which is manifested in the spectrum with a progressive red-shift of the MLCT band from the filled 5d orbitals of Ir(III) to the empty π* ligand orbitals. The pK_a values of the OH group in complexes **1-6** are much lower than that of the free azpy-OH ligand (8.08),[44] with Ir(III) delocalizing the negative electron density of the phenolate. Interestingly, compared with Cp^* analogues bearing the same ligand, all the Cp^{ph} complexes have lower pK_a values, enhanced for CF_3 < Br < H substituents on the ligand, showing that the pK_a values are affected both by the Cp^A ligand as well as the substituents on the phenylazopyridine ligands. Both the extended Cp^{ph} ring and electron-withdrawing groups on the ligand delocalize the negative density from O^-, thus leading to lower pK_a values.

In cell culture media, complexes **1-6** will all exist predominately in zwitterionic forms, which appears to give rise to higher cellular accumulation and contribute to higher anticancer potency compared to complexes **7**-**8** which bear unsubstituted azpy ligands. This was evident for the cellular accumulation of complex **3** which is ca. 2x that of complex **7** at equipotent concentrations, and higher cytotoxicity (IC_{50} 0.33 μM of **3,** versus IC_{50} 8.84 μM of **7**, in **Table 3**). Higher Ir accumulation of zwitterionic complex **3** results from a higher lipophilicity compared to cationic complex **7** ($logP_{7.4}$ = -0.08 for **3** vs -0.59 for **7**). Interestingly the phenolic pK_a values (3.9-6.5) might allow trapping of the complexes by protonation in cell organelles where the pH is lower (e.g. lysosomes ca. 5.6)

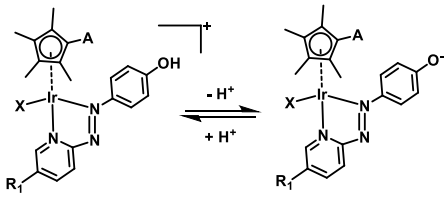

Fig. 11. Acidity of complexes **1-6**.

GSH-mediated ligand-centered activation and ROS production

GSH is an important cellular antioxidant which detoxifies various xenobiotics as well as protects cells from toxic reactive oxygen species.[45] Thus, reactions of metal complexes with GSH can disturb the redox state of cells. Unlike the detoxification of platinum drugs by conjugation with GSH, some chlorido Ru^{II} arene ethylenediamine anticancer complexes form Ru thiolate adducts which are not the 'dead-end' products and can be further oxidized to sulfenato and sulfinato adducts which facilitate the interaction of Ru complexes with DNA.[46] Other Ru(II)[47, 48], Os(II)[41], and Pt (IV)[49] complexes are also thought to be activated by GSH. It is worthy to note that although the pK_a of the Cys thiol in GSH is high (ca. 9.4), there will be a small but significant amount (ca. 0.3%) of deprotonated GSH present at pH 7.[50] Excitingly, although the Ir-I complexes studied here are inert towards hydrolysis (**Fig. S7b**) and do not bind to guanine, they react with the thiolate group on the cysteine of NAC or GSH to form Ir-NAC/SG adducts (**Fig. 3** and **Fig. 4**) and show potent anticancer activity toward A549 cancer cells (**Fig. 10**). DFT calculations suggest that, compared with hydrolysis to form an Ir-aqua complex, displacement of I^- by GS^- to yield an Ir-SG complex is much more thermodynamically favorable, overall being exergonic by 52.1 kcal·mol^{-1} (**Fig. 8**), in accordance with the experimentally-observed preferential reactivity of these iodido iridium complexes with GSH. Furthermore, the observed product that is formed by reaction of complex **7** with GSH is Ir-SG (**Fig. S19a**), in contrast to iodido Os^{II} phenylazopyridine complexes which form the Os-OH species when incubated with low molar ratios of GSH.[41]

Based on previous reports for metal-azo complexes,[51, 52] the first-step reduction can be assigned to one-electron addition into the π* orbital centred on the azo group to give the azo anion radical and the second reduction is assigned to formation of the dianionic

species ([-N-N-]$^{2-}$). However, in aqueous media, the two-electron reduction of azo groups is also accompanied by the proton transfer to give hydrazo groups [-NH-NH-].[53] From the assignment, the azo bond is more likely to be the active centre for reduction of these idodio complexes.

In cells and tissues, the redox potentials of the GSH/GSSG couple (-240 mV)[54] are more negative than the reduction potentials of the azo bonds in the anticancer active complexes **3** and **7** (-130 mV and -70 mV, respectively, **Table 1**), which means that the azo bonds on the ligands of **3**/**7** are likely to be readily reduced by GSH. Complex **7** reacts with 10 mol equiv. GSH under physiological conditions to produce initially the **7-SG** adduct. Then the disappearance of the aromatic signals combined with the broadened Cp* methyl peaks after 15 min in **Fig. 5** suggests that the aromatic ligand is susceptible to redox reactions with the reductant GSH. Hydroxyl radicals were trapped and detected by EPR addition of complex **7** to 20 molar equiv. GSH (**Fig. 6**). It seems likely that these are formed via initial donation of an electron from the reduced azo bind to O_2 to form superoxide radicals which tend to decompose into hydroxyl radicals.[55, 56]

The hydroxyl radicals produced within the first 1.45 h and decayed with time. After 3 h the released 2.0 mol equiv. phenylhydrazopyridine (reduced form of phenylazopyridine) appeared in the solution together with 1.0 mol equiv. tri-SG bridged di-iridium adduct. This might be ascribed to the depletion of oxygen in the solution halting electron transfer from the reduced azo bond.

Thiolate-bridged dimeric Ir(III) complexes $[(Cp^*)_2Ir_2(\mu\text{-}SR)_3]$, have been reported by Therrien et al. to exhibit high anticancer activity toward A2780 and cisplatin-resistant A2780cisR human ovarian cell lines.[57] Procarbazine, an organic molecule with a redox active hydrazine group, was approved in the late 1960s as a cytotoxic anticancer drug.[58] Hence, the potent inert iridium iodido complexes studied in the present work might behave as multi-prodrugs as a “pro-drug”, giving rise to oxidative species (hydroxyl radicals), redox-active phenylhydrazopyridine, as well as active tri-SG bridged dimeric iridium adducts, on intracellular activation by GSH.

In order to elucidate the nature of possible ligand-centred reactivity of these inert iodido complexes, DFT calculations were carried out to investigate whether the formation of Ir-aqua and Ir-SG compounds can be facilitated by the attack of GS^- on the azo bond. Surprisingly, DFT results suggest that loss of the iodido ligand from Ir(II) and the subsequent binding of GS^- or water to Ir is preceded by attack of GS^- on the N=N double bond, as shown in pathways **I**/**II** in **Scheme 1**. Binding of GS^- to the N=N double bond, therefore, increases the lability of the iodido ligand favouring substitution reactions. The energy barriers for the first step of GS^- binding to the non-coordinated N atom of the azo bond to form Ir-OH_2 and Ir-SG are only 9.2 kcal·mol^{-1} (**Fig. 8a**) and 5.6 kcal·mol^{-1} (**Fig. 8b**), respectively. These barriers are much lower than those calculated for the direct replacement of iodide by water or GS^- (19.9 and 20.2 kcal·mol^{-1}, respectively, **Fig. 7**). At the same time, the experimental detection of a faster rate (within 10 min) and 100%

formation of **7-SG** even in presence of 100 mM KI in basic conditions, persuasively indicates that the formation of **7-SG** is likely initiated by the attack of GS^- on the azo bond. Furthermore, DFT calculations show that, after the iodide ligand is released, a step involving attack by a second GS^- on the Ir centre to form a Ir-SG complex requires only 1.3 kcal·mol^{-1} (**Fig. 8b**), whereas along pathway **I**, water binding to the Ir center to form Ir-OH_2 requires 8.7 kcal·mol^{-1} (**Fig. 8a**). Therefore, after the attack of the first GS^- on the N atom of the azo bond, the energy-preferred sequence of steps is that shown by pathway **II** in **Scheme 1**, that is, a second GS^- attack on the Ir centre to form $[(Ir\text{-}SG)(NN\text{-}SG)]^{2-}$ instead of forming the aqua complex $[(Ir\text{-}OH_2)(NN\text{-}SG)]^0$. In the final step of pathway **II**, the $[(Ir\text{-}SG)(NN\text{-}SG)]^{2-}$ complex reacts with a third GS^- and forms the oxidized glutathione species GSSG by the detachment of the GS^- group from the azo bond. One electron is transferred to an oxygen molecule as evidenced by O-O bond elongation. A superoxide anion is formed, whereas another electron is localized on the previously bound N atom. The reaction is calculated to be largely exergonic by 59.4 kcal·mol^{-1}. This correlates well with the ligand-centred reduction observed by ^{1}H NMR (**Fig. 5**), and the formation of hydroxyl radicals as decay products from superoxide radicals trapped in the EPR study (**Fig. 6**). Meanwhile, ROS accumulation in A549 lung cancer cells for complexes **3** and **7** (**Fig. 10**) is consistent with a cellular redox-mediated mechanism of action for these iodido complexes.

Conclusions

We have designed a novel family of half-sandwich cyclopentadienyl Ir(III) complexes containing a soft monodentate iodido ligand and redox-active chelated azo-pyridine ligands with 10-fold higher potency than the anticancer drug cisplatin against A549 human lung cancer cells. Remarkably, iodido complex **1** is more promising than its chlorido analogue for overcoming cisplatin resistance toward A2780 human lung cancer cells and shows lower *in vivo* toxicity toward Zebrafish embryos. Deprotonation of the phenol group on the ligand at physiological pH 7.4 confers zwitterionic characteristics on complexes **1**-**6**. These appear to be the first examples of zwitterionic half-sandwich iridium complexes with high anticancer potency.

Reactions of transition metal anticancer complexes with glutathione are usually considered to be deactivating. In the present case hydrolysis-inert iodido iridium complexes are activated by GSH to form Ir-thiolate adducts combined with production of reactive oxygen species. DFT calculations suggest that energy-favored attack of GS^- on the azo bond, promotes the subsequent release of the iodido ligand, followed by preferential binding of Ir(III) to glutathione rather than water, which matches experimental observations well. In presence of excess GSH, one electron can be donated by GSH to oxygen leading to formation of oxidized glutathione (GSSG), which is largely exergonic. The production of hydroxyl radicals can contribute to the increased cellular ROS level, suggesting that the cellular redox behavior of these iodido complexes may contribute to their cytotoxicity.

Therefore although glutathione is usually considered to deactivate transition metal drugs, the present work shows that it can also have an activating role towards half-sandwich cyclopentadienyl Ir(III) anticancer complexes, one which can involve attack on ligand sites (an azo bond in this case), as well as on the metal itself. Such findings open up new strategies for the design on metallodrugs with novel mechanisms of action which can combat resistance.

Conflicts of Interest

There are no conflicts to declare.

Acknowledgements

This research was supported by the EPSRC (grant nos EP/F034210/1, EP/P030572/1 and MOAC studentship for G. M. H.), a Chancellor's International Ph.D. Scholarship from the University of Warwick (for W.-Y. Z.), and a Royal Society Newton International Fellowship (NF151429 for S. B.). We thank Dr Lijiang Song, Dr Ivan Prokes and Ian Bagley (University of Warwick) for excellent technical assistance with MS, NMR and zebrafish embryo experiments, respectively.

References

1. L. Kelland, *Nat. Rev. Cancer*, 2007, **7**, 573.
2. G. Gasser, I. Ott and N. Metzler-Nolte, *J. Med. Chem.*, 2010, **54**, 3-25.
3. N. P. Barry and P. J. Sadler, *Chem. Commun.*, 2013, **49**, 5106-5131.
4. A. Cusanelli, U. Frey, D. T. Richens and A. E. Merbach, *J. Am. Chem. Soc.*, 1996, **118**, 5265-5271.
5. Z. Liu and P. J. Sadler, *Acc. Chem. Res.*, 2014, **47**, 1174-1185.
6. Y. Geldmacher, M. Oleszak and W. S. Sheldrick, *Inorg. Chim. Acta*, 2012, **393**, 84-102.
7. E. Meggers, *Angew. Chem. Int. Ed.*, 2017, **56**, 5668-5675.
8. M. A. Scharwitz, I. Ott, R. Gust, A. Kromm and W. S. Sheldrick, *J. Inorg. Biochem.*, 2008, **102**, 1623-1630.
9. R. Gao, D. G. Ho, B. Hernandez, M. Selke, D. Murphy, P. I. Djurovich and M. E. Thompson, *J. Am. Chem. Soc.*, 2002, **124**, 14828-14829.
10. L. He, Y. Li, C.-P. Tan, R.-R. Ye, M.-H. Chen, J.-J. Cao, L.-N. Ji and Z.-W. Mao, *Chem. Sci.*, 2015, **6**, 5409-5418.
11. H. Amouri, J. Moussa, A. K. Renfrew, P. J. Dyson, M. N. Rager and L. M. Chamoreau, *Angew. Chem. Int. Ed.*, 2010, **49**, 7530-7533.
12. Z. Liu, I. Romero-Canelón, B. Qamar, J. M. Hearn, A. Habtemariam, N. P. Barry, A. M. Pizarro, G. J. Clarkson and P. J. Sadler, *Angew. Chem. Int. Ed.*, 2014, **53**, 3941-3946.
13. A. J. Millett, A. Habtemariam, I. Romero-Canelón, G. J. Clarkson and P. J. Sadler, *Organometallics*, 2015, **34**, 2683-2694.

14. Y. Yang, L. Guo, Z. Tian, Y. Gong, H. Zheng, S. Zhang, Z. Xu, X. Ge and Z. Liu, *Inorg. Chem.*, 2018, **57**, 11087-11098.
15. Z. Liu, A. Habtemariam, A. M. Pizarro, S. A. Fletcher, A. Kisova, O. Vrana, L. Salassa, P. C. Bruijnincx, G. J. Clarkson and V. Brabec, *J. Med. Chem.*, 2011, **54**, 3011-3026.
16. K. Fagnou and M. Lautens, *Angew. Chem. Int. Ed.*, 2002, **41**, 26-47.
17. P. Štarha, Z. Dvořák and Z. Trávníček, *J. Organomet. Chem.*, 2018, **872**, 114-122.
18. F. Chen, J. Moat, D. McFeely, G. Clarkson, I. J. Hands-Portman, J. P. Furner-Pardoe, F. Harrison, C. G. Dowson and P. J. Sadler, *Journal of Medicinal Chemistry*, 2018, **61**, 7330-7344.
19. J. M. Cross, N. Gallagher, J. H. Gill, M. Jain, A. W. McNeillis, K. L. Rockley, F. H. Tscherny, N. J. Wirszycz, D. S. Yufit and J. W. Walton, *Dalton Trans.*, 2016, **45**, 12807-12813.
20. S. J. Dougan, A. Habtemariam, S. E. McHale, S. Parsons and P. J. Sadler, *Proc. Natl. Acad. Sci. U.S.A.*, 2008, **105**, 11628-11633.
21. Y. Fu, A. Habtemariam, A. M. B. H. Basri, D. Braddick, G. J. Clarkson and P. J. Sadler, *Dalton Trans.*, 2011, **40**, 10553-10562.
22. J. M. Hearn, G. M. Hughes, I. Romero-Canelón, A. F. Munro, B. Rubio-Ruiz, Z. Liu, N. O. Carragher and P. J. Sadler, *Metallomics*, 2018, **10**, 93-107.
23. Y. Fu, M. J. Romero, A. Habtemariam, M. E. Snowden, L. Song, G. J. Clarkson, B. Qamar, A. M. Pizarro, P. R. Unwin and P. J. Sadler, *Chem. Sci.*, 2012, **3**, 2485-2494.
24. S. H. van Rijt, A. J. Hebden, T. Amaresekera, R. J. Deeth, G. J. Clarkson, S. Parsons, P. C. McGowan and P. J. Sadler, *J. Med. Chem.*, 2009, **52**, 7753-7764.
25. J. Kelemen, G. Kormany and G. Rihs, *Dyes Pigments*, 1982, **3**, 249-271.
26. L. Li, W. W. Brennessel and W. D. Jones, *J. Am. Chem. Soc.*, 2008, **130**, 12414-12419.
27. Z. Liu, L. Salassa, A. Habtemariam, A. M. Pizarro, G. J. Clarkson and P. J. Sadler, *Inorg. Chem.*, 2011, **50**, 5777-5783.
28. H. Karoui, N. Hogg, C. Fréjaville, P. Tordo and B. Kalyanaraman, *J. Biol. Chem.*, 1996, **271**, 6000-6009.
29. P. Skehan, R. Storeng, D. Scudiero, A. Monks, J. McMahon, D. Vistica, J. T. Warren, H. Bokesch, S. Kenney and M. R. Boyd, *JNCI: Journal of the National Cancer Institute*, 1990, **82**, 1107-1112.
30. J. Ruiz, C. Vicente, C. n. de Haro and D. Bautista, *Inorg. Chem.*, 2013, **52**, 974-982.
31. T. V. Bowman and L. I. Zon, *ACS Chem. Biol.*, 2010, **5**, 159-161.
32. P. M. Eimon and A. L. Rubinstein, *Expert Opin. Drug Metab. Toxicol.*, 2009, **5**, 393-401.
33. A. J. Rennekamp and R. T. Peterson, *Curr. Opin. Chem. Biol.*, 2015, **24**, 58-70.
34. W. B. Barbazuk, I. Korf, C. Kadavi, J. Heyen, S. Tate, E. Wun, J. A. Bedell, J. D. McPherson and S. L. Johnson, *Genome Res.*, 2000, **10**, 1351-1358.

35. M. J. McKeage, S. J. Berners-Price, P. Galettis, R. J. Bowen, W. Brouwer, L. Ding, L. Zhuang and B. C. Baguley, *Cancer chemotherapy and pharmacology*, 2000, **46**, 343-350.
36. C. X. Zhang and S. J. Lippard, *Curr. Opin. Chem. Biol.*, 2003, **7**, 481-489.
37. L. Messori, G. Marcon, P. Orioli, M. Fontani, P. Zanello, A. Bergamo, G. Sava and P. Mura, *J. Inorg. Biochem.*, 2003, **95**, 37-46.
38. Z. Liu, A. Habtemariam, A. M. Pizarro, S. A. Fletcher, A. Kisova, O. Vrana, L. Salassa, P. C. A. Bruijnincx, G. J. Clarkson, V. Brabec and P. J. Sadler, *J. Med. Chem.*, 2011, **54**, 3011-3026.
39. I. Romero-Canelón, L. Salassa and P. J. Sadler, *J. Med. Chem.*, 2013, **56**, 1291-1300.
40. I. Ritacco, N. Russo and E. Sicilia, *Inorganic Chemistry*, 2015, **54**, 10801-10810.
41. R. J. Needham, C. Sanchez-Cano, X. Zhang, I. Romero-Canelón, A. Habtemariam, M. S. Cooper, L. Meszaros, G. J. Clarkson, P. J. Blower and P. J. Sadler, *Angew. Chem. Int. Ed.*, 2017, **56**, 1017-1020.
42. J. P. C. Coverdale, H. E. Bridgewater, J.-I. Song, N. A. Smith, N. P. E. Barry, I. Bagley, P. J. Sadler and I. Romero-Canelón, *J. Med. Chem.*, 2018, **61**, 9246-9255.
43. R. A. Krause and K. Krause, *Inorg. Chem.*, 1984, **23**, 2195-2198.
44. S. J. Dougan, M. Melchart, A. Habtemariam, S. Parsons and P. J. Sadler, *Inorg. Chem.*, 2006, **45**, 10882-10894.
45. A. Meister, *Trends Biochem. Sci*, 1981, **6**, 231-234.
46. F. Wang, J. Xu, A. Habtemariam, J. Bella and P. J. Sadler, *J. Am. Chem. Soc.*, 2005, **127**, 17734-17743.
47. L. Zeng, S. Kuang, G. Li, C. Jin, L. Ji and H. Chao, *Chem. Commun.*, 2017, **53**, 1977-1980.
48. Q.-X. Zhou, Y. Zheng, T.-J. Wang, Y.-J. Chen, K. Li, Y.-Y. Zhang, C. Li, Y.-J. Hou and X.-S. Wang, *Chem. Commun.*, 2015, **51**, 10684-10686.
49. Y. Shi, S.-A. Liu, D. J. Kerwood, J. Goodisman and J. C. Dabrowiak, *J. Inorg. Biochem.*, 2012, **107**, 6-14.
50. S. G. Tajc, B. S. Tolbert, R. Basavappa and B. L. Miller, *J. Am. Chem. Soc.*, 2004, **126**, 10508-10509.
51. J. L. Sadler and A. J. Bard, *J. Am. Chem. Soc.*, 1968, **90**, 1979-1989.
52. W. Kaim, R. Reinhardt, S. Greulich and J. Fiedler, *Organometallics*, 2003, **22**, 2240-2244.
53. S. J. Dougan, A. Habtemariam, S. E. McHale, S. Parsons and P. J. Sadler, *Proc. Natl. Acad. Sci. U.S.A.*, 2008.
54. W. G. Kirlin, J. Cai, S. A. Thompson, D. Diaz, T. J. Kavanagh and D. P. Jones, *Free Radical Biol. Med.*, 1999, **27**, 1208-1218.
55. V. Khramtsov, L. J. Berliner and T. L. Clanton, *Magn. Reson. Med.*, 1999, **42**, 228-234.
56. S. Dikalov, J. Jiang and R. P. Mason, *Free Radical Res.*, 2005, **39**, 825-836.

57. G. Gupta, A. Garci, B. S. Murray, P. J. Dyson, G. Fabre, P. Trouillas, F. Giannini, J. Furrer, G. Süss-Fink and B. Therrien, *Dalton Trans.*, 2013, **42**, 15457-15463.
58. Y. Kenis, J. De Smedt and H. J. Tagnon, *Eur. J. Cancer*, 1966, **2**, 51-57.

5

CALIXARENES AS VEHICLE SYSTEMS FOR PLATINUM COMPLEXES IN CHEMOTHERAPY

- Calixarenes as vehicle systems for platinum complexes in chemotherapy

Introduction

One of the ongoing challenges in the fight against cancer is to improve the effectiveness of "old" drugs and increase the specificity with which the drug reaches the target. A promising area of research, in this field, is the study of macromolecules including macrocyclic species, as drug delivery agents.

The encapsulation of drugs inside the macrocycle cavity protects the drug from side reactions, increases its targeting and its solubility, stability and bioavailability.

Calix[n]arenes (CX) are one the most widely studied class of synthetic supramolecular macrocycles of bowl or cone shaped whose properties, as molecular hosts and delivery systems, are of increasing interest.

These compounds possess a hydrophobic cavity, which is accessible from a wide number of non-polar molecules of appropriated size, leading to the formation of host-guest inclusion complexes. According to recent literature, the study of calixarenes as encapsulatory vehicles for drugs, has been focused on functionalized calixarenes, in particular anionic derivatives. Among these many derivatives, p-sulfonatocalix[*n*]arene molecules have shown considerable potential in drug delivery and greater solubility and versatility.

The host possesses sulfonate groups that together with the interior surface provide a bipolar structure able to capture both hydrophobic and hydrophilic molecules, respectively.

- Calixarenes as vehicle systems for platinum complexes in chemotherapy

In particular, the para-sulfonatocalix [4] arenes (SC_4) are the most studied macrocycles for platin-based drugs.
It is important to underline, however, that the selectivity of the host is influenced by the size of the drug to be transported and in some cases only the ability of the host to form weak interactions with the drug is exploited.

Aim of the work

The suitability of p-sulfonatocalix[4]arene (SC_4) as drug delivery system has been analyzed, by means of DFT calculations. An inclusion complexation properties, that is complex stability constants and inclusion mode in aqueous media, of a host-guest complex formed between nedaplatin, a second generation platinum derivative, and p-sulfonatocalix[4]arene have been investigated.
The useful information about the supramolecular complex, obtained from theoretical investigation, have been compared with experimental data from ^{1}HNMR,UV, Job's plot analysis, and HPLC. (**Paper 8**)

5.1 Investigation of the host-guest complexation between 4-sulfocalix[4]arene and nedaplatin for potential use in drug delivery

In this study the encapsulation of nedplatin, *cis*-diammine-glycolate-O,O′-platinum II (Figure 1), a cisplatin derivative, with p-sulfonatocalix[4]arene has been examinated.

Nedaplatin is a second generation of platinum based anticancer drug appoved in Japan. This platinum complex was used to treat head and neck, lung, and cervical cancers and showed a siginificantly better antitumor activity and less toxicity than cisplatin.[1–3]

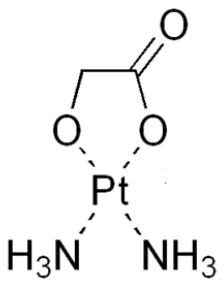

Figure 1. Chemical structure of Nedaplatin

The nedaplatin action mechanism involves two sequential hydrolysis reactions in wich the glycolate bidentate ligand is eliminated to generate the activated drug species that binds the DNA to form intrastrand and interstrand DNA adducts.

Despite the nedaplatin has improved capability compared to cisplatin, it reacts very fast with thiols of the plasma proteins present in the bloodstream leading to the formation of nonactive complexes and the development of side effects. [4]

Calixarenes as vehicle systems for platinum complexes in chemotherapy

A novel strategy to overcome such difficulties is to use of drug carrier agents, water soluble macrocycles with host properties able to protect the platinum drug inside the cavity via weak non-covalent interactions that facilitate release, once the target is reached.

For platinum based complexes, the para-Sulfonatocalix[4]arene has been described as an efficient accomodation.

This anionic receptor possesses a hydrophobic cavity and hydrophilic upper and lower rims and adopts the cone conformation which is stabilized, at the lower rim, by four hydrogen bonds.

So, the interaction energies and bonding properties have been calculated for the host-guest complex formed by nedaplatin and p-Sulfonatocalix[4]arene.

The initial optimized structure for the free SC_4 host and the diameters value of the upper and lower rims are reported in figure 2.

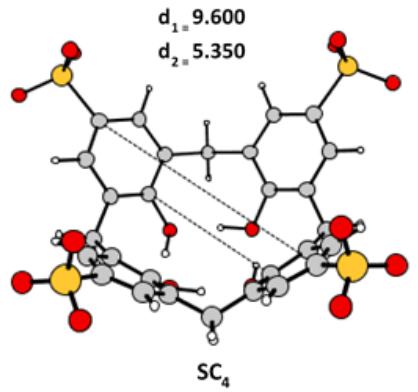

Figure 2. Optimized geometrical structures of SC4

To simulate the insertion of the antineoplatic complex into the host's cavity, several conformations have been proposed. The optimization of supramolecules allowed to consider only two of them plausible.

Calixarenes as vehicle systems for platinum complexes in chemotherapy

The nedaplatin and the SC4 calixarene weakly interact and nedaplatin lies in two different positions: either on top the upper rim, where the drug interacts by the hydrophilic ammine ligands of the platinum complex with the SO_3H groups at the upper rim, (U(a) conformation), or at the bottom of the lower rim, where the drugs's NH_3 groups interact with the O atoms of the OH groups at the lower rim, (L(a) conformation).

A geometry analysis allows to affirm that the supramolecular system is essentially stabilized by hydrogen bridge bonds.

The free energies of complexation have been calculated for both the supramolecular complexes and are -4.9 kcal mol-1 for the U(a) and 0.4 kcal mol^{-1} for the L(a).

The interaction free energy experimentally estimated are -6.2 and -5.9 kcal $mol^{-1.}$ These results agree with the calculated values of the energy of formation of the U(a) complex. This study suggests that the formation of hydrogen-bonds stabilizes the complex, but the complex is not included within the host-cavity.

References Chapter 5

(1) Ota, K. Nedaplatin. *Gan To Kagaku Ryoho* **1996**, *23* (3), 379–387.
(2) Kameyama, Y.; Okazaki, N.; Nakagawa, M.; Koshida, H.; Nakamura, M.; Gemba, M. Nephrotoxicity of a New Platinum Compound, 254-S, Evaluated with Rat Kidney Cortical Slices. *Toxicology Letters* **1990**, *52* (1), 15–24. https://doi.org/10.1016/0378-4274(90)90161-E.
(3) He, Y.-F.; Ji, C.-S.; Hu, B.; Fan, P.-S.; Hu, C.-L.; Jiang, F.-S.; Chen, J.; Zhu, L.; Yao, Y.-W.; Wang, W. A Phase II Study of Paclitaxel and Nedaplatin as Front-Line Chemotherapy in Chinese Patients with Metastatic Esophageal Squamous Cell Carcinoma. *World J Gastroenterol* **2013**, *19* (35), 5910–5916. https://doi.org/10.3748/wjg.v19.i35.5910.
(4) Montagnani, F.; Turrisi, G.; Marinozzi, C.; Aliberti, C.; Fiorentini, G. Effectiveness and Safety of Oxaliplatin Compared to Cisplatin for Advanced, Unresectable Gastric Cancer: A Systematic Review and Meta-Analysis. *Gastric Cancer* **2011**, *14* (1), 50–55. https://doi.org/10.1007/s10120-011-0007-7.

Spectrochimica Acta Part A: Molecular and Biomolecular Spectroscopy 193 (2018) 528–536

Contents lists available at ScienceDirect

Spectrochimica Acta Part A: Molecular and Biomolecular Spectroscopy

journal homepage: www.elsevier.com/locate/saa

Investigation of the host-guest complexation between 4-sulfocalix[4]arene and nedaplatin for potential use in drug delivery

Sherif Ashraf Fahmy [a], Fortuna Ponte [b], Mohamed K. Abd El-Rahman [c], Nino Russo [b,d], Emilia Sicilia [b,*], Tamer Shoeib [a,*]

[a] Department of Chemistry, The American University in Cairo, New Cairo 11835, Egypt
[b] Department of Chemistry and Chemical Technologies, University of Calabria, Arcavacata di Rende, 87036, Italy
[c] Analytical Chemistry Department, Faculty of Pharmacy, Cairo University, Kasr-El Aini Street, Cairo, Egypt 11562
[d] Division de Ciencias Basicas e Ingenieria, Departamento de Quimica, Universidad, Autonoma Metropolitana-Iztapalapa, Av. San Rafael Atlixco No. 186, Col. Vicentina, CP 09340 Mexico, Distrito Federal, Mexico

ARTICLE INFO

Article history:
Received 22 October 2017
Received in revised form 10 December 2017
Accepted 26 December 2017
Available online 27 December 2017

Keywords:
Nedaplatin
Drug delivery
Sulfocalix[4]arene
Complexation
Stability constant

ABSTRACT

Macromolecules including macrocyclic species have been reported to have the potential to encapsulate biologically active compounds such as drugs through host-guest complexation to increase their solubility, stability and bioavailability. In this paper the first experimental and theoretical investigation of the complexation between nedaplatin, a second generation antineoplastic drug, and *p*-4-sulfocalix[4]arene, a macromolecule possessing a bipolar amphiphilic structure with good biocompatibility and relatively low haemolytic toxicity for potential use as a drug delivery system is presented. Data from ^{1}H NMR, UV, Job's plot analysis, HPLC and DFT calculations are detailed and suggest the formation of a 1:1 complex. The stability constant of the complex was experimentally estimated to be 3.6×10^4 M^{-1} and 2.1×10^4 M^{-1} which correspond to values of -6.2 and -5.9 kcal mol^{-1}, respectively for the free energy of complexation while the interaction free energy is calculated to be -4.9 kcal mol^{-1}. The formed species is shown to be stabilised in solution through hydrogen bonding between the host and the guest which may allow for this strategy to be effective for potential use in drug delivery.

1. Introduction

Since the discovery of cisplatin, thousands of platinum based compounds have been synthesized for the hope of obtaining anticancer agents with higher activities and fewer limitations. Among these compounds only carboplatin and oxaliplatin were approved for worldwide use while loboplatin, heptaplatin and nedaplatin were approved in China, South Korea and Japan respectively. Nedaplatin is an analogue of cisplatin, the most commonly used platinum-based anti-cancer drug. Nedaplatin retains the two amine carrier ligands of cisplatin while the two chloride leaving groups are replaced with a glycolate five membered ring structure that binds to the central platinum metal in a bidentate fashion (see Fig. 1). A mechanism of action of nedaplatin has been proposed to entail two sequential hydrolysis steps to eventually eliminate the glycolate moiety resulting in the activated drug species [1]. This proposed mechanism is similar to that of cisplatin, however, it has been observed that the former possesses greater solubility and quicker excretion rates [2]. Nedaplatin has been developed to decrease cisplatin's undesirable side effects such as nephrotoxicity and gastrointestinal toxicity as well as to overcome problems of cisplatin resistance [3,4]. This second generation drug has shown pronounced anticancer activity relative to cisplatin in several clinical studies where it was used to treat head, neck, lung, testicular and cervical cancers [5–10]. Nedaplatin has been available for use in Japan since 1995, however, the ability of cancer cells to become resistant to this chemotherapeutic agent and the potential risk to cause nephrotoxicity at its therapeutic dose without hydration present significant obstacles for its worldwide acceptance.

While novel drug discovery remains a viable route for overcoming such difficulties, the fact remains that the overwhelming majority of platinum compounds synthesized are abandoned for reasons including low solubility, low efficacy, and high toxicity. Thus two other strategies are adopted for the advancement of Pt drug-based chemotherapy. The first of these is the use of combination therapy, where two or more pharmacologically active agents with different mechanisms are co-administered. Substantial effort has therefore been spent recently in identifying new chemotherapy treatments which incorporate nedaplatin in conjunction with other agents to enhance the knowledge of nedaplatin resistance and support the development of nedaplatin-based approaches to cancer therapy. In fact, the resistance to nedaplatin

* Corresponding authors.
E-mail addresses: Emilia.sicilia@unical.it (E. Sicilia), T.Shoeib@aucegypt.edu (T. Shoeib).

https://doi.org/10.1016/j.saa.2017.12.070
1386-1425/

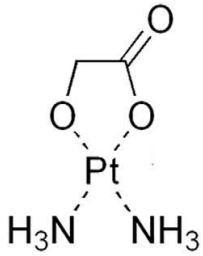

Fig. 1. Chemical Structure of Nedaplatin.

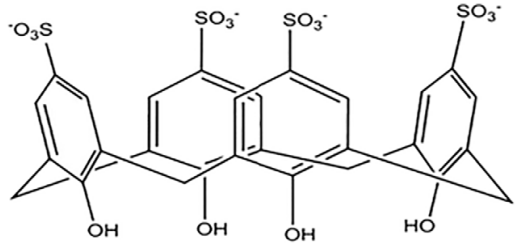

Fig. 2. Chemical Structure of *para*-Sulfonato-calix[4]arine.

was shown to be significantly reduced in combination therapies with 5-fluorouracil, docetaxel, vindesine, paclitaxel, gemcitabine, capecitabine and irinotecan followed by gefitinib [11–23].

Despite nedaplatin's ability for the reduction of some side effects when compared to cisplatin, it still displays significant reactivity much like all Pt drug-based chemotherapeutics toward thiols that are present in the plasma proteins in the bloodstream [24]. This reactivity in turn causes side effects and for the drug to undergo degradation into non-active complexes [24].

Thus considerable energy has been recently exerted on the second strategy for the advancement of chemotherapeutics, including Pt-based drugs, which involves their reformulation. This provides delivery systems with the possibility of protecting these drugs from non-intended side reactions which cause their deactivation while simultaneously increasing their targeting and their uptake into the intended cells. Such drug delivery systems are thought to may be able to revive interest in abandoned compound and possibly lead compounds with limited acceptance such as nedaplatin to wider approval [25]. There are several types of delivery systems reported for full or partial encapsulation of Pt based anti-cancer drugs including liposomes, polymer-based micelles, dendrimers, niosomes, and nanotubes [26–32]. More recently, macromolecules are playing an increasingly important role in drug delivery, for example, a recent clinical trial on patients exhibiting metastatic cervical cancer in which nedaplatin was combined with Albumin-bound paclitaxel where human serum albumin was employed as a novel drug carrier and delivery vehicle has shown great promise [2].

Other macromolecules including macrocyclic species have also been reported to have the potential to encapsulate biologically active compounds such as drugs to increase their solubility, stability and bioavailability [33,34]. Calix[*n*]arenes are a class of synthetic supramolecular macrocycles that are cone shaped, produced through the hydroxyalkylation of phenols and aldehydes to yield phenol units linked by methylene bridges producing hydrophilic upper and lower rims of the truncated cone structures with hydrophobic π-electron rich mid-region cavity. Functionalization of these macrocycles allows them to possess different properties at their phenolic faces and their para-aromatic positions, thus the range of calix[*n*]arene derivatives is very large. Functionalized calix[*n*]arenes ($n = 4, 6$ and 8) have been reported to have anti-cancer, anti-obesity, anti-bacterial and anti-diabetic activities with wide ranging mechanisms of action [35–49]. Among these many derivatives, the *para*-Sulfonato-calix[4]arine, SC_4, (see Fig. 2) possesses a bipolar amphiphilic structure allowing for significant water solubility. More importantly SC_4 exhibits good biocompatibility and has been reported to be relatively innocuous demonstrating no haemolytic toxicity *in-vitro* at concentrations up to 5 mM and is non-toxic *in-vivo* at doses up to 100 mg/kg [50,51]. SC_4 has also been reported to prevent the interactions of platelet-derived growth factor and its receptor leading to the inhibition of angiogenesis [41,42].

In this paper we investigate host-guest complexation between SC_4 and nedaplatin in aqueous media for potential use as a drug delivery system for nedaplatin. To the best of our knowledge there have been no previous reports on this system subject to our investigation. The formed complex has been characterized by means of UV–Vis, and ^{1}H NMR spectroscopy. The stoichiometry and binding constant were determined by means of the continuous variation method (Job's plot) and by HPLC. The derivative ratio method was adopted to resolve the overlap of the absorbance of the SC_4 host spectrum and the spectrum of the complex formed to allow for the measurement of the UV spectrum of the complex in the presence of this overlap. Structural characterization of the host-guest complexes was carried out theoretically employing quantum mechanical calculations at Density Functional Theory (DFT) level whose outcomes are reported. The intermolecular hydrogen bonds of the nedaplatin-SC4 adducts were investigated by means of the Bader theory of Atoms In Molecules (AIM).

2. Experimental and Computational Details

2.1. Chemicals and Reagents

Nedaplatin was obtained from Shandong Boyuan Pharmaceutical Co. Ltd.; *Para*-Sulfonato-calix[4]arine, SC_4, Deuterium Oxide and HPLC-grade water were purchased from Sigma-Aldrich.

2.2. Instrumentation

UV spectrophotometric measurements were carried out on a CARY 500 UV–Vis-NIR Scan dual beam spectrophotometer (Varian, USA). ^{1}H NMR spectra were measured on a Bruker Ascend™-400/R^{-1} MHz spectrometer. HPLC measurements were conducted on a Thermo Fischer Scientific DIONEX ultimate 3000 series HPLC equipped with a RP BDS HYPERSIL C18, 250 × 4.6 mm, 5 μm column.

2.3. Computational Methods

All the calculations were performed using the Turbomole 5.0 software package [52]. Full geometry optimizations were carried out at Density-Functional Theory (DFT) level using the semiempirically dispersion corrected B97-D functional [53], which demonstrated to be able to successfully simulate non covalent interactions [54] and host-guest systems [55]. The Pt atom was described using the Stuttgart/Dresden pseudopotential [56] together with the corresponding basis set for the valence electrons. The standard Pople 6-311G** basis set was used for all other atoms except for oxygen, for which diffuse functions were added (6–311 + G**). Bulk solvent effects were taken into account by means of the Conductor-like Screening Model (COSMO) [57] in water dielectric environment ($\varepsilon = 78.39$) performing single point calculations on optimized gas-phase geometries. Vibrational frequencies were calculated from analytic second derivatives to confirm the nature of minima of optimized structures. Inclusion Gibbs free energies in solution ΔG_{sol} were calculated as the sum of two contributions: a gas-phase free energy ΔG_{gas} and a solvation free energy ΔG_{solv} calculated with the continuum approach. However, such approach does not reflect the real entropic change that occurs when the examined systems go from the gas to the condensed-phase, and the effects are more relevant when association and dissociation are involved. Following one of the adopted correction

schemes, the solvation entropy has been estimated neglecting the translational and rotational components of the gas-phase entropy term and accounting only of the vibrational component of the entropy change for the system optimized in the gas phase [58]. Counterpoise correction calculations, as formulated by Boys and Bernadi [59], were carried out to estimate the Basis Set Superposition Error (BSSE). The nature of the intermolecular hydrogen bonds responsible for the formation of the nedaplatin-SC4 adducts was studied by means of the Bader theory of Atoms In Molecules (AIM) [60]. The AIM analysis is based on the use of the electron density of molecules $\rho(r)$ as a tool for studying the nature of the bonding in molecular systems [61]. The topological properties of $\rho(r)$ and its derivatives were found to be very useful to characterize

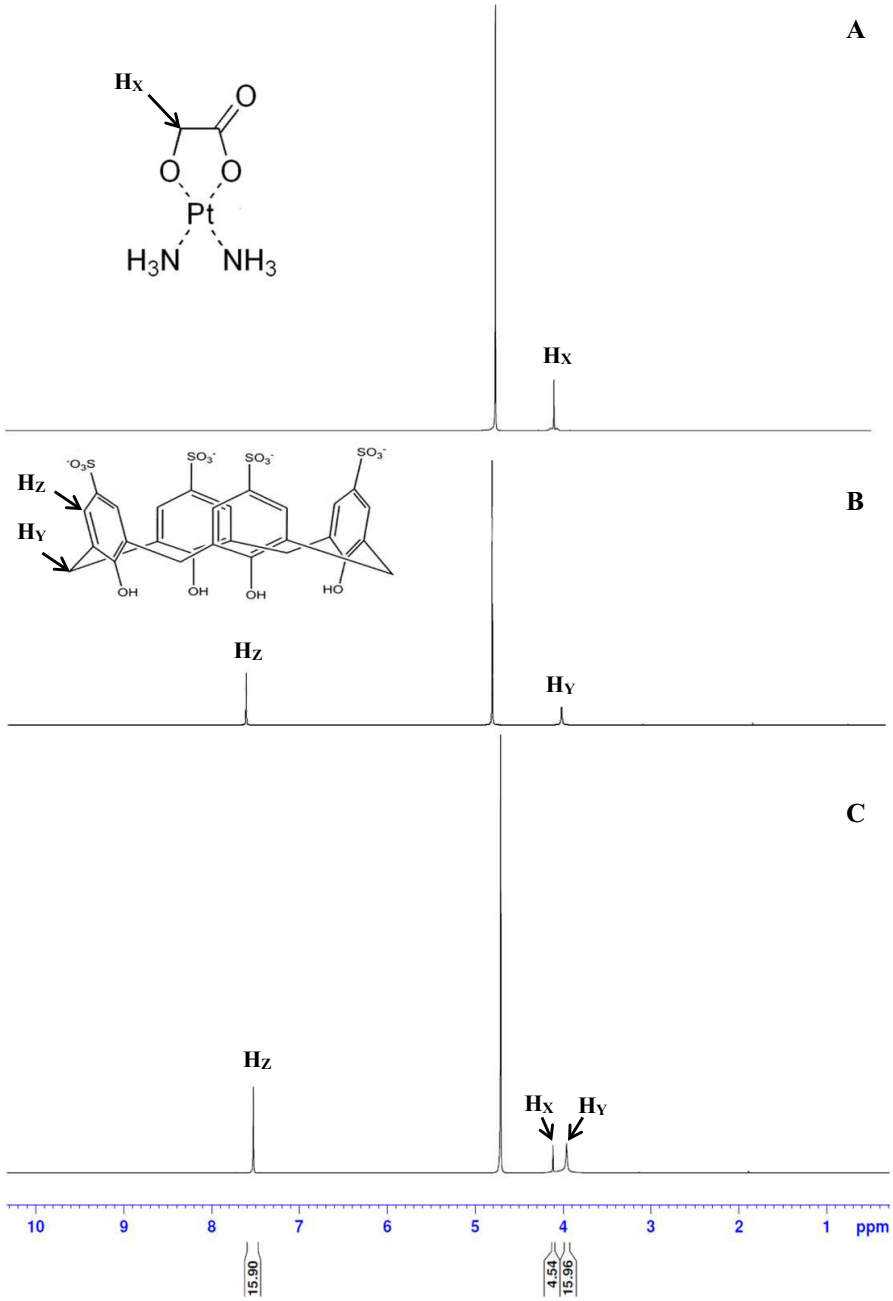

Fig. 3. ^{1}H NMR spectra of nadaplatin alone (panel A), SC_4 alone (panel B) and equal molar ratio of amount of nadaplatin and SC_4 (panel C). Structures of nadaplatin and SC_4 are shown with appropriate protons labeled.

bonding and the so called Critical Points (CPs). The values of ρ (r) and its derivatives at the CPs provide specific information on bonding. Indeed, the derivatives at the CPs are zero, *i.e.* $\nabla\rho(r) = 0$. The nine second order derivatives of ρ (r) are the elements of the real and symmetric Hessian matrix that is diagonalized to obtain the corresponding eigenvalues. CPs are, therefore, characterized by the rank ω, and the signature, σ, where the rank is equal to the number of non-zero eigenvalues, that is non-zero curvatures of ρ(r) at the BCPs and the signature is the algebraic sum of the signs of eigenvalues, that is the signs of curvatures of ρ(r), the Laplacian $\nabla^2\rho(r)$, at the CPs. CPs with $\omega = 3$ and $\sigma = +1$ have two positive curvatures and ρ is a minimum at CP in the plane defined by their corresponding axes, while ρ is a maximum at CP along the third axis, perpendicular to this plane. The presence of a $(3, -1)$ CP highlights that electronic charge density is accumulated within a bond exists between the involved atoms. Such point is referred to as a bond critical point (BCP).

3. Results and Discussion

3.1. ^{1}H NMR Spectroscopy

^{1}H NMR experiments performed in D_2O were employed to investigate the interaction between nedaplatin and SC_4. Fig. 3 shows the ^{1}H NMR spectra for each of nedaplatin (Panel A), SC_4 (Panel B) and 1:1 M ratio mixture of SC_4 and nedaplatin (Panel C) were signal integration was essential in order to distinguish between the peaks due to the CH_2 protons of the glycolate moiety of nedaplatin (labeled Hx) the peak due to the methylene bridges protons in SC_4, (labeled H_y). Examining the observed shielding of the assigned protons as listed in Table 1, it is evident that no significant complexation-induced shifts are observed. The magnitude change in chemical shift of the protons of a guest molecule has been reported to be directly proportional to the depth of these protons resonance within the cavity of a host molecule [62–64]. The very small change in chemical shift of the two assigned CH_2 protons of the glycolate moiety of nedaplatin observed here (0.08 ppm), which is within our instrumental error, suggests that these protons are not imbedded within the cavity of SC_4. It is however, apparent that the signal due to the protons of the methylene bridges in SC_4 in the case of the 1:1 M ratio mixture of SC_4 and nedaplatin shows significant broadening relative to the same signal in SC_4 alone (see Fig. 3 Panels B and C). This observation has previously been reported in other SC_4 complexes and attributed to be due to complexation-induced conformational rigidity of the macrocyclic structure [63,65,66]. This interesting ^{1}H NMR data which suggests that complexation between nedaplatin and SC_4 does exist but without involving the penetration of CH_2 protons of the glycolate moiety of nedaplatin within the cavity of the SC_4 led us to further examine this complex using UV–Vis spectroscopy.

3.2. UV–Vis Spectroscopy

Fig. 4 shows the UV absorbance spectra of 0.2 mM nedaplatin, 0.2 mM SC_4, and several mixtures containing successively increasing concentrations of nedaplatin (ranging from 0.01–0.21 mM) and a fixed concentration of 0.2 mM SC_4 all in deionized water. The spectrum of nedaplatin shows very weak absorbance in the range of 220–240 nm and no observed absorbance beyond 260 nm. The spectrum of SC_4 on the other hand shows strong UV absorbance with a characteristic pair of absorption maxima at 277 and 284 nm. The spectra of the mixtures also show a UV absorbance as seen for SC_4 with an observable hyperchromic shift as evident by the observed increase in absorbance with increasing concentrations of nedaplatin. Throughout this trend of increased absorbance, the characteristic pair of absorption maxima for SC_4 were retained and no significant bathochromic or hypsochromic shifts were observed. This indicates that most likely the observed species formed between nedaplatin and SC_4 is not an inclusion complex. This is in line with previous reports showing a merge of the two absorption maxima of free SC_4 and appearance of a new maximum due to the formation of a host–guest inclusion complex with SC_4 [63].

In order to examine the correlation of this observed hyperchromic shift with increasing concentration of nedaplatin, the zero order spectra of the prepared mixtures were divided by the spectrum of SC_4, and the first derivative of the ratio spectra as described elsewhere were obtained using a scaling factor of 10 and $\Delta\lambda = 4$ nm [67]. The values of the peak amplitudes of the first derivative of the ratio spectra for the mixtures (shown in Fig. S1 of the supplementary material) were then obtained at 265 nm. Fig. 5 shows a plot of the obtained peak amplitudes and the corresponding concentrations of nedaplatin. The nearly perfect linear correlation presented in this plot strongly suggests the hyperchromic shift observed in the absorbance spectra of the mixtures as seen in Fig. 4 to be due to complexation between nedaplatin and SC_4.

The method of continuous variation (commonly known as Job's plot) was adopted to study the stoichiometry and the stability constant of this supramolecular complex. In this method several solutions of varying molar ratios of SC_4 and nedaplatin within the limits of 0 and 1 were prepared while keeping the total concentration of both species constant at 0.1 mM. The UV absorbance of each of these solutions was subsequently measured. While direct determination of the absorbance of the complex between SC_4 and nedaplatin is not possible due to significant overlap with the absorption of SC_4 (see Fig. 4), the derivative ratio method where the resolution of overlapping absorbance in binary and ternary solution mixtures is possible without resorting to prior analytical separation was adopted [68,69]. Another advantage of the derivative ratio method is the fact that the entire spectrum of the interfering signal, in this case due to SC_4, is cancelled making the method much less sensitive to the choice of wavelength used for calibration relative to simple derivative methods [70]. Here, the derivative ratio was obtained by dividing the spectra of the prepared solutions by the spectrum of 0.2 mM SC_4 to obtain the first derivative of the ratio spectra using a scaling factor of 10 and $\Delta\lambda = 4$ nm. The amplitudes of the first derivative ratio spectra peaks at 265 nm which are proportional to the complex concentration were subsequently measured. A Job's plot where the amplitudes of the first derivative ratio spectra peaks are plotted against the mole fraction of the corresponding SC_4 molar fraction was constructed. The maximum amplitude of this plot was observed at a molar fraction of 0.5 indicating a complex stoichiometry of 1:1. A normalized version of this Job's plot where each of the amplitude values, S, were divided by the maximum amplitude, S_{max}, is shown in Fig. 6. The stability constant of the complex was estimated using methods described previously to be $3.6 \times 10^4\ M^{-1}$ [70,71]. This value lies within the range of the stability constants $(0.01 \times 10^3$–$1.7 \times 10^5)\ M^{-1}$ previously reported for complexes, many of which are intended for drug delivery, between three different classes of macromolecule hosts being cyclodextrins, calixarenes and cucurbiturils with various neutral guest molecules [72–88]. Complexes between SC_4 and neutral host molecules were reported to have stability constants of $0.48–6.8 \times 10^4\ M^{-1}$ [88–91]. It is interesting to note that the host-guest complex between SC_4 and benzocaine with a stability constant of just $8.3 \times 10^2\ M^{-1}$ showed improved bioavailability for the benzocaine drug [87].

3.3. HPLC

HPLC coupled with UV detection has been employed to study the interactions between nedaplatin and SC_4. The use of a diode array detector

Table 1
Observed shielding in ppm for assigned protons in nedaplatin and SC_4 individually and in a 1:1 M ratio mixture in D_2O.

Proton signal	Individual molecules	1:1 M ratio
H_X	4.0363	4.1122
H_Y	3.9696	3.9571
H_Z	7.5350	7.5222

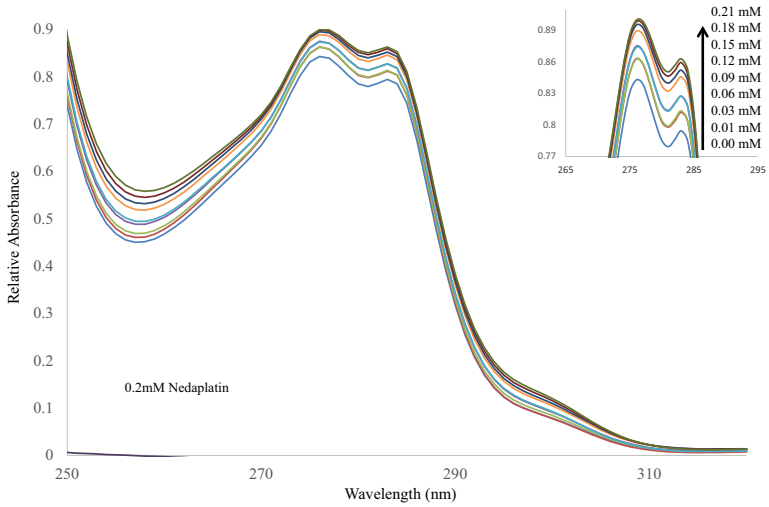

Fig. 4. Absorbance spectra of 0.2 mM nedaplatin, 0.2 mM SC_4, and several mixtures containing successively increasing concentrations of nedaplatin (ranging from 0.00–0.21 mM as marked in the insert) and a fixed concentration of 0.2 mM SC_4 all in distilled water.

allowed for simultaneous absorbance readings at 210 nm to detect nedaplatin and at 265 nm in order to detect both SC_4 and the SC_4–nedaplatin complex. The chromatographic conditions used here allowed for the clear separation of the three species while calibration curves for nedaplatin and SC_4 provided linear relationships. The observed nedaplatin signal was shown to diminish with increasing concentrations of SC_4 used while the nedaplatin concentration was kept fixed; this suggested that nedaplatin was being complexed with SC_4 in line with our previous discussion. This led us to examine several solutions of varying molar ratios of SC_4 and nedaplatin where the latter was fixed at 0.05 mM and the former was allowed to vary from 0.01 to 0.09 mM as shown in Fig. 7. In this figure, it is observed that the free concentration of nedaplatin which was initially fixed at 0.05 mM in solutions where SC_4 was present within the concentration range of 0.09–0.06 mM to be negligible. This suggests that at these molar ratios nearly all the nedaplatin in these solutions was complexed with SC_4. Fig. 7 also shows a signal for nedaplatin to be observed initially only when equal molar ratios of 0.05 mM for each of nedaplatin and SC_4 were present in the solution analyzed, suggesting a weak 1:1 nedaplatin to SC_4 complexation as discussed earlier. The stability constant of the complex was estimated from the data obtained to be $2.1 \times 10^4\ M^{-1}$ which is in line with the stability constant obtained from Job's plot, suggesting a weakly bound complex.

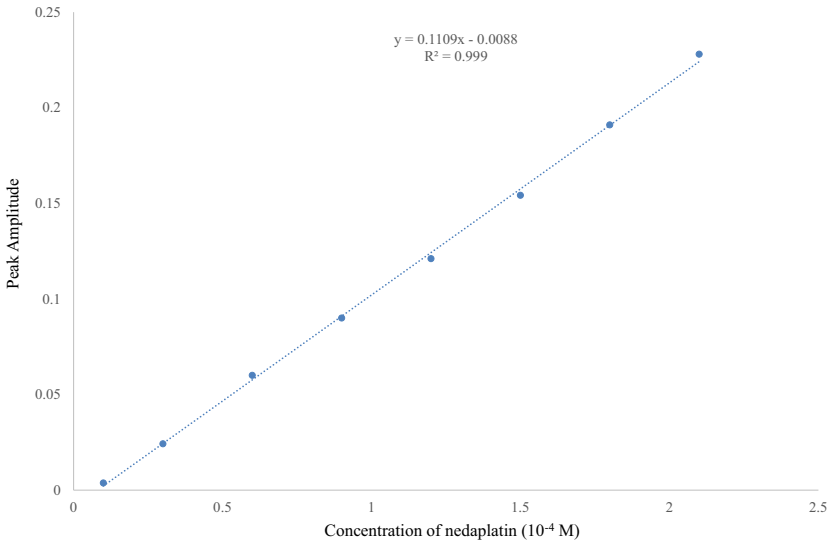

Fig. 5. Plot of peak amplitudes at 265 nm obtained from the mixtures containing successively increasing concentrations of nedaplatin (ranging from 0.01–0.21 mM) and a fixed concentration of 0.2 mM SC4 all in distilled water using the spectrum of 0.2 mM of SC_4 as a divisor against the corresponding concentration of nedaplatin in the complex mixtures.

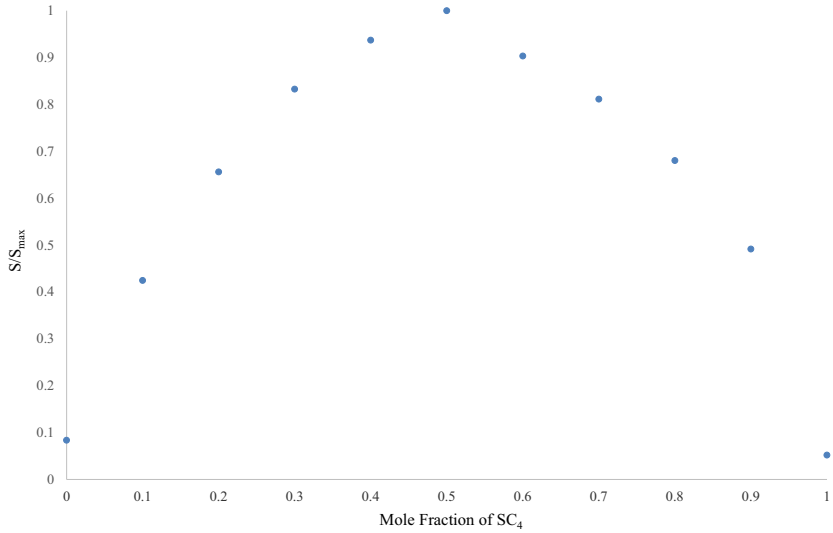

Fig. 6. Normalized Job's plot where each of the amplitude values, S, of the first derivative ratio spectra peaks were divided by the maximum amplitude, S_{max} are plotted against the mole fraction of the corresponding SC4 molar fraction.

3.4. Computational Results

The optimized structure of SC_4 shows values of the diameters at upper ($d_1 = 9.600$ Å) and lower rims ($d_2 = 5.350$ Å) as shown in Fig. 8 while Van der Waals surface graph detailing the maximum distances for height, length and width describing the size for nedaplatin obtained by the intersections of the atomic van der Waals spheres is reported in Fig. 9 for comparison. From such comparison, it appears that based on size it may be possible for nedaplatin to be inserted within the cavity of SC_4. In order to computationally simulate the insertion of nedaplatin drug into the cavity of SC_4, four possible initial arrangements were examined, as it is exemplified in Scheme 1. Indeed, the inclusion can occur from both the side of the wider upper rim (U) and the side of the lower rim (L). In addition, nedaplatin can insert assuming two different orientations with respect to SC_4. That is, the arrangement is labeled as (a) when the ammonia ligands point inwards to the cavity

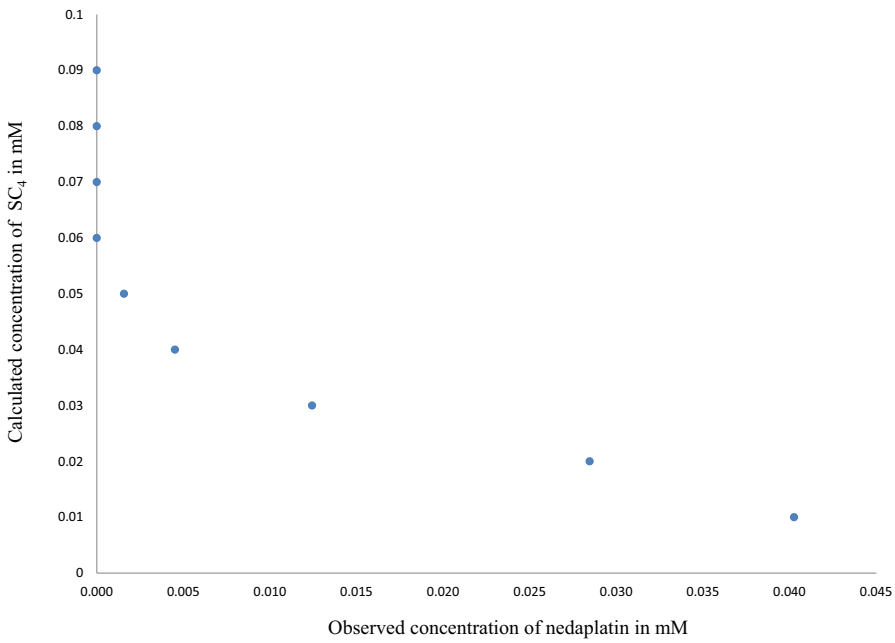

Fig. 7. HPLC observed concentrations of nedaplatin of solutions containing a fixed 0.05 mM of nedaplatin and a varying concentrations of SC4 in the range of 0.01–0.09 mM.

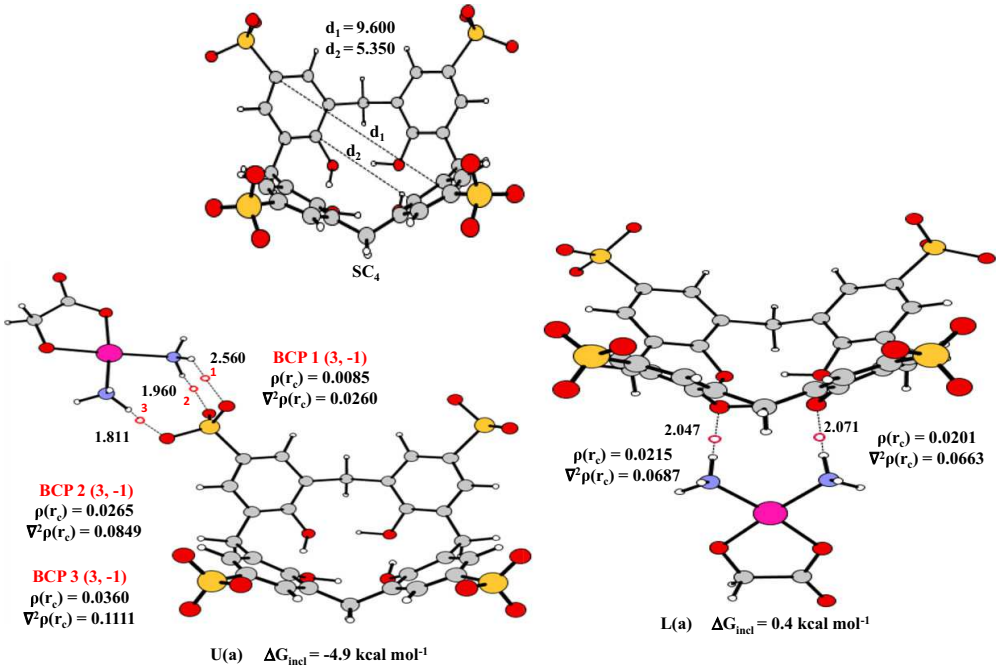

Fig. 8. B97-D optimized geometrical structures of SC_4 and U(a) and L(a) complexes. Upper (d_1) and lower (d_2) rim diameters of the calixarene are reported together with the most relevant distances (Å), calculated interaction energies (kcal mol^{-1}) and electron density (r) and Laplacian of electron density ($\nabla^2\rho$) at the BCPs present between NH and O atoms for the adducts.

and the glycolate ring points outwards and (b) when the glycolate ring points inwards to the cavity and the ammonia ligands point outwards. Fully optimized structures obtained without imposing any constrain for these complexes are shown in Fig. 8, whereas cartesian coordinates can be found in Table S1 of the supplementary material. The most relevant geometrical parameters are reported in the same figure together with the values of the free insertion energies calculated, as detailed above, including BSSE and entropy change corrections. As it is evident from Fig. 8, only the (a) arrangements were obtained for the inclusion from both sides (U and L) of the SC_4 calixarene host. In spite of the numerous attempts carried out starting from different initial reciprocal positions of the host and the guest, the orientation of nedaplatin with respect to the calixarene changed and the optimized geometries collapsed into the two structures shown in Fig. 8. The SC_4 calixarene and the drug weakly interact and nedaplatin lies either on top the upper rim, U(a) conformation, or at the bottom of the lower rim, L(a) conformation. The calculated interaction free energies are −4.9 and 0.4 kcal mol^{-1} for the U(a) and the L(a), respectively indicating that only a weak association complex is formed in the former case. This result agrees with the experimental estimated stability constants reported above to be 3.6×10^4 M^{-1} and 2.1×10^4 M^{-1} which correspond to values of −6.2 and −5.9 kcal mol^{-1}, respectively for the free energy of complexation. The hydrogen bond interactions in complex U(a), evidenced in Fig. 8, established between the hydrogen atoms of the nedaplatin ammonia ligands with the O atoms of the calixarene sulfonato moiety are responsible for the measured stabilization. On the contrary, the hydrogen bonds formed by the hydrogen atoms of the two NH_3 groups with the O atoms of the OH groups at the lower rim perturb the existing charge distribution and the energy of the new interactions compensates the weakening of the already existing hydrogen bonds. Furthermore, AIM analysis was used to better characterize such hydrogen bonding interactions. This analysis was performed as it was demonstrated that the electronic density value -ρBCP at the bond critical point (BCP), and its Laplacian - $\nabla^2\rho_{BCP}$ can be very useful parameters for the characterization of hydrogen bonding. Bader and Essén have reported that covalent interactions correspond to a high value of $\rho(r)$, that is a concentration of electronic charge at the BCP of order $>10^{-1}$ a.u., and negative value of $\nabla^2\rho(r)$ [92]. For weak van der Waals and hydrogen bonding interactions, $\rho(r)$ is quite small, that is $\sim 10^{-2}$ a.u. or less for H-bonded and 10^{-3} a.u. for van der Waals species, and $\nabla^2\rho(r)$ is positive. The values calculated for the density and the Laplacian at the BCPs highlighting the possible formation of hydrogen bonds are reported in Fig. 8. Except for the critical point indicated as BCP1, the electron density values fall in the expected range (0.0102–0.0642 a.u) for H-bonds [93] and the sign of Laplacian of electron density is positive. Due to the correlation existing between the strength of the hydrogen-bond interaction and the value of the electron density, the critical points indicated as BCP2 and BCP3 in U(a) correspond to stronger interactions than those existing in U(b).

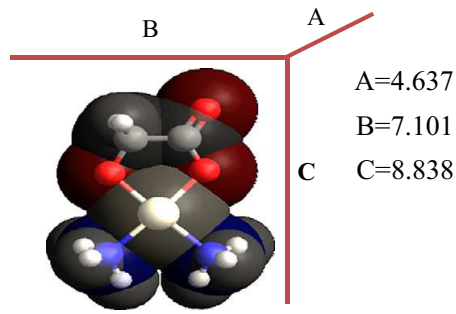

Fig. 9. Calculated van der Waals surface for nedaplatin and height, length and width (in Å) defining its size.

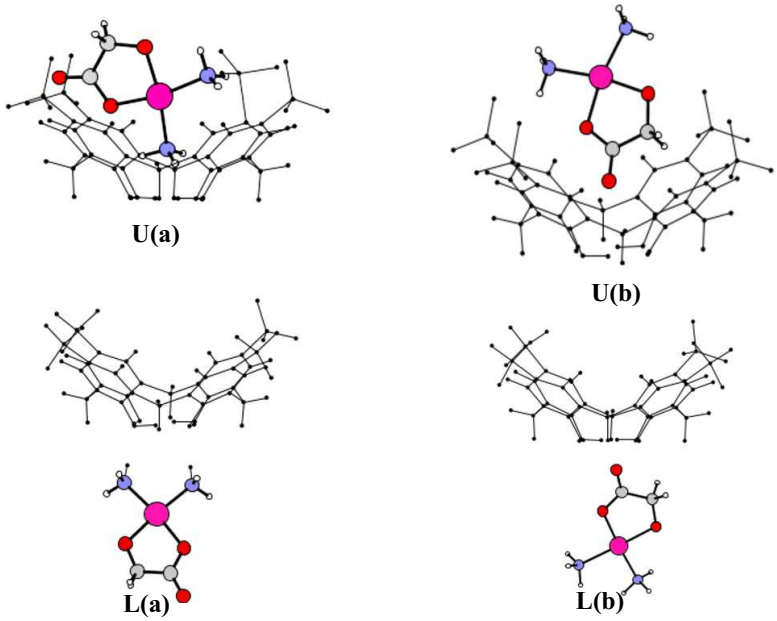

Scheme 1. Four possible inclusion modes of nedaplatin through the upper (U) and lower (L) rims of SC_4, U(a) the ammonia ligands pointing on the inside of the upper cavity and the glycolate ring pointing outwards, U(b) the glycolate ring pointing on the inside of the upper cavity and the ammonia ligands pointing outwards, L(a) the ammonia ligands pointing on the inside of the lower cavity and the glycolate ring pointing outwards, L(b) the glycolate ring pointing on the inside of the lower cavity and the ammonia ligands pointing outwards.

The calculated values of the energy of formation of the adducts U(a) a U(b), indeed, correspond to such description.

4. Conclusions

Data from ^{1}H NMR, UV, Job's plot analysis, HPLC and DFT calculations suggests that complexation between nedaplatin and SC_4 in a 1:1 M ratio under the conditions investigated here does exist. The stability constant of the complex was estimated to be 3.6×10^4 M^{-1} and 2.1×10^4 M^{-1} which correspond to values of -6.2 and -5.9 kcal mol^{-1} respectively for the free energy of complexation. These results agree with calculations which provide an interaction free energy of -4.9 kcal mol^{-1} for the association of nedaplatin with its ammonia ligands pointing inwards toward the wider upper rim of the cavity of SC_4. The formed complex is shown to not involve the penetration of nedaplatin within the cavity of the SC_4, however, it is mainly stabilised due hydrogen bonding between the hydrogen atoms of the nedaplatin ammonia ligands with the O atoms of the calixarene sulfonato moiety. The stability of the complex in solution may allow for its potential use as a drug delivery system.

Supplementary data to this article can be found online at https://doi.org/10.1016/j.saa.2017.12.070.

Acknowledgements

The authors would like to thank the American University in Cairo for the funding sponsorship and provision of resources for the project. The Dipartimento di Chimica e Tecnologie Chimiche of Università della Calabria is also gratefully acknowledged.

References

[1] Marta E. Alberto, Maria Fatima A. Lucas, Matej Pavelka, Nino Russo, J. Phys. Chem. B 113 (43) (2009).
[2] Yifan Li, Jing Zeng, Manni Huang, Jusheng An, Ping Bai, Lingying Wu, Rong Zhang, Cancer 123 (2017) 3420–3425.
[3] Y. Kawai, S. Taniuchi, S. Okahara, Biol. Pharm. Bull. 28 (2005) 1385–1388.
[4] D. Alberts, P. Fanta, K. Running, L. Adair Jr., D. Garcia, R. Liu-Stevens, Cancer Chemother. Pharmacol. 39 (1997) 493–497.
[5] M. Koshiyama, M. Kinezaki, T. Uchida, M. Sumitomo, Anticancer Res. 25 (2005) 4499–4502.
[6] Y. Inuyama, H. Miyake, M. Horiuchi, K. Hayasaki, S. Komiyama, K. Ota, Gan To Kagaku Ryoho 19 (1992) 863–869.
[7] Y.F. He, C.S. Ji, B. Hu, P.S. Fan, Hu CL, F.S. Jiang, J. Chen, L. Zhu, Y.W. Yao, W. Wang, World J. Gastroenterol. 19 (2013) 5910–5916.
[8] K. Ota, Gan To Kagaku Ryoho 23 (1996) 379.
[9] Y. Inuyama, S. Fukuda, N. Satoh, Gan To Kagaku Ryoho 24 (1997) 1902.
[10] Y. Kameyama, N. Okazaki, M. Nakagawa, H. Koshida, M. Nakamura, M. Gemba, Toxicol. Lett. 52 (1990) 15.
[11] H. Yamashita, K. Nakagawa, M. Tago, H. Igaki, N. Nakamura, K. Shiraishi, N. Sasano, K. Ohtomo, Dis. Esophagus 19 (2006) 15–19.
[12] T. Yoshioka, M. Sakayori, S. Kato, N. Chiba, S. Miyazaki, K. Nemoto, H. Shibata, H. Shimodaira, K. Ohtsuka, Y. Kakudo, et al., Int. J. Clin. Oncol. 11 (2006) 454–460.
[13] N. Takigawa, Y. Segawa, H. Ueoka, K. Kiura, M. Tabata, T. Shibayama, I. Takata, H. Miyamoto, K. Eguchi, M. Harada, Cancer Chemother. Pharmacol. 46 (2000) 272–278.
[14] F. Yoshiike, T. Koizumi, Y. Kitaguchi, O. Hatayama, M. Yasuo, M. Sasabayashi, H. Wakamatsu, K. Kubo, J. Chemother. 17 (2005) 550–554.
[15] I. Sekine, M. Sumi, Y. Ito, T. Kato, Y. Fujisaka, H. Nokihara, N. Yamamoto, H. Kunitoh, Y. Ohe, T. Tamura, Jpn. J. Clin. Oncol. 37 (2007) 175–180.
[16] T. Niioka, T. Uno, N. Yasui-Furukori, T. Takahata, M. Shimizu, K. Sugawara, T. Tateishi, Cancer Chemother. Pharmacol. 59 (2007) 575–580.
[17] T. Shirai, T. Hirose, M. Noda, K. Ando, H. Ishida, T. Hosaka, T. Ozawa, K. Okuda, T. Ohnishi, T. Ohmori, N. Horichi, M. Adachi, *Lung Cancer* 52 (2006) 181–187.
[18] F. Oshita, K. Yamada, H. Saito, K. Noda, N. Hamanaka, M. Ikehara, J. Exp. Ther. Oncol. 4 (2004) 343–348.
[19] S. Kawase, T. Okuda, M. Ikeda, S. Ishihara, Y. Itoh, S. Yanagawa, T. Ishigaki, Gynecol. Oncol. 102 (2007) 493–499.
[20] M. Kanai, S. Matsumoto, T. Nishimura, Y. Shimada, G. Watanabe, T. Kitano, A. Misawa, H. Ishiguro, K. Yoshikawa, K. Yanagihara, S. Teramukai, M. Mitsumori, T. Chiba, Y. Sakai, M. Fukushima, Int. J. Clin. Oncol. 12 (2007) 224–227.
[21] T. Kodaira, N. Fuwa, M. Kamata, K. Furutani, H. Tachibana, T. Yamazaki, Anticancer Res. 26 (2006) 471–478.
[22] Y. Sato, T. Takayama, T. Sagawa, T. Okamoto, K. Miyanishi, T. Sato, H. Araki, S. Iyama, S. Abe, K. Murase, R. Takimoto, H. Nagakura, M. Hareyama, J. Kato, Y. Niitsu, Cancer Chemother. Pharmacol. 58 (2006) 570–576.
[23] P. Peng, X. Ou, Z. Chen, H. Liao, Y. Peng, S. Wang, Cancer Chemother. Pharmacol. 72 (2013) 323–328.

[24] F. Montagnani, G. Turrisi, C. Marinozzi, C. Aliberti, G. Fiorentini, Gastric Cancer 14 (2011) 50–55.
[25] T. Boulikas, A. Pantos, E. Bellis, P. Christofis, J. Cancer Ther. 5 (2007) 537–583.
[26] T. Dragovich, D. Mendelson, S. Kurtin, K. Richardson, D. Von Hoff, A. Hoos, Cancer Chemother. Pharmacol. 58 (2006) 759–764.
[27] C. Lu, R. Perez-Soler, B. Piperdi, G.L. Walsh, S.G. Swisher, W.R. Smythe, H.J. Shin, J.Y. Ro, L. Feng, M. Truong, A. Yalamanchili, G. Lopez-Berestein, W.K. Hong, A.R. Khokhar, D.M. Shin, J. Clin. Oncol. 23 (2005) 3495–3501.
[28] B.W. Harper, A.M. Krause-Heuer, M.P. Grant, M. Manohar, K.B. Garbutcheon-Singh, J.R. Aldrich-Wright, Chem. Eur. J. 16 (24) (2010) 7064–7077.
[29] Ma. Galanski, B.K. Keppler, F. Kratz, P. Senter, H. Steinhagen (Eds.),Wiley-VCH Verlag 2012, pp. 1605–1629.
[30] T. Boulikas, A. Pantos, E. Bellis, P. Christofis, Structures and Mechanisms, 5, 2007 537–583.
[31] A. Koshkaryev, R. Sawant, M. Deshpande, V. Torchilin, Adv. Drug Deliv. Rev. 65 (1) (2013) 24–35 (2013).
[32] F. Alexis, E.M. Pridgen, R. Langer, O.C. Farokhzad, M. Schafer-Korting (Eds.),Heidelberg: Springer-Verlag, Vol. 197, 2010, pp. 55–86.
[33] H.M. Dibama, I. Clarot, S. Fontanay, A. Ben Salem, M. Mourer, C. Finance, R.E. Duval, J.B. Regnouf-de-Vains, Bioorg. Med. Chem. Lett. 19 (2009) 2679–2682.
[34] Y. Nakahara, Y. Okazaki, K. Kimura, Soft Matter 8 (2012) 3192–3199.
[35] V.V. Trush, S.O. Cherenok, V.Y. Tanchuk, V.P. Kukhar, V.I. Kalchenko, A.I. Vovk, Bioorg. Med. Chem. Lett. 23 (20) (2013) 5619–5623.
[36] F. Nasuhi Pur, K.A. Dilmaghani, J. Coord. Chem. 67 (3) (2014) 440–448.
[37] K. Hulíková, V. Grobárová, R. Křivohlavá, A. Fišerová, Folia Microbiol. 55 (5) (2010) 528–532.
[38] S.O. Cherenok, O.A. Yushchenko, V.Y. Tanchuk, et al., ARKIVOC 4 (2012) 278–298.
[39] S. Cherenok, A. Vovk, I. Muravyova, et al., Org. Lett. 8 (4) (2006) 549–552.
[40] G.M. Consoli, G. Granata, E. Galante, I. Di Silvestro, L. Salafia, C. Geraci, Tetrahedron 63 (44) (2007) 10758–10763.
[41] H. Zhou, D.A. Wang, L. Baldini, et al., Org. Biomol. Chem. 4 (12) (2006) 2376–2386.
[42] R.P. Dings, X. Chen, D.M. Hellebrekers, et al., J. Natl. Cancer Inst. 98 (13) (2006) 932–936.
[43] R.P. Dings, J.I. Levine, S.G. Brown, et al., Investig. New Drugs 31 (5) (2013) 1142–1150.
[44] R. Kamada, W. Yoshino, T. Nomura, et al., Bioorg. Med. Chem. Lett. 20 (15) (2010) 4412–4415.
[45] K.J. Pelizzaro-Rocha, M.B. de Jesus, R.R. Ruela-de-Sousa, et al., BBA-Mol. Cell. Res. 1833 (12) (2013) 2856–2865.
[46] D. Schrama, R.A. Reisfeld, J.C. Becker, Nat. Rev. Drug Discov. 5 (2) (2006) 147–159.
[47] C. Geraci, G.M.L. Consoli, G. Granata, et al., Bioconjug. Chem. 24 (10) (2013) 1710–1720.
[48] S.D. Brown, J.A. Plumb, B.F. Johnston, N.J. Wheate, Inorg. Chim. Acta 393 (2012) 182–186.
[49] C.D. Gutsche, L.J. Bauer, J. Am. Chem. Soc. 107 (21) (1985) 6052–6059.
[50] D.S. Guo, Y. Liu, J. Chem. Res. 47 (2014) 1925–1934.
[51] A.W. Coleman, S. Jebors, S. Cecillon, P. Perret, D. Garin, D. Marti-Battle, M. Moulin, New J. Chem. 32 (2008) 780–782.
[52] R. Ahlrichs, Turbomole Version 5, Theoretical Chemistry Group, University of Karlsruhe, 2002.
[53] S. Grimme, J. Comput. Chem. 27 (2006) 1787.
[54] R. Peverati, K.K. Baldridge, J. Chem. Theory Comput. 4 (2008) 2030–2048.
[55] C. Mueck-Lichtenfeld, S. Grimme, L. Kobryn, A. Sygula, 2010, 12, 7091–7097.
[56] D. Andrae, U. Häusermann, M. Dolg, H. Stoll, H. Preuss, Theor. Chim. Acta 77 (1990) 123.
[57] A. Klamt, G. Schüürmann, J. Chem. Soc. Perkin Trans. 2 (1993) 799–805.
[58] M. Sumimoto, N. Iwane, T. Takahama, S. Sakaki, J. Am. Chem. Soc. 126 (2004) 10457–10471.
[59] S.F. Boys, F. Bernardi, Mol. Phys. 19 (1970) 553.
[60] R.F.W. Bader, Chem. Rev. 91 (1991) 893–928.
[61] AIMAll (Version 17.11.14), Todd A. Keith, TK Gristmill Software, Overland Park KS, USA, 2017 (aim.tkgristmill.com).
[62] N.J. Wheate, J. Inorg. Biochem. 102 (12) (2008) 2060–2066.
[63] M. Abd El-Rahman, A. Mahmoud, RSC Adv. 5 (2015) 62469–62476.
[64] N.J. Wheate, Grainne M. Abbott, Rothwelle J. Tate, Caorl J. Clements, RuAngelie Edrada-Ebel, B.F. Johnston, J. Inorg. Biochem. 103 (3) (2009) 448–454.
[65] D. Guo, V. Uzunova, X. Su, Y. Liu, W. Nau, Chem. Sci. 2 (2011) 1722.
[66] S. Shinkai, K. Araki, T. Matsuda, O. Manabe, Bull. Chem. Soc. Jpn. 62 (1989) 3856–3862;
S. Shinkai, K. Araki, O. Manabe, J. Am. Chem. Soc. 110 (1988) 7214–7215.
[67] J. Karpińska, Talanta 64 (4) (2004) 801–822.
[68] M.Y. Salem, A.M. El-Kosasy, M.G. El-Bardicy, A.M.K. El-Rahman, Drug Test. Anal. 2 (5) (2010) 225–233.
[69] J. Karpińska, Talanta 64 (4) (2004) 801–822.
[70] M. Nebsen, M.K. Abd El-Rahman, M.Y. Salem, A.M. El-Kosasy, et al, Drug Test. Anal. 3 (4) (2011) 221–227.
[71] J.M. Bosque-Sendra, E. Almansa-Lopez, A.M. Garci-Campana, L. Cuadros-Rodriguez, Anal. Sci. 19 (2003) 1431.
[72] X.Y. Zhang, G. Gramlich, X.J. Wang, W.M. Nau, J. Am. Chem. Soc. 124 (2002) 254–263.
[73] M. Shaikh, J. Mohanty, P.K. Singh, W.M. Nau, H. Pal, Photobiol. Sci. 7 (2008) 408–414.
[74] J. Mohanty, A.C. Bhasikuttan, W.M. Nau, H. Pal, J. Phys. Chem. B 110 (2006) 5132–5138.
[75] I. Enoch, M. Swaminathan, J. Fluoresc. 16 (2006) 697–704.
[76] M. Casolaro, C. Anselmi, G. Picciocchi, Thermochim. Acta 425 (2005) 143–147.
[77] H. Bakirci, A.L. Koner, T. Schwarzlose, W.M. Nau, Chem. Eur. J. 12 (2006) 4799–4807.
[78] R.B. Wang, L. Yuan, D.H. Macartney, Chem. Commun. (2005) 5867–5869.
[79] M. Shaikh, S.D. Choudhury, J. Mohanty, A.C. Bhasikuttan, W.M. Nau, H. Pal, Chem. Eur. J. 15 (2009) 12362–12370.
[80] C.P. Carvalho, V.D. Uzunova, J.P. Da Silva, W.M. Nau, U. Pischel, Chem. Commun. 47 (2011) 8793–8795.
[81] C. Marquez, W.M. Nau, Angew. Chem. Int. Ed. 40 (2001) 3155–3160.
[82] Z. Miskolczy, L. Biczok, J. Phys. Chem. B 115 (2011) 12577–12583.
[83] J. Wu, L. Isaacs, Chem. Eur. J. 15 (2009) 11675–11680.
[84] U. Pischel, V.D. Uzunova, P. Remon, W.M. Nau, Chem. Commun. 46 (2010) 2635–2637.
[85] A. Praetorius, D.M. Bailey, T. Schwarzlose, W.M. Nau, Org. Lett. 10 (2008) 4089–4092.
[86] A.L. Koner, W.M. Nau, Supramol. Chem. 19 (2007) 55–66.
[87] L. Arantes, E. Varejao, K. Pelizzaro-Rocha, C. Cereda, E. Paula, M. Lourenco, H. Duarte, S. Fernandes, Chem. Biol. Drug Des. 83 (2014) 550–559.
[88] N. Wheate, G. Abbott, R. Tate, C. Clements, R. Edrada-Ebel, B. Johnston, J. Inorg. Biochem. 103 (2009) 448–454.
[89] H. Bakirci, A.L. Koner, T. Schwarzlose, W.M. Nau, Chem. Eur. J. 12 (2006) 4799–4807, https://doi.org/10.1002/chem.200501479.
[90] G. Wang, H. Zhang, F. Ding, Y. Liu, J. Incl. Phenom. Macrocycl. Chem. 69 (2011) 85–89.
[91] W. Yang, M. de Villiers, M, AAPS J. 7 (1) (2005) (Article 23 (http://www.aapsj.org)).
[92] R.F.W. Bader, H. Essén, J. Chem. Phys. 80 (1984) 1943–1960.
[93] A. Shahi, E. Arunan, Phys. Chem. Chem. Phys. 16 (2014) 22935–22952.

6

BODIPY DYES AND THEIR APPLICATION IN CANCER THERAPY

Introduction

Photodynamic therapy (PDT) is a clinically approved anti-cancer treatment that exploits the interaction of light with a photosensitizing drug and tissue oxygen. Upon irradiation, the photosensitizer (PS) is activated to the single excited state. This state with a short halflife, undergoes intersystem crossing (ISC) to the longer lived triplet excited state. The interaction of the triplet PS with surrounding molecules results in two types of photooxidative reactions exploited in photodynamic treatment. In the Type II photoreactions, the transfer of triplet PS energy directly to molecular oxygen leads to excited-state singlet oxygen, the most important reactive specie in PDT-mediated cytotoxicity.

In recent years, new sensitizers have been studied for their use in PDT, such as boron-dipyrromethene compounds (BODIPY). However, their application can be achieved by particular structural modifications aimed at modulating their photophysical properties, as the wavelength for their maximum absorption does not fall in the therapeutic window (600-850 nm) and, being highly fluorescent, they hardly can undergo ISC.

In particular, a strategy used to enhanced the intersystem crossing mechanism is the introduction of heavy atoms (*i.e*. Br, I) or heavy metal (*i.e.* Pt(II)) in the BODIPY core which significantly favors spin–orbit coupling. In fact, in vitro and in vivo tests have already showed the efficacy of halogenated BODIPYs and platinum BODIPY conjugates to kill tumor cells. [1–3] In addition, the

conjugation between the BODIPY dyes and the classical platinum based chemotherapy generates multitarget agents able to play a dual action therapy.

Aim of the work

The role played by bromine atoms in influencing the photophysical properties of 8-phenyl boron-dipyrromethene has been elucidated. **(Paper 9)** Moreover, the influence of a platinum moiety on the physicochemical behavior of the BODIPY dyes and the study of Pt(II)-moiety hydrolysis process affected by the photosensitizers have been carried out. **(Paper 10)**

Both the investigations have been performed by means of Density Functional Theory (DFT) and its time-dependent formulation (TDDFT).

6.1 BODIPY for photodynamic therapy applications: computational study of the effect of bromine substitution on $^1O_2$ photosensitization

4,4-Difluoro-4-bora-3a,4a-diaza-s-indacene also known as BODIPY, thanks to its very favourable chemico-physical features, is the most investigated organic compound in the framework of PDT.

Here, the influence of bromine substitution, in different amounts and positions in the BODIPY core, on the photophysical properties of 8-phenyl BODIPY has been investigated (Scheme 1). The heavy atom effect on the absorption wavelength, singlet–triplet energy gap, and spin–orbit coupling constants as well as on the singlet oxygen production has been theoretically studied.

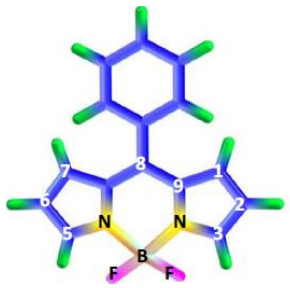

1	8-phenyl BODIPY
2a	1-Br- 8-phenyl BODIPY
2b	2-Br-8-phenyl BODIPY
2c	3-Br-8-phenyl BODIPY
3a	1,7-diBr-8-phenyl BODIPY
3b	2,6-diBr-8-phenyl BODIPY
3c	3,5-diBr-8-phenyl BODIPY
4a	1,2,5,6-tetraBr-8-phenyl BODIPY
4b	1,3,5,6-tetraBr-8-phenyl BODIPY
4c	1,3,5,7-tetraBr-8-phenyl BODIPY
4d	2,3,5,6-tetraBr-8-phenyl BODIPY

Scheme 1. The molecular structure of the 8-phenyl BODIPY and the investigated system names.

All the investigated compounds possess a triplet state T_1 with energy greater than that required to excite the molecular oxygen (0.98 eV), by considering S_0-T_1 energy gaps. Then, in principle, all of them should be able to produce the highly cytotoxic singlet molecular oxygen ($^1\Delta_g$).

Furthermore, to evaluate the influence of the halogen atoms on the photophysical properties, the absorption spectra have been calculated in toluene. The absorption maximum, however, has been changed by the Br presence, which increases the redshift. The comparison between computed and experimental wavelengths shows a reasonable agreement with an error of few tens of nm.[4] However, the introduction of bromine atoms, induces a variation of the spin–orbit matrix elements, whose values depend on the positions. In particular, the 8-phenyl BODIPY substituted in 1 and 7 positions appears to be best for enhancing spin–orbit couplings and thus ISC kinetics.

The theoretical outcomes support the use of these bromine-BODIPY compounds as photosensitizers in photodynamic therapy.

6.2 Photophysical Exploration of Dual-Approach PtII−BODIPY Conjugates: Theoretical Insights

In view of the success of the BODIPY dye in PDT and of cisplatin in chemotherapy practice, particular attention has been given to two - component system PtII-BODIPY, a promising class of compounds for a multitarget approach.

Experimental studies shown how the introduction of platinum in the PS, increases the photodynamic behaviour of BODIPY also improving the cellular accumulation.[5,6]

Here, have been theoretically explored the photophysical and chemical properties of two new synthesized BODIPYs (1 and 2) which have been functionalized with cisplatin moiety (Pt-1 and Pt-2). (Figure 2).

In addition, the hydrolysis process of the platinum complexes, affected by

the photosensitizer, has been investigated.

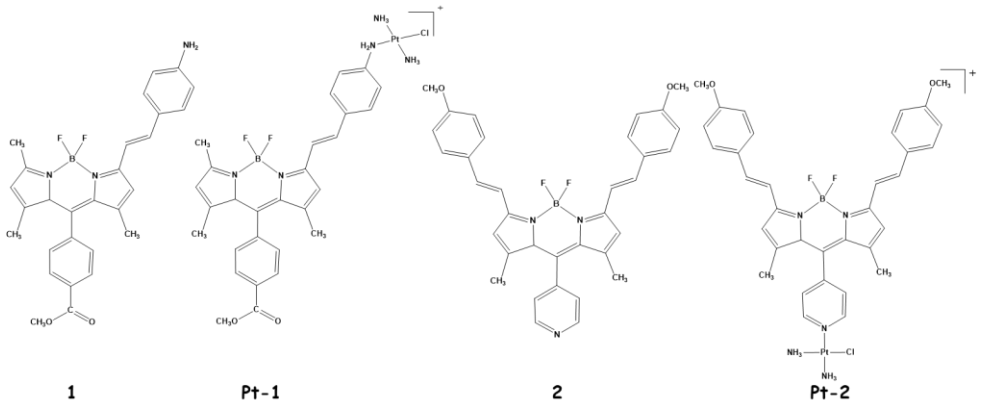

Figure 2.BODIPY Dyes 1 and 2 and Their Complexes with Monofunctional PtII Ligand Pt-1 and Pt-2.

For all compounds, UV−vis spectra have been computed in water.
The electronic absorption spectra show how only the Pt-2 complex, thanks to its extended conjugation, has a wavelength of absorption that falls in the therapeutic window. Other complexes, although they may be suitable in the PDT field, are not useful for treating deep tumors.

The energy gap S0-T1 for all the BODIPYs studied, is high enough (greater than 0.98 eV) to ensure the generation of excited oxygen.
Beside, from the investigation of the intersystem crossing process and therefore from the spin-orbit matrix elements, have been revealed that both the dyes containing the platinum moiety are more efficient to generate the cytotoxic singlet oxygen than the free-metal BODIPY.
The activation mechanism of both platinum complexes, whit three explicit water molecules has been explored and the energy barriers for the chloride/water substitution process are respectively 22.2 kcal/mol for Pt-1 and 20.8 kcal/mol for Pt-2.
Both the platinum complexes have only one labile group, so these complexes form only one covalent bond with DNA.
The obtained date reveal that aquation reaction requires the overcome
an energy barrier very similar to that previously computed for cisplatin and other platinum-based anticancer drugs already used in chemotherapy.

It is possible to conclude that the two-component Pt(II)-BODIPY can open new perspective in the in a dual-action anticancer therapy.

References Chapter 6

(1) Lim, S. H.; Thivierge, C.; Nowak-Sliwinska, P.; Han, J.; van den Bergh, H.; Wagnières, G.; Burgess, K.; Lee, H. B. In Vitro and in Vivo Photocytotoxicity of Boron Dipyrromethene Derivatives for Photodynamic Therapy. *J. Med. Chem.* **2010**, *53* (7), 2865–2874. https://doi.org/10.1021/jm901823u.

(2) Alberto, M. E.; Adamo, C. Synergistic Effects in PtII–Porphyrinoid Dyes as Candidates for a Dual-Action Anticancer Therapy: A Theoretical Exploration. *Chemistry – A European Journal* **2017**, *23* (60), 15124–15132. https://doi.org/10.1002/chem.201702876.

(3) Hopkins, S. L.; Stepanyan, L.; Vahidi, N.; Jain, A.; Winkel, B. S. J.; Brewer, K. J. Visible Light Induced Antibacterial Properties of a Ru(II)–Pt(II) Bimetallic Complex. *Inorganica Chimica Acta* **2017**, *454*, 229–233. https://doi.org/10.1016/j.ica.2016.06.006.

(4) Zhang, X.-F.; Yang, X. Singlet Oxygen Generation and Triplet Excited-State Spectra of Brominated BODIPY. *J. Phys. Chem. B* **2013**, *117* (18), 5533–5539. https://doi.org/10.1021/jp4013812.

(5) Liu, Y.; Li, Z.; Chen, L.; Xie, Z. Near Infrared BODIPY-Platinum Conjugates for Imaging, Photodynamic Therapy and Chemotherapy. *Dyes and Pigments* **2017**, *141*, 5–12. https://doi.org/10.1016/j.dyepig.2017.01.075.

(6) Xue, X.; Zhu, C.; Chen, H.; Bai, Y.; Shi, X.; Jiao, Y.; Chen, Z.; Miao, Y.; He, W.; Guo, Z. A New Approach to Sensitize Antitumor Monofunctional Platinum(II) Complexes via Short Time Photo-Irradiation. *Inorg Chem* **2017**, *56* (7), 3754–3762. https://doi.org/10.1021/acs.inorgchem.6b02148.

Journal of Molecular Modeling (2018) 24:183
https://doi.org/10.1007/s00894-018-3727-3

ORIGINAL PAPER

BODIPY for photodynamic therapy applications: computational study of the effect of bromine substitution on $^1O_2$ photosensitization

Fortuna Ponte[1] · Gloria Mazzone[2] · Nino Russo[1] · Emilia Sicilia[1]

Received: 1 December 2017 / Accepted: 18 June 2018

Abstract
Density functional theory and its time-dependent extension (DFT, TDDFT) were employed to establish the feasibility of using a series of 4,4-difluoro-4-bora-3*a*,4*a*-diaza-*s*-indacenes (BODIPYs) in photodynamic therapy. Their absorption electronic spectra, singlet–triplet energy gaps, and spin–orbit matrix elements were computed and are discussed here. The effects of bromine substitution on the photophysical properties of BODIPY were elucidated. The investigated compounds were found to possess different excited triplet states that lie below the energy of the bright excited singlet state (S_1 or S_2), depending on the positions occupied by the bromine atoms. The computed spin–orbit matrix elements for the radiationless intersystem crossing $S_n \rightarrow T_m$ and the relative singlet–triplet energy gaps allowed the prediction of plausible nonradiative decay pathways for the production of singlet excited molecular oxygen, the key cytotoxic agent in photodynamic therapy.

Keywords PDT · BODIPY · Electronic spectra · Heavy atom effect · Singlet–triplet energy gaps

Introduction

Despite headway in basic research that has provided a better understanding of tumor biology, cancer remains one of the most lethal diseases of our time. Beside conventional therapies, photodynamic therapy (PDT) has emerged as a minimally invasive and nontoxic light-assisted treatment of cancer and other nonmalignant diseases [1–3]. PDT is based on the ability of photosensitizers to selectively accumulate and kill tumor cells via reactive oxygen species (ROS) upon activation by guided light of a particular wavelength. The photophysical cycle for ROS production starts with the excitation of a photosensitizer (PS; $S_0 \rightarrow S_1$) by laser light of a wavelength that falls within the so-called therapeutic window (500–850 nm) in order to maximize penetration into the tissues. After absorbing light, the PS can transfer the absorbed energy to the triplet excited state (T_1) via nonradiative intersystem spin crossing (ISC), which mainly depends on the amplitude of the spin–orbit coupling constants between the two states with different multiplicities. The populated triplet state can react with substrate molecules through either electron or hydrogen transfer reactions, leading to the formation of a superoxide ion and a hydroxyl radical (type I photoreactions), or it can transfer its energy to a ground-state oxygen molecule ($^3\Sigma_g^-$), producing a highly reactive excited singlet state ($^1\Delta_g$; type II photoreactions), which is believed to be responsible for destroying tumor cells. Although these two processes can occur competitively, depending on both the electronic structure of the PS and the concentration of oxygen in the substrate, type II photoreactions can only take place if the energy of the PS triplet is higher than the energy required to excite molecular oxygen (0.98 eV). In PDT, type II photoreactions are preferred, as singlet oxygen is a more selective oxidant [4]. Therefore, the photosensitizer used must possess some specific photophysical properties, such as an absorption wavelength in the range 500–850 nm, a triplet energy greater than 0.98 eV, and efficient intersystem crossing between singlet and triplet states. Furthermore, the PS must be thermodynamically stable

This paper belongs to Topical Collection MIB 2017 (Modeling Interactions in Biomolecules VIII)

Electronic supplementary material The online version of this article (https://doi.org/10.1007/s00894-018-3727-3) contains supplementary material, which is available to authorized users.

✉ Gloria Mazzone
gloria.mazzone@unical.it

[1] Dipartimento di Chimica e Tecnologie Chimiche, Università della Calabria, 87036 Rende, CS, Italy

[2] Dipartimento di Ingegneria Informatica, Modellistica, Elettronica e Sistemistica, Università della Calabria, 87036 Rende, CS, Italy

Published online: 29 June 2018

and resistant to redox processes that can be caused by the cellular environment; it should not aggregate, as this would reduce the amount of singlet oxygen generated; and it must be not cytotoxic in the dark.

Today, most of the PDT photosensitizers that have been approved and used for the clinical treatment of solid tumors are porphyrin- or phthalocyanine-based drugs, but recent experimental and theoretical investigations have suggested that molecules belonging to other classes of compounds may also be good PSs [5]. For instance, interest in using 4,4-difluoro-4-bora-3*a*,4*a*-diaza-*s*-indacene (BODIPY) systems as PSs has recently grown considerably. Because of their absorption and fluorescence spectral features, some of them have been already employed as chemosensors, laser dyes, fluorophores, OLEDs, and labeling reagents [6]. In recent years, they have also been applied as singlet oxygen generators in PDT. BODIPYs have been shown to have interesting photophysical properties for PDT applications, as demonstrated by a very recent study in which their ability to generate singlet oxygen was investigated [7, 8].

In the work reported in the present paper, we theoretically explored the effects of bromine atom substitution in the BODIPY core on the absorption wavelength, singlet–triplet energy gap, and spin–orbit coupling constants. Previous studies [9–19] have demonstrated that introducing a heavy atom significantly increases the spin–orbit matrix element values and consequently facilitates intersystem crossing between states with different spin multiplicities. As shown in Scheme 1, we systematically studied how the photophysical properties of BODIPY are affected by the introduction of a bromine atom at different positions in the core, as well as the impact of inserting more than one heavy atom.

Results and discussion

In order to select the most suitable computational protocol, we performed a preliminary investigation on the abilities of different exchange and correlation functionals (XCs) to accurately reproduce the main geometrical and spectroscopic parameters of compound **4d**, the structure and absorption spectrum of which were recently characterized [8, 20]; see the "Electronic supplementary material" (ESM) for further details. The best agreement was obtained using the PBE functional, which was therefore used for all the calculations carried out on the other compounds of interest in this work. In Table 1, we report the singlet and triplet excitation energies for all the considered systems.

The substitution of a hydrogen atom with a bromine one at positions 2 and 3 of the BODIPY core, resulting in compounds **2b** and **2c**, respectively, slightly redshifts the Q band by 58 and 16 nm, respectively, with respect to the unsubstituted compound **1**, while the insertion of bromine at position 1, **2a**, does not affect the position of the Q band (448 nm). The introduction of two bromine atoms (compounds **3a–c**) further increases the redshift and, again, substitution at position 2 (**2b**) results in the largest wavelength shift. The addition of four Br atoms (see compounds **4a–d**) does not significantly affect the absorption properties. Experimental results for the wavelengths of maximum absorption of the compounds **1**, **2b**, **3b** and **4d** [8] were reproduced well by our theoretical calculations, with errors averaging around 20 nm.

The presence of a bromine atom at position 1 in compounds **2a**, **3a**, and **4c** results in the activation of the S_2 state as the bright one and considerably reduces (**2a**) or eliminates the oscillator strength of S_1. Furthermore, it induces changes in the orbital composition of the transitions. In fact, when Br occupies position 1, S_1 is not HOMO–LUMO in nature, in contrast to the cases in which S_1 is the bright state (see Table 1). Depending on the position of the bromine substituent, there are different triplet states that lie below the bright state S_1 or S_2. In all the investigated compounds, the low-energy triplet (T_1) is always generated by a HOMO → LUMO transition, and the energy gap with respect to the ground singlet state is always significantly greater than the energy required to produce the excited singlet molecular oxygen ($^1\Delta_g$) state (0.98 eV). Consequently, all of the examined compounds could potentially be used as type II photosensitizers in PDT.

Production of cytotoxic singlet oxygen is directly related to the rate constant of the radiationless intersystem crossing

Scheme 1 Structures of the series of brominated 8-phenyl BODIPYs considered in this work

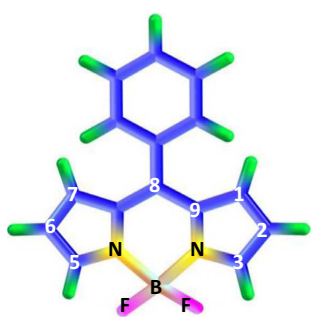

1	8-phenyl BODIPY
2a	1-Br- 8-phenyl BODIPY
2b	2-Br-8-phenyl BODIPY
2c	3-Br-8-phenyl BODIPY
3a	1,7-diBr-8-phenyl BODIPY
3b	2,6-diBr-8-phenyl BODIPY
3c	3,5-diBr-8-phenyl BODIPY
4a	1,2,5,6-tetraBr-8-phenyl BODIPY
4b	1,3,5,6-tetraBr-8-phenyl BODIPY
4c	1,3,5,7-tetraBr-8-phenyl BODIPY
4d	2,3,5,6-tetraBr-8-phenyl BODIPY

Table 1 Main vertical excitation energies (ΔE in eV), absorption wavelengths (λ in nm), oscillator strengths (f), and transitions (molecular orbital contribution in %) for the studied compounds in toluene solvent

Compound	State	Transition	f	ΔE	λ	λ^{exp} [a]
1	T_1	H → L, 99%	0.000	1.69	733	
	T_2	H-1 → L, 98%	0.000	2.47	502	
	T_3	H-2 → L, 72%	0.000	2.63	472	
	T_4	H-3 → L, 73%	0.000	2.75	451	
	S_1	H → L, 78%	0.311	2.77	448	501
2a	T_1	H → L, 100%	0.000	1.69	735	
	T_2	H-1 → L, 98%	0.000	2.24	553	
	T_3	H-2 → L, 60%	0.000	2.52	493	
	S_1	H-1 → L, 82%	0.010	2.61	475	
	T_4	H-3 → L, 50%	0.000	2.64	497	
	S_2	H-2 → L, 58%	0.205	2.80	448	
2b	T_1	H → L, 99%	0.000	1.62	766	
	T_2	H-1 → L, 97%	0.00	2.26	548	
	S_1	H → L, 75%	0.218	2.46	506	521
2c	T_1	H → L, 100%	0.000	1.63	761	
	T_2	H-1 → L, 98%	0.000	2.51	493	
	T_3	H-2 → L, 90%	0.000	2.64	470	
	S_1	H-1 → L, 93%	0.466	2.67	464	
3a	T_1	H → L, 100%	0.000	1.66	745	
	T_2	H-1 → L, 98%	0.000	2.19	565	
	T_3	H-3 → L, 99%	0.000	2.29	543	
	T_4	H-2 → L, 100%	0.000	2.40	517	
	S_1	H-2 → L, 100%	0.000	2.43	511	
	S_2	H-1 → L, 71%	0.062	2.49	497	
3b	T_1	H → L, 99%	0.000	1.54	806	
	T_2	H-1 → L, 99%	0.000	2.22	556	
	T_3	H-2 → L, 98%	0.000	2.25	550	
	S_1	H → L, 84%	0.253	2.29	540	540
3c	T_1	H → L, 100%	0.000	1.57	788	
	S_1	H → L, 98%	0.539	2.60	476	
4a	T_1	H → L, 99%	0.000	1.53	813	
	T_2	H-1 → L, 98%	0.000	1.99	624	
	S_1	H → L, 57%	0.180	2.28	543	
4b	T_1	H → L, 100%	0.000	1.52	817	
	T_2	H-1 → L, 90%	0.000	2.26	548	
	S_1	H → L, 89%	0.485	2.40	516	
4c	T_1	H → L, 100%	0.000	1.57	791	
	T_2	H-1 → L, 96%	0.000	2.29	540	
	T_3	H-2 → L, 100%	0.000	2.40	516	
	T_4	H-3 → L, 98%	0.000	2.42	512	
	S_1	H-2 → L, 100%	0.000	2.43	510	
	S_2	H → L, 56%	0.372	2.53	490	
4d	T_1	H → L, 100%	0.000	1.46	847	
	S_1	H → L, 91%	0.437	2.27	545	559

[a] [8]

(ISC) between S_n and T_m states. As established by an approximation of the Fermi golden rule, the intersystem crossing kinetics are directly related to the spin–orbit matrix elements $\langle S_n|\hat{H}_{SO}|T_m\rangle$ and the Franck–Condon weighted density of states (FCWD):

$$k_{isc}^{nm} = \frac{2\pi}{\hbar}\langle S_n|\hat{H}_{SO}|T_m\rangle^2 \times \text{FCWD}$$

In the framework of Marcus–Levich–Jortner theory [21], the FCWD is proportional to the exponential factor:

$$\text{FCWD} \propto \exp\left[-\frac{(\Delta E_{S-T})^2}{4\lambda k_B T}\right]$$

where λ is the Marcus reorganization energy and ΔE is the difference between the energies of the singlet and triplet states at their equilibrium geometries. Since estimating FCWD is too computationally expensive, we only determined the spin–orbit matrix elements and the singlet–triplet energy gaps, which allowed us to predict the deactivation pathways that lead to the production of the $^1\Delta_g$ state of molecular oxygen. The accuracy of this procedure has already been demonstrated by previous ab initio [22] and DFT studies [9, 13, 15] of a series of compounds that can act as photosensitizers in photodynamic therapy.

The SOCs computed for the $S_n \rightarrow T_m$ transitions together with the corresponding singlet–triplet energy gaps are reported in Table 2. Using these data, we can rationalize how the presence of one or more heavy atoms at different positions can significantly affect the SOC values.

The presence of a bromine atom at position 1 in the BODIBY core significantly increases all of the plausible SOC values as compared to the unsubstituted system. In particular, the values for the $S_1 \rightarrow T_1$ and $S_1 \rightarrow T_3$ transitions increase from 0.05 and 4.3 cm^{-1}, respectively, in compound **1** to 46.3 and 77.1 cm^{-1} in **2a**. Since absorption causes the S_2 excited state of this molecule to be populated, we also computed the SOCs for the transitions from S_2 to the closest triplet states (T_2, T_3, and T_4). The results show how the SOC values for these nonradiative transitions improve upon going from **1** to **2a**. The introduction of a bromine atom at position 2 (**2b**) results in a significant decrease in SOC (e.g., SOC for $S_1 \rightarrow T_1 = 10.9$ cm^{-1}). A further reduction is observed when bromine is inserted at position 3 (e.g., SOC for $S_1 \rightarrow T_1 = 1.9$ cm^{-1} for **2c**). Following the El-Sayed rule [23, 24], the change in orbital composition observed for the $S_1 \rightarrow T_1$ transition in compound **2a** justifies the enhanced SOC values found for this system as compared to the compounds in which the bromine atom occupies other positions, i.e., **2b–c**. In all the compounds, the orbitals of the T_1 state (originated by a H → L transition) extend over the entire molecule, including a considerable contribution from the unpaired electrons of bromine; however, in **2a**, the S_1 state (originated from a H-1 → L

Table 2 SOC values (cm^{-1}) for the $S_n \rightarrow T_m$ transitions and singlet–triplet energy gaps (eV)

Compound	*n.m*	SOC	ΔE
1	1.1	5×10^{-2}	1.08
	1.2	1×10^{-1}	0.30
	1.3	4.3	0.14
	1.4	0.26	0.02
2a	1.1	46.3	0.93
	1.2	18.0	0.37
	1.3	77.1	0.10
	2.2	6.8	0.56
	2.3	25.9	0.28
	2.4	34.4	0.16
2b	1.1	10.9	0.84
	1.2	2.0	0.20
2c	1.1	1.9	1.04
	1.2	6×10^{-1}	0.16
	1.3	3.0	0.03
3a	1.1	70.8	0.76
	1.2	70.4	0.23
	1.3	287.7	0.14
	1.4	9×10^{-2}	0.03
	2.2	7×10^{-2}	0.30
	2.3	4.7	0.21
	2.4	117.2	0.10
3b	1.1	3.2	0.75
	1.2	1.5	0.07
	1.3	2.7	0.04
3c	1.1	2.0	1.03
4a	1.1	2.0	1.03
	1.1	12.6	0.76
4b	1.2	9.1	0.29
	1.1	6.6	0.88
4c	1.2	6.7	0.14
	1.1	51.0	0.86
	1.2	20.5	0.14
	1.3	83.8	0.03
	1.4	283.1	0.01
	2.2	76.4	0.24
	2.3	17.7	0.13
4d	2.4	70.1	0.11

transition) is characterized by a H-1 with a little participation of the heavy atom, whereas in **2b–c**, in which the S_1 state is originated by a H → L transition, both of the orbitals involved are entirely delocalized over the whole molecule, as in the T_1 state (see the ESM).

When two bromine atoms are inserted into the core of BODIPY, the SOCs assume different values depending on the position occupied by the heavy atoms. On one hand, the presence of Br at positions 1 and 7 (**3a**) leads to a marked increase in the SOC values, especially for the $S_1 \rightarrow T_3$ transition (287.7 cm^{-1}). On the other hand, when the bromine atoms occupy positions 2 and 6 (**3b**) or 3 and 5 (**3c**), the resulting SOCs are very small (e.g., the SOC for $S_1 \rightarrow T_1$ is 3.2 and 2.0 cm^{-1} for **3b** and **3c**, respectively).

The SOCs obtained when four bromine atoms were added to the core (compounds **4a–d**) are highest when two of them are located at positions 1 and 7 (**4c**) and smallest when neither of these two positions are occupied by a heavy atom (**4d**).

From Table 1, it is clear that a series of plausible nonradiative decay pathways to populate the lowest triplet state are possible. For molecules in which the S_1 excited state is populated upon irradiation (**1**, **2b–c**, **3b–c**, **4a–b,d**), the lowest triplet excited state can be populated in three ways, depending on the number of triplet excited states lying below the bright singlet one:

a) $S_0 \xrightarrow{A} S_1 \xrightarrow{ISC} T_4 \xrightarrow{IC} T_3 \xrightarrow{IC} T_2 \xrightarrow{IC} T_1$; b) $S_0 \xrightarrow{A} S_1 \xrightarrow{ISC} T_3 \xrightarrow{IC} T_2 \xrightarrow{IC} T_1$;

c) $S_0 \xrightarrow{A} S_1 \xrightarrow{ISC} T_2 \xrightarrow{IC} T_1$; d) $S_0 \xrightarrow{A} S_1 \xrightarrow{ISC} T_1$.

In pathways a–c, an ISC that occurs between S_1 and T_n ($n = 1$–4) is followed by a fast $T_n \rightarrow T_1$ internal conversion (IC), while in pathway d, a direct $S_1 \rightarrow T_1$ ISC leads to the population of the lowest triplet state. Compound **1** can employ all the plausible pathways, while pathways b–d are viable for **2c** and **3b**. For the other compounds, with the exception of **3c** and **4d** (which exclusively have a triplet state below the S_1 one; i.e., only pathway d is feasible), pathways c and d are both viable channels for populating T_1.

For compounds **2a**, **3a**, and **4c**, in which S_2 is the bright state, the following pathways also appear to be feasible:

e) $S_0 \xrightarrow{A} S_2 \xrightarrow{IC} S_1 \xrightarrow{ISC} T_4 \xrightarrow{IC} T_3 \xrightarrow{IC} T_2 \xrightarrow{IC} T_1$; f) $S_0 \xrightarrow{A} S_2 \xrightarrow{IC} S_1 \xrightarrow{ISC} T_3 \xrightarrow{IC} T_2 \xrightarrow{IC} T_1$;

g) $S_0 \xrightarrow{A} S_2 \xrightarrow{IC} S_1 \xrightarrow{ISC} T_2 \xrightarrow{IC} T_1$; h) $S_0 \xrightarrow{A} S_2 \xrightarrow{IC} S_1 \xrightarrow{ISC} T_1$;

i) $S_0 \xrightarrow{A} S_2 \xrightarrow{ISC} T_4 \xrightarrow{IC} T_3 \xrightarrow{IC} T_2 \xrightarrow{IC} T_1$; l) $S_0 \xrightarrow{A} S_2 \xrightarrow{ISC} T_3 \xrightarrow{IC} T_2 \xrightarrow{IC} T_1$;

m) $S_0 \xrightarrow{A} S_2 \xrightarrow{ISC} T_2 \xrightarrow{IC} T_1$; n) $S_0 \xrightarrow{A} S_2 \xrightarrow{ISC} T_1$

Examining the SOC values and energy gaps between the states involved in the nonradiative intersystem spin-crossing processes (Table 2) allows the preferred deactivation channel to be hypothesized for each compound. All of the calculated SOCs for **1** are very small, with $S_1 \rightarrow T_3$ providing the highest value. The ΔE between these two states is just 0.1 eV, with path b the preferred one. For compound **2a**, the highest SOC values are found for the $S_1 \rightarrow T_1$ (46.3 cm^{-1}), $S_1 \rightarrow T_3$ (77.1 cm^{-1}), and $S_2 \rightarrow T_4$ (34.4 cm^{-1}) transitions, so pathways f, h, and i are plausible. However, after looking at the singlet–triplet energy gaps and considering the Kasha rules [25], pathways f and i stand out as the most probable ones. For

2b, the SOC value of 10.9 cm^{-1} for $S_1 \rightarrow T_1$ clearly indicates that the deactivation pathway d is favored over pathway c. The situation appears to be different for **2c**, since the highest SOC value is found for the $S_1 \rightarrow T_3$ ISC, so path b should be the preferred one.

In **3a**, the two halogen atoms at positions 1 and 7 lead to similar photophysical properties to those of **2a**. In fact, the S_2 state is also populated upon irradiation in this case. However, upon considering the Kasha rule and combining the SOC and $\Delta E_{S\text{-}T}$ values, it appears that path f is favored, especially when the SOC of 287.7 cm^{-1} obtained for the $S_1 \rightarrow T_3$ ISC is noted. In the case of **3b**, though the SOC values computed for $S_1 \rightarrow T_1$ and $S_1 \rightarrow T_3$ are of the same magnitude (3.2 and 2.7 cm^{-1}, respectively), the energy gaps suggest that coupling with the T_3 state is favored and pathway b is the most accessible. For **3c**, on the other hand, only pathway d can be considered a viable channel.

For compounds **4a** and **4b**, the data reported in Table 2 suggest that channel c is followed in the deactivation of S_1, in contrast to compound **4d**, for which path d is the only plausible channel for populating T_1. **4c** is characterized by the presence of two Br atoms at positions 1 and 7, and the value of 283.1 cm^{-1} for the $S_1 \rightarrow T_4$ ISC as well as the energy gap of 0.01 eV imply that S_1 deactivates through path i.

Computational methods

All geometry optimizations were performed using the Gaussian 09 code [26] at DFT and TD-DFT [27] levels of theory. A preliminary benchmark study was carried out using several functionals (B3LYP [28, 29], Cam-B3LYP [30], M06 [31], PBE0 [32], and PBE [33, 34]), and their performances were evaluated by comparing both the calculated geometric parameters and the wavelength of maximum absorption for compound **4d** with the corresponding available experimental data [8, 20].

Geometry optimization without symmetry constraints was carried out using the 6-31 + G* basis set for all atoms except Br, which was described using the 6-31G* basis set. When simulating electronic spectra, solvent effects were included by applying the polarizable continuum model (PCM) [35] for implicit toluene ($\varepsilon = 2.379$).

Electronic absorption spectra were calculated via the time-dependent DFT formalism at the corresponding optimized geometries in toluene.

Spin–orbit matrix elements were computed within the atomic mean field approximation as implemented in the DALTON code [36] (previous studies have demonstrated that the Breit–Pauli method and the atomic mean field approximation give very similar values [37], but the latter is less computationally demanding). For this purpose, the quadratic response TDDFT approach was applied, employing B3LYP in conjunction with the cc-pVDZ basis set for all the atoms, as suggested by the authors of the software, and using the first singlet excited state structures optimized at the TD-PBE level.

$$\mathrm{SOC}_{ij} = \sqrt{\sum_n \left| \left\langle \psi_{S_i} \middle| \hat{H}_{SO} \middle| \psi_{T_{j,n}} \right\rangle \right|^2}; \qquad n = x, y, z,$$

where $\hat{H}_{SO}$ is the spin–orbit Hamiltonian.

This computational protocol has been successfully applied to study the photophysical properties of several potential photosensitizers for use in PDT [9–19].

Conclusions

Based on the computed excitation energies, singlet–triplet energy gaps, and spin–orbit matrix elements for a series of BODIPYs with different numbers of bromine substituents at different positions, the following conclusions can be drawn:

- Benchmarking performed on the tetrabromo-substituted compound **4d** indicates that PBE is the functional that best reproduces experimental structural and absorption data;
- Introducing bromine atoms at positions 1 and 7 significantly changes the photophysical properties, as S_2 becomes the populated singlet excited state upon irradiation instead of S_1;
- All of the investigated compounds possess a low-lying triplet state at a higher energy than that required to produce the cytotoxic singlet molecular oxygen;
- SOC values strongly depend on the position(s) of the heavy atom(s) in the BODIPY core, and substitution at positions 1 and 7 appears to be best for enhancing spin–orbit couplings and thus ISC kinetics.
- The preferred intersystem spin-crossing pathway for populating the lowest triplet state also seems to effectively depend on the position(s) of the bromine atom(s) in the BODIPY core.

Our computations of their photophysical properties demonstrate that all of the bromine-substituted systems examined here are candidate photosensitizers for PDT.

Acknowledgements The authors thank the Università della Calabria for financial support.

References

1. Dolmans DEJGJ, Fukumura D, Jain RK (2003) Photodynamic therapy for cancer. Nature 3:380–387
2. Dąbrowski JM, Arnaut LG (2015) Photodynamic therapy (PDT) of cancer: from local to systemic treatment. Photochem Photobiol Sci 14:1765–1780

3. González-Delgado JA, Kennedy PJ, Ferreira M, Tomé JP, Sarmento B (2015) Use of photosensitizers in semisolid formulations for microbial photodynamic inactivation. J Med Chem 59:4428–4442
4. Dabrowski JM, Pucelik B, Regiel-Futyra A, Brindell M, Mazuryk O, Kyzioł A, Stochel G, Macyk W, Arnaut LG (2016) Engineering of relevant photodynamic processes through structural modifications of metallotetrapyrrolic photosensitizers. Coord Chem Rev 32:567–101
5. Yanoa S, Hirohara S, Obata M, Hagiyad Y, Ogura S, Ikeda A, Kataoka H, Tanaka M, Joh T (2011) Current states and future views in photodynamic therapy. J Photochem Photobiol C: Photochem Rev 12:46–67
6. Zhao J, Xu K, Yang W, Wang Z, Zhong F (2015) The triplet excited state of Bodipy: formation, modulation and application. Chem Soc Rev 44:8904–8939
7. Epelde-Elezcano N, Martınez-Martínez V, Pena-Cabrera E, Gómez-Duran CFA, Lopez Arbeloa I, Lacombe S (2016) Modulation of singlet oxygen generation in halogenated BODIPY dyes by substitution at their meso position: towards a solvent-independent standard in the vis region. RSC Adv 6:41991–41998
8. Zhang X–F, Yang X (2013) Singlet oxygen generation and triplet excited-state spectra of brominated BODIPY. J Phys Chem B 117: 5533–5539
9. De Simone BC, Mazzone G, Russo N, Sicilia E, Toscano M (2017) Metal atom effect on the photophysical properties of Mg(II), Zn(II), Cd(II), and Pd(II) tetraphenylporphyrin complexes proposed as possible drugs in photodynamic therapy. Molecules 22:1093–1103
10. Alberto ME, De Simone BC, Mazzone G, Sicilia E, Russo N (2015) The heavy atom effect on Zn(II) phthalocyanine derivatives: a theoretical exploration of the photophysical properties. Phys Chem Chem Phys 17:23595–23601
11. Alberto ME, De Simone BC, Mazzone G, Marino T, Russo N (2015) Photophysical properties of free and metallated meso-substituted tetrabenzotriazaporphyrin from density functional theory investigation. Dyes Pigments 120:335–339
12. Pirillo J, Mazzone G, Russo N (2018) Theoretical insights into the switch off/on $^1O_2$ photosensitization in chemicontrolled photodynamic therapy. Chem Eur J 24:3512–3519
13. Pirillo J, Mazzone G, Russo N, Bertini L (2017) Photophysical properties of S, Se and Te-substituted deoxyguanosines: insight into their ability to act as chemotherapeutic agents. J Chem Inf Model 57:234–242
14. Mazzone G, Quartarolo AD, Russo N (2016) PDT-correlated photophysical properties of thienopyrrole BODIPY derivatives. Theoretical insights. Dyes Pigments 130:9–15
15. De Simone BC, Mazzone G, Pirillo J, Russo N, Sicilia E (2017) Halogen atom effect on the photophysical properties of substituted aza-BODIPY derivatives. Phys Chem Chem Phys 19:2530–2536
16. De Simone BC, Mazzone G, Russo N, Sicilia E, Toscano M (2018) Computational investigation on the influence of halogen atoms on the photophysical properties of tetraphenylporphyrin and its zinc(II) complexes. J Phys Chem A 122:2809–2815
17. De Simone BC, Mazzone G, Russo N, Sicilia E, Toscano M (2018) Excitation energies, singlet-triplet energy gap, spin-orbit matrix elements and heavy atom effect in BOIMPYs as possible photosensitizers in photodynamic therapy. A computational investigation. Phys Chem Chem Phys 20:2656–2661
18. Alberto ME, Pirillo J, Russo N, Adamo C (2016) Theoretical exploration of type I/type II dual photoreactivity of promising Ru(II) dyads for PDT approach. Inorg Chem 55:11185–11192
19. Alberto ME, Russo N, Adamo C (2016) Synergistic effects of metals in a promising RuII−PtII assembly for a combined anticancer approach: theoretical exploration of the photophysical properties. Chem Eur J 22:9162–9168
20. Jiao L, Pang W, Zhou J, Wei Y, Mu X, Bai G, Hao E (2011) Regioselective stepwise bromination of boron dipyrromethene (BODIPY). Dyes J Org Chem 76:9988–9996
21. Brédas JL, Beljonne D, Coropceanu V, Cornil J (2004) Charge-transfer and energy-transfer processes in π-conjugated oligomers and polymers: a molecular picture. Chem Rev 104:4971–5004
22. Marian CM (2012) Spin–orbit coupling and intersystem crossing in molecules. WIREs Comput Mol Sci 2:187–203
23. El-Sayed MA (1962) The radiationless processes involving change of multiplicity in the diazenes. J Chem Phys 36:573–574
24. El-Sayed MA (1963) Spin-orbit coupling and the radiationless processes in nitrogen heterocycles. J Chem Phys 38:2834–2838
25. Kasha M (1950) Characterization of electronic transitions in complex molecules. Discuss Faraday Soc 9:14–19
26. Frisch MJ, Trucks GW, Schlegel HB, Scuseria GE, Robb MA, Cheeseman JR, Scalmani G, Barone V, Mennucci B, Petersson GA, Nakatsuji H, Caricato M, Li X, Hratchian HP, Izmaylov AF, Bloino J, Zheng G, Sonnenberg JL, Hada M, Ehara M, Toyota K, Fukuda R, Hasegawa J, Ishida M, Nakajima T, Honda Y, Kitao O, Nakai H, Vreven T, Montgomery Jr JA, Peralta JE, Ogliaro F, Bearpark M, Heyd JJ, Brothers E, Kudin KN, Staroverov VN, Kobayashi R, Normand J, Raghavachari K, Rendell A, Burant JC, Iyengar SS, Tomasi J, Cossi M, Rega N, Millam JM, Klene M, Knox JE, Cross JB, Bakken V, Adamo C, Jaramillo J, Gomperts R, Stratmann RE, Yazyev O, Austin AJ, Cammi R, Pomelli C, Ochterski JW, Martin RL, Morokuma K, Zakrzewski VG, Voth GA, Salvador P, Dannenberg JJ, Dapprich S, Daniels AD, Farkas Ö, Foresman JB, Ortiz JV, Cioslowski J, Fox DJ (2009) Gaussian 09, revision D.01. Gaussian, Inc., Wallingford
27. Casida ME, Jamorski C, Casida KC, Salahub DR (1998) Molecular excitation energies to high-lying bound states from time-dependent density-functional response theory: characterization and correction of the time-dependent local density approximation ionization threshold. J Chem Phys 108:4439–4449
28. Becke AD (1993) Density-functional thermochemistry. III. The role of exact exchange. J Chem Phys 98:5648–5652
29. Lee C, Yang W, Parr RG (1988) Development of the Colle–Salvetti correlation-energy formula into a functional of the electron density. Phys Rev B 37:785–789
30. Yanai T, Tew D, Handy N (2004) A new hybrid exchange-correlation functional using the Coulomb-attenuating method (CAM-B3LYP). Chem Phys Lett 393:51–57
31. Zhao Y, Truhlar DG (2008) The M06 suite of density functionals for main group thermochemistry, thermochemical kinetics, noncovalent interactions, excited states, and transition elements: two new functionals and systematic testing of four M06-class functionals and 12 other functionals. Theor Chem Accounts 120:215–241
32. Adamo C, Barone V (1999) Toward reliable density functional methods without adjustable parameters: the PBE0 model. J Chem Phys 110:6158–6169
33. Perdew JP, Burke K, Ernzerhof M (1996) Generalized gradient approximation made simple. Phys Rev Lett 77:3865–3868
34. Perdew JP, Burke K, Ernzerhof M (1997) Errata: generalized gradient approximation made simple. Phys Rev Lett 78:1396
35. Scalmani G, Frisch MJ (2010) Continuous surface charge polarizable continuum models of solvation. I. General formalism. J Chem Phys 132:114110
36. Aidas K et al (2011) Dalton, a molecular electronic structure program. http://daltonprogram.org/
37. Alberto ME, Marino T, Quartarolo AD, Russo N (2013) Photophysical origin of the reduced photodynamic therapy activity of temocene compared to Foscan®: insights from theory. Phys Chem Chem Phys 15:16167–16171

Inorganic Chemistry
Cite This: Inorg. Chem. 2019, 58, 9882−9889
Article
pubs.acs.org/IC

Photophysical Exploration of Dual-Approach Pt^{II}−BODIPY Conjugates: Theoretical Insights

Fortuna Ponte, Marta E. Alberto,* Bruna C. De Simone, Nino Russo, and Emilia Sicilia

Dipartimento di Chimica e Tecnologie Chimiche, Università della Calabria, I-87036, Arcavacata di Rende, Italy

Supporting Information

ABSTRACT: Two-component Pt^{II}−BODIPY dyes were recently proposed as potential multitarget agents able to conjugate the photobased photodynamic therapy (PDT) treatment with the classical chemotherapy approach based on Pt^{II} complexes. A careful first-principle investigation is herein presented on the above-mentioned conjugates (**Pt-1** and **Pt-2**) and on the two metal-free precursors (**1** and **2**), aimed at revealing the influence of the platinum moiety on the physicochemical behavior of the photosensitizer (PS) and to inspect, in turn, the possible modulation of the hydrolysis rate of the Pt^{II} ligand induced by the PS. The investigated photophysical properties for singlet and triplet states and the amplitude of the computed spin−orbit matrix elements reveal that the Pt-containing systems are able to enhance the cytotoxic $^1O_2$ production. The Pt^{II} moiety, instead, follows an activation mechanism similar to that previously found for cisplatin and its analogues already used in cancer therapy.

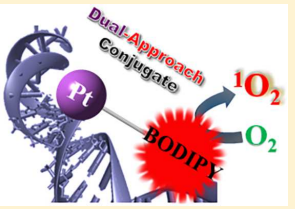

INTRODUCTION

Two-component systems made up of a photosensitizer (PS) linked to a Pt^{II} moiety recently garnered increasing attention due to the possibility to combine photodynamic therapy (PDT) treatment with classical Pt chemotherapy. These assemblies attempt to circumvent the chemotherapy drawbacks also promoting an improved distribution of the PS inside the tumor.[1−7]

In such kinds of conjugates, the light absorber should possess fundamental physicochemical properties to allow the photodynamic process to efficiently take place, therefore allowing the photobased treatment to exert its highly reliable tumor ablative ability.[8−11] Actually, PDT is a worldwide accepted, less invasive medical treatment able to efficiently destroy tumors through a light-triggered sequence of photochemical processes leading to the production of the extremely reactive singlet oxygen species $^1O_2$. The photodynamic process involves the promotion of the PS from its ground state S_0 to the excited one S_1 upon absorption of proper wavelengths, followed by intersystem crossing (ISC) transition to a lower triplet state.[12,13] Such a nonradiative process, usually prohibited, can take place if the relativistic spin−orbit coupling value between the two states $\langle S_1|\hat{H}|T_1\rangle$ is large enough and if the involved states are close in energy to permit the process to be efficient. Once in the triplet excited state, the PS can relax back to the ground state via a triplet−singlet emission process (phosphorescence) or via a radiationless transition by transferring energy to other molecules. In oxygenated tissues, two different routes are possible for the T_1 quenching mechanisms. Type II photoreactions originate from the direct energy transfer to ground-state molecular oxygen ($^3O_2$), producing the highly reactive singlet oxygen $^1O_2$, which oxidizes biomolecules of all kinds, such as lipids, proteins, and nucleic acids, ultimately killing tumors cells via a combination of necrosis and/or apoptosis. The oxygen triplet to singlet transition requires an energy equal to 0.98 eV to take place.

Alternatively, the excited PS can be involved in direct electron exchange reactions with organic substrates ultimately leading to the generation of the superoxide oxygen radical species $O_2^{\bullet(-)}$ and other radicals (type-I photoreactions). Due to the high chemical reactivity of singlet oxygen, which irreversibly destroys tumor cells, type II photoreactions should be the predominant mechanism. Accordingly, a good PS must possess a series of intrinsic properties to selectively favor that process. In particular, (*i*) the singlet−triplet splitting (ΔE_{S-T}) should be higher than 0.98 eV to allow the production of the singlet oxygen; (*ii*) the intersystem crossing between these two states should be efficient to guarantee an effective singlet oxygen generation;[13] and (*iii*) the PS should possess a red-shifted absorption wavelength to allow penetration into the tissues without interfering with the physiological processes in the cell.[12]

The tissue penetration turns out to be optimal within the so-called therapeutic window, which is limited at shorter and longer wavelengths by the light absorption of endogenous biomolecules and by water absorption, respectively. Although several ranges have been reported in the literature, the PDT window can be comprised between 600 and 1200 nm. While some of these properties can be easily achieved during the synthesis, others are required to be rationally designed beforehand. In that preliminary phase, theoretical and computational chemistry can offer a valuable contribution. In particular, the density functional theory (DFT) and its time-

Received: April 8, 2019
Published: July 25, 2019

DOI: 10.1021/acs.inorgchem.9b01002
Inorg. Chem. 2019, 58, 9882−9889

Scheme 1. BODIPY Dyes 1 and 2 and Their Complexes with Monofunctional Pt^{II} Ligand Pt-1 and Pt-2, herein Investigated

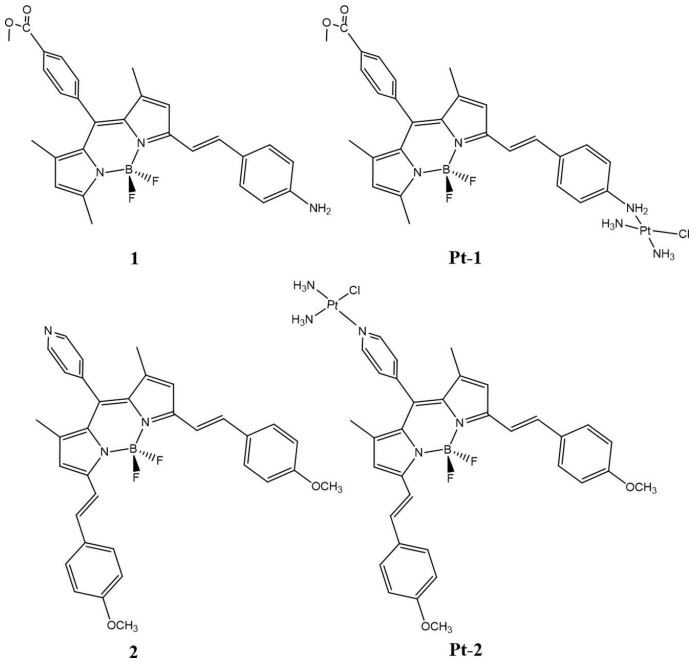

dependent version (TDDFT) allow prediction of the excitation energies, the splittings between states with different spin multiplicity and spin couplings in systems of medium-large size and complexity, with a certain reliability.[14−17] Recently, a Pt^{II} moiety has been used to functionalize two different boron dipyrromethene (BODIPY) dyes **1** and **2**, leading to the **Pt-1** and **Pt-2** metal complexes (Scheme 1). Such compounds were synthesized and tested in vitro.[6,7] Due to the high fluorescence quantum yields of BODIPYs dyes, the triplet formation is generally negligible. Nevertheless, the introduction of heavy atoms or even atoms belonging to the third-row in the core region could enhance the intersystem crossing, thereby favoring spin−orbit coupling.[18] Platinum plays an important role since experimental studies revealed how the platination process increases the photodynamic effect of BODIPY also improving the cellular accumulation.[6,7] While the properties of BODIPY dyes were extensively explored in the past for their potential application in PDT,[19] the modulation of their properties caused by the introduction of a platinum moiety has not yet been elucidated. To explore these interesting conjugates, we thus focused on their photophysical properties carrying out a careful DFT and TDDFT investigation. The used approach was extensively employed in the literature to elucidate the photochemistry of several classes of photosensitizers.[18,20] Herein, the effect of the Pt^{II} ligand on the photochemical behavior of the BODIPY light absorber has been accurately elucidated, providing information on the type II photoreactions also computing spin orbit coupling (SOC) values and comparing the obtained data with the metal-free BODIPY **1** and **2** dyes. On the other hand, the possible modulation of the Pt^{II}-moiety hydrolysis process affected by the photosensitizer has been evaluated analyzing the ligand substitution mechanisms by water, which represents the most energetically relevant process preceding the drugs' interaction with DNA. The obtained results have also been compared with those computed for cisplatin and its previously investigated analogues.[21−24]

EXPERIMENTAL SECTION

All the computations presented in this paper were performed at DFT and time-dependent DFT levels of theory, as implemented in the Gaussian 09 program code.[25] Ground singlet state optimizations were carried out in water by using the B3LYP exchange-correlation functional (XC)[26,27] and adopting the IEFPCM model (integral equation formalism polarizable continuum model[28,29]) to reproduce the solvent environment (ε = 80). The Stuttgart−Dresden pseudopotential[30] was selected to describe the heavy Pt^{II} ion while all the other atoms were described by using a 6-31+G(d,p) basis set. Although the Pt^{II} chloride−water exchange process was studied in implicit solvent, two explicit extra water molecules, in addition to the catalytic one, were also added in the system to better account for the hydrogen bonding network and to allow a proper solvation of the leaving chloride.

To explore and confirm the nature of the transition states, vibrational frequency analysis was carried out at the same level of theory. In addition, to accurately describe the hydrolysis process, single-point calculations were performed with the larger basis set 6-31++G(2df,2pd) and using the DFT-D3 atom pairwise additive schemes,[31] which account for the dispersion corrections for nonbonding interaction. The energetic profiles were also evaluated in a less polar solvent (ε = 8), which should account for the hydrophobic nature of the several macromolecules present in the cell and the water medium surrounding them.

UV−vis spectra reported in the manuscript were computed in water as vertical electronic excitations on the ground-state structures adopting the B3LYP XC functional in conjunction with 6-31+G(d,p)/SDD bases. Such a protocol was established testing several XC

DOI: 10.1021/acs.inorgchem.9b01002
Inorg. Chem. 2019, 58, 9882−9889

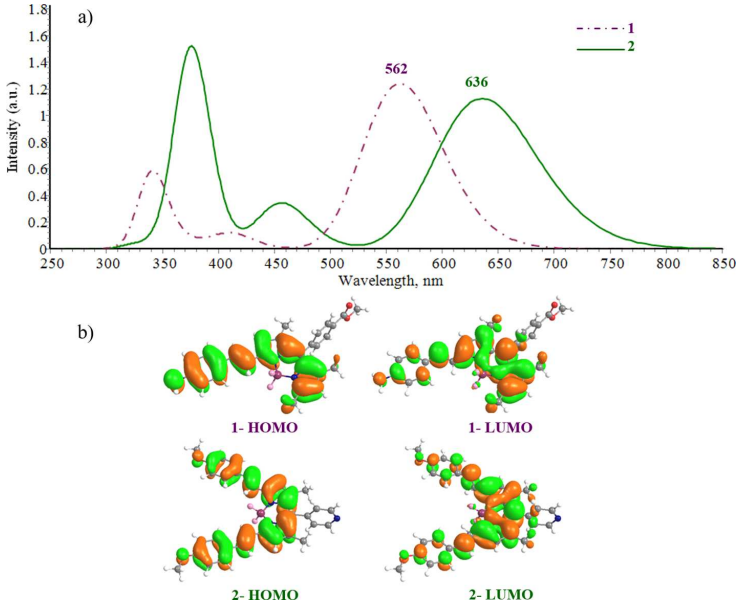

Figure 1. (a) Calculated UV−vis spectra of **1** and **2** at the B3LYP/6-31+G(d,p) level of theory, in a water environment. (b) Highest occupied (HOMO) and lowest unoccupied (LUMO) molecular orbital plots (MOs) for **1** and **2** BODIPY dyes.

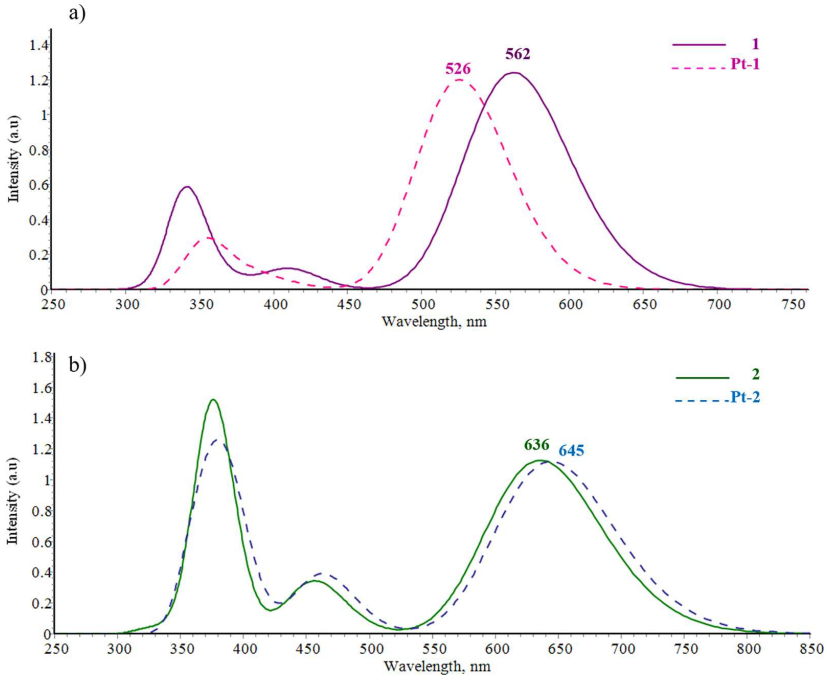

Figure 2. Calculated UV−vis spectra of (a) BODIPY **1** and **Pt-1** and (b) BODIPY **2** and **Pt-2** at the B3LYP/6-31+G(d,p) level of theory, in a water environment.

DOI: 10.1021/acs.inorgchem.9b01002
Inorg. Chem. 2019, 58, 9882−9889

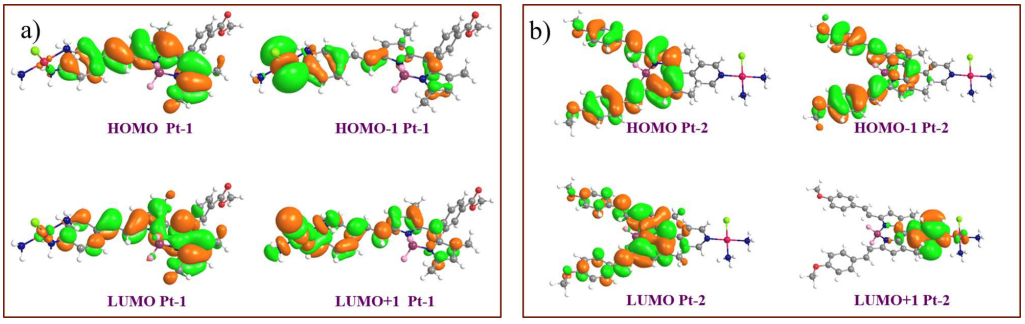

Figure 3. HOMO, LUMO, HOMO−1, and LUMO+1 MOs for (a) **Pt-1** and (b) **Pt-2** conjugates.

functionals against the experimental λ_{max} available in methanol[6] for molecule **2**. Results are reported in the Supporting Information, Figure S1. Singlet−Triplet (S-T) energy gaps discussed in the text were obtained at the same level of theory and compared with the oxygen S-T splitting (0.90 eV) previously computed adopting a similar protocol.[20a] It is worthy of note that S-T gaps are particularly functional-dependent,[15] and their values tend to be generally underestimated by the use of fixed exact exchange functionals.[32] Anyway, we are interested in a comparison between PSs and O_2 splittings that are all obtained under the same conditions, rather than at determining absolute triplet energies for the systems under investigation. To trace the spectra, a value of the fwhm equal to 0.33 eV was adopted. The quadratic-response (QR-TDDFT)[33] approach, as implemented in the Dalton code,[34] was applied to obtain spin−orbit matrix elements at the S_1 optimized geometries of the studied systems. The approximate one-electron spin−orbit operator with scaled nuclear charges[35] was used for platinum containing molecules (**Pt-1**, **Pt-2**), while the atomic-mean field approximation[36] was adopted in the other cases (**1**, **2**). B3LYP combined with the cc-pVDZ basis set was chosen to describe all atoms, while the SDD pseudopotential was used for metal ions. The SOC values were obtained according to the following formula:

$$SOC_{ij} = \sqrt{\sum_{n} |\psi_{S_i}|\hat{H}_{SO}|\psi_{T_{j,n}}|^2}\,;\ n = x, y, z$$

RESULTS AND DISCUSSION

BODIPY dyes possess remarkable optical and photophysical properties, such as very intense absorption bands at visible wavelengths. As the dye scaffold allows versatile functionalization, their spectroscopic properties can be easily modulated introducing structural chemical modifications. The *meso* position, in particular, was extensively studied.[37] The presently investigated BODIPY dyes **1** and **2** are both meso-substituted (Scheme 1), and they also contain styryl substituents on the BODIPY core. Just one styryl group is present on the BODIPY structure **1**, while BODIPY **2** is a distyryl complex with a consequent extended π system resulting also in an appreciable shift of the absorbance toward longer wavelengths. Nevertheless, in going from **1** to **2**, the observed shift is smaller than expected due to the weaker electron-donor character of the methoxy substituent compared to the NH_2 one of the BODIPY **1**. The computed UV−vis spectra of **1** and **2** in water are reported in Figure 1.

Both dyes efficiently absorb light throughout the UV and visible regions. Although they show intense high-energy absorption bands in the lowest UV region of the spectrum, especially in the case of BODIPY **2**, those bands are not suitable to treat deep tumors. On the contrary, low-energy bands are generally used for PDT. A strong absorption at 562 nm is found for system **1**, and it experiences a significant red-shift in BODIPY **2** in which the λ_{max} is located at 636 nm. Our findings are in nice agreement with the available experimental values (592 and 645 nm for **1** and **2**, respectively). Both the mentioned bands are characterized by a HOMO → LUMO transition and turn out to be $\pi-\pi^*$ in nature, the donor and acceptor orbitals in both cases being localized mainly on the BODIPY core and on the styryl ligands (Figure 1b).

To establish the influence of the Pt^{II} moiety on the photophysics of the two metal-free chromophores **1** and **2**, the UV−vis spectra of complexes **Pt-1** and **Pt-2** were computed in water and compared with those previously obtained (Figure 2). The presence of the Pt^{II} ligand generates two opposite effects on the BODIPY systems.

Indeed, when the monofunctional **Pt-1** is formed, the maximum absorption band experiences a hypsochromic shift to 526 nm due to the platination process (See Figure 2). Looking at the involved orbitals, the λ_{max} band in the case of the metallic complex is also due to a HOMO−LUMO $\pi-\pi^*$ transition. The molecular orbitals involved in such a transition indeed are visibly localized on the BODIPY and on the styryl ligand and clearly indicate the IL nature of the band. On the contrary, part of the electron density is localized on the Pt metal only when the HOMO−1 orbital is analyzed. Such an orbital is involved in the transition found at 358 nm, which, thus, possesses a partial MLCT character (HOMO−1 → LUMO). That transition is blue-shifted with respect to the weak IL band found at 411 nm also due to a HOMO−1→ L transition found for BODIPY **1**. This effect originates from the great stabilization that the HOMO−1 orbital experiences after platination. The other IL band detected below 400 nm for BODIPY **1** disappeared with the introduction of the Pt moiety.

In contrast, when BODIPY **2** undergoes a platination process generating the **Pt-2** conjugate, the effects on the UV−vis spectrum are different from those observed in **Pt-1**. Actually, the presence of the metallic moiety just slightly influences the position of the maximum absorption band, bathochromically shifting it to 645 nm. As in the previous case, the λ_{max} can be characterized as an IL $\pi-\pi^*$ transition involving a BODIPY styryl-based HOMO and LUMO orbitals.

In this case, differently from the **Pt-1** conjugate, no metal contribution is detected in the next-HOMO and the next-LUMO orbital plots for the **Pt-2** system. As a consequence, the UV region of the spectrum remains almost unchanged, the involved orbitals not being affected at all by the presence of the Pt moiety (see Figure 3).

DOI: 10.1021/acs.inorgchem.9b01002
Inorg. Chem. 2019, 58, 9882−9889

In order to shed light on the influence of the Pt^{II} moiety on the crucial PDT properties of the explored systems, it is essential to evaluate if its presence influences the energy of the triplet state. It is well known that for the type II photoreactions to take place, the energy transfer process from the ^3PS to molecular oxygen must ensure the $O_2\,^3\Sigma g^- \rightarrow {}^1\Delta g$ transition. Obviously, to achieve a good singlet oxygen quantum yield, the PS singlet−triplet (S-T) splitting should be larger than the oxygen S-T one, computed to be 0.90 eV,[20a] in good agreement with the experimental value of 0.98 eV. Besides this important issue, an efficient triplet state population via the ISC mechanism is also indispensable. It is worthy of note that just one triplet state is found below the bright S_1 state for systems under investigation, so that it is the only one that could be populated through an ISC mechanism (see Figure S2, SI). From the plot of the singlet−triplet energy gap Δ_{S-T} (Figure 4), it can be inferred that all compounds are able to promote the production of singlet oxygen, the T_1 state of all the investigated dyes lying above the $^1O_2$ one.

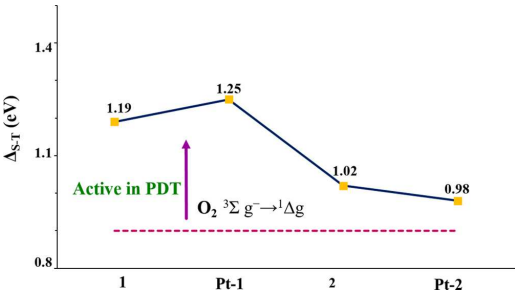

Figure 4. Singlet−triplet energy gap (eV) for **1** and **2** and their Pt complexes **Pt-1** and **Pt-2**, at the B3LYP/6-31+G(d,p) level of theory, in a water environment.

Looking at the triplet states of platinated deriatives **Pt-1** and **Pt-2**, no involvement of the metal ion has been detected in the molecular orbital plots (see Figure S3, SI). The inspection of the electronic density difference between singlet and triplet state unequivocally shows that there is no movement of the density on the Pt^{II} moiety after excitation. This is the reason why the triplet energies of **1** and **Pt-1** are quite similar, the same being true also comparing **2** and **Pt-2**.

As previously mentioned, a good photosensitizer should efficiently populate the triplet state through an efficient nonradiative intersystem crossing from the singlet exited state. The ISC rate constant K_{ISC} for the S_1-T_1 transition in the limit of the Franck−Condon approximation can be obtained in the framework of Fermi's golden rule expression, considering that both the states are harmonic:[38]

$$k_{ISC}^{nm} = \frac{2\pi}{\hbar}\langle \psi_{S_n}|\hat{H}_{SO}|\psi_{T_m}\rangle^2 \times \mathrm{FCWD} \quad (1)$$

In that expression, the main terms are the spin−orbit coupling between the considered states and the Franck−Condon weighted density of states (FCWD). In the framework of Marcus−Levich−Jortner theory, this term is proportional to the exponential factor:

$$\mathrm{FCWD} \propto \exp\left[-\frac{(\Delta E_{S-T})^2}{4\lambda k_B T}\right] \quad (2)$$

where λ is the Marcus reorganization energy and $\Delta E_{S\text{-}T}$ is the singlet−triplet gap in their equilibrium geometries. Many previous works on a series of different kinds of molecular systems[18,20] have emphasized that the spin−orbit coupling is the most important perturbation operator of the ISC process. From the obtained values collected in Table 1, it is evident as

Table 1. Spin−Orbit Matrix Elements (cm^{-1}) Calculated at the B3LYP/6-31G(d)//B3LYP Level of Theory, Using the S_1 Geometry, and the Corresponding Vertical $\Delta E_{S_1-T_1}$ (eV) Values

compound	$\lvert\psi_{S_1}\rvert\hat{H}_{so}\rvert\psi_{T_1}$	$\Delta E_{S_1-T_1}$	Φ_F[6]	Φ_Δ[7]
1	0.33	1.032		0.13
Pt-1	156.7	1.126		
2	0.01	0.978	0.13	
Pt-2	86.86	0.985	0.08	

compound **1** and **2**, possessing a very small value of the spin−orbit coupling, should be considered bad photosensitizers to be used in photodynamic therapy. On the contrary, values reveal a strong enhancement of the S_1-T_1 spin−orbit coupling matrix elements with the introduction of the Pt heavy atom. In particular, values of 156.7 and 86.9 cm^{-1} have been herein obtained for **Pt-1** and **Pt-2**, respectively. This difference can be explained in the framework of the El Sayed rule[39] affirming that a significant SOC enhancement can be produced if the radiationless transition involves a change of orbital type. While no significant differences in the MOs electronic distribution between singlet and triplet can be detected for **Pt-1**, a movement of the density from the central core toward the pyridyl group is observed after excitation in the case of the **Pt-2** conjugate, producing an increase of the SOC values (see Figure 3 and Figure S3). Anyway, such high values suggest that both the two-component systems could produce the cytotoxic $^1O_2$ molecular oxygen, providing that an appropriate light irradiation is used.

Aiming at providing a picture of the influence of the BODIPY core on the Pt^{II} activation mechanism, we have also explored the chloride−water substitution process. Indeed, it is well established that cisplatin-like drugs have DNA as their main target. In particular, they establish bonds (in mono- or bicoordinated fashion) with the N7 nitrogen atoms of guanosine, thus preventing the transcription process. To perform this action, the complexes need to replace the chloride ligands once they enter the cell nucleus. This process occurs in the dark, producing an aquated form of the complex able to reach and bind to DNA bases. For cisplatin and a series of other similar anticancer drugs, that reaction was widely studied[5,21−24,40] and the reaction path follows an SN_2 mechanism through a five-coordinated transition state (TS). With the aim to maximize the anticancer action and to reduce the dangerous side effect, the aquation process must be not too slow nor too fast, and as an average reference value, that of cisplatin is considered.[21] Differently from cisplatin, the complexes under investigation possess a monofunctional Pt^{II} ligand each, so that just one leaving chloride ion could be substituted by water (Scheme 2). Accordingly, similar to other

DOI: 10.1021/acs.inorgchem.9b01002
Inorg. Chem. 2019, 58, 9882−9889

Scheme 2. Investigated Hydrolysis Process for Pt-1 (a) and Pt-2 (b)[a]

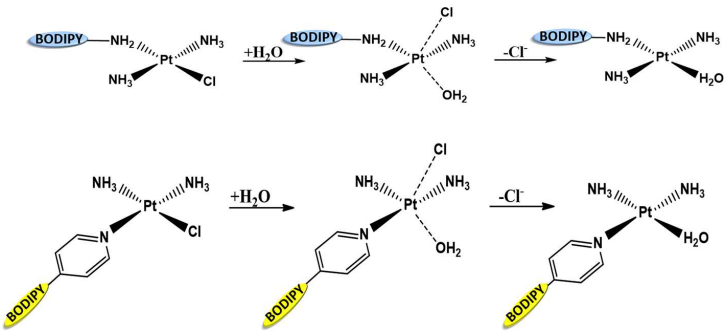

[a]Reaction mechanism and free-energy profiles are reported in the Supporting Information.

two-component systems[5] already investigated, they are expected to establish only one covalent bond with DNA.

In the hydrolysis inspection, besides the catalytic water, two extra H_2O molecules were added to the system to better account for the hydrogen bonding network and to allow a proper solvation of the leaving chloride. The potential energy surfaces for the hydrolysis of the **Pt-1** and **Pt-2** complexes, computed in water and in a less polar solvent (ε = 8), are reported in Figure S4 of the Supporting Information. All the stationary points intercepted along the reaction paths, together with more detailed information, are collected in Figure S5.

At the initial stage, water approaches the Pt^{II} center (3.61 and 3.71 Å for **Pt-1** and **Pt-2**, respectively) forming a weak interaction, leaving almost unchanged the Pt−Cl bond compared to the corresponding starting complexes. As expected, the transition state (TS) adopts a trigonal bipyramidal geometry in which the Pt−Cl bond is sensibly elongated (2.73 Å in **Pt-1** and 2.79 in **Pt-2**), while water is forming its bond with platinum (2.49 and 2.40 Å for **Pt-1** and **Pt-2**, respectively). The analyses of the TS vibrational modes unequivocally show the Pt−Cl bond breaking and the simultaneous metal−water bond formation. In the product, the Pt−OH_2 bond is completely formed, and the chloride lies far from Pt center. According to our calculations, the **Pt-1** and **Pt-2** hydrolysis reactions require energy barriers of 22.2 and 20.8 kcal/mol to be overcome in water, respectively. The activation energy values computed for **Pt-1** and **Pt-2** complexes compared with those previously obtained for cisplatin[21] and its analogues[5a,22−24] are collected in Figure 5.

The inspection of the hydrolysis process in the dark reveals that the Pt^{II} moiety follows an activation mechanism similar to that previously found for cisplatin and its analogues already used in cancer therapy. The exploration of the hydrolysis process, indeed, reveals no consistent differences between the two computed energy barriers, meaning that the Pt^{II}-coordinated chromophore has a negligible effect on the aquation process. On the other hand, the heights of the barriers found are similar to those determined in other platinum-based anticancer drugs used in chemotherapy.

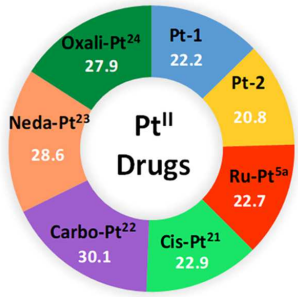

Figure 5. Computed activation energies in solution (kcal mol^{-1}) for **Pt-1**, **Pt-2**, and cisplatin analogues previously investigated.

CONCLUSIONS

Two Pt^{II}−BODIPY conjugates (**Pt-1** and **Pt-2**) and the two metal-free precursors (**1** and **2**) have been herein investigated at DFT and TDDFT levels of theory in order to explore how the Pt^{II} moiety affects the photophysics of the light absorber and to inspect, in turn, the possible modulation of the hydrolysis rate of the Pt^{II} ligand before reaching the biological target, induced by the presence of the BODIPY core.

The investigated photophysical properties for singlet and triplet states and the amplitude of the computed spin−orbit matrix elements reveal that the Pt-containing systems are both able to enhance the cytotoxic $^1O_2$ production. In particular, results also show a significant enhancement of the spin−orbit matrix elements in complex **Pt-1**, suggesting a more efficient intersystem crossing process along the investigated S_1-T_1 channel and better meeting the criteria to be successful in the PDT application. Nevertheless, due to the more extended conjugation in the chromophore moiety, the absorption wavelength of **Pt-2** better falls in the so-called photo-therapeutic window. The Pt^{II} moiety, instead, follows an activation mechanism similar to that previously found for cisplatin and its analogues already used in cancer therapy. The exploration of the hydrolysis process indeed reveals no noteworthy differences between the two computed energy barriers, meaning that the Pt^{II}-coordinated chromophore has no influence on the aquation process. On the other hand, the heights of the barriers found are similar to those determined for other previously investigated platinum-based anticancer drugs used in chemotherapy.

DOI: 10.1021/acs.inorgchem.9b01002
Inorg. Chem. 2019, 58, 9882−9889

■ ASSOCIATED CONTENT

Supporting Information

The Supporting Information is available free of charge on the ACS Publications website at DOI: 10.1021/acs.inorgchem.9b01002.

HOMO, LUMO, HOMO−1, and LUMO+1 molecular orbital plots for **Pt-2** conjugate; diagram of S_n and T_n vertical excitation states for **1**, **Pt-1**, **2**, and **Pt-2** molecules; HOMO and LUMO orbitals for T_1 state of **Pt-1** and **Pt-2** conjugates; B3LYP-D3 free energy profiles for the hydrolysis of **Pt-1** and **Pt-2** conjugates in water; optimized stationary points along the hydrolysis pathways of the **Pt-1** and **Pt-2** conjugates (PDF)

■ AUTHOR INFORMATION

Corresponding Author

*E-mail: marta.alberto@unical.it.

ORCID

Marta E. Alberto: 0000-0001-9925-7233

Nino Russo: 0000-0003-3826-3386

Emilia Sicilia: 0000-0001-5952-9927

Notes

The authors declare no competing financial interest.

■ ACKNOWLEDGMENTS

Università della Calabria is acknowledged for financial support.

■ REFERENCES

(1) Naik, A.; Rubbiani, R.; Gasser, G.; Spingler, B. Visible-light-induced annihilation of tumor cells with platinum-porphyrin conjugates. *Angew. Chem., Int. Ed.* **2014**, *53*, 6938−6941.

(2) (a) Jain, A.; Winkel, B.; Brewer, K. J. In vivo inhibition of E. coli growth by a Ru(II)/Pt(II) supramolecule [(tpy)RuCl(dpp)$PtCl_2$]-(PF_6). *J. Inorg. Biochem.* **2007**, *101*, 1525−1528. (b) Higgins, S. L. H.; Tucker, A. J.; Winkel, B. S. J.; Brewer, K. J. Metal to ligand charge transfer induced DNA photobinding in a Ru(II)-Pt(II) supramolecule using red light in the therapeutic window: a new mechanism for DNA modification. *Chem. Commun.* **2012**, *48*, 67−69. (c) Higgins, S. L. H.; White, T. A.; Winkel, B.S J.; Brewer, K. J. Redox, Spectroscopic, and Photophysical Properties of Ru-Pt Mixed-Metal Complexes Incorporating 4,7-Diphenyl-1,10-phenanthroline as Efficient DNA Binding and Photocleaving Agents. *Inorg. Chem.* **2011**, *50*, 463−470.

(3) Herman, A.; Tanski, J. M.; Tibbetts, M. F.; Anderson, C. M. Synthesis, Characterization, and in Vitro Evaluation of a Potentially Selective Anticancer, Mixed-Metal [Ruthenium(III)-Platinum(II)] Trinuclear Complex. *Inorg. Chem.* **2008**, *47*, 274−280.

(4) (a) Lottner, C.; Bart, K. C.; Bernhardt, G.; Brunner, H. Soluble Tetraarylporphyrin-Platinum Conjugates as Cytotoxic and Phototoxic Antitumor Agents. *J. Med. Chem.* **2002**, *45*, 2079−2089. (b) Lottner, C.; Bart, K.C.; Bernhardt, G.; Brunner, H. Hematoporphyrin-Derived Soluble Porphyrin-Platinum Conjugates with Combined Cytotoxic and Phototoxic Antitumor Activity. *J. Med. Chem.* **2002**, *45*, 2064−2078.

(5) (a) Alberto, M. E.; Russo, N.; Adamo, C. Synergistic Effects of Metals in a Promising $Ru^{II}Pt^{II}$ Assembly for a Combined Anticancer Approach: Theoretical Exploration of the Photophysical Properties. *Chem. - Eur. J.* **2016**, *22*, 9162−9168. (b) Alberto, M. E.; Adamo, C. Synergistic effects in Pt(II)-Porphyrinoid Dyes as candidates for a dual anticancer approach: a theoretical exploration. *Chem. - Eur. J.* **2017**, *23*, 15124−15132.

(6) Liu, Y.; Li, Z.; Chen, L.; Xie, Z. Near infrared BODIPY-Platinum conjugates for imaging, photodynamic therapy and chemotherapy. *Dyes Pigm.* **2017**, *141*, 5−12.

(7) Xue, X.; Zhu, C.; Chen, H.; Bai, Y.; Shi, X.; Jiao, Y.; Chen, Z.; Miao, Y.; He, W.; Guo, Z. A New Approach to Sensitize Antitumor Monofunctional Platinum(II) Complexes via Short Time Photo-Irradiation. *Inorg. Chem.* **2017**, *56*, 3754−3762.

(8) Dougherty, T. J.; Grindey, G. B.; Fiel, R.; Weishaupt, K. R.; Boyle, D. G. Photoradiation Therapy. II. Cure of Animal Tumors With Hematoporphyrin and Light. *J. Natl. Cancer Inst* **1975**, *55*, 115−121.

(9) Dabrowski, J. M.; Arnaut, L. G. Photodynamic therapy (PDT) of cancer: from local to systemic treatment. *Photochem. Photobiol. Sci.* **2015**, *14*, 1765−1780.

(10) Quirk, B. J.; Brandal, G.; Donlon, S.; Vera, J. C.; Mang, T. S.; Foy, A. B.; Lew, S. M.; Girotti, A. W.; Jogal, S.; LaViolette, P. S.; Connelly, J. M.; Whelan, H. T. Photodynamic therapy (PDT) for malignant brain tumors. Where do we stand? *Photodiagn. Photodyn. Ther.* **2015**, *12*, 530−544.

(11) Dolmans, D.E.J.G.J; Fukumura, D.; Jain, R. K. Photodynamic therapy for cancer. *Nat. Rev. Cancer* **2003**, *3*, 380−387.

(12) Yano, S.; Hirohara, S.; Obata, M.; Hagiya, Y.; Ogura, S.-I.; Ikeda, A.; Kataoka, H.; Tanaka, M.; Joh, T. Current states and future views in photodynamic therapy. *J. Photochem. Photobiol., C* **2011**, *12*, 46−67.

(13) Lang, K.; Mosinger, J.; Wagnerova, D.M. Photophysical properties of porphyrinoid sensitizers non-covalently bound to host molecules; models for photodynamic therapy. *Coord. Chem. Rev.* **2004**, *248*, 321−350.

(14) (a) Le Guennic, B.; Jacquemin, D. Taking Up the Cyanine Challenge with Quantum Tools. *Acc. Chem. Res.* **2015**, *48*, 530−537. (b) Laurent, A.; Jacquemin, D. TD-DFT benchmarks: A review. *Int. J. Quantum Chem.* **2013**, *113*, 2019−2039.

(15) Adamo, C.; Jacquemin, D. The calculations of excited-state properties with Time-Dependent Density Functional Theory. *Chem. Soc. Rev.* **2013**, *42*, 845−856.

(16) Eriksson, E. S. E.; Eriksson, L. A. Predictive power of long-range corrected functionals on the spectroscopic properties of tetrapyrrole derivatives for photodynamic therapy. *Phys. Chem. Chem. Phys.* **2011**, *13*, 7207−7217.

(17) (a) Francés-Monerris, A.; Magra, K.; Darari, M.; Cebrián, C.; Beley, M.; Domenichini, E.; Haacke, S.; Pastore, M.; Assfeld, X.; Gros, P. C.; Monari, A. Synthesis and Computational Study of a Pyridylcarbene Fe(II) Complex: Unexpected Effects of fac/ mer Isomerism in Metal-to-Ligand Triplet Potential Energy Surface. *Inorg. Chem.* **2018**, *57*, 10431−10441. (b) Francés-Monerris, A.; Gattuso, H.; Roca-Sanjuan, D.; Tunon, I.; Marazzi, M.; Dumont, E.; Monari, A. Dynamics of the excited-state hydrogen transfer in a (dG).(dC) homopolymer: intrinsic photostability of DNA. *Chem. Sci.* **2018**, *9*, 7902−7911.

(18) (a) Alberto, M. E.; De Simone, B. C.; Mazzone, G.; Quartarolo, A. D.; Russo, N. Theoretical determination of Electronic Spectra and Intersystem Spin-Orbit Coupling: the case of Isoindole-BODIPY dyes. *J. Chem. Theory Comput.* **2014**, *10*, 4006−4013. (b) Mazzone, G.; Quartarolo, A. D.; Russo, N. PDT-correlated photophysical properties of thienopyrrole BODIPY derivatives. Theoretical insights. *Dyes Pigm.* **2016**, *130*, 9−15. (c) De Simone, B. C.; Mazzone, G.; Pirillo, J.; Russo, N.; Sicilia, E. Halogen atom effect on the photophysical properties of substituted aza-BODIPY derivatives. *Phys. Chem. Chem. Phys.* **2017**, *19*, 2530−2536. (d) Ponte, F.; Mazzone, G.; Russo, N.; Sicilia, E. BODIPY for photodynamic therapy applications: computational study of the effect of bromine substitution on $^1O_2$ photosensitization. *J. Mol. Model.* **2018**, *24*, 183.

(19) (a) Kamkaew, A.; Lim, S. H.; Lee, H. B.; Kiew, L. V.; Chung, L. Y.; Burgess, K. BODIPY dyes in photodynamic therapy. *Chem. Soc. Rev.* **2013**, *42*, 77−88. (b) Zhao, J.; Wu, W.; Sun, J.; Guo, S. Triplet photosensitizers: from molecular design to applications. *Chem. Soc. Rev.* **2013**, *42*, 5323−51. (c) Awuah, S. G.; You, Y. Boron dipyrromethene (BODIPY)-based photosensitizers for photodynamic therapy. *RSC Adv.* **2012**, *2*, 11169−11183. (d) Boens, N.; Leen, V.; Dehaen, W. Fluorescent indicators based on BODIPY. *Chem. Soc. Rev.* **2012**, *41*, 1130. (e) Leen, V.; Yuan, P.; Wang, L.; Boens, N.; Dehaen,

DOI: 10.1021/acs.inorgchem.9b01002
Inorg. Chem. 2019, 58, 9882−9889

W. Synthesis of *Meso*-Halogenated BODIPYs and Access to *Meso*-Substituted Analogues. *Org. Lett.* **2012**, *14*, 6150−6153. (f) Pang, W.; Zhang, X.-Fu; Zhou, J.; Yu, C.; Hao, E.; Jiao, L. Modulating the singlet oxygen generation property of *meso*-*β* directly linked BODIPY dimers. *Chem. Commun.* **2012**, *48*, 5437−5439.

(20) (a) Alberto, M. E.; De Simone, B. C.; Mazzone, G.; Sicilia, E.; Russo, N. Heavy atom effect on Zn(II) phthalocyanines derivatives: a theoretical exploration of the photophysical properties. *Phys. Chem. Chem. Phys.* **2015**, *17*, 23595−23601. (b) Mazzone, G.; Alberto, M. E.; De Simone, B. C.; Marino, T.; Russo, N. Can Expanded Bacteriochlorins Act as Photosensitizers in Photodynamic Therapy? Good News from Density Functional Theory Computations. *Molecules* **2016**, *21*, 288. (c) Ji, S.; Ge, J.; Escudero, D.; Wang, Z.; Zhao, J.; Jacquemin, J. Molecular Structure-Intersystem Crossing Relationship of Heavy-Atom-Free BODIPY Triplet Photosensitizers. *J. Org. Chem.* **2015**, *80*, 5958−5963.

(21) Raber, J.; Zhu, C.; Eriksson, L. A. Activation of anti-cancer drug cisplatin — is the activated complex fully aquated? *Mol. Phys.* **2004**, *102*, 2537−2544.

(22) Pavelka, M.; Lucas, M. F. A.; Russo, N. On the Hydrolysis Mechanism of the Second-Generation Anticancer Drug Carboplatin. *Chem. - Eur. J.* **2007**, *13*, 10108−10116.

(23) Alberto, M. E.; Lucas, M. F.A.; Pavelka, M.; Russo, N. The Second-Generation Anticancer Drug Nedaplatin: A Theoretical Investigation on the Hydrolysis Mechanism. *J. Phys. Chem. B* **2009**, *113*, 14473−14479.

(24) Lucas, M. F. A.; Pavelka, M.; Alberto, M. E.; Russo, N. Neutral and Acidic Hydrolysis Reactions of the Third Generation Anticancer Drug Oxaliplatin. *J. Phys. Chem. B* **2009**, *113*, 831−838.

(25) Frisch, M. J.; Trucks, G. W.; Schlegel, H. B.; Scuseria, G. E.; Robb, M. A.; Cheeseman, J. R.; Scalmani, G.; Barone, V.; Mennucci, B.; Petersson, G. A.; Nakatsuji, H.; Caricato, M.; Li, X.; Hratchian, H. P.; Izmaylov, A. F.; Bloino, J.; Zheng, G.; Sonnenberg, J. L.; Hada, M.; Ehara, M.; Toyota, K.; Fukuda, R.; Hasegawa, J.; Ishida, M.; Nakajima, T.; Honda, Y.; Kitao, O.; Nakai, H.; Vreven, T.; Montgomery, J. A., Jr.; Peralta, J. E.; Ogliaro, F.; Bearpark, M.; Heyd, J. J.; Brothers, E.; Kudin, K. N.; Staroverov, V. N.; Keith, T.; Kobayashi, R.; Normand, J.; Raghavachari, K.; Rendell, A.; Burant, J. C.; Iyengar, S. S.; Tomasi, J.; Cossi, M.; Rega, N.; Millam, J. M.; Klene, M.; Knox, J. E.; Cross, J. B.; Bakken, V.; Adamo, C.; Jaramillo, J.; Gomperts, R.; Stratmann, R. E.; Yazyev, O.; Austin, A. J.; Cammi, R.; Pomelli, C.; Ochterski, J. W.; Martin, R. L.; Morokuma, K.; Zakrzewski, V. G.; Voth, G. A.; Salvador, P.; Dannenberg, J. J.; Dapprich, S.; Daniels, A. D.; Farkas, O.; Foresman, J. B.; Ortiz, J. V.; Cioslowski, J.; Fox, D. J. *Gaussian 09*, Revision D.01; Gaussian, Inc.: Wallingford, CT, 2010.

(26) Becke, A. D. J. Density-functional thermochemistry. III. The role of exact exchange. *J. Chem. Phys.* **1993**, *98*, 5648−5652.

(27) Lee, C.; Yang, W.; Parr, R. G. Development of the Colle-Salvetti correlation-energy formula into a functional of the electron density. *Phys. Rev. B: Condens. Matter Mater. Phys.* **1988**, *37*, 785−789.

(28) Cossi, M.; Barone, V. Solvent effect on vertical electronic transitions by the polarizable continuum model. *J. Chem. Phys.* **2000**, *112*, 2427−2435.

(29) Tomasi, J.; Mennucci, B.; Cammi, R. Quantum Mechanical Continuum Solvation Models. *Chem. Rev.* **2005**, *105*, 2999−3094.

(30) Andrae, D.; Häusermann, U.; Dolg, M.; Stoll, H.; Preuss, H. Energy-adjusted*ab initio* pseudopotentials for the second and third row transition elements. *Theor. Chim. Acta* **1990**, *77*, 123.

(31) Grimme, S.; Antony, J.; Ehrlich, S.; Krieg, H. A consistent and accurate *ab initio* parametrization of density functional dispersion correction (DFT-D) for the 94 elements H-Pu. *J. Chem. Phys.* **2010**, *132*, 154104−154122.

(32) Peach, M. J. G.; Williamson, M. J.; Tozer, D. J. Influence of Triplet Instabilities in TDDFT. *J. Chem. Theory Comput.* **2011**, *7*, 3578−3585.

(33) (a) Rinkevicius, Z.; Tunell, I.; Salek, P.; Vahtras, O.; Ågren, H. Restricted density functional theory of linear time-dependent properties in open-shell molecules. *J. Chem. Phys.* **2003**, *119*, 34−46. (b) Ågren, H.; Vahtras, O.; Minaev, B. Response Theory and Calculations of Spin-Orbit Coupling Phenomena in Molecules. *Adv. Quantum Chem.* **1996**, *27*, 71−162.

(34) Dalton, a molecular electronic structure program, Release Dalton 2016. http://daltonprogram.org.

(35) Koseki, S.; Schmidt, M. W.; Gordon, M. S. Effective Nuclear Charges for the First-through Third-Row Transition Metal Elements in Spin-Orbit Calculations. *J. Phys. Chem. A* **1998**, *102*, 10430−10436.

(36) Ruud, K.; Schimmelpfennig, B.; Ågren, H. Internal and external heavy-atom effects on phosphorescence radiative lifetimes calculated using a mean-field spin-orbit Hamiltonian. *Chem. Phys. Lett.* **1999**, *310*, 215−221.

(37) Epelde-Elezcano, N.; Martinez-Martinez, V.; Pena-Cabrera, E.; Gomez-Duran, C. F. A.; Arbeloa, I. L.; Lacombe, S. Modulation of singlet oxygen generation in halogenated BODIPY dyes by substitution at their *meso* position: towards a solvent-independent standard in the vis region. *RSC Adv.* **2016**, *6*, 41991−41998.

(38) Marian, C. M. Spin-orbit coupling and intersystem crossing in molecules. *Wiley Interdiscip. Rev. Comput. Mol. Sci.* **2012**, *2*, 187−203.

(39) El-Sayed, M. A. Triplet state. Its radiative and nonradiative properties. *Acc. Chem. Res.* **1968**, *1*, 8−16.

(40) Alberto, M. E.; Russo, N. Methionine ligand selectively promotes monofunctional adducts between trans-EE platinum anticancer drug and guanine DNA base. *Chem. Commun.* **2011**, *47*, 887−889. (b) Alberto, M. E.; Butera, V.; Russo, N. Which One among the Pt-Containing Anticancer Drugs More Easily Forms Monoadducts with G and A DNA Bases? A Comparative Study among Oxaliplatin, Nedaplatin, and Carboplatin. *Inorg. Chem.* **2011**, *50*, 6965−6971. (c) Alberto, M. E.; Lucas, M. F.; Pavelka, M.; Russo, N. The Degradation Pathways in Chloride Medium of the Third Generation Anticancer Drug Oxaliplatin. *J. Phys. Chem. B* **2008**, *112*, 10765−10768. (d) Zhang, Y.; Guo, Z.; You, X.-Z. Hydrolysis Theory for Cisplatin and Its Analogues Based on Density Functional Studies. *J. Am. Chem. Soc.* **2001**, *123*, 9378−9387.

DOI: 10.1021/acs.inorgchem.9b01002
Inorg. Chem. 2019, 58, 9882−9889